THE UNIVERSITY *of* EDINBURGH

Molecular torsion balances for quantifying non-covalent interactions

Ioulia Mati

Thesis presented for the degree of

Doctor of Philosophy

The University of Edinburgh

2013

Declaration

I declare that this thesis is written by myself and that the work presented here is entirely my own, except where indicated in the text. The work was carried out in the School of Chemistry at the University of Edinburgh. It has not been submitted in part, or in a whole, for any other degree.

Ioulia Mati
February 2013

Acknowledgements

First of all, I would like to express my sincere thanks to my supervisor Dr Scott L. Cockroft for giving me the opportunity to work on this project of great interest in his research group, and also for his continuous help, support and guidance.

Secondly, I want to thank Catherine Adam who also worked in this project and we had an excellent collaboration. John Brazier, who worked as a post-doc in the group, was always very willing to help me, give important ideas and answer my questions. I also want to thank everyone in the Cockroft group, previous and current members for their friendship and help. They are all great guys and it was wonderful to be working in a nice environment.

I would like to thank Prof. Christopher Hunter for the idea of the solvation model used to analyse our experimental data.

In addition, thanks are expressed to the technical staff of the Chemistry Department of Edinburgh (NMR, mass spectrometry and organic-inorganic undergraduate lab technical staff) for their help. Many thanks to Dr Juraj Bella for the valuable help with the more demanding NMR experiments.

Furthermore, I would like to thank the University of Edinburgh and EPSRC for funding my Ph.D.

Finally, a thousand thanks go to my family and friends back in Greece for their love and support.

Abstract

Non-covalent interactions underpin the whole of chemistry and biology, but their study is extremely difficult in complicated biological systems. This thesis presents the application of synthetic molecular balances for gaining fundamental insights into the physicochemical phenomena that govern molecular recognition processes.

Chapter 1 reviews the use of small synthetic molecules that exist in two conformational states *via* slow rotation of a bond, in the quantification of non-covalent interactions.

Chapter 2 presents a new molecular torsion balance, based on a slowly rotating tertiary formyl amide for the study of non-covalent interactions. The incorporation of a fluorine atom in one of the rings allows the quantification of solvent effects in a wide range of solvents. Intramolecular electrostatic interactions and intermolecular solvation effects (but not solvophobic effects) are shown to be important in determining the position of the conformational equilibria. Correlations with calculated molecular properties show that solvent effects are fully dissected, revealing the idealistic behavior of the system in the gas phase.

Chapter 3 discusses through-space substituent effects on the properties of aromatic rings. Electronic communication between both electron-rich and electron-deficient substituents with the electron density of an adjacent aromatic ring is predicted by molecular electrostatic potential calculations. The effect is confirmed to occur experimentally and is quantified using synthetic molecular balances.

Chapter 4 describes the work done towards the investigation of solvent bridging interactions in molecular torsion balances. No experimental evidence of bridging interactions was observed. This might be attributed to the entropic penalty associated with this binding mode, or the non-ideal geometry of the potential bridging sites.

Chapter 5 outlines a steric blocking effect observed in certain balances with bulky substituents in chloroform and dichloromethane.

Chapter 6 presents synthetic procedures and compound characterisation including a thorough analysis of NMR data obtained in this study.

List of papers

Sections of the work presented in the thesis have contributed to the following publications:

Chapter 1
Molecular Balances for Quantifying Non-covalent Interactions
Chem. Soc. Rev. 2010, 39, 4195-4205
I. K. Mati, S. L. Cockroft

Chapter 2
Dissecting Electronic and Solvent Effects on Conformational Equilibria
in preparation
I. K. Mati, C. A. Adam, S. L. Cockroft

Chapter 3
Experimental Measurement of Through-space Substituent Effects
in preparation
I. K. Mati, C. A. Adam, S. L. Cockroft

Chapter 5
Electrostatic Polarisation of Aromatic Ring via Solvation of Substituents
in preparation
K. B. Muchowska, I. K. Mati, C. A. Adam, S. L. Cockroft

Abbreviations

1-D or 2-D	1 or 2 dimentional
Bu	butyl
CCDB	Cambridge crystallographic database
COSY	correlation spectroscopy
d	doublet
Dab	diaminobutyric acid
DCM	dichloromethane
DFT	density functional theory
DME	dimethoxyethane
DMF	dimethylformamide
DMSO	dimethyl sulfoxide
EDG	electron donating group
EI	electron ionization
ESI	electrospray ionization
ESP	electrostatic potential
Et_3N	triethylamine
Et_2O	diethyl ether
EtOAc	ethyl acetate
EtOH	ethanol
EWG	electron withdrawing group
EXSY	exchange spectroscopy
HMBC	heteronuclear multiple-bond correlation spectroscopy
HOMO	highest occupied molecular orbital
HRMS	high resolution mass spectrometry
HSQC	heteronuclear single-quantum correlation spectroscopy
IR	infrared spectroscopy
Lys	lysine
m	multiplet
MeOH	methanol
MEP	molecular electrostatic potential
m.p.	melting point
NMR	nuclear magnetic resonance
NOE	nuclear overhauser effect
NOESY	nuclear overhauser effect spectroscopy
Orn	ornithine

$PdCl_2$(dppf)	[1,1′-bis(diphenylphosphino)ferrocene]dichloropalladium(II)
PEG	polyethylene glycol
Ph	phenyl
ppm	parts per million
Pr	propyl
prep-TLC	preparative thin layer chromatography
r.t.	room temperature
s	singlet
sat.	saturated
t	triplet
TFA	trifluoroacetic acid
THF	tetrahydrofuran
TOCSY	total correlation spectroscopy
UV	ultraviolet
VT-NMR	variable temperature NMR

Contents

Chapter 1

Molecular balances for quantifying non-covalent interactions

Abstract

Molecular interactions underlie the whole of chemistry and biology. This chapter illustrates the use of rotameric folding molecules, topoisomers, atropoisomers, and tautomers as molecular balances for quantifying non-covalent interactions. This intramolecular approach enables a wide variety of interactions to be examined with a degree of geometric control that is difficult to achieve in supramolecular complexes. Synthetic variation of molecular balances allows the fundamental physicochemical origins of molecular recognition to be systematically examined by providing insights into the interplay of geometry and solvation on non-covalent interactions

1.1. Introduction

Non-covalent interactions are fundamental aspects of all chemical and biological processes. In the chemical sciences, non-covalent interactions have essential roles in template-directed synthesis,[1] the transmission of stereochemical information,[2] and in determining the structure and properties of materials.[3] Meanwhile, in biological systems, non-covalent interactions govern the secondary and tertiary structure of proteins,[4] and are responsible for enzyme-ligand binding and base-pairing in nucleic acids.[5]

Detailed study of non-covalent interactions in biological systems is often complicated by arrays of interactions featuring multiple molecular contacts and solvent molecules. Furthermore, the precise geometry of an interaction of interest is hard to determine in conformationally-dynamic biomolecules. Such complexities can

be side-stepped by using minimal synthetic compounds in the study of non-covalent interactions.[6] Synthetic chemistry facilitates the design of molecules that allow the systematic study of the underlying phenomena that determine the strength of non-covalent interactions. Whilst non-covalent interactions have been examined extensively using supramolecular complexes,[7] unimolecular approaches often offer improved control over the geometry of an intramolecular interaction of interest, which is a major advantage since small alterations in geometry may have a considerable effect on the strength of an interaction. Furthermore, very weak interactions that are too weak to overcome the entropic penalty associated with intermolecular association, or that would otherwise provide only a minor perturbation to the overal stability of an intermolecular complex can often be measured accurately using molecular balances.

1.2. Quantifying non-covalent interactions with molecular balances

Folding molecules offer an attractive platform for the study of non-covalent interactions, since the relative stabilities of the conformational states are governed by intramolecular contacts and solvent interactions that are present in one conformation, but absent in the others. Although it is not possible to experimentally assess the relative stabilities of all accessible conformations of a flexible molecule, thermodynamic information can be extracted from simple model systems with limited degrees of conformational freedom. The most elegant molecular torsion balances possess high degrees of symmetry, which minimises the contributions of background steric, solvent and secondary intramolecular interactions to the folding behaviour of the molecule. When the system lacks symmetry or when changing functional groups perturbs multiple interactions in the system, then the interaction of interest can be dissected from the background secondary effects by reference to suitable control compounds and application of thermodynamic double-mutant cycles.[8]

Though not all molecules have the desired folding properties to permit ΔG determination, numerous molecular systems have been successfully applied to the quantitative study of non-covalent interactions. Rotational barriers ($\Delta G^{\ddagger}$) and differences in the free energies of ground-state conformers (ΔG) are used most frequently to assess the thermodynamics of non-covalent interactions.

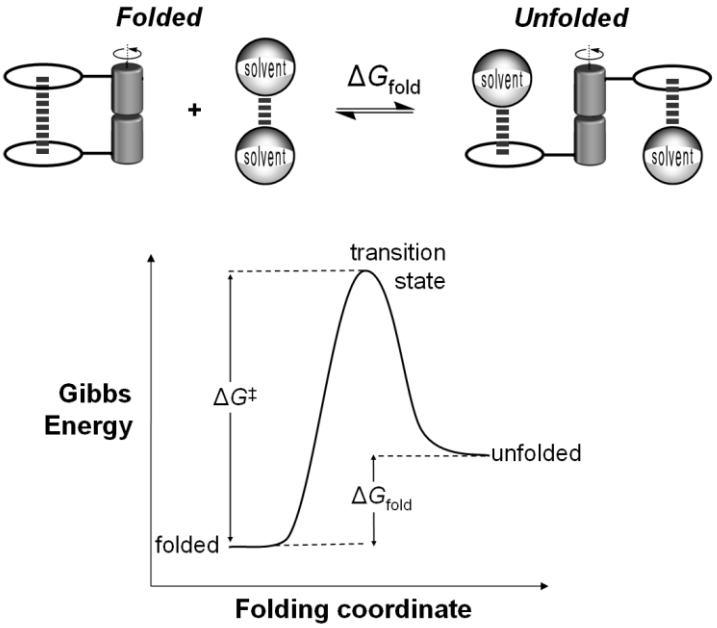

Figure 1.1. Simplified folding equilibrium for a molecular torsion balance including the solvent and the corresponding energy profile showing the energy barrier to rotation, $\Delta G^{\ddagger}$ and the free energy of folding, ΔG_{fold}. In this example, folding involves the formation of an intramolecular interaction accompanied by desolvation of the interacting functional groups.

$\Delta G^{\ddagger}$ Rotational barrier measurement - theoretical requirements & limitations

The barrier to rotation about a single covalent bond ($\Delta G^{\ddagger}$) quantifies the free energy difference between a ground-state conformation and the transition state, and can provide insight into the strength of non-covalent interactions (Figure 1.1). Although $\Delta G^{\ddagger}$ values can be readily determined using variable-temperature dynamic NMR

spectroscopy, the interpretation of these measurements is not always straightforward since the nature of the transition state can be hard to define.[9] The conformation of the transition state cannot be observed directly, and the energetic effects of substituents on the stability and the structure of highly strained or sterically crowded transition states can be particularly difficult to predict.

ΔG Conformational equilibrium measurement - theoretical requirements & limitations

The free energy difference between ground-state conformers (ΔG) is more easily interpreted than $\Delta G^{\ddagger}$ rotational barrier measurements because the interactions present in the ground-state conformations can often be calculated with a high degree of certainty or observed experimentally (*i.e.* in X-ray crystal structures or NMR solution structures). However, interaction energies should always be interpreted with care; the role of the solvent in determining molecular conformation should never be overlooked (Figure 1.1).[10-13]

The foremost requirement for ΔG measurement using folding molecules is that the relative populations of each distinct conformer must be quantifiable. NMR spectroscopy is a powerful technique for assessing the conformation of small molecules. However, it is not always possible to quantify folding equilibria because most forms of molecular flexibility are rapid on the NMR timescale and result in conformationally averaged signals. Thus, not all folding molecules are suited to the quantitative study of non-covalent interactions. For example, the folding compounds depicted in Figure 1.2 have been used to investigate aromatic stacking interactions.[14,15] Qualitative information about the preferred geometry of these molecules can be obtained from spectroscopic techniques, but thermodynamic information cannot be extracted from the system because the precise position of the conformational equilibrium cannot be determined.

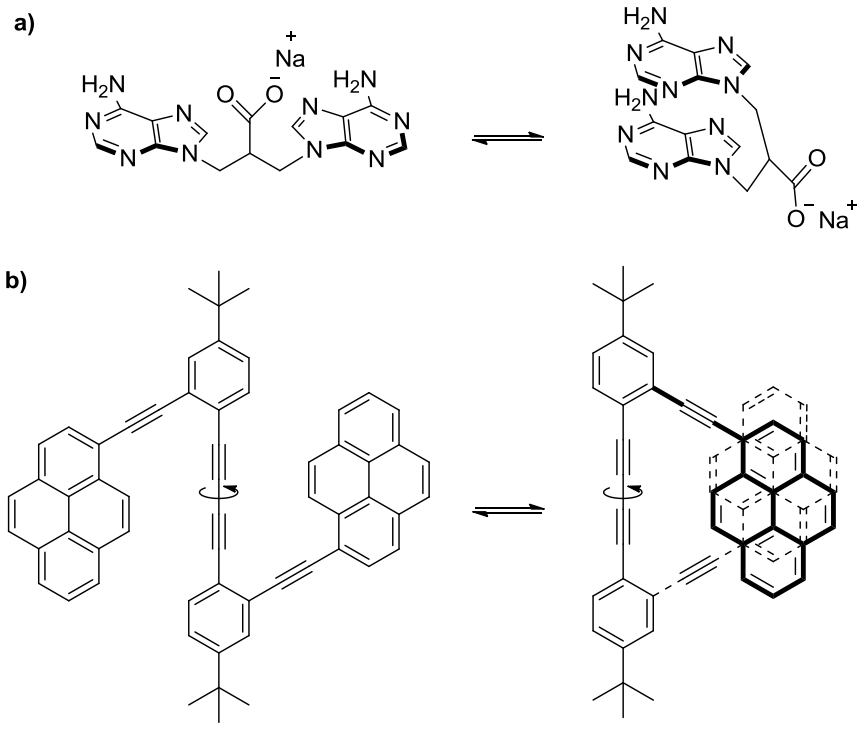

Figure 1.2. Folding molecules synthesised by a) Newcomb and Gellman,[14] and b) Sankararaman *et al.* for studying aromatic interactions.[15] Despite the elegant, simplistic designs, neither system can be used to quantify the interaction of interest as no method of accurately determining the position of the equilibrium has been established.

One approach to quantifying ground-state non-covalent interactions is to exploit molecules featuring a single restricted bond that rotates slowly enough for distinct conformational populations to be directly quantified by NMR, but rapidly enough for conformational equilibrium to be reached within a reasonable timescale. For room-temperature analysis using ^{1}H NMR this typically requires a barrier to rotation, $\Delta G^{\ddagger} >$ 65 kJ mol^{-1}. Integration of distinct NMR conformer signals allows the conformational equilibrium constant K_{fold} to be determined from a single NMR spectrum. One advantage of this approach is that time-consuming titrations, or variable-temperature experiments are not required to extract thermodynamic information from the system. Provided that the system under investigation is sufficiently geometrically well-defined,

the approach allows both attractive and repulsive interactions to be measured with a high degree of accuracy (often ±0.5 kJ mol^{-1}). The precise range and accuracy of the approach depends upon the sensitivity of the spectroscopic technique employed. For example, ^{1}H-NMR spectra with an integral accuracy ~5% provides an interaction window of 14.6 kJ mol^{-1} since the most extreme conformational populations that can be measured accurately correspond to $\Delta G_{fold} = -RT \ln K_{fold} = -RT \ln(5/95) = +7.3$ kJ mol^{-1} and $\Delta G_{fold} = -RT \ln(95/5) = -7.3$ kJ mol^{-1}.

1.3. Classes of interaction investigated using molecular balances

CH···O Interactions

Ōki's pioneering studies of restricted bond rotation in triptycene derivatives date back to the 1970s. Ōki *et al.* were quick to realise that interactions between substituents in the 1-(*peri*) and 9-(bridge-head) positions influenced the rotational barrier about the C-C bond indicated in Figure 1.3.[16] Furthermore, when the substituents in these positions were large enough, the increased barrier to rotation meant that distinct conformers could be observed in ^{1}H-NMR spectra at low temperatures.[17] The substituents attached to the 1- and 9- positions are able to interact with each other in the folded ±*syn* conformation, whilst they are splayed apart in the unfolded *anti* conformation. Based on the equilibrium shown in Figure 1.3, the magnitude of the intramolecular interaction between the 1- and 9-substituents (including steric and solvophobic effects) can be determined by measuring the deviation from the statistically expected ±*syn*/*anti* ratio of 2:1.[16] Ōki went on to study many types of non-covalent interactions using triptycene balances,[18] and some of these findings are summarised below and interpreted from a contemporary point of view.[19]

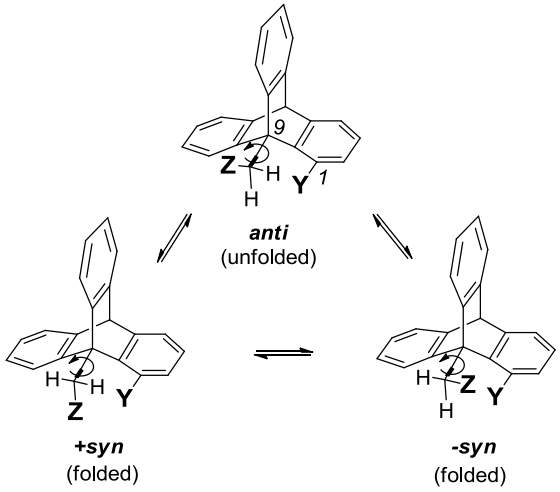

Figure 1.3. Conformational equilibrium in 1,9-disubstituted triptycenes.[16,18]

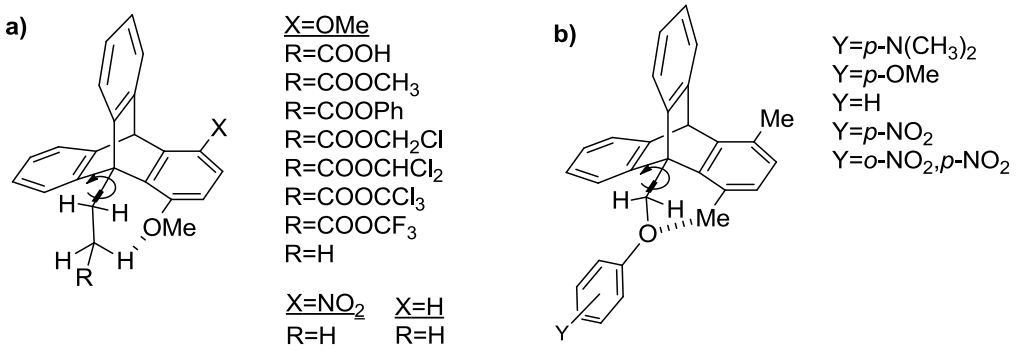

Figure 1.4. 1,9-disubstituted triptycenes for investigating CH···O interactions in $CDCl_3$. a) The folded *syn* conformer (depicted) becomes more prevalent as the R-group becomes more electron-withdrawing, which is consistent with the presence of a polar CH···O interaction. However when R = H, steric and desolvation effects dominate and the unfolded *anti* conformer is favoured (Figure 1.5a).[20-23] b) The folded *syn* conformer depicted is most favoured when the phenolic Y-substituents are electron donating.[24]

A series of triptycene torsion balances was synthesised to study the interactions of methoxy groups with a range of functional groups in $CDCl_3$ (Figure 1.4a).[20-22] In general, the folded ±*syn* conformers were most favoured when the R-groups were

electron-withdrawing, which was consistent with an electrostatically dominated interaction between the electron-rich oxygen and the δ+ CH_2 groups adjacent to the carbonyl group.[21] There were a few exceptions to this rule that were attributed to conformational and steric differences related to the positioning of the functional groups as the R-group was varied.[20,22] When the methoxy group was replaced with a chlorine atom, the ±*syn*/*anti* ratios decreased due to the increased size and decreased electron density of chlorine compared to oxygen.

Two different families of torsion balances were then synthesised to investigate CH···O interactions (Figure 1.4a bottom, R = H and Figure 1.4b).[24,23] In both series, the unfolded *anti* conformer was always favoured, which was attributed to the dominance of van der Waals repulsion over the electrostatic CH···O interactions. Consistent with the presence of a favourable CH···O non-covalent interaction, the population of the folded *syn* conformer increased as the oxygen atom became more electron-rich for the compounds depicted in Figure 1.4b. In contrast, the population of the unfolded *anti* conformer increased as the X-substituent became more electron donating for the other compound series (R = H, Figure 1.4a).[23]

This inconsistency was reasoned as being due to the increased polarity of the benzyl CH *vs.* ethyl CH, although modern-day electrostatic surface potential calculations show that these functional groups have only a marginal difference in polarity (+49 kJ mol^{-1} for the toluene CH_3 *cf.* +43 kJ mol^{-1} for the CH_3 in ethyl benzene at DFT/B3LYP/6-31G*). Further insight into this discrepancy can be gained from examination of molecular models (Figure 1.5). Space-filling models indicate that the ethyl group occludes most of the methoxy oxygen in the folded *syn* conformation, whereas the phenolic oxygen in the other compound series remains accessible to solvation by chloroform in the *syn* conformation. Since chloroform is a stronger H-bond donor (α = 2.2) than an alkyl group (α = 0.4) solvation of the methoxy group by chloroform outcompetes the Et···O interaction.[19] Thus, the steric occlusion of the methoxy oxygen in the folded *syn* conformer means that desolvation dominates the population ratios for the compound series where R = H (Figure 1.4a), whilst the phenolic compounds (Figure 1.4b) are much less affected by desolvation

and the CH···O interaction governs the folding behaviour as the Y-substituents are varied. These experiments highlight the subtle interplay of geometry and the effects of desolvation on non-covalent interactions.

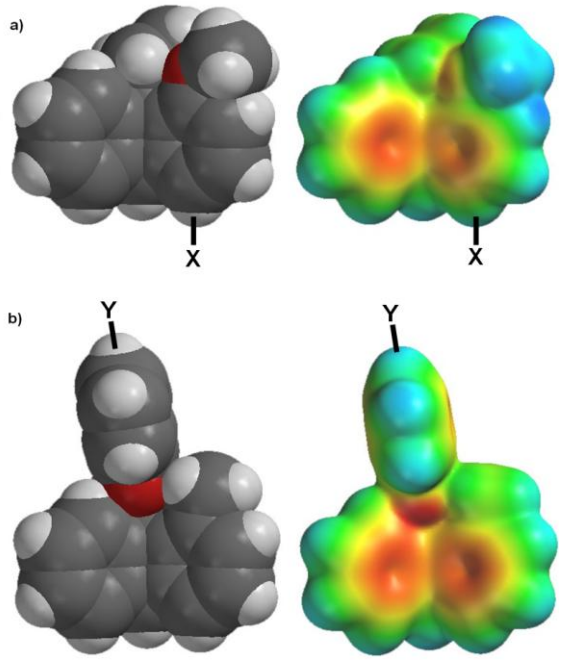

Figure 1.5. Space-filling models (left) and electrostatic surface potentials (right) of triptycene balances minimised at the DFT/B3LYP/6-31G* level. Electrostatic potentials are scaled from –115 kJ mol^{-1} (red) to +115 kJ mol^{-1} (blue); green corresponds to neutral charge. a) The negative charge on the oxygen atom is solvent-occluded in the *syn* conformer of the ethyl balance shown (Figure 1.4a, R = H), but solvent exposed in the *anti* conformation (not shown). Thus, the trend in the folding behaviour as the X-substituent is varied is dominated by the effects of chloroform desolvation. b) In contrast, the electron density of the oxygen atom is not sterically occluded in the *syn* conformer of the phenoxy balance and can be freely solvated by the polar C-H of chloroform (Figure 1.4b). As a result the trends in the folding behaviour of the phenoxy balance are governed by the strength of the CH···O interaction as the Y-substituents are varied rather than by the effects of desolvation.

Arene···functional-group interactions

Building on his earlier studies of CH···O interactions, Ōki and more recently, Gung, have synthesised a series of 9-benzyl triptycene derivatives for investigating arene···functional group interactions (Figure 1.6). The compounds shown in Figure 1.6a were synthesised for studying CH_3···arene interactions as the X and Z substituents were varied.[18] Chlorine atoms were used in two of the *peri*-positions in this compound series to approximately balance the influence of steric effects on the *syn*/*anti* conformer ratio (Cl has a similar van der Waals radius to Me). Thus, the position of the folding equilibrium should be mostly determined by the relative energies of the Cl/CH_3···arene interactions and desolvation effects. Consistent with the formation of a dominant CH···arene interaction, higher ±*syn*/*anti* ratios were observed for the compounds with the most electron-rich aromatic ring (Z = NMe_2) and the most positively polarised CH_3-group (X = $COOCH_3$).

Oxygen···arene and halogen···arene interactions were studied using the compounds shown in Figure 1.6b.[18] Introduction of electron-donating Z-substituents was seen to decrease the *syn/anti* ratio, and this was attributed to the increase in electrostatic repulsion between the oxygen atom and the face of the aromatic ring. The *syn/anti* ratio was reduced when the X-substituents were replaced with larger chlorine or bromine atoms.

Gung and co-workers have investigated interactions between aromatic rings and a series of esters (Figure 1.6c)[25] and methoxymethyl ether groups (Figure 1.6d).[26] There was a preference for the folded *syn* conformer in almost all cases. The greatest preference for the folded conformation was observed in the methoxymethyl ether series (Figure 1.6d), particularly when the arene contained electron-withdrawing Z-substituents. Interpretation of these data may be complicated by the conformational freedom of the functional groups studied, which permits multipoint contacts of both positively polarised CH-groups and electron-rich oxygen atoms with the rotameric phenyl ring. Although the role of the solvent on these conformational equilibria has yet to be systematically examined, the authors suggest that the preference for the folded state points towards the importance of van der Waals

dispersion forces, with the position of the equilibrium being modulated by electrostatic interactions.

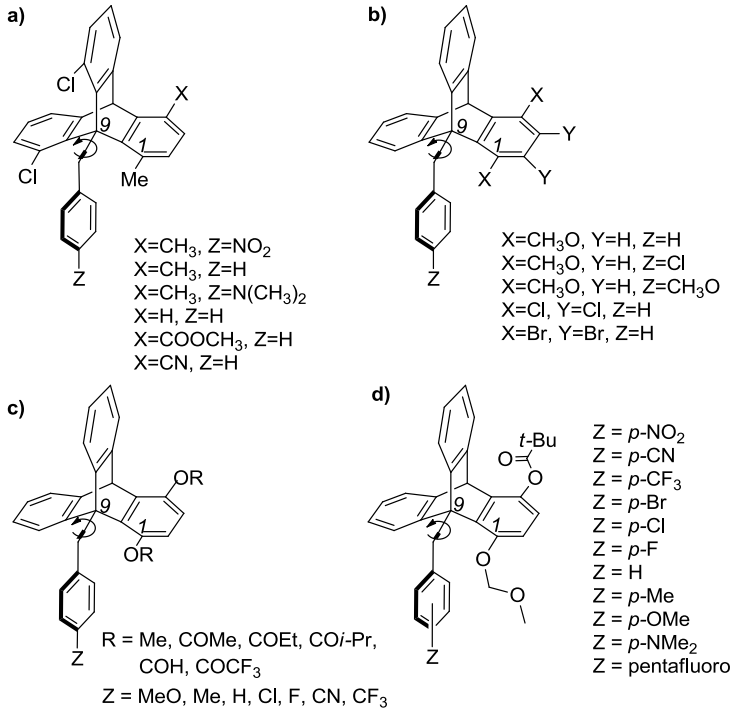

Figure 1.6. 9-Benzyl triptycene derivatives for investigating functional group···arene interactions. a) and b) Ōki's compounds for studying CH···arene and oxygen/halogen···arene interactions.[18] c) and d) Gung's systems for studying oxygen···arene interactions,[25] and methoxymethyl···arene interactions.[26]

Gung and co-workers used the 1,9-disubstituted triptycenes shown in Figure 1.7 for the quantification of CH···π interactions between an α-substituted acetate group and a benzene ring.[27] The *syn* conformer was the major conformer for all the balances in this study. For the balances of type a, electron-withdrawing groups increase the hydrogen bond donor ability of the CH protons and favour the CH···π interaction. Electron-withdrawing substituents in the b series balances reduce the electron density of the benzene ring and weaken the CH···π interaction. The folding free energies for both series correlate linearly with the Hammett constants (σ_m) of the substituents X and Y. In

addition for the series a, there is a linear correlation of the folding energies with the computationally calculated deprotonation energies, and thus also with the acidity of the α-substituted acetates.

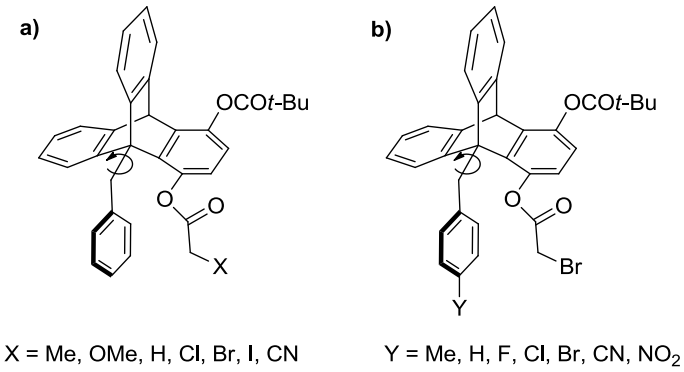

Figure 1.7. 1,9-disubstituted triptycenes synthesised by Gung and co-workers for quantifying CH···π interactions.[27]

Motherwell and co-workers have used minimal dibenzobicyclo[3,2,2]-nonane derivatives to study interactions between functional groups and aromatic rings (Figure 1.8).[28,29] These compounds exist in two conformations, where either the Y or Z group interacts with the face of an aromatic ring. In contrast to many of the other folding molecules presented in this chapter, the barrier to isomerisation in these derivatives is small and the rate of the conformational interconversion is not slow on the NMR timescale. Nevertheless, accurate population ratios were determined from the ^{1}H-NMR *J*-couplings of the conformers.[28] When Y = Me and Z = OH, the conformation in which the hydroxyl group interacts with the aromatic ring is observed in the solid-state and also dominates in low polarity solvents such as cyclohexane, carbon tetrachloride, benzene, toluene and chloroform (population of *D* > 89%). Meanwhile, solvents that act as H-bond acceptors, such as pyridine, methanol, and dimethylsufoxide ($\beta_s \approx 6$-9) compete with the OH···arene interaction and the equilibrium is shifted towards the *U* conformation (population of *D* = 50-55%). Acetronitrile competes less strongly with the OH···arene interaction

(population of *D* = 74%) since it is a weaker H-bond acceptor (β_s = 4.7). When the hydroxyl group in the *Z*-position was replaced by an amino group, the populations of the *D* conformer were seen to decrease in most of the solvents studied, indicating that the OH···arene interaction is stronger than the NH···arene interaction in these compounds.[29]

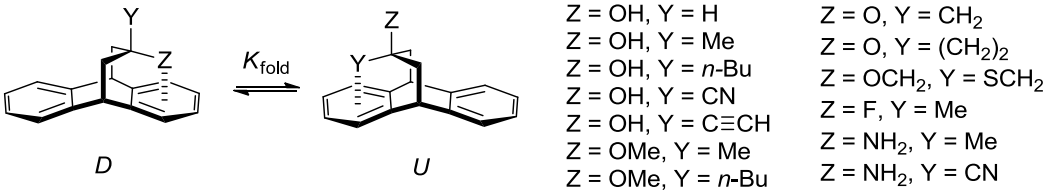

Figure 1.8. Motherwell's molecular torsion balance for quantifying functional group···arene interactions in organic solvents.[28,29]

Not all molecular balances reveal information about non-covalent interactions through changes in the position of a conformational equilibrium. Indeed, Elguero, Cornago and co-workers have used the position of tautomeric equilibria in pyrazole derivatives to investigate intramolecular NH···arene interactions (Figure 1.9).[30] At low concentrations, the tautomers are in slow exchange on the ^{1}H-NMR timescale in a range of deuterated solvents (chloroform, dichloromethane, dimethylsulfoxide and hexamethylphosphoramide). The barrier to tautomerisation decreases as the concentration of the pyrazole increases, presumably due to intermolecular association and proton exchange *via* the adjacent pyrazole ring nitrogen and NH groups. ^{1}H NMR showed a large shielding of the NH proton in tautomer 1 consistent with the NH···arene interaction shown. Tautomer 1 was >98% abundant when R = CF_3 in all solvents examined, which was attributed to the strengthening of polar NH···arene interaction by the strong electron-withdrawing effect of the CF_3 group.

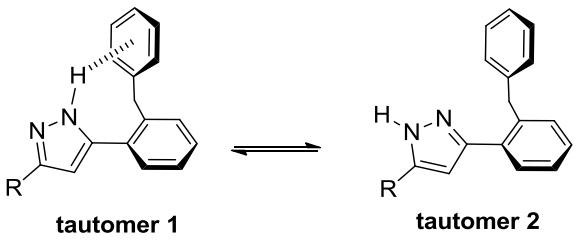

Figure 1.9. Polar NH···arene interactions have been quantified by using the tautomeric equilibria in pyrazoles when R = Me, CF_3 and Ph.[30]

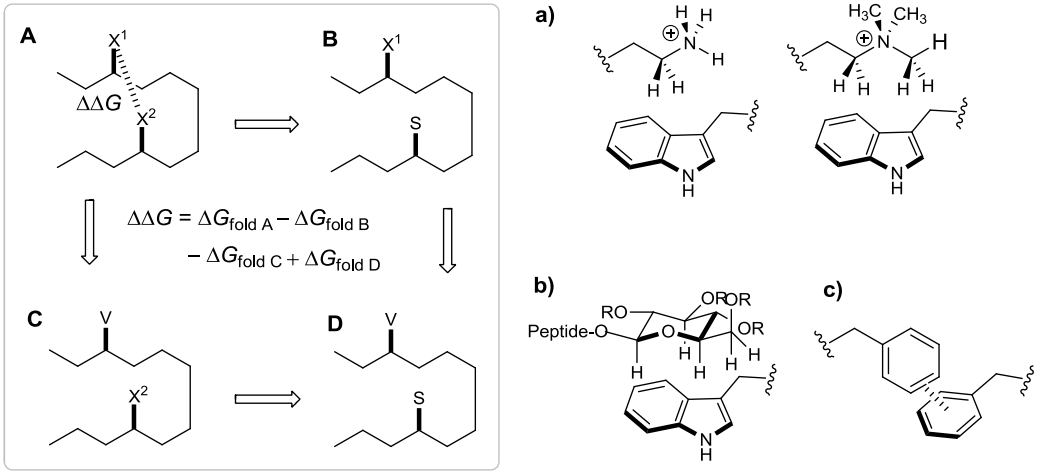

Figure 1.10. Example of a thermodynamic double-mutant cycle used by Waters and co-workers for the quantification of a range of arene···functional-group interactions in folded β-hairpin peptides. a) cation···arene interactions, b) carbohydrate···arene interactions (R = H or Ac), and c) aromatic edge-to-face interactions.[8,31-34]

Functional-group···arene interactions have also been studied in a more biological context using simple folding peptides in aqueous solution. Waters and co-workers used thermodynamic double-mutant cycles,[8] to quantify non-covalent interactions between the X^1 and X^2 side-chains in β-hairpin folds (Figure 1.10, left). This model system has been used to study cation···arene interactions between an aromatic tryptophan residue and cationic amine side-chains (Figure 1.10a).[31]

Shielding of the protons in the lysine side-chain was observed by NMR spectroscopy due to close proximity of the tryptophan ring in the folded conformation. The chain length of the cationic side-chain was found to affect the interaction with tryptophan, and thus the stability of the β-hairpin fold. Shortening of the side-chain in the sequence: Lys > Orn > Dab decreased the favourability of the cation···arene interaction, with lysine having the optimal length for a diagonal interaction. The strength of this interaction and the stability of the β-hairpin were also seen to increase upon *N*-methylation of the lysine analogues.

In addition, β-hairpin peptides have been used to quantify carbohydrate···arene interactions (Figure 1.10b).[32,33] The carbohydrate protons are shifted upfield in the NMR spectra due to the close proximity to the aromatic tryptophan ring in the folded peptide. There was an insignificant change in the stability of the fold when the tryptophan indole side-chain was substituted for a 1-naphthyl or 2-naphthyl group. In contrast, replacing the tryptophan residue with the smaller aromatic amino acid, phenylalanine, decreased the stability of the peptide fold. Similar destabilisation was also observed upon substitution of the tryptophan residue for a non-aromatic cyclohexyl side-chain. A strong solvophobically driven interaction was only seen between tryptophan and fully acylated carbohydrates (Figure 1.10b, R = Ac) and not with the unprotected carbohydrates due to the high energetic penalty required to desolvate the unprotected hydroxyl groups. Strikingly, the carbohydrate···arene interaction was found to be stronger than the arene···arene interaction between two phenylalanine side-chains (Figure 1.10c), or the cation···arene interaction between tryptophan and lysine (Figure 1.10a).[32,34]

Shimizu and co-workers synthesised a series of *N*-arylimide molecular torsion balances for the quantification of CH···π interactions between alkyl and arene groups.[35] Slow rotation of the C_{aryl}–N_{imide} bond results in two conformers, but only in the folded conformation the alkoxy group is placed above the arene shelf and forms a CH···π interaction. The balances in Figure 1.11a could only be crystallised in the unfolded conformation, but the crystal structures of the two-armed balances (Figure 1.11b) show a definite CH···π interaction. The two-armed balances with an ethyl group could form a

second weak CH···π interaction. The balance c acts as a control compound because it cannot form a CH···π interaction, but it can still account for the lone pair···π interaction between the oxygen of the ether linker and the benzene shelf. The unfolded conformer was the major one because apart from the attractive CH···π interaction (~ 4.2 kJ/mol), there was a repulsive lone pair···π interaction and an entropic penalty on folding for the balances with larger alkoxy arms. The repulsive lone pair···π interaction, calculated from the $\Delta\Delta G_{fold}$ between balances c and d, was slightly larger than the CH···π interaction. By calculating the enthalpic and entropic terms for the balances, the rotational entropy was found to be the reason for the weaker CH···π interaction of the balances with larger alkoxy arms.

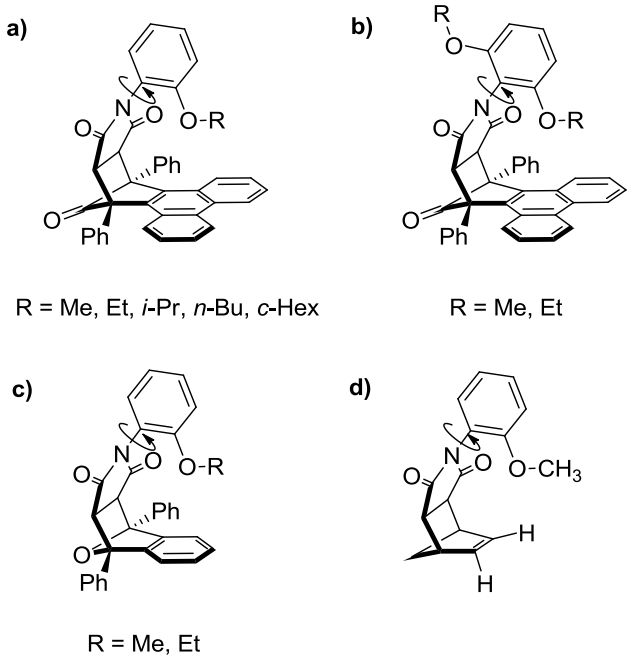

Figure 1.11. Molecular torsion balances designed by Shimizu *et al.* for quantifying CH···π interactions.[35]

Datta *et al.* performed computational calculations on Shimizu's balances.[35,36] According to these calculations, the folded conformer in Figure 1.11a was stabilised by removing the repulsive lone pair···π interaction or by strengthening the CH···π

interaction. Datta also showed that the lone pair···π interaction can be removed by replacing the oxygen of the alkoxy arm with a CH_2 group. The CH···π interaction can be enhanced by inserting electron-donating substituents at the aromatic shelf. For example, an NH_2 substituent polarises the C-H bond towards the arene shelf and at the same time increases the distance of the oxygen linker from the arene shelf. In addition the larger arene shelf, moving from naphthalene to phenanthrene and pyrene, was seen to increase the CH···π interaction in the calculations.

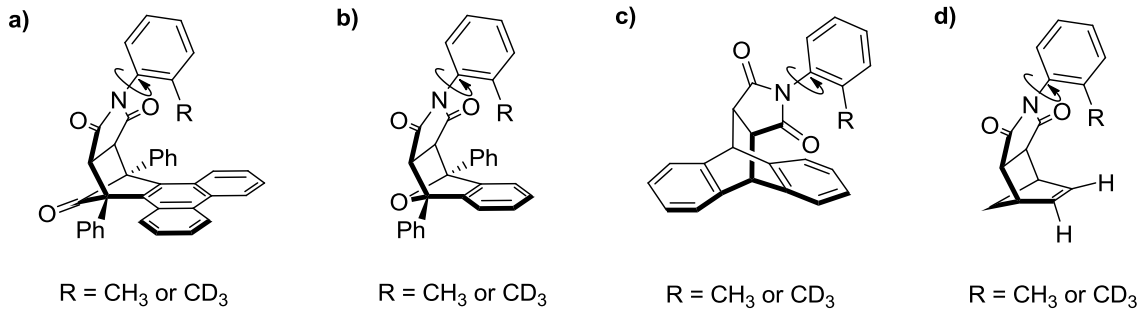

Figure 1.12. Molecular torsion balances synthesised by Shimizu and co-workers to study the D/H isotope effect for the CH···π interaction.[37]

Very recently Shimizu and co-workers used the molecular balances shown in Figure 1.12 to study the D/H isotope effect for the CH···π interaction.[37] The balances a, b and c form in the folded conformation a CH···π interaction between the *o*-methyl group R and the arene shelf, which is also apparent in the X-ray crystal structures. The balance a, posseses a large phenanthrene shelf compared to the benzene shelves in balances b and c. In addition, the different bridges in the three balances affect the distance between the *o*-methyl group and arene face to a different extent. The torsion balance d was used as a control compound, as no CH···π interaction could take place due to the lack of an aromatic shelf. The folded conformation was preferred only in the balance a, with the phenanthrene shelf. The close proximity of the methyl group to the arene face caused steric repulsion, especially in balance b in which the interacting moieties were closer compared to the rest of the balances. The steric

repulsion destabilised the folded conformer, favouring the unfolded one, despite the presence of the attractive CH···π interaction. D/H isotope effects were not observed, as the folding free energies for the protic and deuterated balances were about identical both in chloroform and acetone. Computation studies in a model benzene-methane system did not also show any D/H isotope effect.

Wilcox and co-workers have also studied alkyl···arene contacts using molecular torsion balances (Figure 1.13).[38,39] Indeed, Wilcox *et al.* were the first to coin the phrase 'molecular torsion balance', with the most recent studies building upon measurements published in 1994.[38]

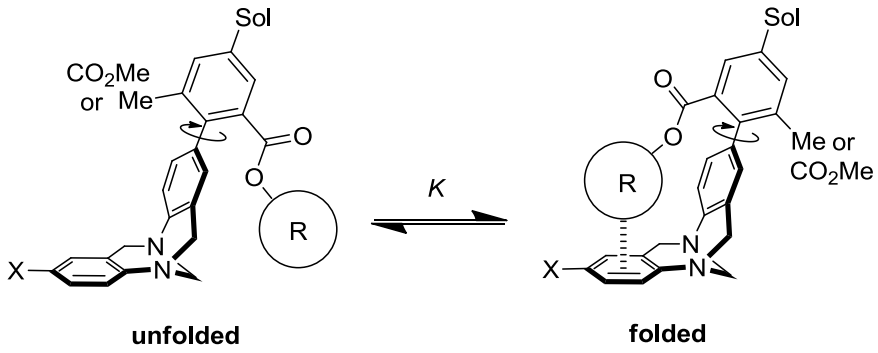

Figure 1.13. Molecular torsion balances designed by Wilcox and later used by others for measuring aromatic edge-to-face interactions in organic solvents (R = substituted phenyl rings), and alkyl···arene interactions (R = Me, *i*-Pr, *t*-Bu, cyclohexyl, 1-adamantyl, 2-adamantyl) in $CDCl_3$ (Sol = NO_2, H, NH_2) and D_2O (Sol = $NHCO(CH_2)_3$-COO^-K^+).[11-13, 38-43]

Like the triptycene balances discussed earlier, the folded and unfolded conformations in Wilcox's balance are visible as distinct signals in ^{1}H-NMR spectra. The two conformations arise from the hindered rotation about the biaryl bond. Deviation from a 1:1 ratio of states indicates the presence of a non-covalent interaction or solvent effect. When R = Me there is little or no preference for either conformation, as the methyl group is too far from the face aromatic ring to interact.[40]

However, when R is replaced by a larger alkyl group the folded conformation is seen to dominate in both D_2O and $CDCl_3$. The balance is most folded in aqueous solution and when R = *i*-Pr, highlighting the importance of the hydrophobic effect and shape complementarity in non-covalent interactions.[40,39]

A modification of the bridgehead of the Wilcox molecular torsion balance, performed by Ams *et al.* was seen to affect the folding of the balance.[44] If the methano-bridgehead is replaced by an ethano-bridgehead, then the dihedral angle between the two aromatic rings of the Tröger's base decreases, thus providing a shorter interaction distance. When the group R in Figure 1.14 is an isopropyl or *tert*-butyl group the folding free energies for the methano and ethano-bridged balances differ little. However, when there is a cyclohexyl or phenyl ester the folding energy changes significantly and the unfolded conformation dominates. Due to the close proximity of the group R and the benzene face in the case of the ethano-bridgehead, the steric repulsion dominates over the attractive edge-to-face interaction. This is more pronounced in the case of the bulkier cyclohexyl and phenyl groups.

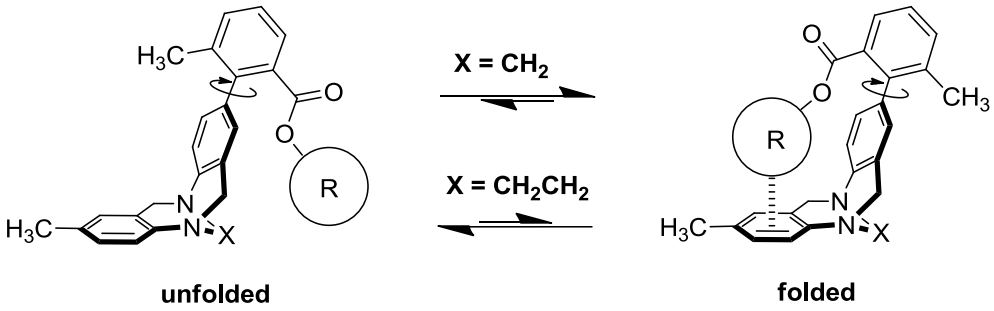

Figure 1.14. The Wilcox molecular torsion balance modified by Ams, featuring a NCH_2CH_2N instead of the NCH_2N bridgehead.[44]

Aromatic edge-to-face interactions

Aromatic edge-to-face interactions have received considerable attention from supramolecular chemists, partly due to their importance in stabilising the structure of

proteins and peptides.[34,45]

Wilcox and co-workers pioneered the use of molecular torsion balances for studying aromatic edge-to-face interactions (Figure 1.13).[38] By varying both the R-group with differently substituted phenyl rings, and the X-substituent on the 'face-ring', it was possible to systematically examine the effects of substituents on the folding free energy. Aromatic R-groups featuring electron-withdrawing groups such as CN, CF_3 and NO_2 shift the equilibrium towards the folded conformation, which can be explained by an increase in the electrostatic attraction between the partial positive charge of the edge of the aromatic ring with the electron-density of the aromatic face.[12,13,38,42,43]

Other experiments involving variation of the X-substituents on the 'face-ring' revealed a much more surprising result; the folding free energies of the torsion balances appeared to be insensitive to variation of the X-substituents in $CDCl_3$ when R was an unsubstituted phenyl ring.[40-43] This observation led Wilcox to conclude that dispersion forces, and not electrostatic forces, dominate aromatic edge-to-face interactions in this system.[40] However, experimental work published by Ren in 1997, and Diederich in 2004 and 2008, revealed that the solvent has a significant influence on the folding behaviour of these molecules.[41-43] Particularly worthy of note was the observation that folding free energies when R = *p*-trifluoromethyl phenyl correlated linearly with Hammett substituent constants in both C_6D_6 and $CDCl_3$. This implies an important role for electrostatic effects in edge-to-face interactions, and contradicts Wilcox's earlier conclusions.

Cockroft and Hunter used a simple solvation model to rationalise the apparent discrepancy (Figure 1.1, top).[12] The key point is that solvation of the face-ring competes with the edge-to-face aromatic interaction formed upon folding. Thus, when R is a phenyl ring with an electron-withdrawing substituent, the positively polarised edge of the aromatic ring outcompetes the solvation of the face ring by both chloroform and benzene and the folding free energies vary significantly as the electrostatic potential of the aromatic face is modulated by changing the X-substituents. In contrast, when R is an unsubstituted phenyl ring, the edge-to-face

interaction formed in the folded conformation is similar in magnitude to the interaction between the face aromatic ring and the solvent (in $CDCl_3$ and C_6D_6), so the folding free energies change only slightly upon variation of the X-substituents on the face ring. The most obvious prediction made by this model is that benzene solvation should compete equally as well for the edge-to-face interaction as R = Ph, a result that was later confirmed experimentally by Diederich and co-workers.[13,43]

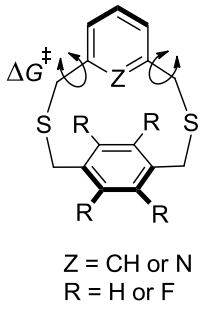

Figure 1.15. Topomeric model compounds designed by Cozzi to measure tilted edge-to-face aromatic interactions.[46]

Recently, Cozzi and co-workers studied the interaction of the face of a phenyl ring with both the edge of another phenyl ring, and the nitrogen of a pyridine ring using variable-temperature NMR experiments (Figure 1.15).[46] The barriers to topomeric flipping of the *meta*-substituted ring were increased upon fluorination of the face-ring, with the highest barrier being observed with the pyridine ring. The lowest barrier to flipping was observed with the benzene ring and the non-fluorinated face ring. Despite the appealing simplistic design of these molecules, calculated energy landscapes for the topomerisation process contained multiple transition states, highlighting the complexities involved in the interpretation of $\Delta G^{\ddagger}$ measurements. Rationalisation of the observed barriers to rotation was further convoluted because the energetics of the ground-state conformations and each of the transition states were modulated to different extents as the substituents were varied.

Cozzi and co-workers studied the interaction of thiophene and furan rings with the face of an aromatic ring by using computational calculations and VT-NMR experiments (Figure 1.16a).[47] The large size of the sulfur atom and the small distance from the benzene ring, forces the thiophene derivatives to adopt a parallel-stacked conformation in the ground state, whereas the edge-to-face arrangement is only adopted at the transition state. The energy barrier was larger for the fluoro-substituted derivative because it possesses a more stable ground state with less repulsion between the stacked rings compared to the H-substituted derivative. The oxygen atom in furan adducts is smaller than sulfur, but more electron rich, thus the parallel-stacked conformation is disfavoured and the furan adducts adopt an edge-to-face conformation in the ground state. The isomerisation process in this case happens through rotation of the bridges, thus the threshold barriers are identical for the two furan adducts.

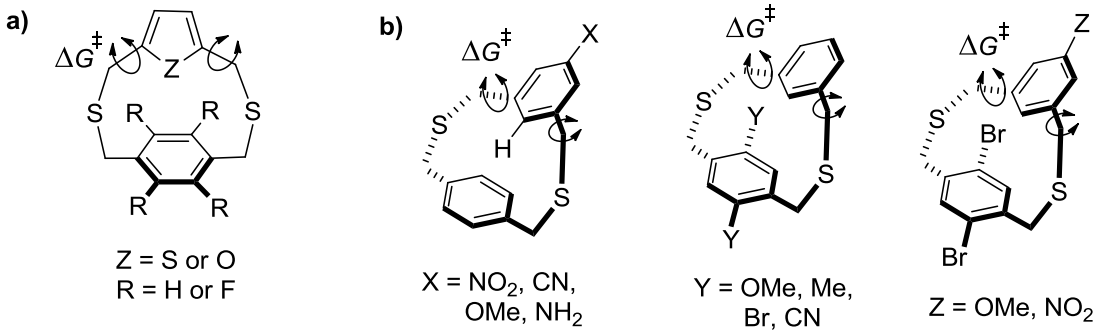

Figure 1.16. Model compounds designed by Cozzi and co-workers to study a) the interaction of thiophene and furan rings with the face of an aromatic ring[47], b) the effect of substituents on aromatic-aromatic interactions.[48]

Cozzi and co-workers also used the model compounds shown in Figure 1.16b to study the effects of substituents on aromatic-aromatic interactions.[48] The compounds in all three series (substituted on either or both rings) adopted a slightly tilted conformation in the X-ray structures. The variation of the energy barriers in all three series was small and could not be correlated with the effect of substituents based on electrostatic rules.

Generally, the barrier was lower when there were no substituents on one or both rings and became larger with the presence of either kind of substituent.

Siegel and co-workers designed a series of 2,6-diaryltolans and tetraarylditolans and studied the structure of these molecular rotors with computational calculations and X-ray crystallography (Figure 1.17).[49] The A and B rings of the 2,6-diaryltolan rotors can be either coplanar, giving an umbrella-like conformation stabilised by CH···π interactions between the CH of ring B and the face of the flanking rings, or perpendicular (Figure 1.17a). In the crystal structure of this series neither of the two absolute conformations was achieved. When a CH···π interaction was possible, the alkyne axis was bent, favouring a closer contact.

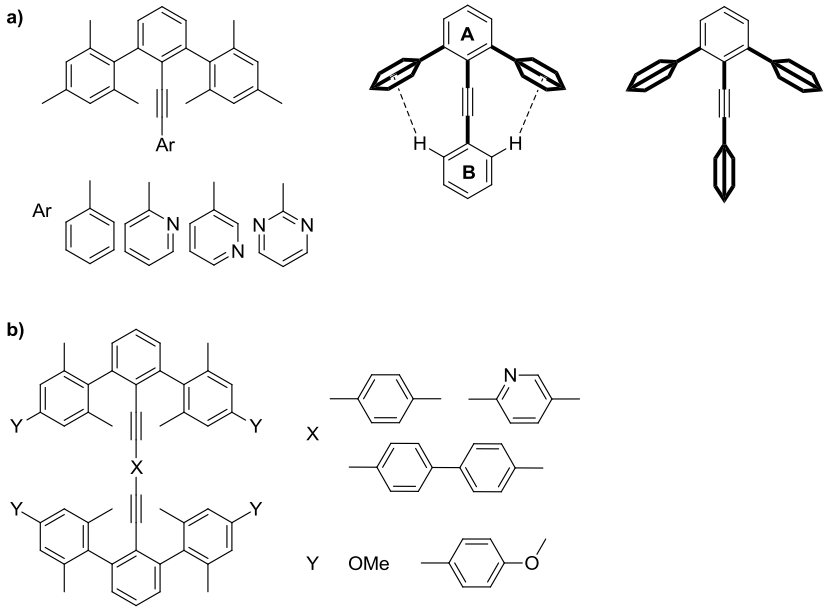

Figure 1.17. α) 2,6-diaryltolan series and conformations α and β, b) tetraarylditolan series.[49]

Aromatic stacking interactions

Gellman and co-workers expanded on their earlier qualitative studies of aromatic stacking interactions (Figure 1.2a) by developing a series of folding molecules for quantifying aromatic interactions (Figure 1.18).[10,50,51] These compounds exist as two

slowly interconverting conformers *via* rotation about the tertiary amide C-N bond (Figure 1.18a). In the Z-conformation the aromatic rings are splayed apart and cannot interact with each other, but in the *E* conformation the aromatic rings can come into a stacked arrangement (as supported by X-ray crystal structures). The conformer ratios of the compounds shown in Figures 1.18a and 1.18b were similar in $CDCl_3$ solution, but were quite different in D_2O. This was attributed to the hydrophobic stabilisation of the *E* conformer, which minimises the solvent-exposed surface area of the apolar aromatic moieties (Figure 1.1, top).

A derivative where one of the aromatic groups was replaced with a phenyl ring was seen to have similar folding ratios in both water and chloroform, presumably because the phenyl group does not reach far enough to interact with the naphthyl group (Figure 1.18b, Y = H). Thus, the contribution of the arene···arene interaction to the observed folding free energies could be quantified by subtracting the folding free energy of this reference compound from those observed in the other variations shown in Figures 1.18a and 1.18b.

The folded *E* configuration was favoured when nitrogen atoms were introduced into one or both of the aromatic rings, (Figure 1.18b, Y= pyridyl or pyrimidyl).[51] This observation cannot be attributed to the hydrophobic effect since the nitrogen heterocycles are less hydrophobic than the naphthyl group. Instead, these observations are consistent with the formation of electrostatically dominated edge-to-face aromatic contacts. Indeed, the stacked geometry is not enforced in these compounds, the terminal aromatic groups are free to rotate in solution, and the lowest energy conformation of the biaryl compounds employed are twisted propeller conformations. Furthermore, the *E/Z* ratios increased in-line with the positive polarisation of the aromatic edges induced by the addition of electronegative nitrogen atoms.

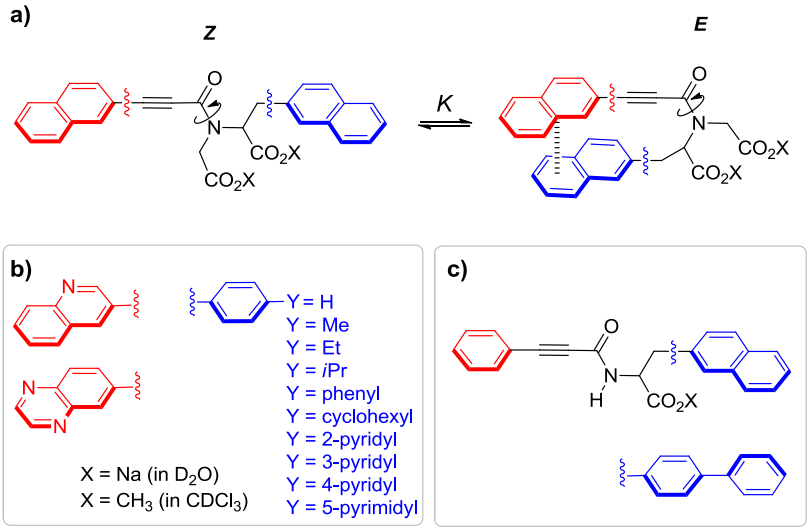

Figure 1.18. Folding molecules designed by Gellman *et al.* for quantifying aromatic stacking interactions in D_2O and $CDCl_3$.[10,50,51]

Unlike tertiary amides, secondary amides typically exist predominantly in the *Z* conformation due to repulsive steric interactions between the substituents on the amide carbon and nitrogen atoms. Despite this, the hydrophobic stacking of the aromatic groups in the secondary amides depicted in Figure 1.18c was substantial enough that significant populations of the *E* conformers could be observed in aqueous solution.[10]

Cozzi, Siegel and co-workers have investigated aromatic stacking interactions in a range of geometries by measuring the barrier to rotation ($\Delta G^{\ddagger}$) about biaryl bonds (Figure 1.19).[52-54] Parallel-offset stacking interactions were investigated by varying the X-substituent using the system shown in Figure 1.19a.[52] The barrier to rotation increased as the X-substituent became more electron-withdrawing, since this decreases repulsion between the rings and stabilises the stacked ground state. Linear relationships were observed between $\Delta G^{\ddagger}$ and the Hammett substituent constants, indicating that electrostatic effects dominate the system. The same trends were observed in the 1,8-diarylnaphthalene system (Figure 1.19b), where the aromatic groups are forced into a sterically strained stacked arrangement, but the changes in

the barrier to rotation were larger than those observed in the offset stacked system (Figure 1.19a). It was reasoned that the parallel-offset stacking interactions were less repulsive than parallel stacked interactions in these strained systems.[52] To further test the proposed electrostatic model, the successive addition of electronegative fluorine atoms to one of the rings in the strained stacked system (Figure 1.19b) was seen to increase the barrier to rotation.

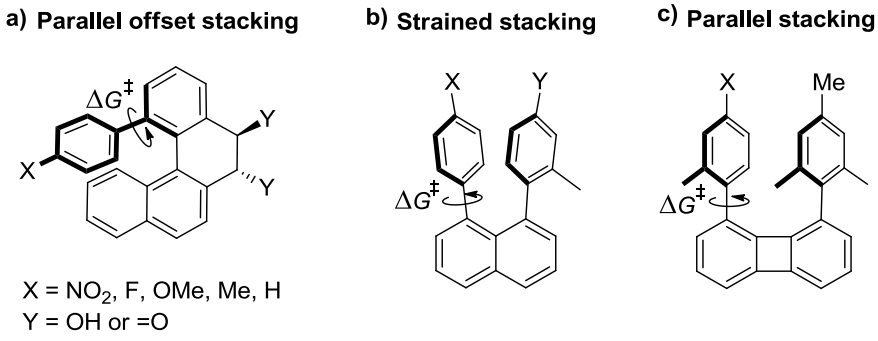

Figure 1.19. Model systems used by Cozzi *et al.* for studying aromatic stacking interactions in a variety of geometries.[52-54]

Cozzi *et al.* have recently expanded their research on aromatic interactions using a series of substituted 1,8-diarylbiphenylenes where the distance between the stacked aromatic groups was much closer to the equilibrium separation of stacking interactions observed in X-ray crystal structures (Figure 1.19c).[54] As seen in the earlier stacked systems, electron-donating X-substituents lowered the barrier to biaryl rotation, but these systems were much less sensitive to substituent effects. Surprisingly, the barrier to rotation was insensitive to variation of the X-substituents when one of the rings was fluorinated. This was postulated to arise from a combination of van der Waals dispersive interactions and secondary interactions between the fluorine atoms and the X-substituents.

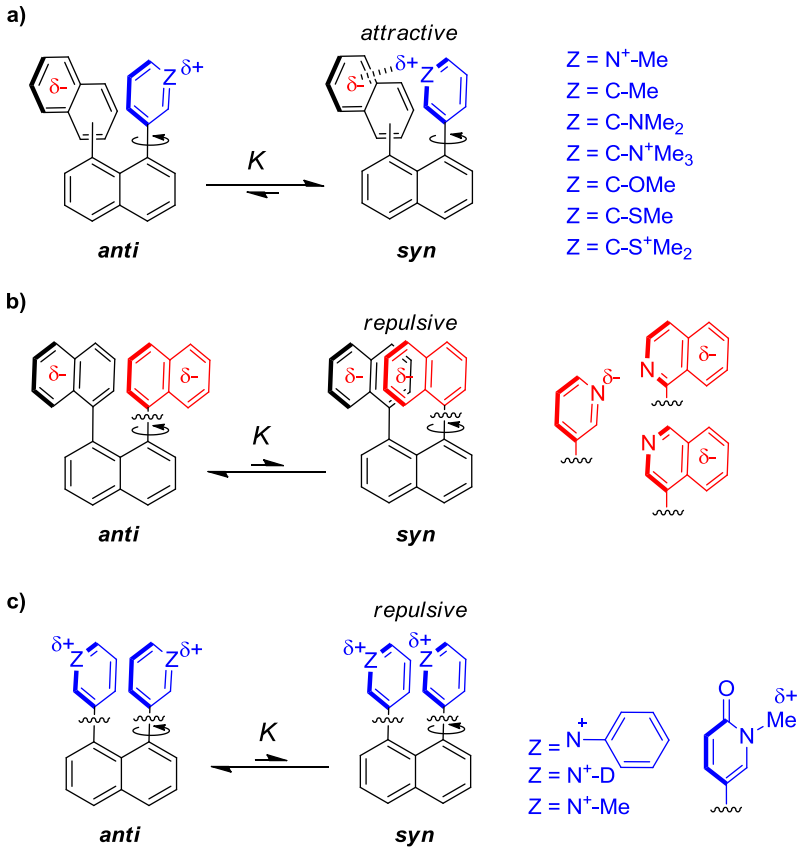

Figure 1.20. Model systems used by Zoltewicz *et al.* for studying aromatic stacking interactions. [55-60]

Zoltewicz and co-workers have also adopted strained 1,8-naphthalene derivatives to investigate a wide range of stacking interactions, but rather than measuring barriers to rotation, compounds that display *syn-anti* conformational isomerisation were studied (Figures 1.20a-c).[55-60] The *syn* conformation was dominant for all of the compounds depicted in Figure 1.20a. The large upfield shielding of the ^{1}H-NMR methyl signals and the preference for the *syn* conformation can be attributed to the existence of favourable cation···arene and CH···arene interactions between the positively polarised methyl substituents of one ring and electron-rich naphthalene face of the other. Although solvent molecules cannot enter the space between the aromatic rings, they can easily interact with the edges of the

aromatic rings and the substituents in the *anti* conformation. Polar solvents were found to stabilise the *anti* conformer most. Thus, changing the solvent from $CDCl_3$ to DMSO decreased the degree of stacking of the methylpyridinium moiety with naphthalene ring.[59] In contrast, when both aromatic rings were either electron-rich or electron-poor, electrostatic and steric repulsion dominated and the *anti* conformers were preferred (Figures 1.20b and 1.20c).

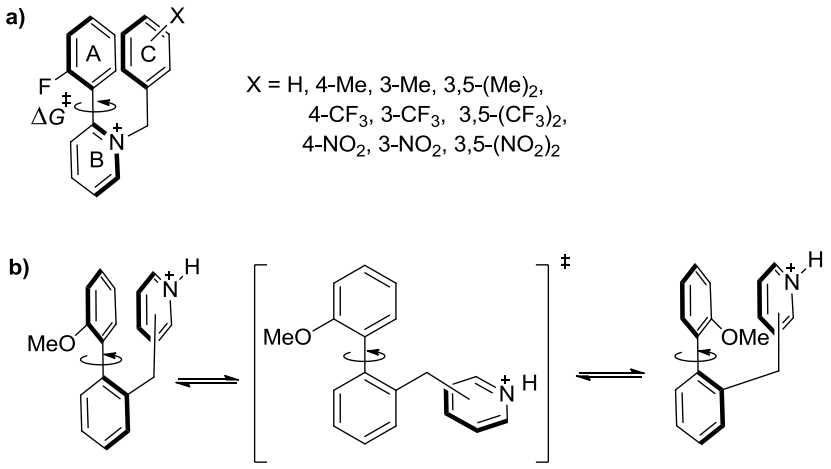

Figure 1.21. Torsion balances designed by Waters *et al.* to measure aromatic cation···arene interactions in aqueous solution.[61,62]

In 2002, Waters examined substituent effects in offset stacking interactions using a related class of rotameric compounds (Figure 1.21a).[61] Whilst earlier studies had predominantly been performed in organic solvents, the polar nature of these cationic compounds enabled measurements to be obtained in aqueous solution. In line with the earlier findings of Siegel and co-workers, electron-withdrawing groups increased the barrier of rotation, which was also larger for *meta vs. para*-substituents. Further work examined how the interaction between a positively charged nitrogen and the face of another aromatic ring varied as the point of contact was changed (Figure 1.21b).[62] The offset-stacked geometry that places the *ortho* hydrogen of the pyridinium ring close to the phenyl ring was favoured.

Computational models suggested that the two rings were splayed apart in the transition state and no stacking interaction was taking place. The compound with the nitrogen atom in the *ipso* position showed the largest $\Delta G^{\ddagger}$ followed by the *ortho*, *meta* and *para* analogues. Small changes to the barrier to rotation were observed upon alkylation of the nitrogen atom. This indicated that specific $^{+}$NH···π or $^{+}$NMe···π interactions were not dominant in the system, which was consistent with the fact that the positive charge of the pyridinium ion is delocalised over the entire aromatic surface.

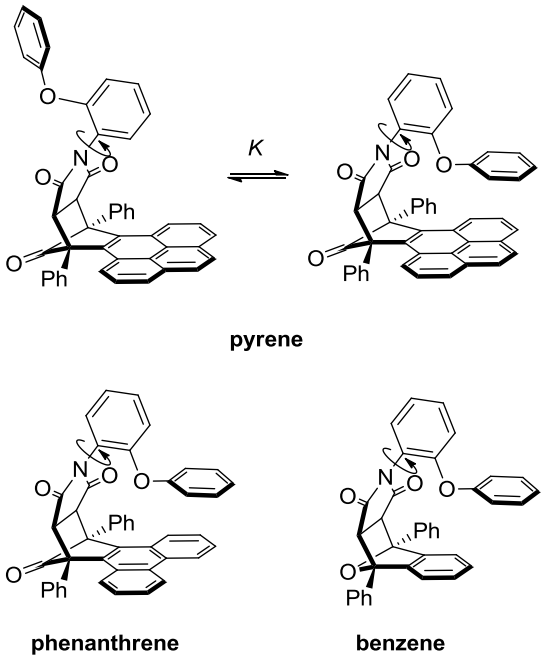

Figure 1.22. Molecular torsion balances designed by Shimizu *et al.* for quantifying aromatic stacking interactions.[63]

Shimizu and co-workers recently synthesised a series of molecular balances for quantifying aromatic stacking interactions (Figure 1.22).[63] In the folded conformation, only a face-to-face aromatic stacking interaction can occur because the distance between the two arenes is too small to accommodate an edge-to-face interaction. The compounds with the phenanthrene or pyrene 'shelves' were found to

have higher folded/unfolded ratios than the compound with the smaller phenyl shelf. The phenyl platform is too small to facilitate an aromatic stacking interaction with the phenyl ether arm, thus this compound was used as a control compound to measure secondary interactions. The free energy of the interaction was measured in different solvents, with more polar solvents shifting the equilibrium towards the folded conformation, consistent with solvophobically driven folding (Figure 1.1, top left).

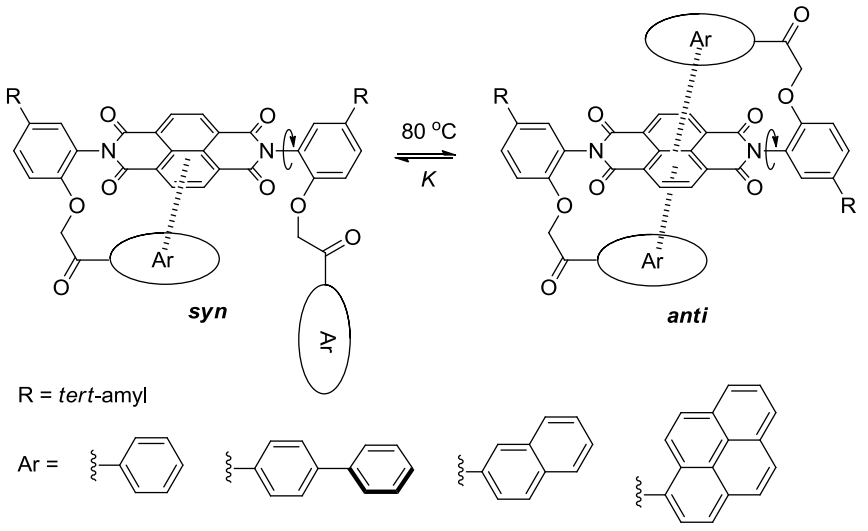

Figure 1.23. Molecular torsion balances synthesised by Shimizu and co-workers for quantifying aromatic stacking interactions between the central electron-poor naphthalene diimide surface and a range of aromatic groups.[64]

Most recently, Shimizu and co-workers synthesised a new torsion balance for quantifying interactions between extended aromatic face-to-face contacts (Figure 1.23).[64] The high barrier to *syn*/*anti* interconversion (113 kJ mol^{-1}) in these compounds meant that the *anti* atropoisomers could be isolated and the X-ray crystal structures determined. These solid-state snapshots showed that the aromatic groups were stacked on either face of the naphthalene diimide as depicted on the right-hand side of Figure 1.23. The folding free energies increased in an upwardly curving trend

as the area of contact between the interacting aromatic groups was increased. This could be attributed to an increase in dispersion interactions as the size of the aromatic contacts increase, or alternatively may be the result of an entropic co-operative effect.[65] The folding free energies did not change significantly upon changing the solvent from tetrachloroethane to dimethylsulfoxide.

Building on the seminal work of Ōki, Gung and co-workers have adopted triptycenes in the study of substituent effects on aromatic stacking interactions in both the face-to-face and offset-stacked geometries in organic solvents (Figures 1.24-1.26).[66-68]

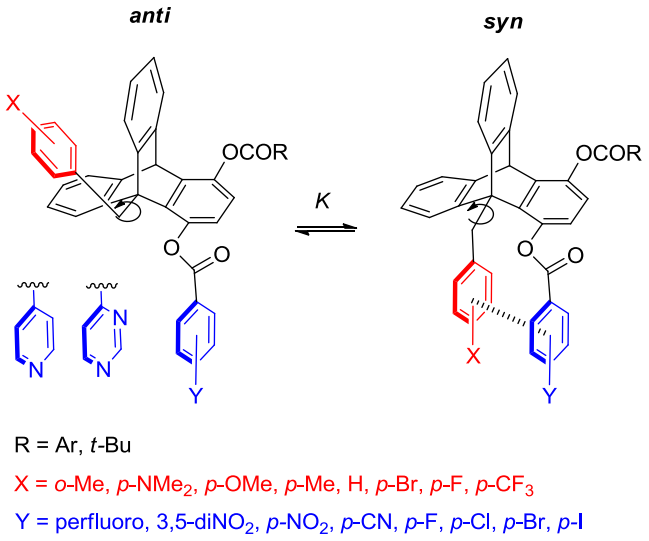

Figure 1.24. 1,9-disubstituted triptycenes used by Gung and co-workers for quantifying offset aromatic stacking interactions.[66-69]

A non-linear relationship between interaction energies and Hammett *para*-substituent constants was reported and attributed to charge-transfer interactions. Correlating these results against calculated ring-centre electrostatic potentials (Figure 1.25), or Hammett constants from another source[70] removes much of the curvature in the trends. However, curvature does remain for the pentafluorophenyl data series (dark blue points in Figure 1.25), which may be consistent with a role for charge-transfer

interactions between the most electron-deficient and electron-rich aromatic rings. Just as Cozzi, Siegel[53] and Hunter[71,72] have found in other stacked systems, the gradient of the stacking interaction trend in Figure 1.25 is inverted when an electron-rich aromatic group is replaced by an electron-poor pentafluorophenyl group.

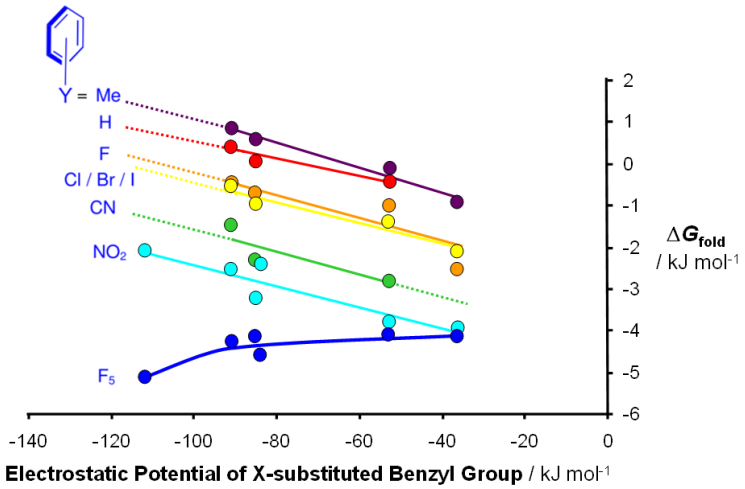

Figure 1.25. Experimental folding free energies (ΔG)[66,67] plotted against the DFT/B3LYP-6-31G*-calculated electrostatic surface potentials taken above the ring centroids of the X-substituted aromatic ring for the triptycene balances depicted in Figure 1.24. Values were measured in $CDCl_3$ at –40 ^{o}C, and the NO_2-, Cl-, I- and perfluoro-substituted phenyl ester groups were measured at –15 ^{o}C. Data for the Cl, Br and I-substituted phenyl ester series were very similar - as would be expected from calculated electrostatic potentials - despite being obtained at different temperatures (only the chlorophenyl ester series are plotted for purposes of clarity). The *syn*/*anti* ratios of some nitrophenyl ester compounds were measured at both –15 ^{o}C and –40 ^{o}C and the interaction trends are very similar.

Furthermore, the *syn*/*anti* ratios for the compounds were reduced in bromobenzene-d_5 compared to $CDCl_3$, in accordance with increased solvent competition. In the most recent work, the stacking interaction was found to be more favourable when a methyl group was installed in the *ortho*-position *vs.* the

para-position on the X-substituted ring.[68] The *syn* conformation became dominant when the Y-substituted ring was replaced by a pyridine or pyrimidine ring (Figure 1.24).[69] The most favourable interaction was observed when an electron-rich X-substituted benzene ring interacted with the electron-poor pyrimidine ring, mirroring the results obtained by Gellman (Figure 1.18b).

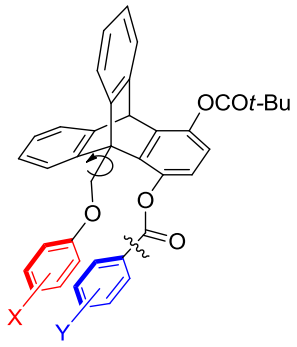

X = *p*-NMe_2, *p*-OMe, *p*-Me, H, *p*-NO_2, 3,5-diMe, 3,4,5-triMe

Y = *p*-OMe, H, *p*-NO_2, *p*-Me, *p*-F, 2,6-diF, 2,4,6-triF, 2,3,5,6-tetraF, pentaF

Figure 1.26. 1,9-disubstituted triptycenes used by Gung and co-workers for quantifying near-sandwich stacked aromatic interactions. Note the additional oxygen atom adjacent to the X-substituted ring compared to the compounds shown in Figure 1.24.[73]

Gung went on to investigate near-perfect face-to-face stacking interactions by inserting an oxygen atom into the linker attached to the X-substituted arene (Figure 1.26).[73] Again, interactions were found to be repulsive with electron-rich monosubstituted rings, but attractive when an electron-poor arene ring was involved. A linear correlation of the folding free energy with the number of fluorine atoms attached to the phenyl ester, indicated that the more electron-deficient the system, the more attractive the interaction. It should be noted that the stacking interaction is not enforced in Gung's system and the additional oxygen atom may provide enough conformational flexibility to accommodate an edge-to-face aromatic contact in solution.

Interactions with carbonyl groups

Another type of non-covalent interactions that can be found in the literature is the interaction of carbonyl groups with other moieties.

The hydrogen bonding interaction with carbonyl groups has been used by Wennemers, Ochsenfeld and co-workers in a biological context. The Xaa-Pro amide bonds (Xaa = any amino acid, Pro = proline) exist in the *cis* and *trans* conformers as shown in Figure 1.27a.[74] When there is an electron-withdrawing substituent, such as F or N_3, in the C4 position of the ring, the C4-*endo* and C4-*exo* conformations exist (Figure 1.27b). The C4-*exo* ring pucker favours the *trans* conformer, which is also proposed as being stabilised by an $n \rightarrow \pi^*$ interaction between the adjacent amide bonds, whereas the C4-*endo* ring pucker favours the *cis* conformation.

Wennemers, Ochsenfeld and co-workers synthesised proline derivatives that adopt the C4-*endo* conformation and favour the *trans* conformer (Figure 1.27c).[74] In the C4-*endo* conformation there is repulsion between the C4 substituent and the carbonyl oxygen in the *trans* conformer. However if a hydrogen bond donor is used in the C4 position which will interact with the oxygen of the methyl ester, then the C4-*endo* conformation could favour the *trans* conformer. When an ammonium, acetamide, *tert*-butyl carbamate and hydroxyl group was used in the C4 position, the *trans* conformer was most favoured in the *endo* pucker compared to the *exo* form in $CDCl_3$ solution. In contrast, the C4-*exo* pucker favoured the *trans* conformer when an azido substituent was used. The results were not the same when D_2O was used as solvent, because the interacting groups are preferentially solvated by the D_2O. The researchers were also able to stabilise the *trans* conformation in oligoprolines by using this hydrogen bonding strategy.

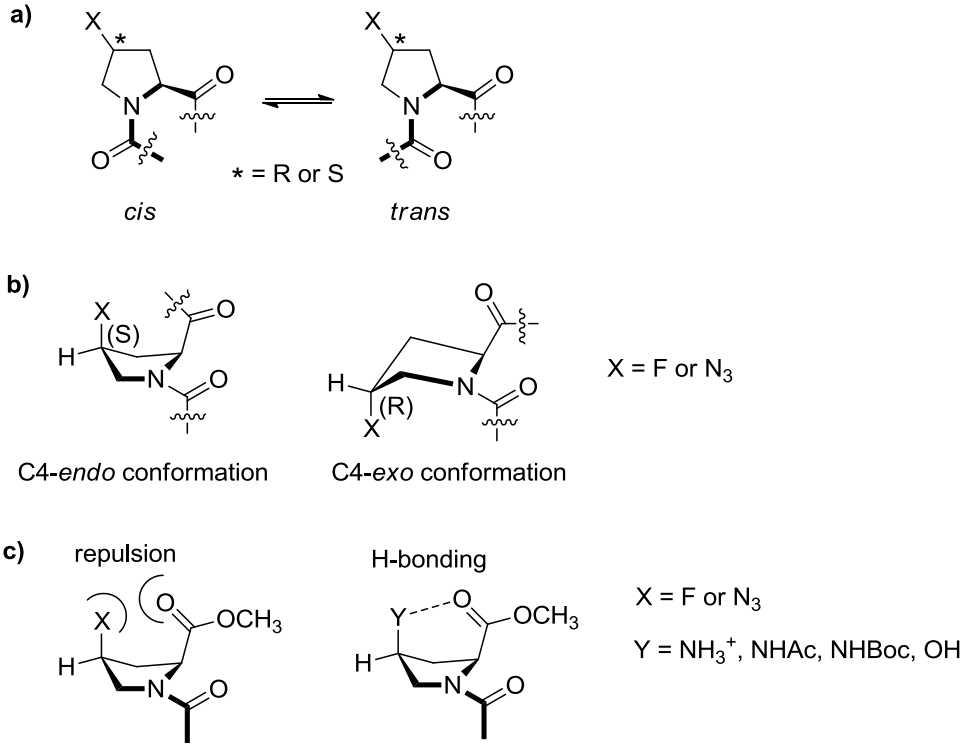

Figure 1.27. a) *cis*/*trans* amide conformers in Xaa-Pro bond, b) C4-*endo* and *exo* conformations, c) C4-*endo* conformations destabilised when there is an electron-withdrawing substituent and stabilised when there is a hydrogen bond donor group.[74]

Diederich *et al.* have utilised the desirable geometry of the Wilcox torsion balance described earlier in combination with thermodynamic double-mutant cycles[8] to quantify C-F···carbonyl, and carbonyl···carbonyl interactions between orthogonally orientated aromatic substituents (Figure 1.28).[42,75,76] In Figure 1.28a a weak C-F···amide interaction was measured in $CDCl_3$ and C_6H_6 (–1.05 kJ/mol and –0.85 kJ/mol respectively).[42] Two new double-mutant cycles with greater validity were designed and the C-F···amide interaction was studied in a variety of solvents (Figure 1.28b and c).[75] In apolar solvents (C_6H_6 and $C_2D_2Cl_4$) the interaction energy is in the range of –0.8 to –1.2 kJ/mol. In smaller dipolar chlorinated solvents ($CDCl_3$ and CD_2Cl_2) there is a weaker interaction (value range of –0.2 to –0.6 kJ/mol) due to

solvent competition for the solvation of the indole. The orthogonal dipolar interaction between two amide carbonyl groups was measured with the molecular balance shown in Figure 1.28d.[76] The energy of this interaction is –2.7 kJ/mol in C_6H_6, whereas in the chlorinated solvents ($CDCl_3$, $C_2D_2Cl_4$ and CD_2Cl_2) is in the range of –1.2 to –1.7 kJ/mol as the solvent molecule preferentially solvates the amide groups and the folded conformation is destabilised.

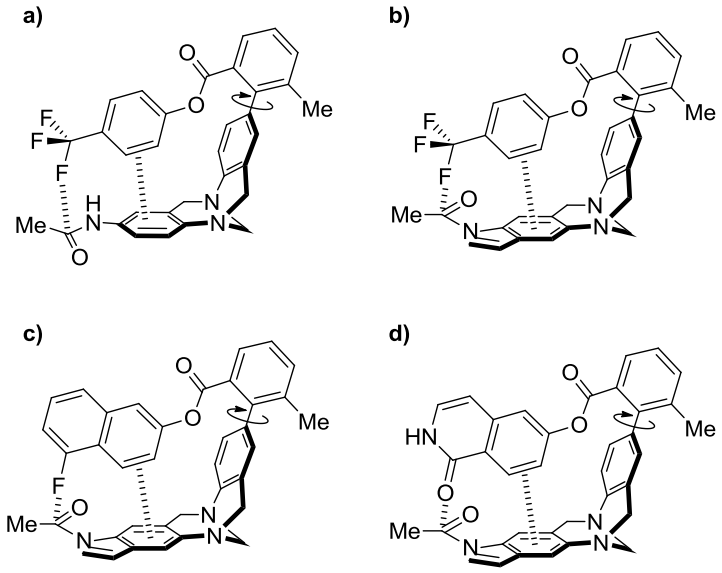

Figure 1.28. a)-c) Wilcox torsion balances synthesised by Diederich and co-workers for examining F···amide[42,75] and d) carbonyl···amide interactions.[76]

Hamilton and co-workers designed a series of diphenylacetylene molecular switches that exist in two H-bonded conformations in equilibrium.[77-79] The design consists of two amides which can act as hydrogen bond donors to the benzoate hydrogen-bond acceptor. The equilibrium can be biased towards one conformation by making the one amide a better H-bond donor compared to the other. As shown in Figure 1.29, by inserting an electron donating or withdrawing X-group to the system, the hydrogen-bond donor constant of the amide NH was changed, which influenced the strength of the intramolecular hydrogen bond. If an electron-withdrawing NO_2 group is

placed *para* to the amide, then the amide NH will become a better hydrogen-bond donor than the unsubstituted compound. Thus, the conformation in which the benzoate group is bonded to the specific amide will be favoured.[77] On the contrary, when an electron-donating NMe_2 group is present, the corresponding amide NH will become a weaker H-bond donor. The position of the molecular switch is also pH-dependent, because with the addition of trifluoroacetic acid, the NMe_2 can be protonated, reversing the electronic properties of the substituent, and switching the position of the equilibrium.[78]

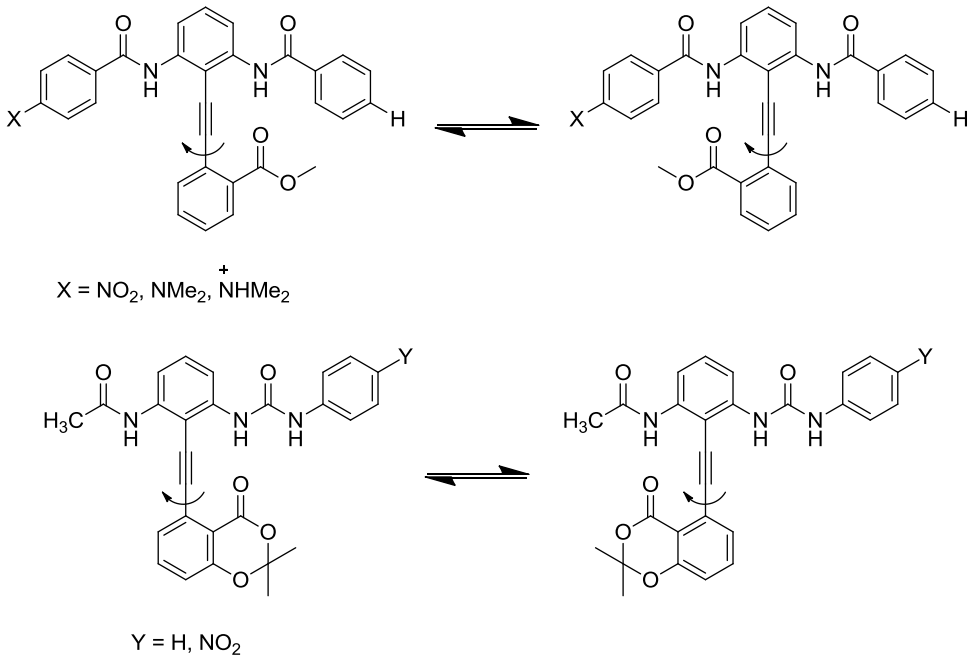

Figure 1.29. Molecular switches designed by Hamilton *et al.*[77-79]

An anion-dependent molecular switch was also synthesised, by using a urea group in place of one of the amide groups (Figure 1.29).[79] The urea is a better hydrogen-bond donor than the amide, shifting the equilibrium towards the urea H-bonded conformation. A conformational switch can occur if NBu_4Cl is added, as the urea will preferentially bind to the chlorine anions, forcing the H-bond acceptor to bind to the amide NH instead.

1.4. Conclusions

The study of non-covalent interactions leads to a greater understanding of the principles governing the behaviour of chemical and biological systems. Molecular balances and folding molecules offer several advantages that make them excellent tools for expanding our understanding of non-covalent interactions:

- Simple model compounds overcome the difficulties of studying complicated biological systems.
- Synthetic modifications allow systematic variation of functional groups and interaction geometries to test current theories of molecular interactions.
- Very weak, repulsive, or entropically disfavoured interactions can be measured using conformationally well-designed compounds.

Several classes of molecular balances have been developed for the quantitative study of non-covalent interactions to date. Aromatic interactions have been particularly well-studied, and the scope of the approach continues to expand. The subtle interplay of numerous factors contributing to non-covalent interactions probably limits the transferability of absolute interaction energies measured using molecular balances. Despite this caveat, molecular balances are able to provide insights into the physicochemical origins of molecular recognition; they have already contributed to the development of empirical solvation models, and future investigations have the potential to reveal previously overlooked or unidentified phenomena.

1.5. Acknowledgements

The major part of Chapter 1 has been already published as a review:
Ioulia K. Mati and Scott L. Cockroft, *Chem. Soc. Rev.*, **2010**, 39, 4195–4205
Reproduced by permission of the Royal Society of Chemistry. The Figure 1.25 was drawn by Scott L. Cockroft and published as part of this review.

1.6. References

1. Amabilino, D. B.; Stoddart, J. F., *Chem. Rev.* **1995,** 95, 2725-829.
2. Clayden, J., *Chem. Soc. Rev.* **2009,** 38, 817-829.
3. Lehn, J. M., *Science* **2002,** 295, 2400-3.
4. Deechongkit, S.; Nguyen, H.; Powers, E. T.; Dawson, P. E.; Gruebele, M.; Kelly, J. W., *Nature* **2004,** 430, 101-5.
5. Krueger, A. T.; Kool, E. T., *Curr. Opin. Chem. Biol.* **2007,** 11, 588-594.
6. Kool, E. T.; Waters, M. L., *Nat. Chem. Biol.* **2007,** 3, 70-73.
7. Schneider, H. J., *Angew Chem Int Ed Engl* **2009,** 48, 3924-77.
8. Cockroft, S. L.; Hunter, C. A., *Chem. Soc. Rev.* **2007,** 36, 172-188.
9. Sandström, J., *Dynamic NMR Spectroscopy*. Academic Press: London, UK, 1982.
10. Gardner, R. R.; McKay, S. L.; Gellman, S. H., *Org. Lett.* **2000,** 2, 2335-2338.
11. Nakamura, K.; Houk, K. N., *Org. Lett.* **1999,** 1, 2049-2051.
12. Cockroft, S. L.; Hunter, C. A., *Chem. Commun.* **2006**, 3806-3808.
13. Cockroft, S. L.; Hunter, C. A., *Chem. Commun.* **2009**, 3961 - 3963.
14. Newcomb, L. F.; Gellman, S. H., *J. Am. Chem. Soc.* **1994,** 116, 4993-4.
15. Sankararaman, S.; Venkataramana, G.; Varghese, B., *J. Org. Chem.* **2008,** 73, 2404-7.
16. Nakamura, M.; Ōki, M.; Nakanishi, H.; Yamamoto, O., *Bull. Chem. Soc. Jpn.* **1974,** 47, 2415-19.
17. Ōki, M., *Angew. Chem. Int. Ed. Engl.* **1976,** 15, 87-93.
18. Ōki, M., *Acc. Chem. Res.* **1990,** 23, 351-6.
19. Hunter, C. A., *Angew. Chem., Int. Ed.* **2004,** 43, 5310-5324.
20. Ōki, M.; Izumi, G.; Yamamoto, G.; Nakamura, N., *Chem. Lett.* **1980**, 213-16.
21. Izumi, G.; Yamamoto, G.; Ōki, M., *Chem. Lett.* **1980**, 969-72.
22. Ōki, M.; Izumi, G.; Yamamoto, G.; Nakamura, N., *Bull. Chem. Soc. Jpn.* **1982,** 55, 159-66.
23. Tamura, Y.; Yamamoto, G.; Ōki, M., *Bull. Chem. Soc. Jpn.* **1987,** 60, 1781-8.
24. Tamura, Y.; Yamamoto, G.; Ōki, M., *Chem. Lett.* **1986**, 1619-22.
25. Gung, B. W.; Xue, X.; Reich, H. J., *J. Org. Chem.* **2005,** 70, 7232-7237.
26. Gung, B. W.; Zou, Y.; Xu, Z.; Amicangelo, J. C.; Irwin, D. G.; Ma, S.; Zhou, H. C., *J. Org. Chem.* **2008,** 73, 689-693.
27. Gung, B. W.; Emenike, B. U.; Lewis, M.; Kirschbaum, K., *Chem. Eur. J.* **2010,** 16, 12357-12362.
28. Motherwell, W. B.; Moïse, J.; Aliev, A. E.; Nič, M.; Coles, S. J.; Horton, P. N.; Hursthouse, M. B.; Chessari, G.; Hunter, C. A.; Vinter, J. G., *Angew. Chem., Int. Ed.* **2007,** 46, 7823-7826.
29. Aliev, A. E.; Moïse, J.; Motherwell, W. B.; Nič, M.; Courtier-Murias, D.; Tocher, D. A., *Phys. Chem. Chem. Phys.* **2009,** 11, 97-100.
30. Cornago, P.; Claramunt, R. M.; Bouissane, L.; Elguero, J., *Tetrahedron* **2008,** 64, 3667-3673.
31. Hughes, R. M.; Benshoff, M. L.; Waters, M. L., *Chem. Eur. J.* **2007,** 13, 5753-5764.

32. Kiehna, S. E.; Laughrey, Z. R.; Waters, M. L., *Chem. Commun.* **2007**, 4026-4028.
33. Laughrey, Z. R.; Kiehna, S. E.; Riemen, A. J.; Waters, M. L., *J. Am. Chem. Soc.* **2008,** 130, 14625-14633.
34. Tatko, C. D.; Waters, M. L., *J Am Chem Soc* **2002,** 124, 9372-3.
35. Carroll William, R.; Zhao, C.; Smith Mark, D.; Pellechia Perry, J.; Shimizu Ken, D., *Org. Lett.* **2011,** 13, 4320-3.
36. Nijamudheen, A.; Jose, D.; Shine, A.; Datta, A., *J. Phys. Chem. Lett.* **2012**, 3, 1493-96.
37. Zhao, C.; Parrish, R. M.; Smith, M. D.; Pellechia, P. J.; Sherrill, C. D.; Shimizu, K. D., *J. Am. Chem. Soc.*, **2012**, 134, 14306-309.
38. Paliwal, S.; Geib, S.; Wilcox, C. S., *J. Am. Chem. Soc.* **1994,** 116, 4497-8.
39. Bhayana, B.; Wilcox, C. S., *Angew. Chem., Int. Ed.* **2007,** 46, 6833-6836.
40. Kim, E.-i.; Paliwal, S.; Wilcox, C. S., *J. Am. Chem. Soc.* **1998,** 120, 11192-11193.
41. Ren, T.; Jin, Y.; Kim, K. S.; Kim, D. H., *J. Biomol. Struct. Dyn.* **1997,** 15, 401-405.
42. Hof, F.; Scofield, D. M.; Schweizer, W. B.; Diederich, F., *Angew. Chem., Int. Ed.* **2004,** 43, 5056-5059.
43. Fischer, F. R.; Schweizer, W. B.; Diederich, F., *Chem. Commun.* **2008**, 4031-4033.
44. Bhayana, B.; Ams, M. R., *J. Org. Chem.* **2011,** 76, 3594-3596.
45. Burley, S. K.; Petsko, G. A., *Science* **1985,** 229, 23-8.
46. Annunziata, R.; Benaglia, M.; Cozzi, F.; Mazzanti, A., *Chem. Eur. J* **2009,** 15, 4373-81.
47. Benaglia, M.; Cozzi, F.; Mancinelli, M.; Mazzanti, A., *Chem. Eur. J.* **2010,** 16, 7456-7468.
48. Xia, J. L.; Liu, S. H.; Cozzi, F.; Mancinelli, M.; Mazzanti, A., *Chem. Eur. J.* **2012,** 18, 3611-3620.
49. Karim, A. R.; Linden, A.; Baldridge, K. K.; Siegel, J. S., *Chem. Sci.* **2010,** 1, 102-110.
50. Gardner, R. R.; Christianson, L. A.; Gellman, S. H., *J. Am. Chem. Soc.* **1997,** 119, 5041-5042.
51. McKay, S. L.; Haptonstall, B.; Gellman, S. H., *J. Am. Chem. Soc.* **2001,** 123, 1244-1245.
52. Cozzi, F.; Annunziata, R.; Benaglia, M.; Cinquini, M.; Raimondi, L.; Baldridge, K. K.; Siegel, J. S., *Org. Biomol. Chem.* **2003,** 1, 157-162.
53. Cozzi, F.; Siegel, J. S., *Pure Appl. Chem.* **1995,** 67, 683-9.
54. Cozzi, F.; Annunziata, R.; Benaglia, M.; Baldridge, K. K.; Aguirre, G.; Estrada, J.; Sritana-Anant, Y.; Siegel, J. S., *Phys. Chem. Chem. Phys.* **2008,** 10, 2686-2694.
55. Zoltewicz, J. A.; Maier, N. M.; Fabian, W. M. F., *J. Org. Chem.* **1996,** 61, 7018-7021.
56. Zoltewicz, J. A.; Maier, N. M.; Fabian, W. M. F., *J. Org. Chem.* **1997,** 62, 2763-2766.
57. Zoltewicz, J. A.; Maier, N. M.; Fabian, W. M. F., *J. Org. Chem.* **1997,** 62, 3215-3219.
58. Zoltewicz, J. A.; Maier, N. M.; Lavieri, S.; Ghiviriga, I.; Abboud, K. A.; Fabian, W. M. F., *Tetrahedron* **1997,** 53, 5379-5388.

59. Zoltewicz, J. A.; Maier, N. M.; Fabian, W. M. F., *J. Org. Chem.* **1998,** 63, 4985-4990.
60. Lavieri, S.; Zoltewicz, J. A., *J. Org. Chem.* **2001,** 66, 7227-7230.
61. Rashkin, M. J.; Waters, M. L., *J. Am. Chem. Soc.* **2002,** 124, 1860-1861.
62. Rashkin, M. J.; Hughes, R. M.; Calloway, N. T.; Waters, M. L., *J. Am. Chem. Soc.* **2004,** 126, 13320-13325.
63. Carroll, W. R.; Pellechia, P.; Shimizu, K. D., *Org. Lett.* **2008,** 10, 3547-3550.
64. Chong, Y. S.; Carroll, W. R.; Burns, W. G.; Smith, M. D.; Shimizu, K. D., *Chem. Eur. J.* **2009,** 15, 9117-9126.
65. Hunter, C. A.; Anderson, H. L., *Angew. Chem., Int. Ed.* **2009,** 48, 7488-7499.
66. Gung, B. W.; Xue, X.; Reich, H. J., *J. Org. Chem.* **2005,** 70, 3641-3644.
67. Gung, B. W.; Patel, M.; Xue, X., *J. Org. Chem.* **2005,** 70, 10532-10537.
68. Gung, B. W.; Emenike, B. U.; Alverez, C. N.; Rakovan, J.; Kirschbaum, K.; Jain, N., *Tetrahedron Lett.* **2010,** 51, 1648-1650.
69. Gung, B. W.; Wekesa, F.; Barnes, C. L., *J. Org. Chem.* **2008,** 73, 1803-1808.
70. Hansch, C.; Leo, A.; Taft, R. W., *Chem. Rev.* **1991,** 91, 165-95.
71. Cockroft, S. L.; Perkins, J.; Zonta, C.; Adams, H.; Spey, S. E.; Low, C. M.; Vinter, J. G.; Lawson, K. R.; Urch, C. J.; Hunter, C. A., *Org Biomol Chem* **2007,** 5, 1062-80.
72. Cockroft, S. L.; Hunter, C. A.; Lawson, K. R.; Perkins, J.; Urch, C. J., *J Am Chem Soc* **2005,** 127, 8594-5.
73. Gung, B. W.; Xue, X.; Zou, Y., *J. Org. Chem.* **2007,** 72, 2469-2475.
74. Kuemin, M.; Nagel, Y. A.; Schweizer, S.; Monnard, F. W.; Ochsenfeld, C.; Wennemers, H., *Angew. Chem., Int. Ed.* **2010,** 49, 6324-6327.
75. Fischer, F. R.; Schweizer, W. B.; Diederich, F., *Angew. Chem. Int. Ed.* **2007,** 46, 8270-8273.
76. Fischer, F. R.; Wood, P. A.; Allen, F. H.; Diederich, F., *Proc. Natl. Acad. Sci. U. S. A.* **2008,** 105, 17290-17294.
77. Jones, I. M.; Hamilton, A. D., *Org. Lett.* **2010,** 12, 3651-3653.
78. Jones, I. M.; Lingard, H.; Hamilton, A. D., *Angew. Chem., Int. Ed.* **2011,** 50, 12569-12571.
79. Jones, I. M.; Hamilton, A. D., *Angew. Chem., Int. Ed.* **2011,** 50, 4597-4600.

Chapter 2

Dissecting electronic and solvent effects on conformational equilibria

Abstract

Non-covalent interactions have a fundamental role in chemistry and biology. The structure of proteins[1,2] and nucleic acids[3,4], drug-receptor binding[5,6] and the stereochemical outcome of reactions[7,8] are just a few examples where these interactions are encountered. Non-covalent interactions include the classical hydrogen bond, as well as electrostatic and van der Waals interactions. Complicated arrays of interactions, combined with steric and solvophobic effects often complicate the study of molecular interactions. In this work we have used a simple molecular balance to show that it is possible to dissect the electronic and solvent effects that determine the position of conformational equilibria. Such structurally simple model systems can be useful for testing theoretical models of solvation and for revealing the underlying principles that determine molecular behaviour and recognition phenomena.[9]

2.1. Solvent effects on non-covalent interactions

When a non-covalent interaction takes place in a vacuum or an idealistic gas-phase environment, then only the properties of the two interacting molecules need to be considered. Most computational models of non-covalent interactions are performed in such an environment, where the solvent is not considered.[10] The Lennard-Jones potential describes the effect of separation on the interaction between two neutral atoms in a vacuum (Figure 2.1).[11,12] When two separated atoms approach one another there is a weak favourable interaction between them due to attractive van der Waals forces. At the minimum point on the energy curve, the system is at the equilibrium separation and the

attractive forces are exactly cancelled by repulsive steric interactions. Beyond this point the repulsive force dominates due to overlapping orbitals. The Lennard-Jones potential is valid in the gas phase, where the solvent is not included in the system. In the liquid phase, solvation effects play an important role in the energy of the interaction of interest.

Computational solvation models with various applications have been developed.[13-16] Computational solvation models have been used to study a variety of events such as protein folding[17], protein-ligand binding[18] and solvent effects on the pK_a of benzoic acids.[19]

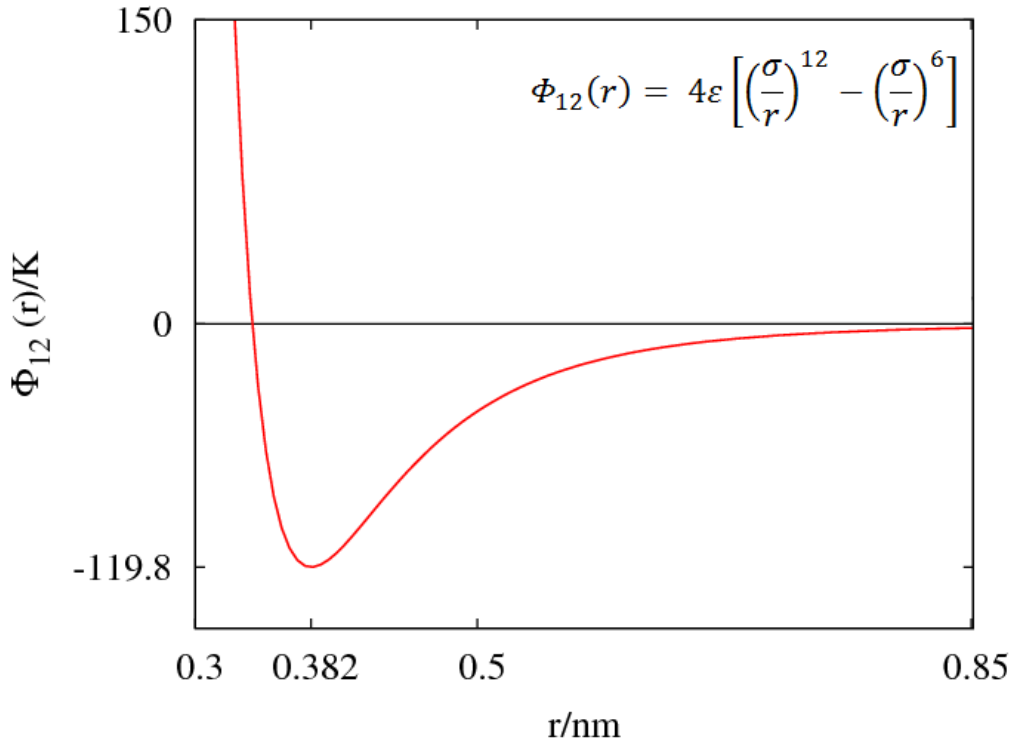

Figure 2.1. An example of Lennard-Jones potential for argon.[20,21] The x-axis in the graph is r : the distance between the particles and the y-axis is Φ_{12}(r) : the intermolecular pair potential between two particles. (reprinted with adaptation from: http://www.sklogwiki.org/SklogWiki/index.php/Lennard-Jones_model)

A simple model for the prediction of the free energy of a hydrogen-bond between two interacting species was introduced by Hunter in 2004 (Figure 2.2).[22] Each molecule

is solvated in the free state and therefore the properties of the solvent affect the overall energy of the system. Hunter's α/β model can be used to estimate the energy of a hydrogen-bond between a donor and acceptor in solution. In this method, α is the H-bond donor constant of one molecule and β is the H-bond acceptor constant of the other molecule. The hydrogen-bond parameters α and β, can either be measured experimentally or calculated from the maxima and minima of the molecular electrostatic potential surfaces. The contribution of the solvent in the system can be determined by using the corresponding α_s and β_s hydrogen-bond parameters of the solvent. Thus, the free energy of the apparent interaction between A and HD can be calculated by using the equation shown in Figure 2.2. The α/β model has been used to study a variety of non-covalent interactions like hydrogen bonds, halogen bonds and edge-to-face interactions.[23-27]

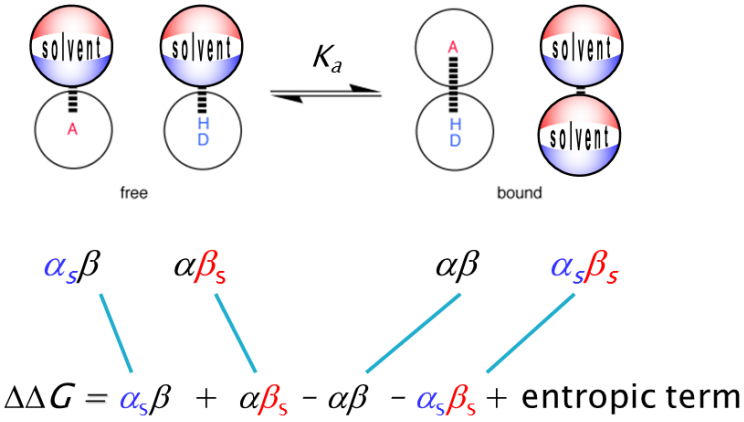

Figure 2.2. Hunter's model for estimating the free energy of a hydrogen-bond in solution.[22] (part of the figure is adapted with permission from: Hunter, C. A., *Angew. Chem., Int. Ed.* **2004**, 43, 5310-5324)

2.2. Aims

Experimentally, the quantification of non-covalent interactions and the study of the effects of solvation could be performed by designing structurally simple synthetic model systems. A great variety of molecular torsion balances has been designed in the literature

to study different types of non-covalent interactions,[28-31] as shown in Chapter 1, but only in few cases a solvation study was undertaken.[32-37] The aim in this chapter is to design a small and synthetically simple molecular torsion balance and investigate the forces that affect the position of the conformational equilibria. A full solvation study in a range of solvents was performed and a model that dissects the electrostatic and solvation effects on the system was introduced.

2.3. Methodology for investigating substituent and solvent effects on conformational equilibria

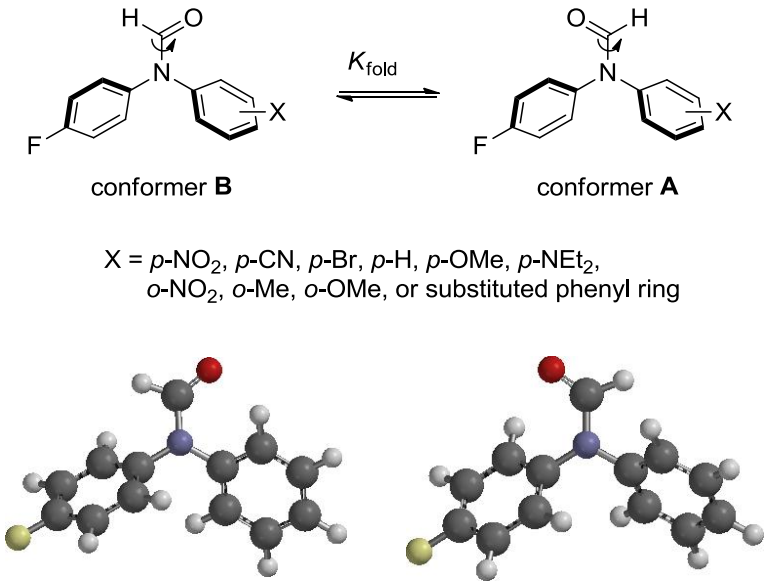

Figure 2.3. General design and DFT/B3LYP/6-31G* calculated structures of the molecular torsion balance when X = H.

The general design of the molecular torsion balances to be synthesised in this study is shown in Figure 2.3 alongside DFT/B3LYP/6-31G* calculated structures. Throughout this study conformer A is defined as the isomer where the oxygen atom of

the formyl group lies above the fluorinated aromatic ring, while the isomer where the proton of the formyl group lies above the fluorinated ring is denoted as conformer B. The design is similar to that of Kagechika and co-workers who studied conformational switching in a similar series of molecules featuring acetyl groups rather than the formyl groups used here.[38,39]

The tertiary amide in these molecules rotates slowly on the NMR timescale due to the double-bond character of the carbon-nitrogen bond. Thus, the balance exists in equilibrium between two slowly exchanging conformations and distinct peaks corresponding to each conformer are apparent in the NMR spectrum. The fluorine atom *para* to the formamide nitrogen in this design allows ^{19}F-NMR spectroscopy to be used for determining the A/B conformer ratio in variety of cheap and readily accessible, non-deuterated solvents. These ^{19}F-NMR spectra are very simple, having only two sets of peaks corresponding to the two conformers, compared to the more complicated proton spectrum as shown in Figure 2.4.

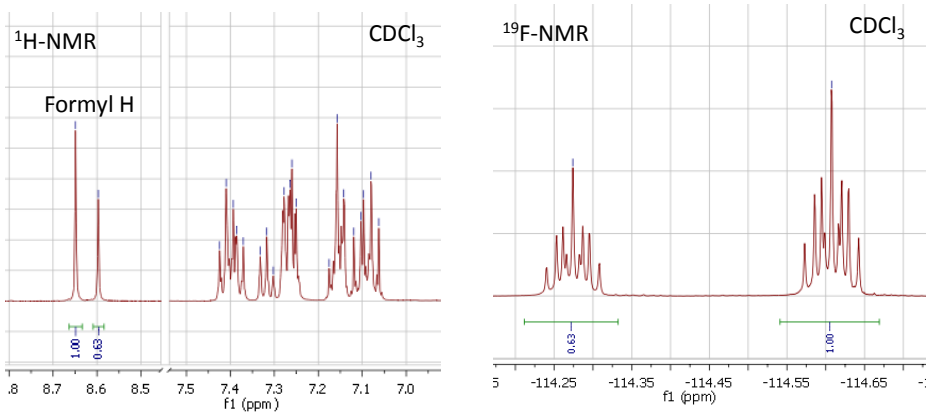

Figure 2.4. Calculation of K_{fold} and ΔG_{fold} for the molecular balance shown in Figure 2.3, where X = H in $CDCl_3$.

Either the ^{19}F-NMR peaks or the ^{1}H-NMR signal corresponding to the formyl protons of the two conformers can be integrated to determine the folding equilibrium constant, K_{fold} using:

$$K_{fold} = \frac{\text{conformer A}}{\text{conformer B}}$$

Finally, the free energy difference between the two conformations can be calculated using the equation:

$$\Delta G_{\text{fold}} = -RTlnK_{\text{fold}} \text{ (in kJ/mol)}$$

where R = 8.314 x 10^{-3} kJ/mol K and T = 298 K

Experimentally determined free energies in this system are associated with an error ± 0.2 kJ/mol (details of how this value was determined are provided in the Experimental Chapter 6).

This method therefore allows the factors governing the position of the conformational free energy (ΔG_{fold}) to be quantified by systematically varying the solvent and the substituents on the aromatic rings. A range of balances with a variety of electron-donating (EDG) and electron-withdrawing groups (EWG) in both the *para* and *ortho* positions was synthesised.

2.4. Synthesis of *para*-substituted molecular torsion balances

The synthetic procedure to obtain the *para*-substituted balances was based on the *N*-amidation of an aryl iodide mediated by a CuI catalyst, a 1,2-diamine ligand as a pre-catalyst, and a base.[40,41] In the case of the phenyl torsion balance (**3**) the procedure described in the literature was modified to improve the yield. Thus, the amounts used for the catalyst and the ligand were increased from 5 mol% CuI and 10 mol% ethylenediamine to 20 mol% and 40 mol% respectively.[40] The cross-coupling reaction of 1-fluoro-4-iodobenzene (**1**) and formanilide (**2**) occurred in 54% yield using CuI, ethylenediamine and K_3PO_4 (Figure 2.5).

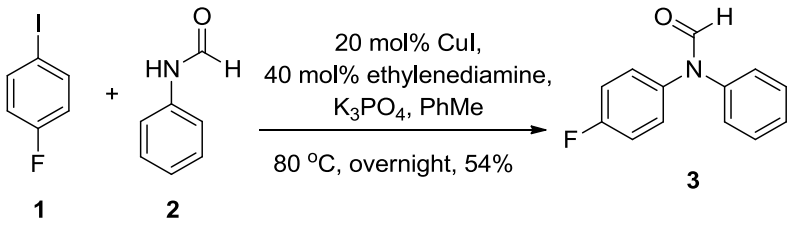

Figure 2.5. Synthesis of *N*-(4-fluorophenyl)-*N*-phenylformamide (**3**).

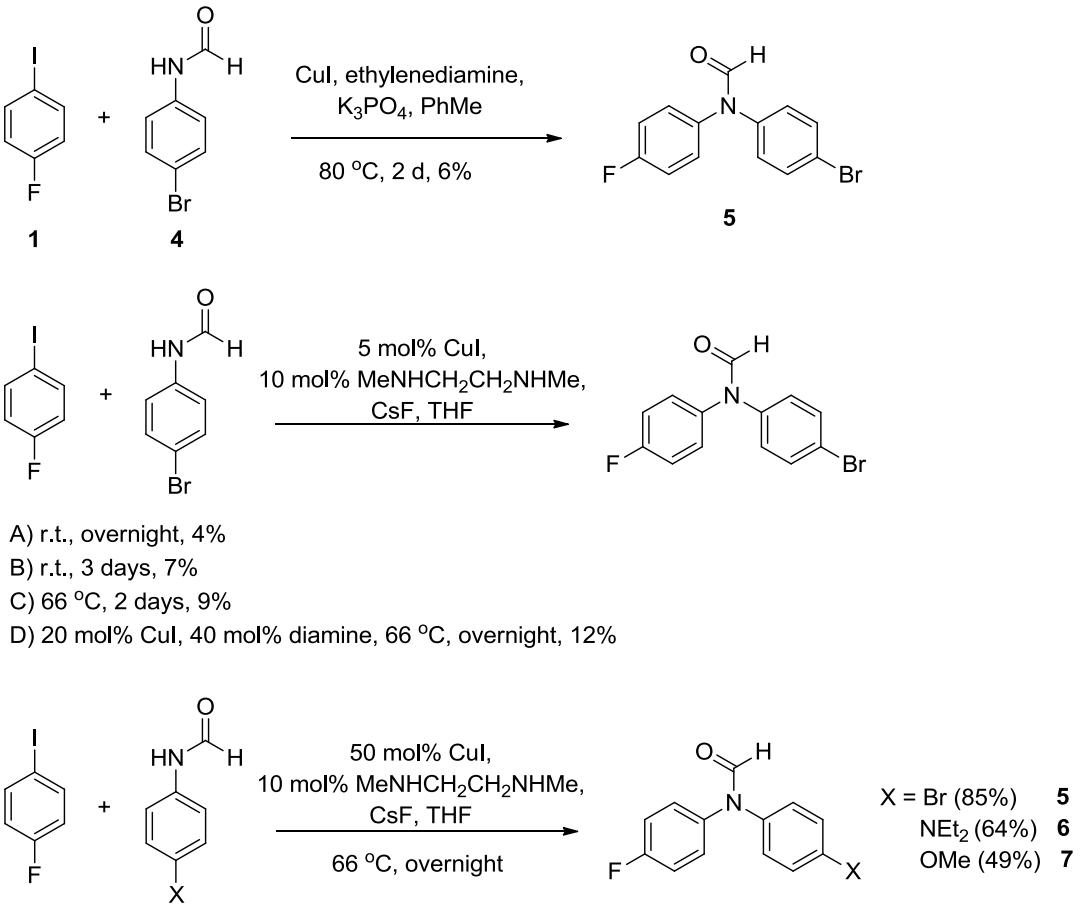

Figure 2.6. Reaction trials and synthesis of *N*-(4-bromophenyl)-*N*-(4-fluorophenyl)formamide (**5**), *N*-(4-(diethylamino)phenyl)-*N*-(4-fluorophenyl)formamide (**6**) and *N*-(4-fluorophenyl)-*N*-(4-methoxyphenyl)formamide (**7**).

The *p*-bromo phenyl balance (**5**) proved more difficult to synthesise. Despite using the same procedure and increasing the catalyst loading, the yield remained low (6%).[40]

A new reaction was carried out between 1-fluoro-4-iodobenzene (**1**) and *N*-(4-bromophenyl)formamide (**4**) by using CuI and changing the ligand to *N*,*N*-dimethylethylenediamine and the base to caesium fluoride.[41] The literature procedure described a mild reaction at room temperature with the use of 5 mol% catalyst and 10 mol% ligand.[41] However, after screening various reaction parameters it was found that heating at 66 ^{o}C and increasing the amount of CuI to 50 mol% gave much better results. This procedure provided *N*-(4-bromophenyl)-*N*-(4-fluorophenyl)formamide (**5**) in 85% yield and the *p*-NEt_2 phenyl torsion balance (**6**) in 64% yield (Figure 2.6).

The syntheses, characterisation and solvent screening of the *p*-OMe (**7**), *p*-CN (**10**) and *p*-NO_2 (**11**) balances were performed by Catherine Adam, another PhD student in the Cockroft group. However, differences in the synthetic procedure are noted here, and an analysis of the solvent effects on their conformational equilibria will be discussed later in this chapter. For syntheses involving an electron-donating X-substituent, the synthesis involves the use of 1-fluoro-4-iodobenzene (**1**) and the appropriately *para*-substitued *N*-phenylformamide. This procedure was not successful in the cases where X = CN and NO_2, presumably due to the poor nucleophilicity of the amide as a result of the electron-withdrawing effects of the X-substituents. To overcome this barrier, the *N*-(4-fluorophenyl)formamide (**9**) was therefore synthesised by the formylation of 4-fluoroaniline (**8**) using formic acid.[42] The resulting *N*-(4-fluorophenyl)formamide (**9**) was then coupled with 4-iodobenzonitrile and 1-iodo-4-nitrobenzene to give the desired molecular torsion balances (Figure 2.7).[41]

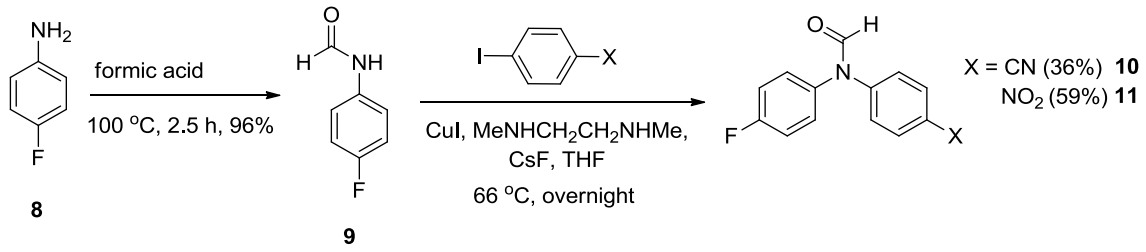

Figure 2.7. Synthetic routes for *N*-(4-cyanophenyl)-*N*-(4-fluorophenyl)formamide (**10**) and *N*-(4-fluorophenyl)-*N*-(4-nitrophenyl)-formamide (**11**).

2.5. Synthesis of the *ortho*-substituted molecular torsion balances

In order to explore greater chemical diversity in the model system beyond the *para*-substituted series of balances described above, a series with a substituent placed in the *ortho* position was synthesised (Figure 2.3).

The synthesis, characterisation and solvent screening of the *o*-Me (**14**), *o*-OMe (**15**) and *o*-NO_2 (**17**) balances were performed by Catherine Adam. The same synthetic procedures as those used for the *para*-substituted balances were used for the *ortho*-substituted molecular torsion balances. In the case of *N*-(4-fluorophenyl)-*N*-(*o*-tolyl)formamide (**14**) and *N*-(4-fluorophenyl)-*N*-(2-methoxyphenyl)formamide (**15**) a reaction between 1-fluoro-4-iodobenzene (**1**) and the formamide with the *o*-Me and *o*-OMe substituents produced the desired products in 88% and 65% yields respectively.[41] The *N*-(2-methoxyphenyl)formamide (**13**) was synthesised via initial formylation of 2-methoxyaniline (**12**) (Figure 2.8).[42]

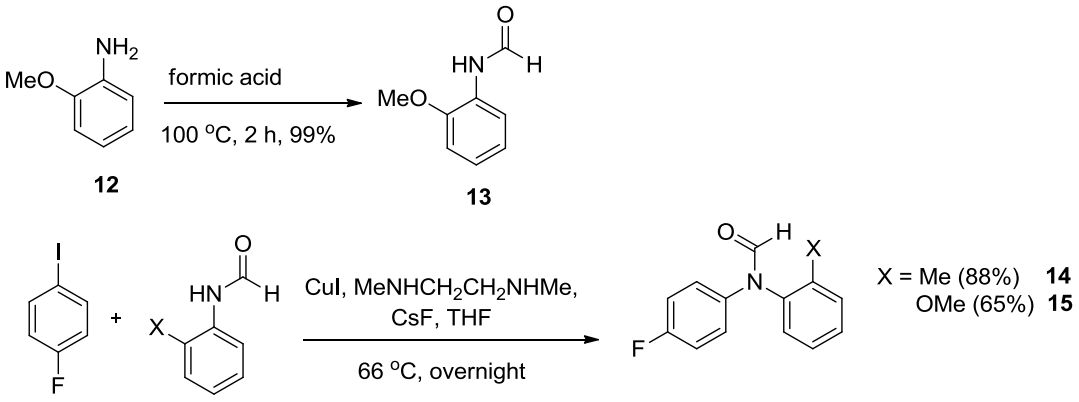

Figure 2.8. Synthetic routes for *N*-(4-fluorophenyl)-*N*-(*o*-tolyl)formamide (**14**) and *N*-(4-fluorophenyl)-*N*-(2-methoxyphenyl)formamide (**15**).

Since the *o*-Me (**14**), *o*-OMe (**15**) torsion balances bear electron-donating substituents, *ortho*-substituted formamides could be used in their syntheses. However, as was the case for the *para*-substituted balances, electron-withdrawing substituents

dramatically reduce the nucleophilicity of the formamide which meant that the synthesis of *N*-(4-fluorophenyl)-*N*-(2-nitrophenyl)formamide (**17**) required the use of the *N*-(4-fluorophenyl)formamide (**9**) and 1-iodo-2-nitrobenzene (**16**) (24% yield) (Figure 2.9).[41]

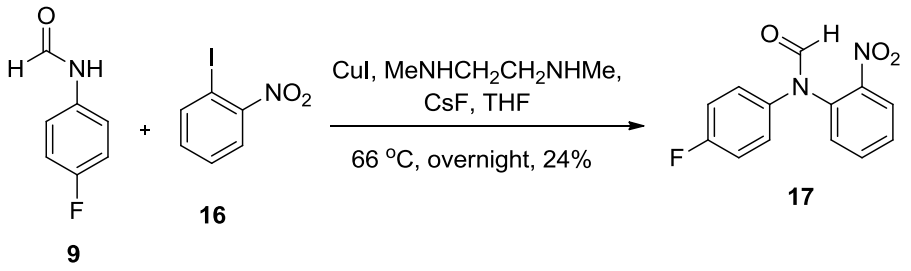

Figure 2.9. Synthesis of *N*-(4-fluorophenyl)-*N*-(2-nitrophenyl)formamide (**17**).

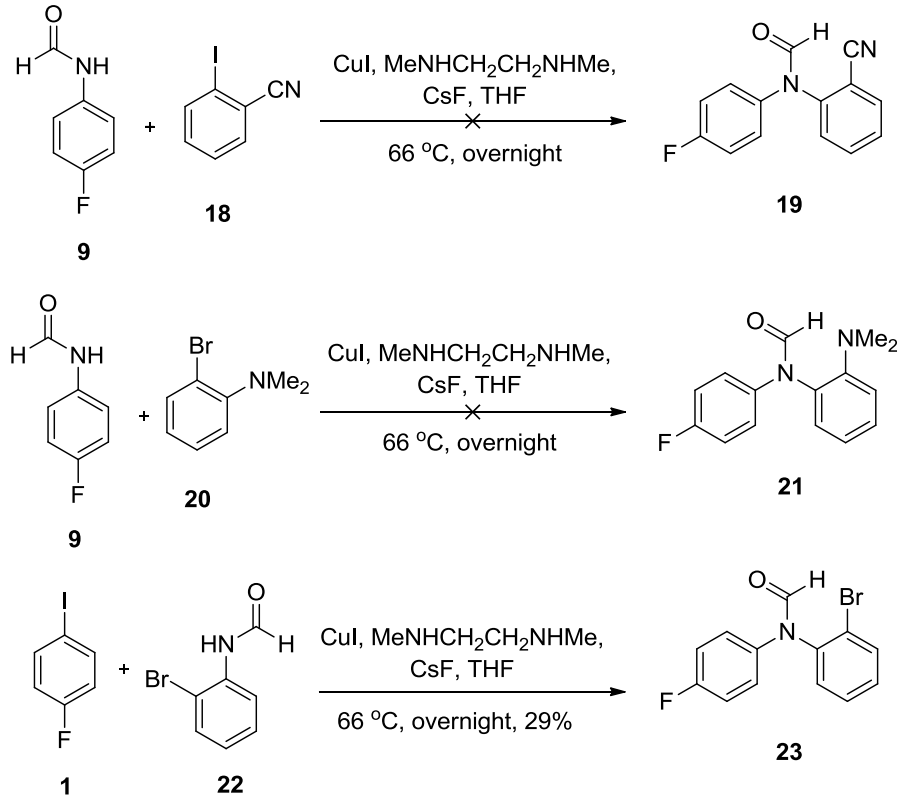

Figure 2.10. Synthetic trials for the *ortho*-CN (**19**) and *ortho*-NMe_2 (**21**) balances. Synthesis of the *ortho*-Br (**23**) torsion balance.

The molecular balances *N*-(2-cyanophenyl)-*N*-(4-fluorophenyl)formamide (**19**) and *N*-(2-(dimethylamino)phenyl)-*N*-(4-fluorophenyl)formamide (**21**) could not be synthesised by following the previously established procedure, even after increasing the catalyst loading. A problem was also encountered in the case of the *N*-(2-bromophenyl)-*N*-(4-fluorophenyl)formamide (**23**) which appeared in four conformational states in NMR spectra. This was proposed as being due to the slow rotation of the *N*-aryl bond due to the steric influence of the *ortho*-bromo substituent. As a result this compound was not included in further analyses (Figure 2.10).

2.6. Synthesis of the extended molecular torsion balances

The syntheses of the extended molecular torsion balances bearing a third aromatic ring (Figure 2.11) were based on the Suzuki coupling reaction between an aryl boronic acid and a halide in the presence of a base and a palladium catalyst. The previously synthesised *N*-(4-bromophenyl)-*N*-(4-fluorophenyl)formamide (**5**) served as a suitable halide which was coupled with an aryl boronic acid to construct several three-ringed balances (compounds **26**-**30**, **34**, **36**).

Torsion balances with a simple phenyl ring (**26**), an *ortho*-dimethylphenyl (**27**) and *ortho*-diethylphenyl (**28**) substituents were synthesised in 78%, 59% and 42% yields respectively (Figure 2.11). In these reactions the *para*-bromo balance (**5**) was used as a precursor, with a tetrakis(triphenylphosphine)palladium(0) catalyst and Na_2CO_3 base.[43] The phenylboronic acid and (2,6-dimethylphenyl)boronic acid were commercially available. The (2,6-diethylphenyl)boronic acid (**25**) had to be synthesised in 82% yield by the reaction of 2,6-diethyl bromobenzene with *n*-BuLi and trimethyl borate to make the boronic ester which was subsequently hydrolysed by hydrochloric acid (Figure 2.11).[44]

The Suzuki coupling reaction between *N*-(4-bromophenyl)-*N*-(4-fluorophenyl)formamide (**5**) and 2-aminobenzeneboronic acid or (2,6-dimethoxyphenyl)boronic acid under the same conditions, gave the *N*-(2'-amino-[1,1'-

biphenyl]-4-yl)-*N*-(4-fluorophenyl)formamide (**29**) and *N*-(2',6'-dimethoxy-[1,1'-biphenyl]-4-yl)-*N*-(4-fluorophenyl)formamide (**30**) balances in 67% and 91% yields respectively (Figure 2.12).[43]

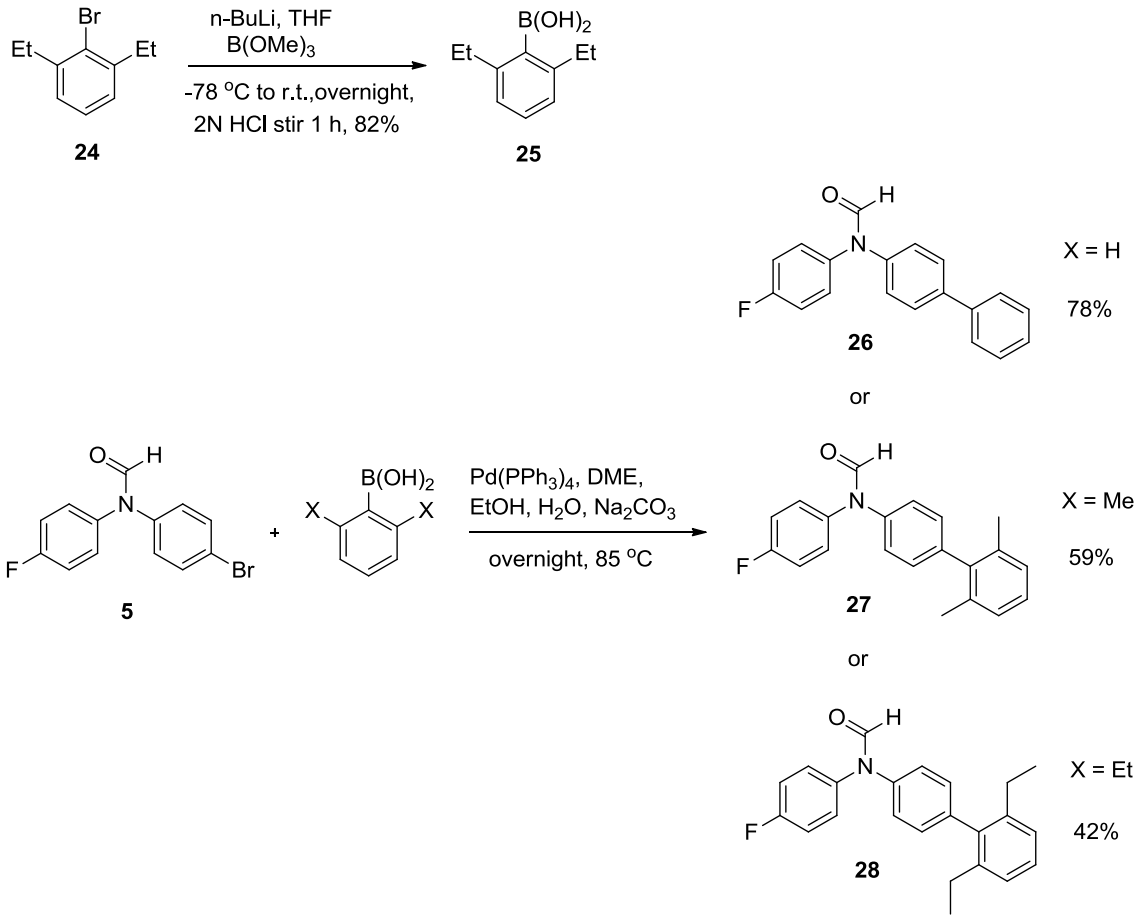

Figure 2.11. Synthetic routes for the *N*-([1,1'-biphenyl]-4-yl)-*N*-(4-fluorophenyl)formamide (**26**), *N*-(2',6'-dimethyl-[1,1'-biphenyl]-4-yl)-*N*-(4-fluorophenyl)formamide (**27**) and *N*-(2',6'-diethyl-[1,1'-biphenyl]-4-yl)-*N*-(4-fluorophenyl)formamide (**28**) torsion balances.

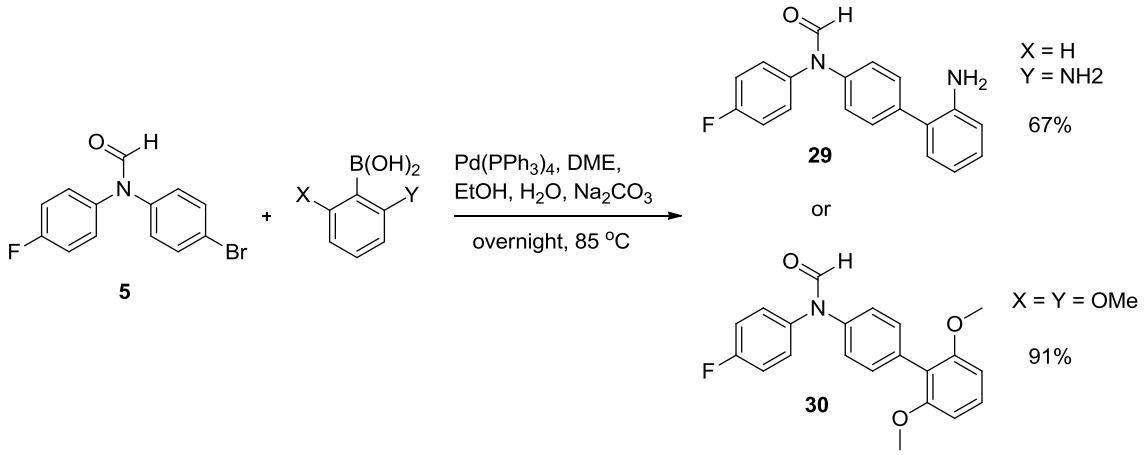

Figure 2.12. Synthesis of *N*-(2'-amino-[1,1'-biphenyl]-4-yl)-*N*-(4-fluorophenyl)formamide (**29**) and *N*-(2',6'-dimethoxy-[1,1'-biphenyl]-4-yl)-*N*-(4-fluorophenyl)formamide (**30**).

The synthesis of *N*-(3',5'-di-*tert*-butyl-2',6'-dimethoxy-[1,1'-biphenyl]-4-yl)-*N*-(4-fluorophenyl)formamide (**34**) occurs in three steps as shown in Figure 2.13. It starts with the methylation reaction of 4,6-di-*tert*-butylresorcinol (**31**) with methyl iodide and sodium hydride in 68% yield.[45] The conditions for the synthesis of 3,5-di-*tert*-butyl-2,6-dimethoxyphenyl)boronic acid (**33**) had to be changed compared to the synthesis of (2,6-diethylphenyl)boronic acid (**25**). After further optimisation, the reaction was found to work in 27% yield (by delaying the addition of the trimethyl borate by 3.5 h after initial stirring at room temperature).[46] Finally, a Suzuki reaction performed under the same conditions as described above, provided the *N*-(3',5'-di-*tert*-butyl-2',6'-dimethoxy-[1,1'-biphenyl]-4-yl)-*N*-(4-fluorophenyl)formamide (**34**) in 33% yield (Figure 2.13).[43]

Several sets of reaction conditions were attempted for the coupling reaction of *N*-(4-bromophenyl)-*N*-(4-fluorophenyl)formamide (**5**) with (2,6-bis(trifluoromethyl)phenyl) boronic acid (**35**), as the tetrakis(triphenylphosphine) palladium and Na_2CO_3 approach used previously was not successful here.[43] Neither changing the catalyst to $PdCl_2$(dppf) and the base to Et_3N,[47] nor the *in situ* production of the tetrakis(triphenylphosphine)palladium catalyst from palladium(II) acetate and

triphenylphosphine were successful.[48] A possible explanation for the lack of success could be the sterically hindered boronic acid used in the reaction (Figure 2.14).

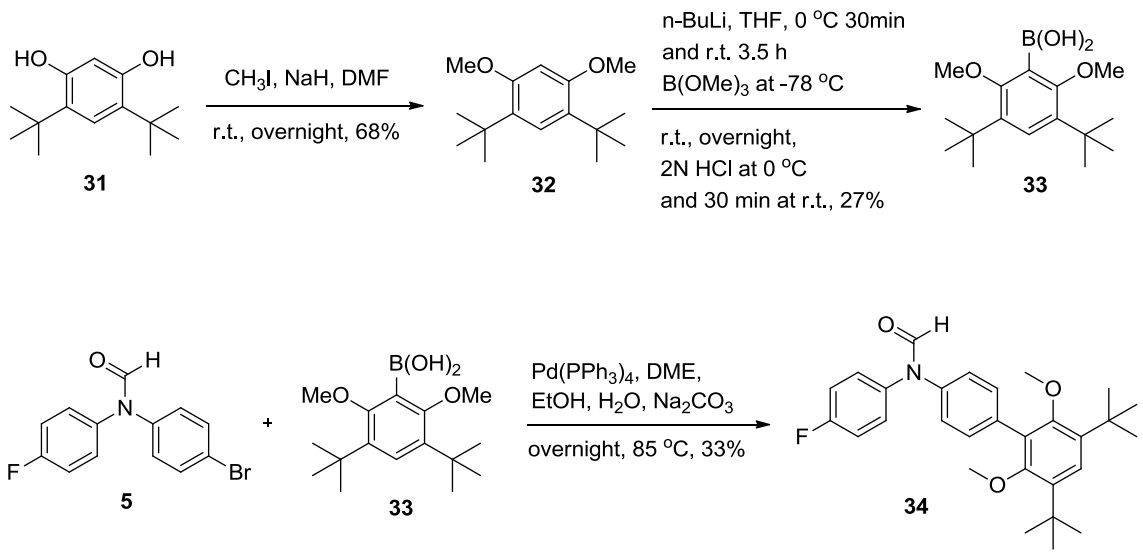

Figure 2.13. Synthetic route for *N*-(3',5'-di-*tert*-butyl-2',6'-dimethoxy-[1,1'-biphenyl]-4-yl)-*N*-(4-fluorophenyl)formamide (**34**).

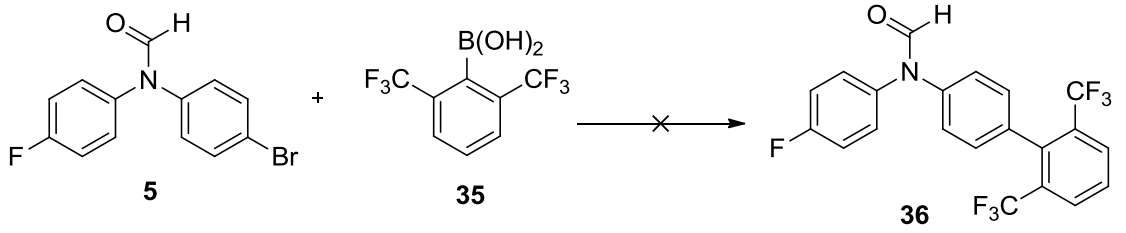

Conditions:
1) $Pd(PPh_3)_4$, DME, EtOH, H_2O, Na_2CO_3, overnight, 85 °C
2) $PdCl_2(dppf)$, Et_3N, EtOH, overnight, 78 °C
3) $Pd(OAc)_2$, PPh_3, *n*-propanol, H_2O, Na_2CO_3, overnight, 97 °C

Figure 2.14. Trials for the synthesis of *N*-(2',6'-bis(trifluoromethyl)-[1,1'-biphenyl]-4-yl)-*N*-(4-fluorophenyl)formamide (**36**).

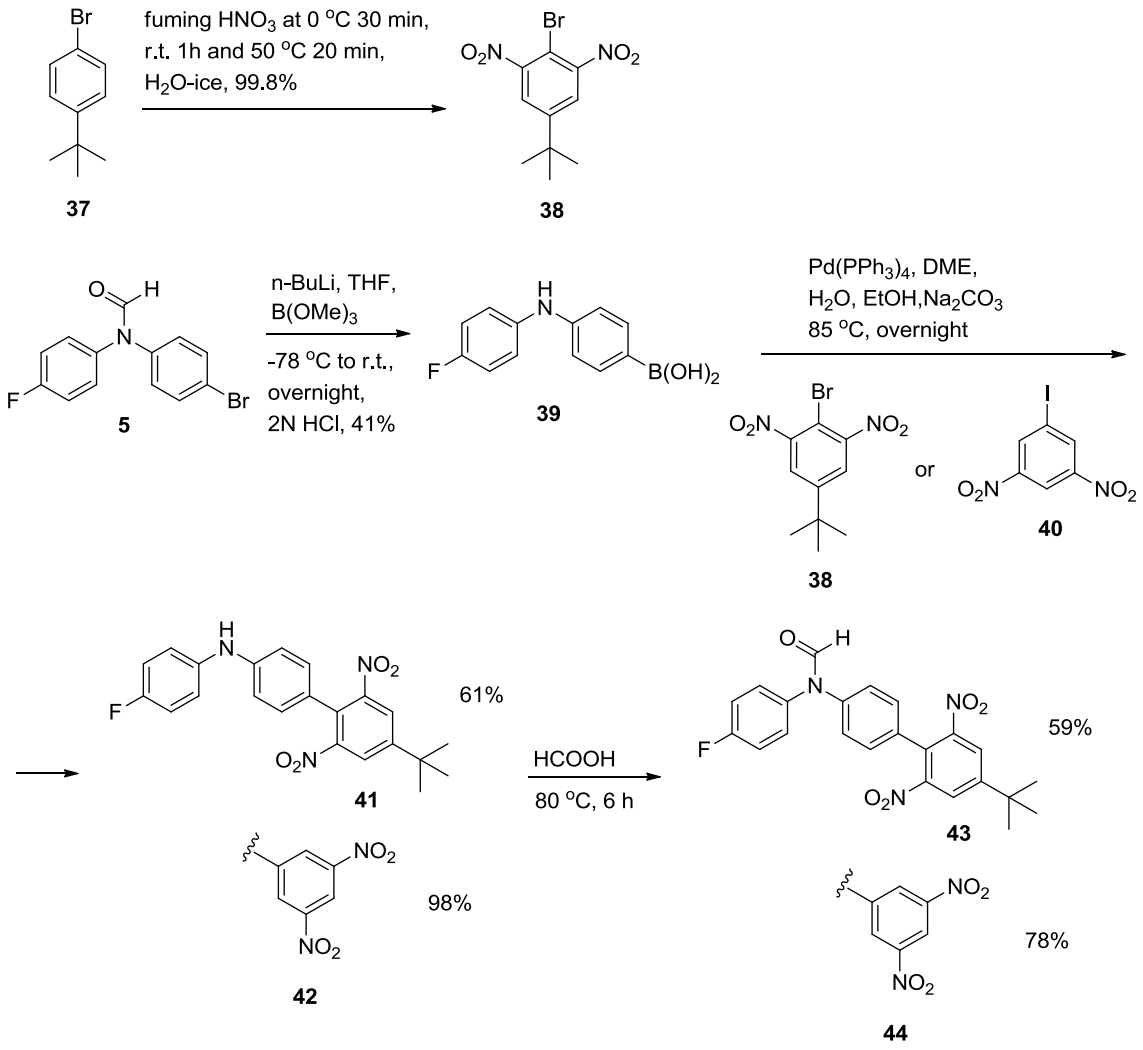

Figure 2.15. Synthetic routes for *N*-(4'-(*tert*-butyl)-2',6'-dinitro-[1,1'-biphenyl]-4-yl)-*N*-(4-fluorophenyl)formamide (**43**) and *N*-(3',5'-dinitro-[1,1'-biphenyl]-4-yl)-*N*-(4-fluorophenyl)formamide (**44**).

The synthesis of *N*-(4'-(*tert*-butyl)-2',6'-dinitro-[1,1'-biphenyl]-4-yl)-*N*-(4-fluorophenyl)formamide (**43**) proved to be quite difficult (Figure 2.15). Firstly, the 2-bromo-5-(*tert*-butyl)-1,3-dinitrobenzene (**38**) was obtained by nitration of 4-*tert*-butylbromobenzene (**37**) with fuming nitric acid in excellent yield.[49] The corresponding boronic acid from 2-bromo-5-(*tert*-butyl)-1,3-dinitrobenzene (**38**) required for coupling

with the *para*-bromo balance (**5**) could not be synthesised. This problem was overcome by reversing the orientation of the Suzuki coupling by forming the boronic acid from *N*-(4-bromophenyl)-*N*-(4-fluorophenyl)formamide (**5**) followed by direct coupling to 2-bromo-5-(*tert*-butyl)-1,3-dinitrobenzene (**38**).[61,43] The formyl group fell off the *para*-bromo balance (**5**) during the formation of this boronic acid and the reaction did not always proceed in reasonable yield.

The (4-((4-fluorophenyl)amino)phenyl)boronic acid (**39**) was then coupled to 2-bromo-5-(*tert*-butyl)-1,3-dinitrobenzene (**38**) in 61% yield under the same Suzuki conditions as before.[43] Finally, a formylation reaction with formic acid provided the torsion balance (**43**) in 59% yield (Figure 2.15).[42]

As shown in Figure 2.15, by following the same synthetic route and using 1-iodo-3,5-dinitrobenzene (**40**) instead of 2-bromo-5-(*tert*-butyl)-1,3-dinitrobenzene (**38**), the *N*-(3',5'-dinitro-[1,1'-biphenyl]-4-yl)-*N*-(4-fluorophenyl)formamide (**44**) molecular balance was synthesised in 78% yield.[61,43,42]

2.7. Conformational assignment and barrier to rotation of the molecular torsion balances

The molecular balances of the type shown in Figure 2.3 exist in two conformational states (A and B) due to slow rotation of the carbon-nitrogen bond in the formyl group. In order for the free energy of folding to be precisely defined, it is essential to fully characterise and assign each conformer spectroscopically. The two conformers of each balance were fully assigned by NMR analysis in $CDCl_3$. A series of NMR experiments (^1H, ^{13}C, HSQC, COSY, NOESY and HMBC) was performed for each balance. Following the assignment of the protons and the corresponding carbons using the ^1H, ^{13}C and HSQC spectrum, the conformers A and B were assigned using NOESY and HMBC experiments. An example of the conformational assignment of *N*-(4-fluorophenyl)-*N*-phenylformamide (**3**) by these methods is presented in the Experimental section (Chapter 6) of this thesis.

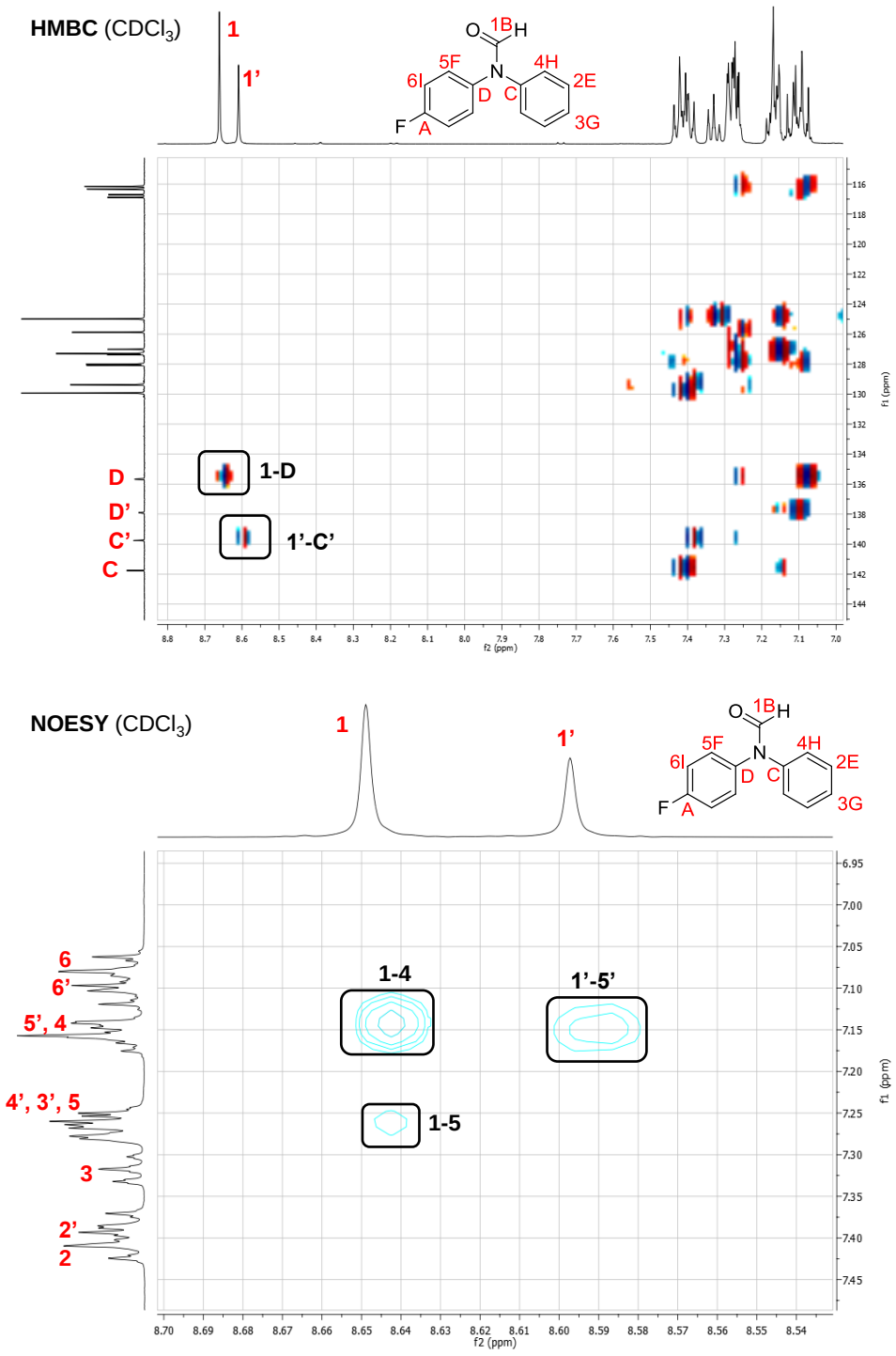

Figure 2.16. The HMBC and NOESY spectra of the balance (**3**) in $CDCl_3$.

In HMBC spectra, a correlation between the formyl proton and the quaternary aromatic carbon positioned *trans* to the formyl proton of each conformer was observed (Figure 2.16 and Figure 2.17). In the NOESY spectra, a major NOE was apparent between the formyl and the aromatic protons that were closest in space in each conformer (i.e. on the same side of the molecule) (Figure 2.16 and Figure 2.17). Minor NOE correlations were also observed in these spectra since there is exchange between the two conformers on the timescale of the NOESY experiment at room temperature. Furthermore, the formyl proton and the aromatic protons on opposite sides of the balance in each conformer are still within the range for an NOE signal to be observed. This information in combination with the HMBC result provided an accurate assignment of the two conformers.

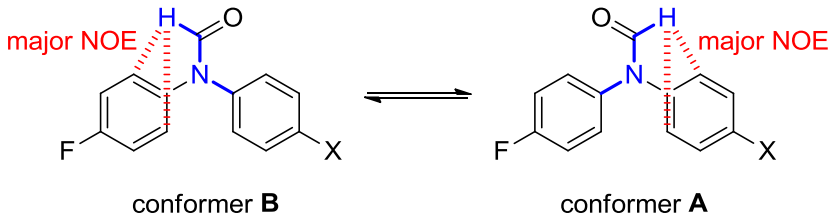

Figure 2.17. The two conformations of the molecular torsion balance. The major NOEs observed in the NOESY experiment are shown in red and the *trans* correlations observed in the HMBC spectrum are shown in blue.

In the case of *N*-(4-fluorophenyl)-*N*-phenylformamide (**3**), additional NMR experiments were performed to further confirm the conformational assignment (see experimental chapter for more details, Figures 6.9, 6.10 and 6.11). A sample of the compound in $CDCl_3$ was cooled to –35 ^{o}C to slow down the conformational exchange. A 1-dimensional NOESY experiment was then performed by irradiating the formyl proton for each conformer and monitoring the response signal. By using this method, the aromatic proton which is nearest in space to the formyl proton can be identified. A TOCSY NMR was also taken for the major conformer, which shows how magnetisation

is transferred around the aromatic ring after passing from the formyl proton to the aromatic protons that are nearest in space.

It was also important to prove that the NMR signals correspond to the two conformers of the same compound rather than from impurities or other effects. This was proven by a variable-temperature NMR experiment in which a series of ^{1}H-NMR spectra were taken in DMSO. This experiment was performed for several of the balances and the results can be found in the Experimental section of this thesis (Chapter 6, Figures 6.12 – 6.14). As the temperature was increased, the two signals corresponding to the formyl protons became broad and eventually coalesced into a singlet, which sharpened at higher temperatures. At high temperatures the exchange of the conformers is fast and therefore the compound does not appear as two conformers in the NMR spectrum. Upon cooling, the two conformer signals were seen to reappear confirming the existence of a conformational equilibrium separated by a high-rotational barrier (Figure 2.18).

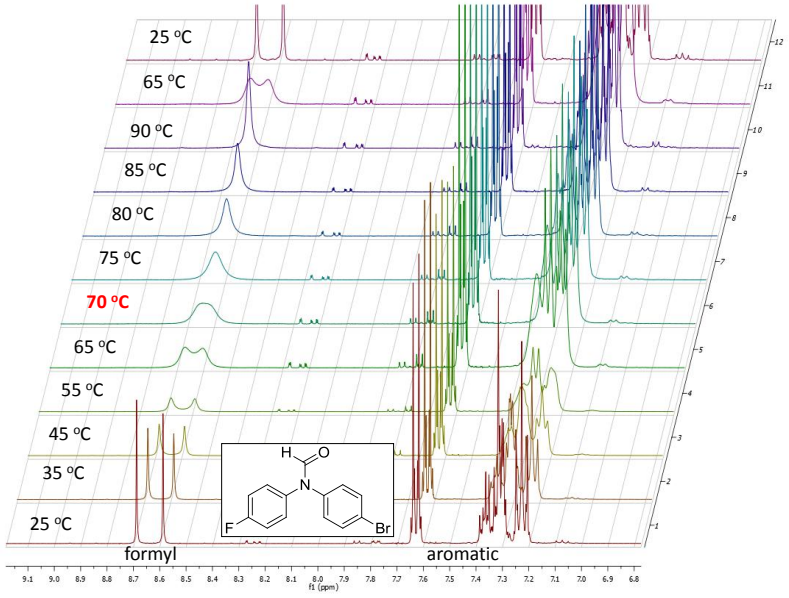

Figure 2.18. Variable temperature NMR experiment for balance (**5**) in DMSO-d_6.

Further insight into the barrier of rotation was gained by EXSY NMR. These experiments consist of a series of 1D NOESY experiments with varying mixing times,

which can then be used to calculate the barrier to rotation about the C-N formamide bond.[50,51] In this method, the integral ratio in response to selectively irradiated peak is plotted against the mixing times for each experiment to give a linear correlation. The slope of the graph corresponds to the rate constant of rotation, from which the energy barrier to rotation can then be calculated. By using this method, the barrier to rotation of the formyl group in *N*-(4-fluorophenyl)-*N*-phenylformamide (**3**) was determined to be 74.9 kJ/mol, which is quite similar to that reported for the acetyl group of *N*,*N*-dimethylacetamide (~71.1 kJ/mol).[52] Further details of this experiment can be found in the Experimental section (Chapter 6) of this thesis (Figure 6.15).

Given the number of combinations of torsion balances and solvents investigated in this study it was not possible to perform such detailed conformational assignments for all 204 possible experimental combinations (17 balances in 12 different solvents). However, differences in the ^{19}F-NMR chemical shifts of each conformer were found to be useful for assigning conformers in the range of solvents investigated (Figure 2.19).

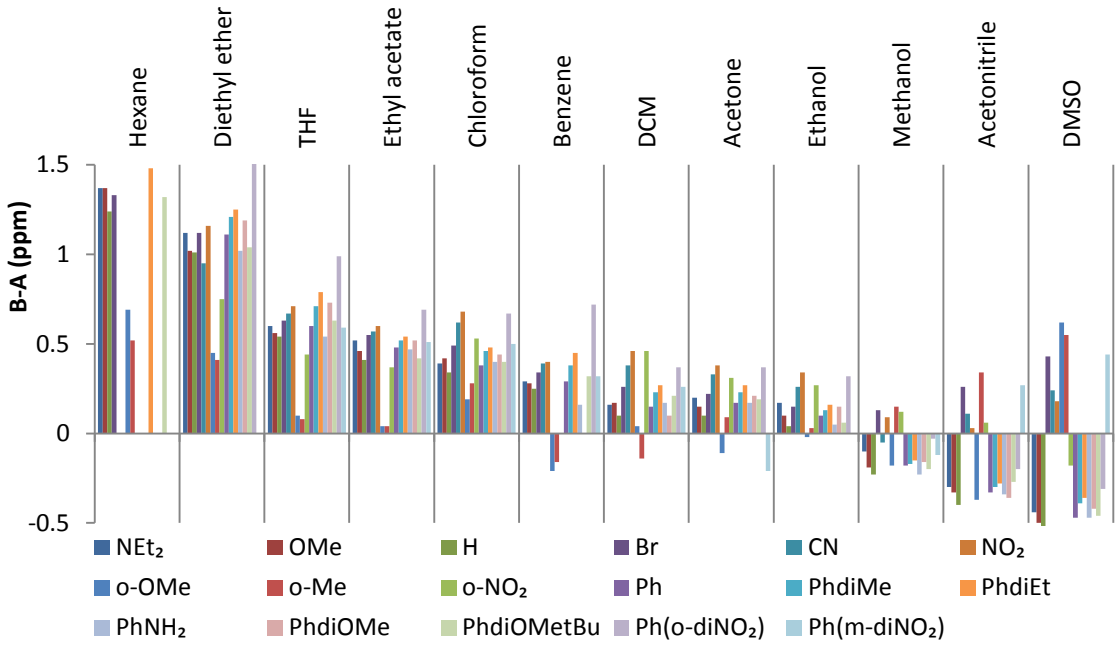

Figure 2.19. Graph showing the trends in the ^{19}F-NMR chemical shift differences between conformers A and B.

Conformer assignments were based on the detailed assignments performed in $CDCl_3$ compared to the differences between the chemical shifts of each conformer. The graph in Figure 2.19 shows the trends that appeared in these ^{19}F-NMR chemical shift differences [B-A (ppm)].

The typical [B-A (ppm)] chemical shift differences shown in Figure 2.19 are positive for the less polar solvents (from hexane to ethanol) and negative for the majority of balances in methanol, acetonitrile and DMSO. However, several outlying balance/solvent combinations, that behave differently compared to the majority of balances, could be identified by this analysis as follows (see coloured boxes in Table 6.2 in the experimental section):

1) *p*-Br (**5**): CH_3CN, MeOH, DMSO
2) *p*-CN (**10**): CH_3CN, DMSO
3) *p*-NO_2 (**11**): CH_3CN, MeOH, DMSO
4) *o*-Me (**14**): CH_3CN, benzene, DCM, MeOH, DMSO
5) *o*-OMe (**15**): acetone, benzene, EtOH, DMSO
6) *o*-NO_2 (**17**): CH_3CN, MeOH
7) Ph(*m*-diNO_2) (**44**): acetone, CH_3CN, DMSO

Detailed NMR analysis and assignment was performed for each of these outliers to identify whether the major conformer of a particular balance was different to that observed in $CDCl_3$. The outliers in DCM and EtOH were not checked due to the relatively high cost of the deuterated solvent required for the NMR experiments and the similarity of the behaviour of these types of balances in $CDCl_3$ and MeOH respectively. In these cases it was assumed that the dominant conformer was the same as the assignment in $CDCl_3$ in the case of DCM outliers, and MeOH in the case of EtOH outliers. After this additional NMR analysis only 15 of over 200 possible balance/solvent combinations were found to have dominant conformers that differed from those observed in $CDCl_3$ as listed below:

1) *p*-Br (**5**): CH_3CN, EtOH, MeOH, DMSO
2) *p*-CN (**10**): CH_3CN, DMSO

3) *p*-NO_2 (**11**): DMSO

4) *o*-Me (**14**): CH_3CN, EtOH, MeOH, DMSO

5) *o*-OMe (**15**): DMSO

6) Ph(*m*-diNO_2) (**44**): acetone, CH_3CN, DMSO

Most of these cases are of low significance with respect to the quantitative free energy analysis that follows, because the A/B conformer ratio lies close to 1:1 ($\Delta G_{fold} \approx 0$). The more significant cases are the *p*-CN (**10**), *p*-NO_2 (**11**) and Ph(*m*-diNO_2) (**44**) balances in DMSO and the *o*-Me (**14**) balance in CH_3CN, EtOH, MeOH and DMSO.

Additional experiments were performed to check that the folding ratios of the balances were not affected by aggregation. Chloroform and DMSO solutions of the X = $PhNH_2$ (**29**) and X = PhdiOMe (**30**) balances at three different concentrations covering the range used in the general NMR studies showed that the position of the conformation equilibrium was not concentration dependent. Similar tests were also performed for the X = *para*-NEt_2 (**6**) balance in chloroform and methanol, and the X = Ph(*o*-diNO_2) balance (**43**) in chloroform. In all cases the conformer ratios for each balance was found to be the same at all concentrations (Figure 2.20).

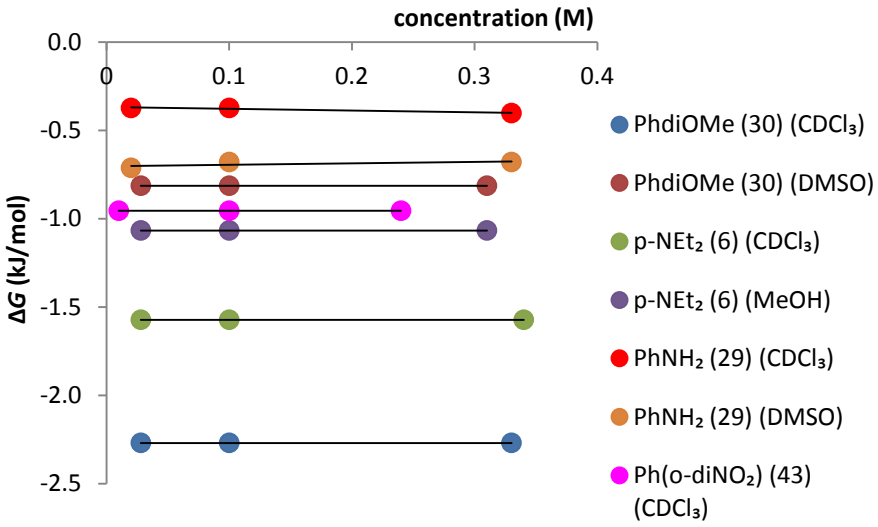

Figure 2.20. Concentration studies. Graph correlating concentration-Δ*G* for some balances in particular solvents.

2.8. Initial analyses of electronic and solvent effects on the conformations of the balances

Following the assignment of conformers described above, Table 2.1 summarises the experimentally determined folding free energies, ΔG_{fold} for each of the balances in the range of solvents examined.

Table 2.1. Table showing experimental folding free energies, ΔG_{exp} in every solvent, ΔG_{calc} calculated in Spartan '08 using B3LYP/6-31G* and the Hammett substituent constants for simple X-substituents. The entry "n.s." stands for not soluble cases.

X-substituent and compound number	Hammett constants (σ_m)	Hammett constants (σ_p)	ΔG (kJ/mol) calc	ΔG exp (kJ/mol) Chloroform	ΔG exp (kJ/mol) Acetone	ΔG exp (kJ/mol) Acetonitrile	ΔG exp (kJ/mol) Benzene	ΔG exp (kJ/mol) Ethyl acetate	ΔG exp (kJ/mol) Hexane	ΔG exp (kJ/mol) THF	ΔG exp (kJ/mol) DCM	ΔG exp (kJ/mol) Ethanol	ΔG exp (kJ/mol) Methanol	ΔG exp (kJ/mol) DMSO	ΔG exp (kJ/mol) Diethyl ether
***p*-H (3)**	0	0	-0.89	-1.14	-0.85	-0.78	-0.68	-1.07	-1.14	-0.88	-0.81	-0.81	-0.81	-0.75	-1.11
***p*-Br (5)**	0.39	0.23	0.67	0.08	0.05	-0.15	0.08	0.18	0.37	0.23	0.08	-0.05	-0.08	-0.10	0.37
***p*-NEt_2 (6)**	-0.23	-0.72	-3.71	-1.57	-1.53	-0.99	-1.39	-2.15	-2.75	-2.09	-1.11	-1.53	-1.07	-0.81	-2.40
***p*-OMe (7)**	0.12	-0.27	-2.03	-0.78	-0.71	-0.52	-0.75	-0.92	-1.48	-1.07	-0.58	-0.68	-0.52	-0.37	-1.27
***p*-CN (10)**	0.56	0.66	2.59	1.03	0.29	-0.15	0.78	0.65	n.s.	0.68	0.71	0.37	0.15	-0.55	1.27
***p*-NO_2 (11)**	0.71	0.78	3.07	1.39	0.46	0.02	1.07	0.96	n.s.	0.88	0.99	0.58	0.18	-0.37	1.98
***o*-Me (14)**	-	-	-1.19	-0.15	-0.55	1.18	-0.15	-0.05	-1.35	-0.13	-0.29	0.78	1.18	1.48	-0.88
***o*-OMe (15)**	-	-	-3.09	-0.75	-0.81	-0.13	-0.78	-1.07	-1.87	-1.44	-0.55	-0.49	-0.02	0.08	-1.82
***o*-NO_2 (17)**	-	-	6.51	3.99	4.25	4.11	n.s.	4.11	n.s.	4.11	4.39	4.11	4.11	4.54	3.75
Ph (26)	-	-	-0.45	-0.68	-0.58	-0.58	-0.46	-0.68	n.s.	-0.65	-0.58	-0.55	-0.62	-0.58	-0.65
PhdiMe (27)	-	-	-0.77	-0.99	-0.65	-0.55	-0.62	-0.65	n.s.	-0.85	-0.85	-0.62	-0.68	-0.65	-0.85
PhdiEt (28)	-	-	-1.01	-1.03	-0.62	-0.55	-0.58	-0.65	-0.92	-0.65	-0.96	-0.65	-0.75	-0.55	-0.78
$PhNH_2$ (29)	-	-	-0.37	-0.37	-0.62	-0.49	-0.13	-0.71	n.s.	-0.52	-0.49	-0.43	-0.49	-0.68	-0.55
PhdiOMe (30)	-	-	-3.52	-2.27	-1.11	-0.78	-1.82	-1.57	n.s.	-1.57	-1.14	-1.31	-1.14	-0.81	-2.09
PhdiOMetBu (34)	-	-	-1.45	-1.18	-0.71	-0.85	-0.32	-0.58	-0.85	-0.75	-1.07	n.s.	-0.71	-0.58	-0.49
Ph(*o*-diNO_2) (43)	-	-	-0.87	-0.96	-0.68	-0.32	-0.71	-0.55	n.s.	-0.75	-0.55	n.s.	-0.55	-0.75	-0.49
Ph(*m*-diNO_2) (44)	-	-	2.91	0.62	-0.02	-0.21	1.48	0.35	n.s.	0.21	0.32	n.s.	0.05	-0.35	n.s.

An initial overview of the behaviour of these balances can be obtained by looking at the major conformers of each of the balances in $CDCl_3$ (Figure 2.21). It can be seen that A is the major conformer for the *p*-H (**3**), *p*-NEt_2 (**6**), *p*-OMe (**7**), *o*-Me (**14**) and *o*-OMe (**15**) balances, whereas the *p*-CN (**10**), *p*-NO_2 (**11**) and *o*-NO_2 (**17**) balances prefer the B conformation in $CDCl_3$.

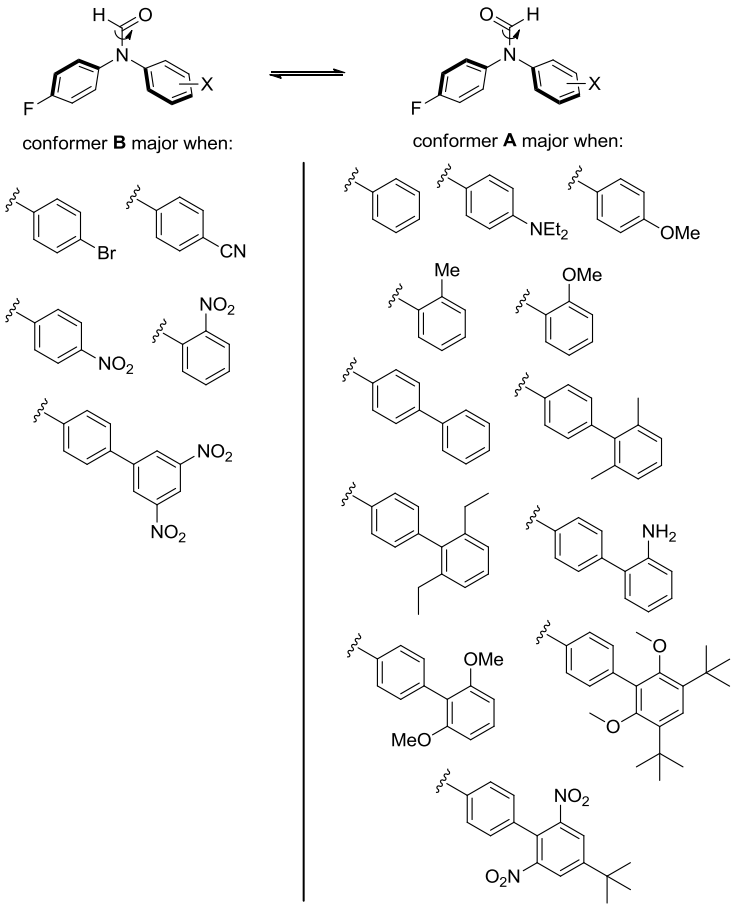

Figure 2.21. Conformational assignment of the major conformer for each molecular torsion balance in $CDCl_3$.

Thus, the simple interpretation is that A is the major conformer when X is electron-donating, but conformer B dominates when X is more strongly electron-

withdrawing. Electron-donating substituents increase the electron density of the aromatic ring to which they are attached, thus the proton, and not the oxygen, of the formyl group prefers to be located above the most electron-rich aromatic ring. Electron-withdrawing X-substituents decrease the electron density of the adjacent ring making the ring more electron-poor compared to the fluoro-substituted ring, and conformer B is more abundant. In the *p*-Br (**5**) balance the conformational ratio is about 1:1, slightly favouring the B conformer, since in this case the electronic effects of the fluorine and bromine substituents are similar. Interesting electronic effects are observed for the extended phenyl balances and these are discussed in more detail in Chapter 3.

Similarly, an initial overview of the effects of the solvent on the conformational equilibria in the balances can be obtained by performing a Hammett analysis on the simple *para*-substituted balances.[53,54] By definition, the Hammett constants for X = H are 0, electron-withdrawing groups have positive constants (Br < CN < NO_2) and the electron-donating groups have negative values (NEt_2). The OMe substituent is electron-withdrawing relative to the *meta*-position but is electron-donating via resonance relative to the *para* position.[54]

The graphs in Figure 2.22 show the correlation of the Hammett constants with the folding free energies in each solvent. With the minor exception of hexane and THF, σ_m provides better correlations than σ_p.

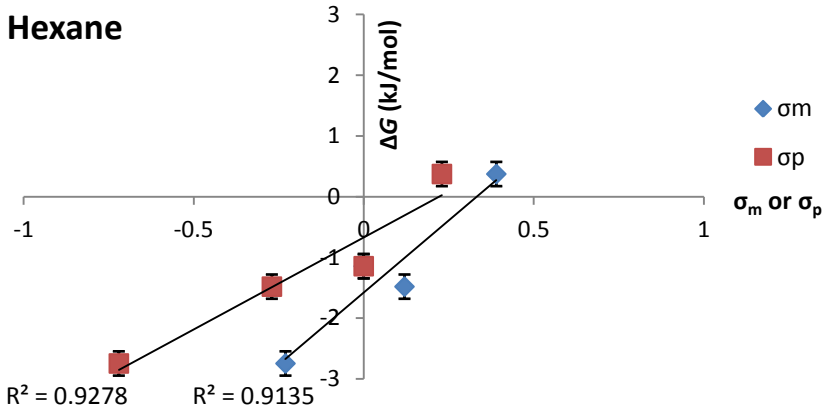

Diethyl ether

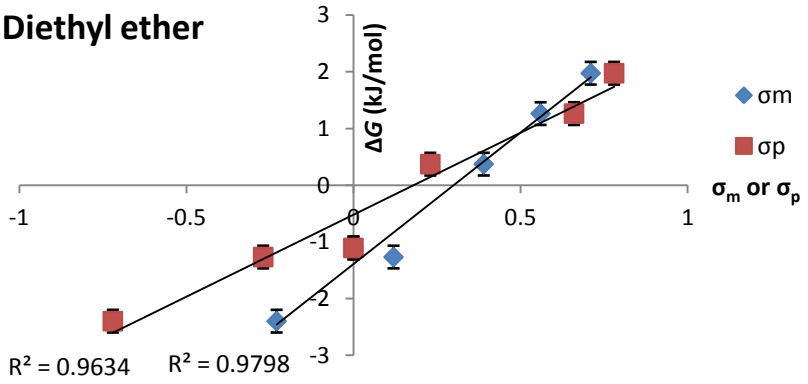

Chloroform

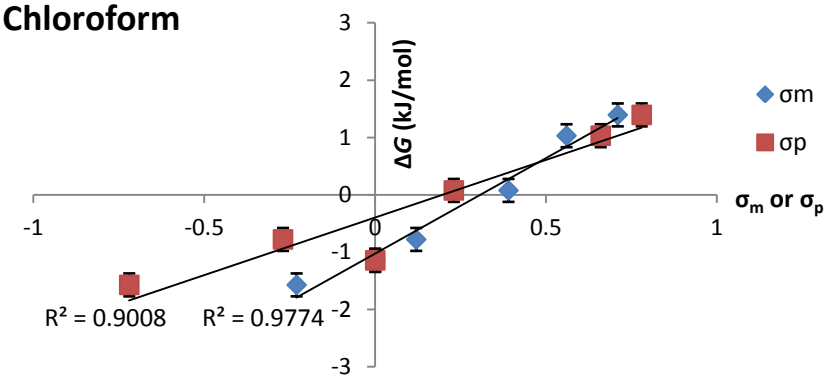

Ethyl acetate

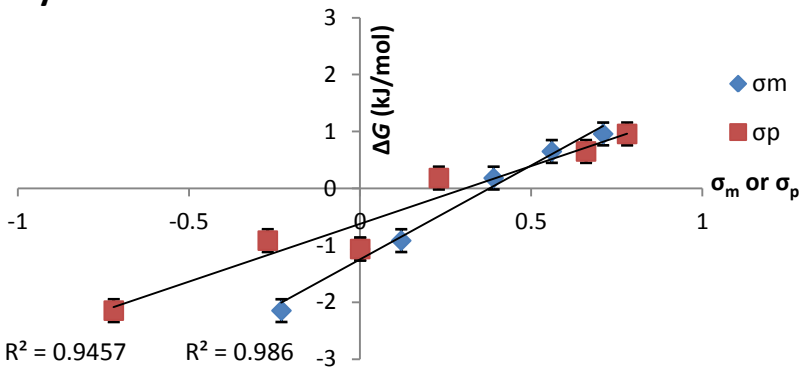

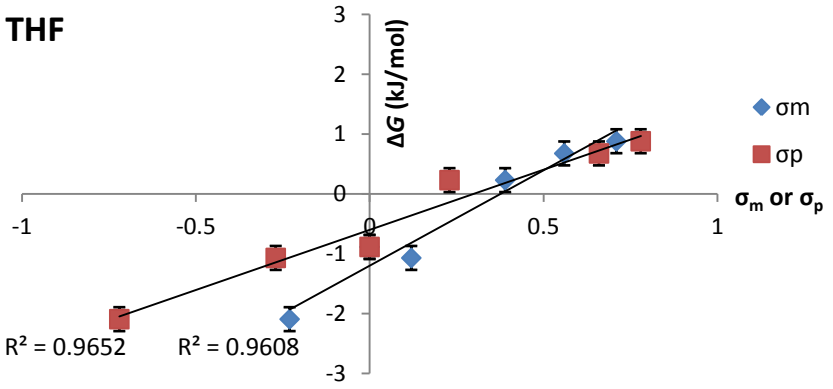
THF
3
2
1
0
-1
-2
-3
-1
-0.5
0
0.5
1
ΔG (kJ/mol)
σm
σp
σm or σp
R² = 0.9652
R² = 0.9608

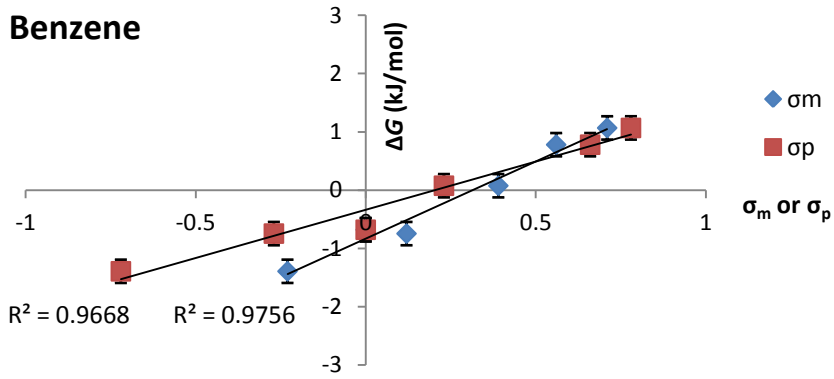
Benzene
3
2
1
0
-1
-2
-3
-1
-0.5
0
0.5
1
ΔG (kJ/mol)
σm
σp
σm or σp
R² = 0.9668
R² = 0.9756

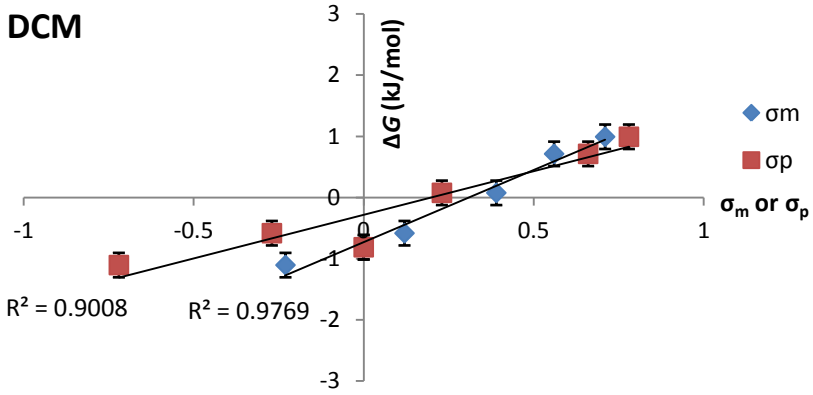
DCM
3
2
1
0
-1
-2
-3
-1
-0.5
0
0.5
1
ΔG (kJ/mol)
σm
σp
σm or σp
R² = 0.9008
R² = 0.9769

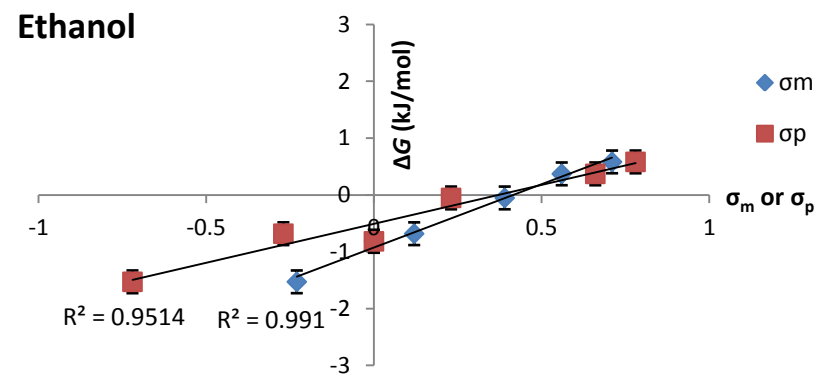
Ethanol
ΔG (kJ/mol)
σm
σp
σm or σp
R² = 0.9514
R² = 0.991

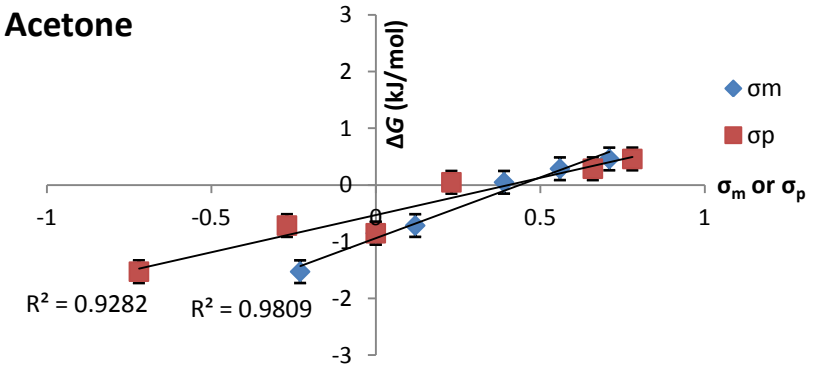
Acetone
ΔG (kJ/mol)
σm
σp
σm or σp
R² = 0.9282
R² = 0.9809

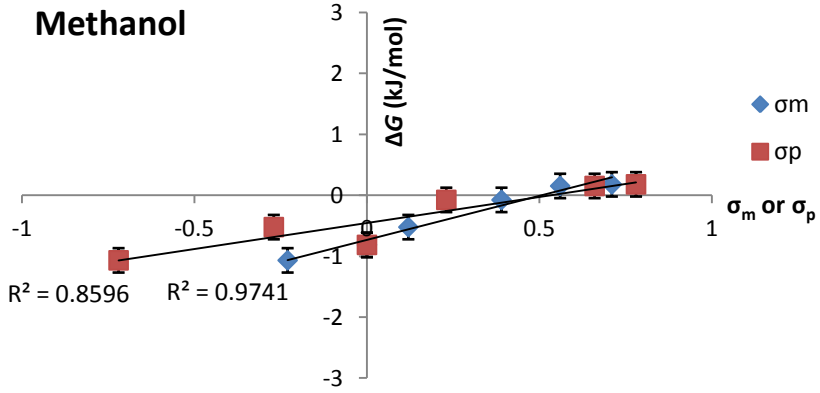
Methanol
ΔG (kJ/mol)
σm
σp
σm or σp
R² = 0.8596
R² = 0.9741

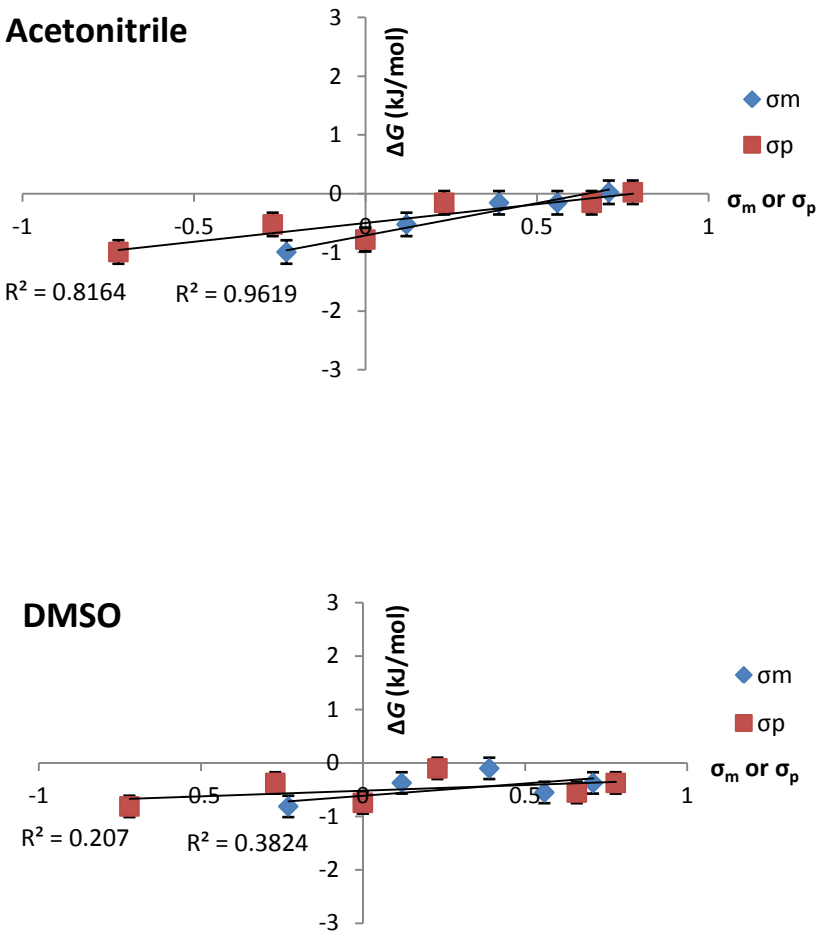

Figure 2.22. Graphs correlating the Hammett constants and ΔG_{fold} of the *para*-substituted balances in each solvent. The error bar for ΔG_{fold} is ± 0.2 kJ/mol.

Excellent linear correlations between σ_m and ΔG_{fold} were observed in most solvents ($R^2 > 0.9$). This observation indicates that intramolecular electrostatic effects are important in determining the trends in the conformational equilibrium. It can also be seen that the gradient of these σ_m graphs varies dramatically between the solvents. Table 2.2 lists the gradients of these graphs alongside the dielectric constant of the solvent,[55,56] and these are plotted in Figure 2.23. From this graph it can be concluded that the more polar the solvent, the shallower the gradient of the ΔG_{fold} vs. Hammett substituent plot

(Figure 2.23). This means that the folding free energy of these balances is less sensitive to electrostatic effects in polar solvents than in apolar solvents.

Table 2.2. Table showing the dielectric constants for every solvent and the gradient of the correlation with σ_m in the graphs of Figure 2.22.[55,56]

	ε	gradient
Chloroform	4.806	3.3317
Acetone	20.7	2.1447
Acetonitrile	37.5	1.1042
Benzene	2.284	2.6483
Ethyl acetate	6.02	3.3031
Hexane	1.88	4.7532
THF	7.6	3.1916
DCM	9.08	2.3624
Ethanol	24.3	2.2299
Methanol	32.6	1.4469
DMSO	46.8	0.4602
Diethyl ether	4.3	4.6427

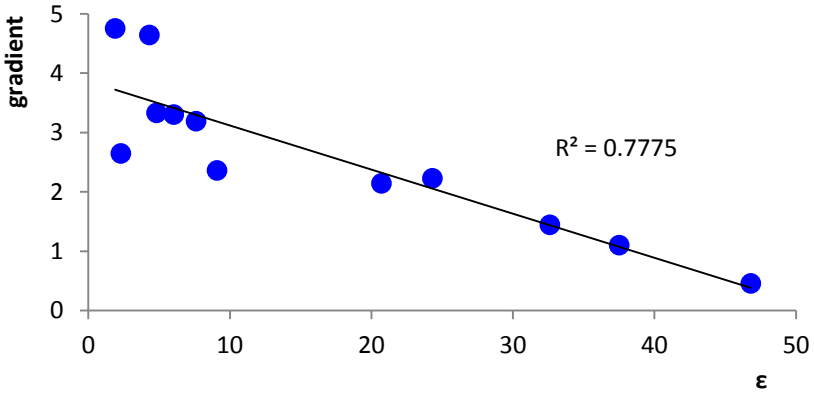

Figure 2.23. Graph correlating the dielectric constant and the gradient taken from the σ_m–ΔG_{exp} correlation of the *para*-series in every solvent as shown in Figure 2.22.

Following this analysis of solvent dielectric constants, simple correlations of the experimentally determined folding free energies with various solvent parameters were attempted (Table 2.3), but no significant correlations were seen with E_T30,[57,56] calculated electrostatic potentials (MEP_{min} and MEP_{max}), hydrogen bond donor ability (α_s), acceptor ability (β_s), or the solvophobicity term ($\alpha_s\beta_s$). [22,58-60]

Table 2.3. Solvent parameters used in this study (dielectric constants, E_T30, electrostatic potentials calculated using B3LYP/6-31G*, and experimental α_s and β_s values taken from the literature).[55,56,57,22,58,59,60]

Solvent	ε	E_T30 (kcal/mol)	MEP_{max} (kJ/mol)	MEP_{min} (kJ/mol)	α_s	β_s
Chloroform	4.806	39.1	170	-45	2.2	0.9
Acetone	20.7	42.2	92	-175	1.5	5.8
Acetonitrile	37.5	45.6	133	-190	1.7	5.1
Benzene	2.284	34.3	64	-89	1.1	2.1
Ethyl acetate	6.02	38.1	113	-205	1.5	5.3
Hexane	1.88	31	36	-20	1.0	0.6
THF	7.6	37.4	63	-180	0.9	5.9
DCM	9.08	40.7	143	-70	1.9	1.1
Ethanol	24.3	51.9	212	-178	2.7	5.3
Methanol	32.6	55.4	214	-178	2.7	5.3
DMSO	46.8	45.1	121	-218	2.2	8.7
Diethyl ether	4.3	34.5	51	-162	0.9	5.3

Overall, these initial analyses show that the trends in the folding behaviour of the molecular torsion balances are mainly governed by electronic substituent effects, but that the magnitude of these effects are highly solvent dependent. Hammett analyses and correlations with bulk solvent properties such as the dielectric constant are incapable of completely rationalising the behaviour of this model system. This raises the question of whether it is possible to dissect and quantify the array of non-covalent interactions and solvent effects that govern the behaviour of the system.

2.9. Introducing a model for the dissection of electrostatic and solvent effects on conformational equilibria

From the initial analyses described above, it was apparent that no single electronic or solvent parameter is sufficient to describe the folding behaviour of the molecular balances examined in this study. Thus, it was proposed that a model that involves both electrostatic and solvation terms is required to gain a complete understanding of the behaviour of this system.

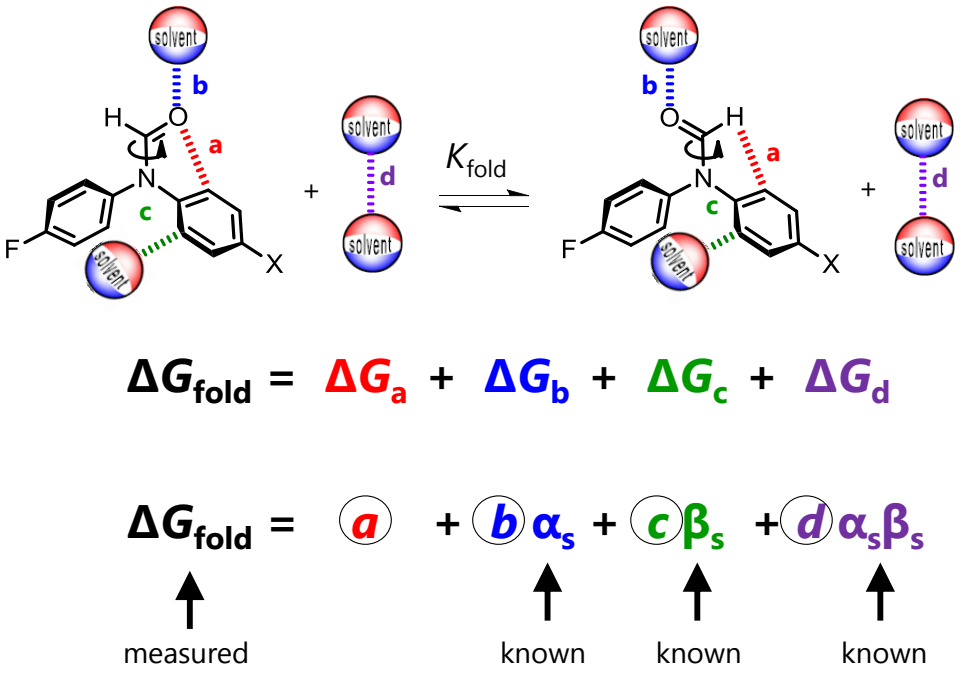

Figure 2.24. Model for the dissection of electrostatic and solvent effects on the molecular torsion balances.

An equation which represents the folding free energy as the sum of the energies due to electrostatic interactions, solvent interactions and solvophobic effects was introduced. For simplicity, the interactions in the schematic representation in Figure 2.24 show only a single hydrogen-bond donor site and a single hydrogen-bond acceptor site, but in reality the position of the conformational equilibrium is likely to be determined by

a complicated mixture of different solvation sites. An *a* coefficient (red) can be proposed as encoding the differences in the electrostatic interactions of the formyl group with the aromatic rings in each conformer, since steric effects are likely to be similar in each conformation. The $b\alpha_s$ term (blue) is related to the difference in the hydrogen-bond acceptor constant in each conformation of the balance (e.g. solvent interactions with the formyl oxygen or the faces of aromatic rings). The $c\beta_s$ term (green) is related to changes in the hydrogen-bond donor ability of the balance in each conformation (e.g. solvent interactions with the aromatic protons). Finally, the term $d\alpha_s\beta_s$ (purple) encodes changes in solvophobic effects that might contribute to the conformational equilibrium.

The coefficients *a*, *b*, *c* and *d* in the equation $\Delta G_{fold} = a + b\alpha_s + c\beta_s + d\alpha_s\beta_s$, are unknowns that can be solved for every balance by fitting experimental folding free energies to this equation upon systematic variation of the solvent (i.e. with known α_s and β_s values).

2.10. Determination of the *a*, *b*, *c* and *d* coefficients

Table 2.4 shows how the *a*, *b*, *c* and *d* coefficients were determined in the case of the *N*-(4-fluorophenyl)-*N*-phenylformamide balance (**3**). The hydrogen bond donor and acceptor constants, α_s and β_s, for each solvent were obtained from the literature where in most cases they were experimentally measured.[22,58-60] The solver function in Excel was then used to obtain optimised *a*, *b*, *c* and *d* coefficients such that the sum of the squared difference between the experimental and fitted energies, $\Sigma(\Delta G_{exp} - \Delta G_{calc})^2$ was minimised. This process was then repeated to obtain the coefficients for the other balances.

Table 2.4. Determination of the *a*, *b*, *c* and *d* coefficients for the *N*-(4-fluorophenyl)-*N*-phenylformamide (**3**).

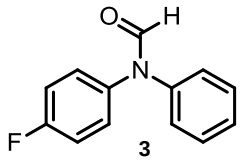

3

ΔG exp = -RTln(A/B)

ΔG calc = *a* + *b* α_s + *c* β_s + *d* $\alpha_s\beta_s$

Solvent	α_s	β_s	$\alpha_s\beta_s$	A/B	ΔG exp	ΔG calc	ΔG exp - ΔG calc	(ΔG exp - ΔG calc)²
Chloroform	2.2	0.9	2.0	1.59	-1.14	-1.00	-0.15	0.02151
Acetone	1.5	5.8	8.7	1.41	-0.85	-0.90	0.05	0.00258
Acetonitrile	1.7	5.1	8.7	1.37	-0.78	-0.89	0.11	0.01309
Benzene	1.1	2.1	2.3	1.32	-0.68	-0.95	0.27	0.07292
Ethyl acetate	1.5	5.3	8.0	1.54	-1.07	-0.91	-0.16	0.02585
Hexane	1.0	0.6	0.6	1.59	-1.14	-0.95	-0.19	0.03786
THF	0.9	5.9	5.3	1.43	-0.88	-0.96	0.07	0.00538
DCM	1.9	1.1	2.1	1.39	-0.81	-0.98	0.17	0.02790
Ethanol	2.7	5.3	14.3	1.39	-0.81	-0.81	-0.01	0.00003
Methanol	2.7	5.3	14.3	1.39	-0.81	-0.81	-0.01	0.00003
DMSO	2.2	8.7	19.1	1.35	-0.75	-0.73	-0.01	0.00014
Diethyl ether	0.9	5.3	4.8	1.56	-1.11	-0.96	-0.15	0.02250

Σ(ΔGexp - ΔGcalc)²	*a*	*b*	*c*	*d*
0.23	-0.89	-0.07	-0.03	0.03

2.11. Refinement of the solvation model using the *para*-substituted molecular torsion balances

The validity of the solvation model introduced above for the dissection of electrostatic and solvent effects was first examined using the *para*-substituted balances (Table 2.5). The conformational ratios, the ΔG_{exp} and ΔG_{calc} for the *para*-substituted balances for all the solvents can be found in the Chapter 6 – Table 6.3. The *a* term was determined as having the largest coefficient indicating that intramolecular electrostatic interactions were a major force governing the position of the conformational equilibrium. The *a* coefficients were seen to have negative values in balances bearing electron-donating substituents and positive values for the balances with electron-withdrawing substituents.

Table 2.5. The *a*, *b*, *c* and *d* coefficients determined for the *para*-substituted balances.

$$\Delta G_{calc} = a + b\,\alpha_s + c\,\beta_s + d\,\alpha_s\beta_s$$

X-substituent	*a*	*b*	*c*	*d*
NEt_2	-2.87	0.64	0.06	-0.01
OMe	-1.65	0.42	0.06	-0.02
H	-0.89	-0.07	-0.03	0.03
Br	0.45	-0.17	-0.01	0.00
CN	0.36	0.37	0.14	-0.15
NO_2	0.67	0.37	0.18	-0.17

The *a* coefficient should be expected to have the most obvious physical significance, since it should relate to the differences in the intramolecular electrostatic interactions in the A and B conformers. Thus, the *a* coefficients were initially correlated against the molecular electrostatic potentials (MEP) of simple X-substituted phenyl moieties calculated at the DFT/B3LYP/6-31G* level using the program Spartan '08. Table 2.6 lists the molecular electrostatic potentials corresponding to each *para*-substituted balance at the *ipso*, *ortho*, ring centre and *ortho* aromatic proton positions of the X-substituted ring with respect to the point of attachment to the nitrogen atom of the formyl group.

The MEP calculated at the *ipso* position of the substituted aromatic ring gave a linear correlation with the electrostatic term *a* with an $R^2 = 0.89$ (Figure 2.25). Given the simplicity of the model system, this correlation was not considered satisfactory and prompted closer examination of the *b*, *c* and *d*, coefficients.

Table 2.6. The molecular electrostatic potentials at different points on the surfaces of the *para*-substituted balances.

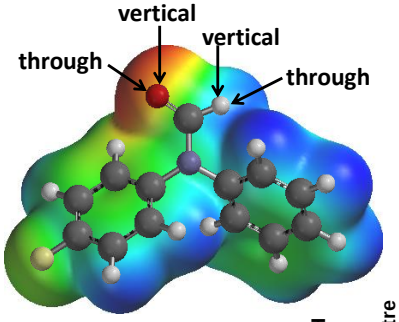

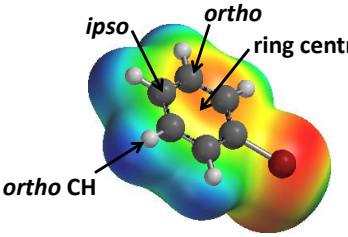

X-substituent	MEP *ipso*	MEP *ortho*	MEP *ortho* CH	MEP ring centre	MEP through O bond (conf. A)	MEP vertical O bond (conf. A)	MEP vertical H bond (conf. A)	MEP through H bond (conf. A)	MEP through O bond (conf. B)	MEP vertical O bond (conf. B)	MEP vertical H bond (conf. B)	MEP through H bond (conf. B)
NEt_2	-104.7	-96.5	44.5	-113.4	-189	-187.1	7.5	51.4	-194.5	-187.9	10.9	53.5
OMe	-82.4	-76.8	60.5	-84.1	-182.7	-184.8	23.3	64	-186	-185.4	26	68
H	-70.6	-70.6	64.2	-84.4	-178.4	-178.3	33.2	71.4	-178.7	-178.1	33.8	74.2
Br	-41.3	-40.9	90.2	-44.5	-166.3	-167.6	46.1	89.2	-161.9	-164.9	47.5	87.5
CN	-11.7	-14.6	109.3	-12	-153	-152.1	65.9	109.8	-144	-149	64.1	104.3
NO_2	-3.3	-7.5	113.2	0.1	-148.6	-148	71.1	115.3	-138.6	-144.1	68.3	108.9

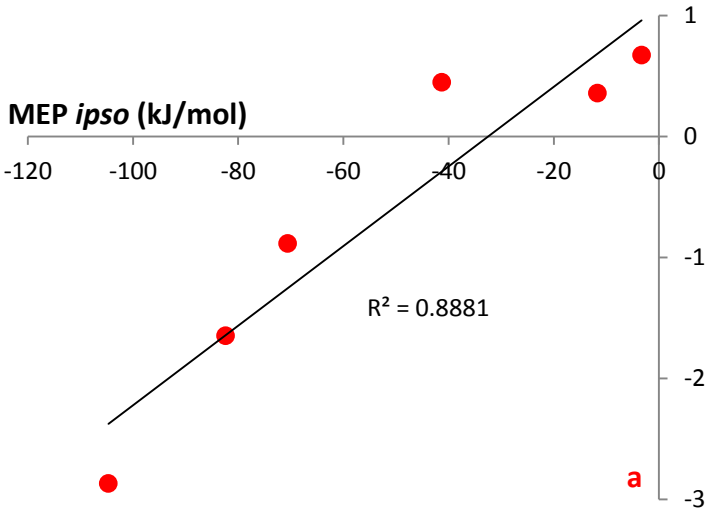

Figure 2.25. Graph correlating the *a* coefficient for the *para*-substituted balances with the molecular electrostatic potential at the *ipso* position defined in Table 2.6.

While the *b* coefficient was significant for many of the balances, the *c* and *d* coefficients, which correspond to the change in the hydrogen bond donor ability of the balance in the A and B conformers, and the desolvation term respectively, were generally found to be quite small (Table 2.5). Furthermore, due to the similar steric influence of the proton and oxygen of the formyl group in each conformer, it could be reasonably anticipated that changes in the desolvation coefficient *d* might not be significant. For these reasons it was decided to recalculate the *a*, *b* and *c* coefficients with the *d* coefficient set to 0, and these new values are listed in Table 2.7.

Table 2.7. *a*, *b* and *c* coefficients determined from experimental folding free energies in a range of solvents for the *para*-substituted balances when coefficient $d = 0$.

$$\Delta G_{calc} = a + b\,\alpha_s + c\,\beta_s$$

X-substituent	a	b	c
NEt_2	-2.78	0.59	0.04
OMe	-1.51	0.34	0.03
H	-1.10	0.06	0.02
Br	0.48	-0.19	-0.02
CN	1.76	-0.36	-0.14
NO_2	2.34	-0.50	-0.16

The new values for the *a* coefficient after the setting $d = 0$ were then correlated with the MEP values as before. The new correlations were much improved compared to the previous model where $d \neq 0$ ($R^2 = 0.89$), giving correlations with $R^2 = 0.998$ and

0.997 for the *ipso* and *ortho* positions of the *para*-substituted aromatic ring respectively (Figure 2.26).

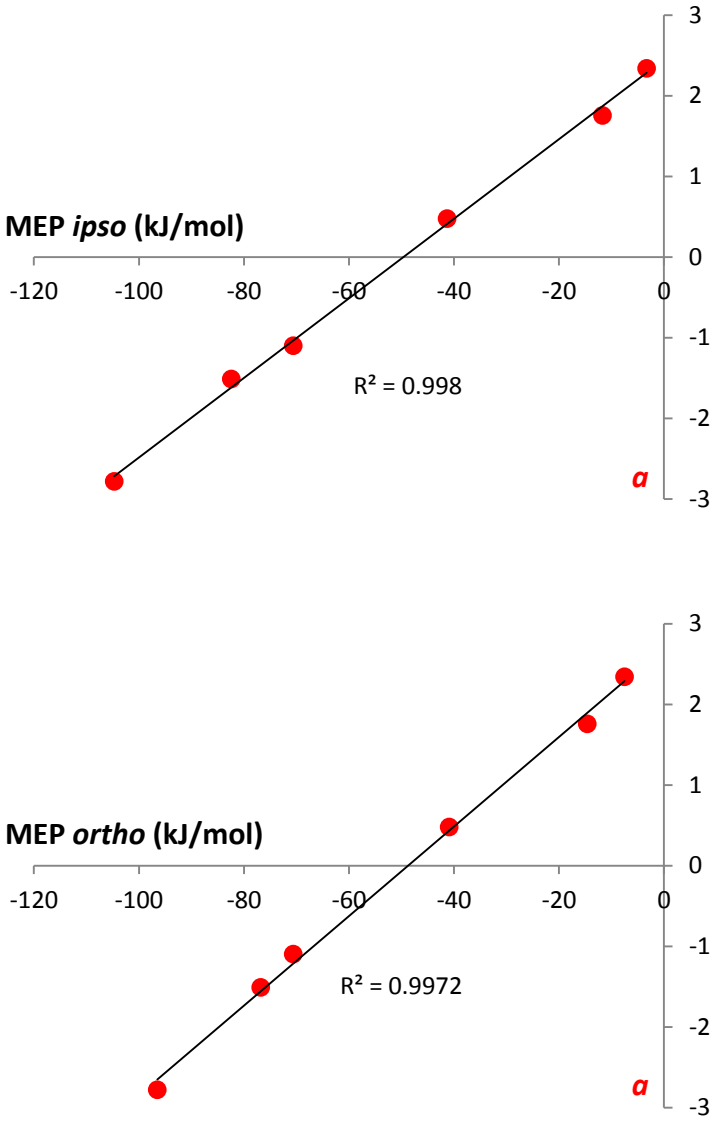

Figure 2.26. Graphs correlating the *a* coefficient, when *d* = 0, for the *para*-substituted balances with the molecular electrostatic potential at the *ipso* and *ortho* position.

The qualities of these correlations suggest that the dissection of solvent effects using the Hunter model was possible, and that the model is improved if desolvation

effects are not included. Thus, it was decided to apply this refined solvation model to the data for all of the molecular balances synthesised as described below.

2.12. Dissection of solvent and intramolecular effects for all molecular torsion balances using the refined solvation model

The refined solvation model where $d = 0$ was applied to all of the torsion balances to determine the *a*, *b* and *c* coefficients (Table 2.8).

Table 2.8. The *a*, *b* and *c* coefficients for all the balances after setting $d = 0$.

X-substituent	compound number	a	b	c
NEt_2	6	-2.78	0.59	0.04
OMe	7	-1.51	0.34	0.03
H	3	-1.10	0.06	0.02
Br	5	0.48	-0.19	-0.02
CN	10	1.76	-0.36	-0.14
NO_2	11	2.34	-0.50	-0.16
o-Me	14	-2.06	0.84	0.17
o-OMe	15	-2.30	0.75	0.05
o-NO_2	17	3.80	0.12	0.03
Ph	26	-0.59	0.00	0.00
PhdiMe	27	-0.90	0.03	0.03
PhdiEt	28	-0.87	-0.05	0.05
$PhNH_2$	29	-0.28	-0.01	-0.05
PhdiOMe	30	-2.38	0.27	0.11
PhdiOMetBu	34	-0.65	-0.19	0.05
Ph(*o*-diNO_2)	43	-0.65	-0.03	0.01
Ph(*m*-diNO_2)	44	1.54	-0.36	-0.14

Table 2.9 shows the calculated free energies from the solvation model for all the balances in the range of different solvents used in this study. Figure 2.27 shows the correlation of the calculated and experimental folding free energies for all of the balances in each solvent. The closer to the line the points appear in the graph, the closer the calculated and experimental values. The quality of this correlation (R^2 = 0.96) indicates that the solvation model is reasonable, and suggests that the derived *a*, *b* and *c* coefficients may appropriately encode the intramolecular and solvent effects.

Table 2.9. The ΔG_{calc} for all the balances across the different solvents, when $d = 0$.

Δ*G* calc	**Chloroform**	**Acetone**	**Acetonitrile**	**Benzene**	**Ethyl acetate**	**Hexane**	**THF**	**DCM**	**Ethanol**	**Methanol**	**DMSO**	**Diethyl ether**
NEt_2	-1.45	-1.67	-1.58	-2.05	-1.69	-2.17	-2.01	-1.62	-0.98	-0.98	-1.14	-2.04
OMe	-0.74	-0.82	-0.78	-1.07	-0.84	-1.15	-1.02	-0.83	-0.43	-0.43	-0.49	-1.04
H	-0.94	-0.88	-0.89	-0.99	-0.89	-1.02	-0.92	-0.96	-0.82	-0.82	-0.78	-0.93
Br	0.05	0.10	0.07	0.24	0.11	0.28	0.21	0.10	-0.12	-0.12	-0.08	0.22
CN	0.83	0.40	0.43	1.06	0.47	n.s.	0.61	0.91	0.04	0.04	-0.26	0.69
NO_2	1.10	0.68	0.69	1.46	0.76	n.s.	0.97	1.22	0.16	0.16	-0.12	1.06
***o*-Me**	-0.05	0.18	0.23	-0.78	0.10	-1.11	-0.31	-0.27	1.11	1.11	1.26	-0.41
***o*-OMe**	-0.61	-0.87	-0.75	-1.36	-0.89	-1.52	-1.31	-0.82	0.00	0.00	-0.19	-1.34
***o*-NO_2**	4.09	4.13	4.14	n.s.	4.12	n.s.	4.06	4.06	4.27	4.27	4.30	4.05
Ph	-0.59	-0.61	-0.60	-0.60	-0.60	n.s.	-0.61	-0.59	-0.60	-0.60	-0.61	-0.61
PhdiMe	-0.82	-0.70	-0.71	-0.81	-0.71	n.s.	-0.71	-0.82	-0.68	-0.68	-0.59	-0.73
PhdiEt	-0.92	-0.64	-0.68	-0.81	-0.66	-0.88	-0.60	-0.90	-0.72	-0.72	-0.52	-0.63
$PhNH_2$	-0.33	-0.55	-0.52	-0.38	-0.53	n.s.	-0.55	-0.34	-0.54	-0.54	-0.69	-0.52
PhdiOMe	-1.69	-1.36	-1.38	-1.86	-1.42	n.s.	-1.52	-1.75	-1.09	-1.09	-0.87	-1.58
PhdiOMetBu	-1.02	-0.63	-0.71	-0.75	-0.66	-0.81	-0.52	-0.95	n.s.	-0.89	-0.62	-0.55
Ph(*o*-diNO_2)	-0.70	-0.61	-0.62	-0.65	-0.61	n.s.	-0.59	-0.69	n.s.	-0.65	-0.58	-0.60
Ph(*m*-diNO_2)	0.62	0.17	0.20	0.84	0.24	n.s.	0.37	0.70	n.s.	-0.19	-0.50	n.s.

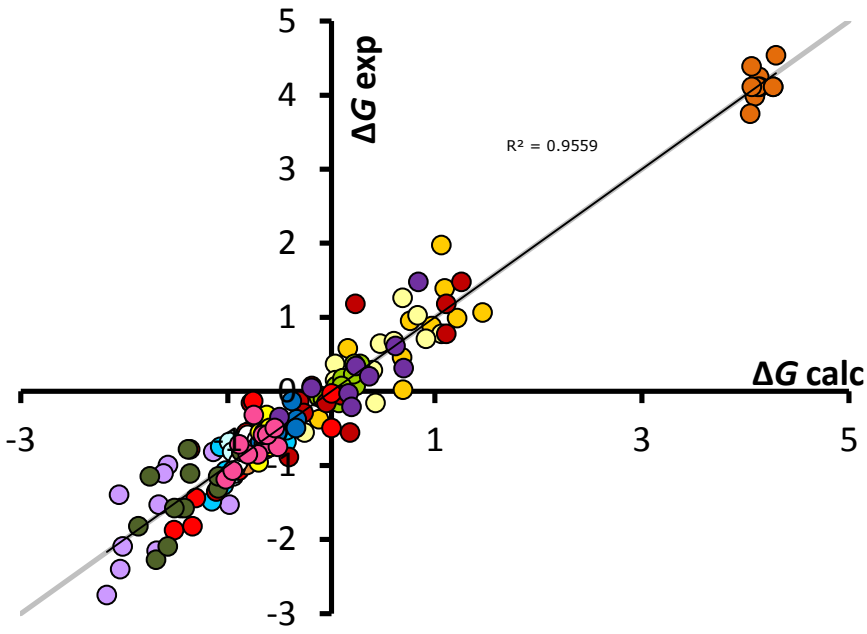

Figure 2.27. Graph correlating the ΔG_{calc} and ΔG_{exp} for all the balances (every balance has a different colour of points) in all the solvents.

2.13. Physical interpretation of the *a*, *b* and *c* coefficients

Having established that this simple solvation model seems capable of describing conformational free energies in this series of molecular balances, it becomes necessary to determine whether the derived *a*, *b* and *c* coefficients are physically meaningful and provide any physicochemical insight.

Analysis of the *a* coefficient for all balances

According to the solvation model employed, the *a* coefficient is proposed as corresponding to the intramolecular electrostatic effect on the position of the conformational equilibrium. The large magnitude of the *a* coefficient in most cases suggests that following dissection of solvent effects, intramolecular electrostatic effects has the largest influence on the conformational behaviour of the balances. The *a* coefficient had negative values for the EDG and positive values for the EWG, which is

consistent with the electrostatic intramolecular effects described in Section 2.8-Table 2.1. To further test the electrostatic model initially examined using the *para*-substituted series, each substituted aromatic ring was minimised at the DFT/B3LYP/6-31G* level in Spartan '08 and the molecular electrostatic potential (MEP) was taken at various positions (Tables 2.6 and 2.10).

Two MEP values were recorded for the non-identical *ortho*-positions in the *ortho*-substituted series, from which the average MEP was also calculated. The values for the *ipso*, *ortho* and ring centre positions for the mono-substituted $PhNH_2$ biphenyl model for compound **(29**) were taken on the same side as the NH_2 group, as these values were found to correlate better compared to the values of the other side of the molecule (Table 2.10).

Table 2.10. The MEPs for the substituted aromatic rings and biphenyls at the *ipso* and *ortho* positions with respect to the point of attachment to the nitrogen atom of the formyl group. For the *ortho*-substituted rings the *ortho* MEP is taken on both the unsubstituted and substituted aromatic carbons. The MEP for the *para*-substituted series were given in Table 2.6 above.

X-substituent	MEP *ipso*	MEP *ortho* 1	MEP *ortho* 2 (substituent)	MEP *ortho average*
***o*-Me**	-74.4	-74.3	-61.0	-67.7
***o*-OMe**	-75.3	-76.1	-53.4	-64.8
***o*-NO_2**	-4.80	-7.7	7.8	0.0
Ph	-66.4	-66.1	-	-
PhdiMe	-64.5	-62.9	-	-
PhdiEt	-62.4	-61.6	-	-
$PhNH_2$	-56.8	-55	-	-
PhdiOMe	-95.5	-97.9	-	-
PhdiOMetBu	-61.0	-60.5	-	-
Ph(*o*-diNO_2)	-63.9	-68.5	-	-
Ph(*m*-diNO_2)	-16.4	-15.3	-	-

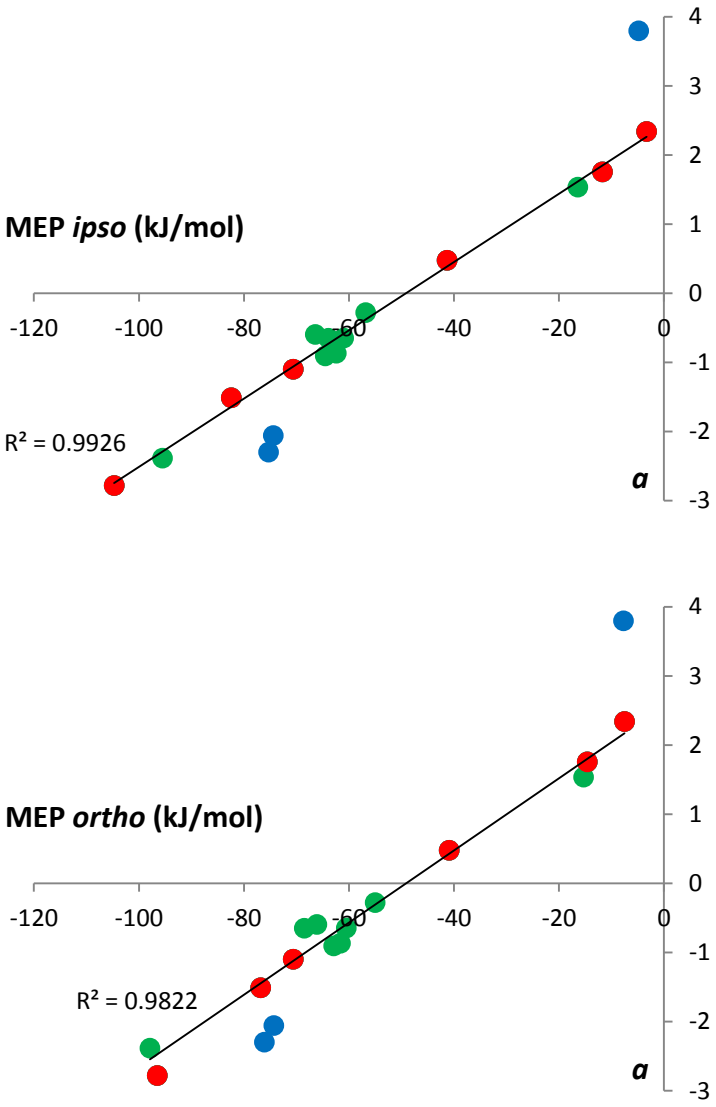

Figure 2.28. Graphs correlating the *a* coefficient with the MEP at the *ipso* and *ortho* positions. The red points correspond to the *para*-series, the blue points to the *ortho*-series and the green points to the extended balances. The best fit lines correspond to the *para*-extended pair of series.

The correlations in Figure 2.28 of the *a* coefficient against the MEP in both the *ortho* and *ipso* positions are excellent for all the series examined ($R^2 > 0.9$). Even the extreme case of the *ortho*-NO_2 balance (**17**) (*a* = 3.80), which is unusual in that it had

very large positive folding free energies in all solvents examined can be accounted for, which points to the dominance of intramolecular electrostatic effects in this example.

The results of the model analysis were further tested by correlating the electrostatic coefficient *a* for each balance against the difference in energy between the two conformers of each molecular balance calculated for the minimised structures in the gas-phase using Spartan '08 at the DFT/B3LYP/6-31G* (Table 2.11).

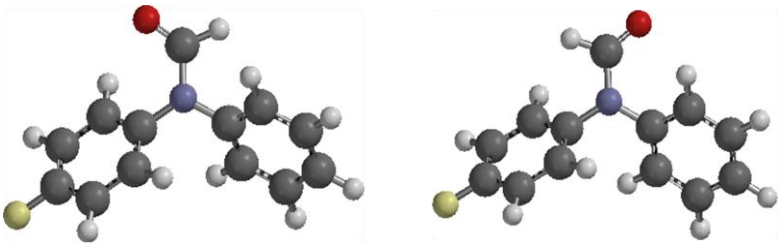

Conformer A **Conformer B**

Table 2.11. *a* coefficients for all balances and the B3LYP/6-31G* energies and differences calculated in Spartan '08.

X-substituent	a	E (kJ/mol) conf. A	E (kJ/mol) conf. B	ΔE (kJ/mol) A-B
H	-1.10	-1919817.02	-1919816.13	-0.89
Br	0.48	-8675968.28	-8675968.95	0.67
NEt_2	-2.78	-2477995.06	-2477991.35	-3.71
OMe	-1.51	-2220496.48	-2220494.45	-2.03
CN	1.76	-2161998.43	-2162001.02	2.59
NO_2	2.34	-2456733.13	-2456736.2	3.07
o-Me	-2.06	-2023045.22	-2023044.03	-1.19
o-OMe	-2.30	-2220490.2	-2220487.11	-3.09
o-NO_2	3.80	-2456702.52	-2456709.03	6.51
Ph	-0.59	-2526459.38	-2526458.93	-0.45
PhdiMe	-0.90	-2732900.24	-2732899.47	-0.77
PhdiEt	-0.87	-2939331.65	-2939330.64	-1.01
$PhNH_2$	-0.28	-2671786.29	-2671785.92	-0.37
PhdiOMe	-2.38	-3127802.49	-3127798.97	-3.52
PhdiOMetBu	-0.65	-3953499.15	-3953497.7	-1.45
Ph(o-diNO_2)	-0.65	-4013108.96	-4013108.09	-0.87
Ph(m-diNO_2)	1.54	-3600279.47	-3600282.38	2.91

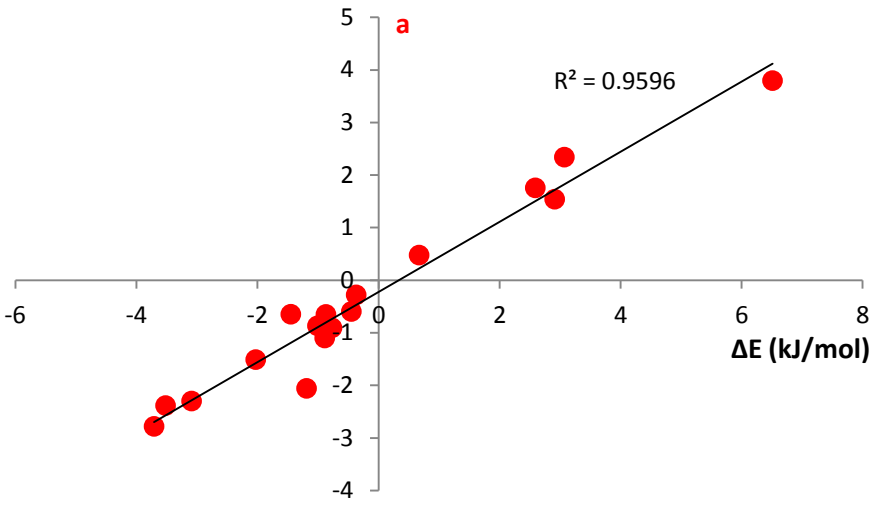

Figure 2.29. Graph correlating the *a* coefficient for all the balances with the difference of the energy between the two conformers calculated in Spartan '08 using B3LYP/6-31G*.

Figure 2.29 reveals an excellent correlation of the *a* coefficient with these gas-phase folding free energies (R^2 = 0.96). This correlation and those with MEPs (Figure 2.28) indicate that this approach allows intramolecular electrostatic effects (encoded by *a*) to be dissected from the solvation phenomena encoded by the *b* and *c* coefficients.

Analysis of the *b* coefficient for all balances

The derived *b* coefficients refer to the solvation of the balance when the solvent acts as a hydrogen bond donor. Potential solvation points by hydrogen-bond donors include the faces of the aromatic rings, the oxygen atom of the formyl group and in some cases, electron-rich aromatic substituents. Thus, the MEP on the ring centre and on the formyl oxygen (through O bond) and parallel to the carbon – nitrogen bond (vertical O bond) were calculated as before and listed in Table 2.12.

Table 2.12. The MEP values for potential hydrogen-bond acceptor sites in the molecular balances. Corresponding MEP values for the *para*-substituted series are given in Table 2.6 above.

X-substituent	MEP through O bond (conf. A)	MEP vertical O bond (conf. A)	MEP through O bond (conf. B)	MEP vertical O bond (conf. B)	MEP ring centre
***o*-Me**	-174.2	-178.1	-182	-180.2	-88.7
***o*-OMe**	-186.6	-188.4	-196.1	-193.9	-84.1
***o*-NO_2**	-168.2	-166.9	-180	-179.5	0.1
Ph	-178.6	-179	-177.4	-177.2	-77.5
PhdiMe	-177.3	-177.8	-177	-176.7	-74.9
PhdiEt	-176.9	-177.8	-175.6	-176.1	-69.4
$PhNH_2$	-177.8	-178.7	-174.1	-176	-63.6
PhdiOMe	-189.7	-190.5	-190.2	-188.8	-118
PhdiOMetBu	-178.5	-178.2	-179.8	-177.9	-61
Ph(*o*-diNO_2)	-178.3	-179.7	-176.7	-176.7	-78.9
Ph(*m*-diNO_2)	-155.5	-154.9	-144.3	-149.7	-16.5

The graphs in Figure 2.30 show the correlation of the coefficient *b* with the MEP values taken at different hydrogen-bond acceptor sites. Although some trends are seen, no single site of solvation by hydrogen-bond donors can be derived across all of the series. The situation is likely to be further complicated by the differing conformational preferences of the *ortho*-substituted balances. However, it can be seen that the correlations with the MEPs of the formyl group oxygen give the best correlation across all three series of balances examined.

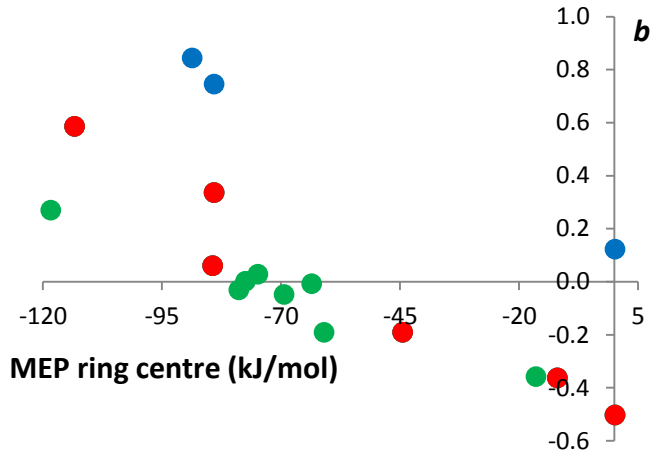
b
1.0
0.8
0.6
0.4
0.2
0.0
-0.2
-0.4
-0.6
-120
-95
-70
-45
-20
5
MEP ring centre (kJ/mol)

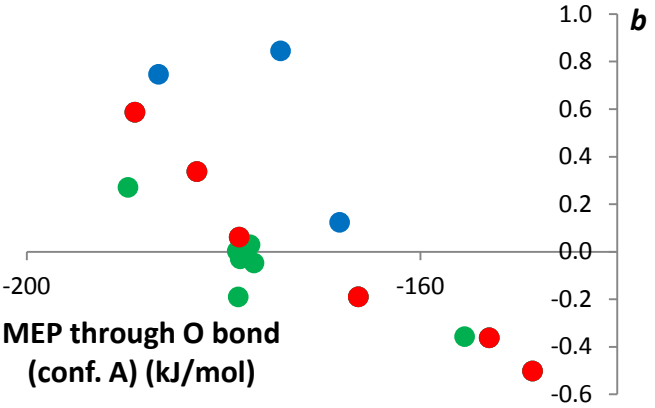
b
1.0
0.8
0.6
0.4
0.2
0.0
-0.2
-0.4
-0.6
-200
-160
MEP through O bond
(conf. A) (kJ/mol)

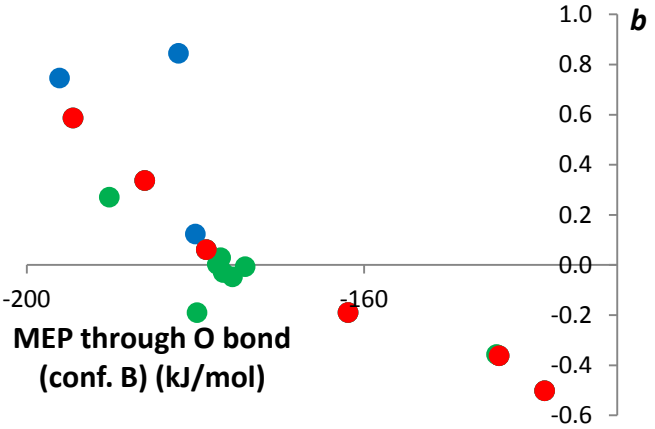
b
1.0
0.8
0.6
0.4
0.2
0.0
-0.2
-0.4
-0.6
-200
-160
MEP through O bond
(conf. B) (kJ/mol)

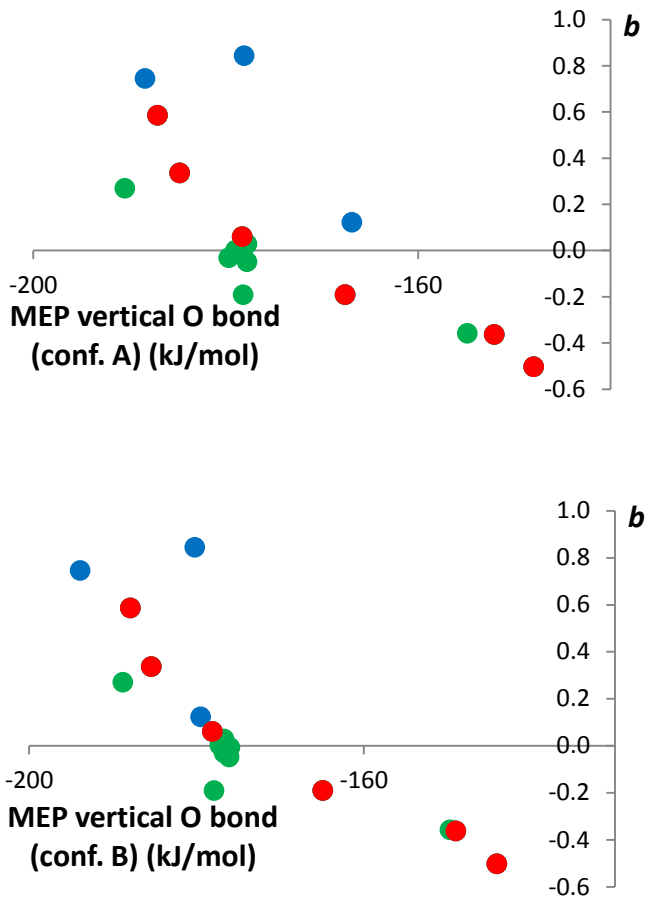

Figure 2.30. Graphs correlating the *b* coefficient with the MEPs at the ring centre and at the formyl oxygen. The red points correspond to the *para*-series, the blue points to the *ortho*-series and the green points to the extended balances.

Analysis of the *c* coefficient for all balances

The coefficient *c*, was found to be one of the smaller coefficients in the analysis described above. It can be interpreted as arising from the solvation of the balance when the solvent acts as a hydrogen bond acceptor. Again, it might be expected that prediction of a single major solvation site will be difficult, since potential solvation sites include the aromatic protons, the hydrogen atom of the formyl group and the solvation of the substituent in some cases. Thus, the MEP on the *ortho* aromatic proton and on the

formyl proton (through H bond) and parallel to the carbon – nitrogen bond (vertical H bond) were calculated as before and listed in Table 2.13.

Table 2.13. The MEP for hydrogen-bond donor sites in the molecular balances. The MEP for the *para*-substituted series are given above in Table 2.6.

X-substituent	MEP through H bond (conf. A)	MEP vertical H bond (conf. A)	MEP through H bond (conf. B)	MEP vertical H bond (conf. B)	MEP *ortho* aromatic CH
***o*-Me**	68.1	27.7	74.6	33.6	59.9
***o*-OMe**	59.6	19.2	58.4	18.7	60.5
***o*-NO_2**	94.6	47.9	82.7	40.3	113.2
Ph	72.9	32.5	75.3	33.4	66.8
PhdiMe	74.3	33.5	75.3	35.6	67.4
PhdiEt	74.8	33.8	75.2	35.3	67.9
$PhNH_2$	77.3	34.3	75.3	36.2	66.2
PhdiOMe	53.3	15.7	63	21.4	43.9
PhdiOMetBu	73.2	32.1	75	34.4	64.8
Ph(*o*-diNO_2)	69	32.3	75.4	35.7	71.4
Ph(*m*-diNO_2)	106.5	61.4	103.7	63.4	107.1

The graphs in Figure 2.31 show the correlation of the coefficient *c* with the calculated MEPs at the *ortho* aromatic proton and the formyl proton for all the three series of balances. As for the *b* coefficient, weak correlations are seen with the *c* coefficient against the MEPs of various points on the balances. Once again the *ortho*-substituted balances are seen to be the largest outliers, which may be due to solvation or conformational differences compared to the *para*-substituted balances.

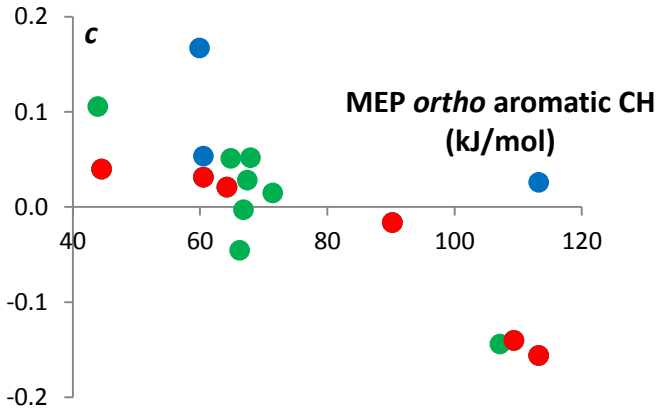
c
MEP ortho aromatic CH (kJ/mol)
0.2
0.1
0.0
-0.1
-0.2
40
60
80
100
120

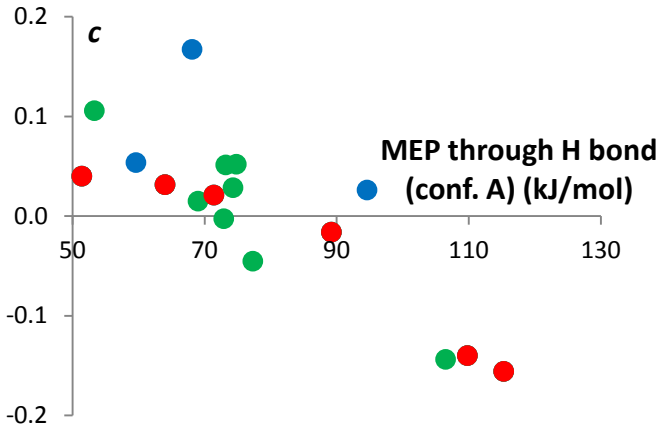
c
MEP through H bond (conf. A) (kJ/mol)
0.2
0.1
0.0
-0.1
-0.2
50
70
90
110
130

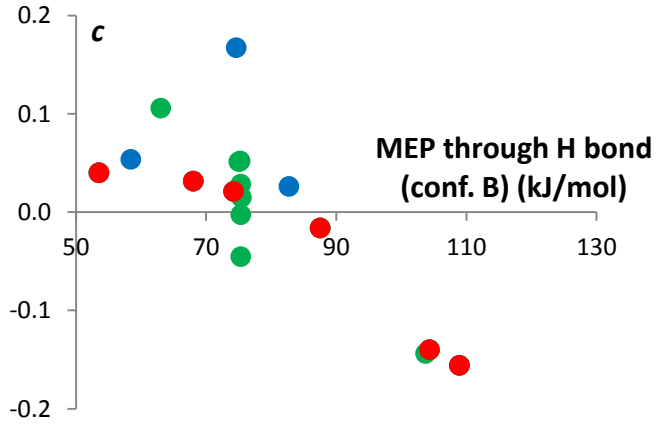
c
MEP through H bond (conf. B) (kJ/mol)
0.2
0.1
0.0
-0.1
-0.2
50
70
90
110
130

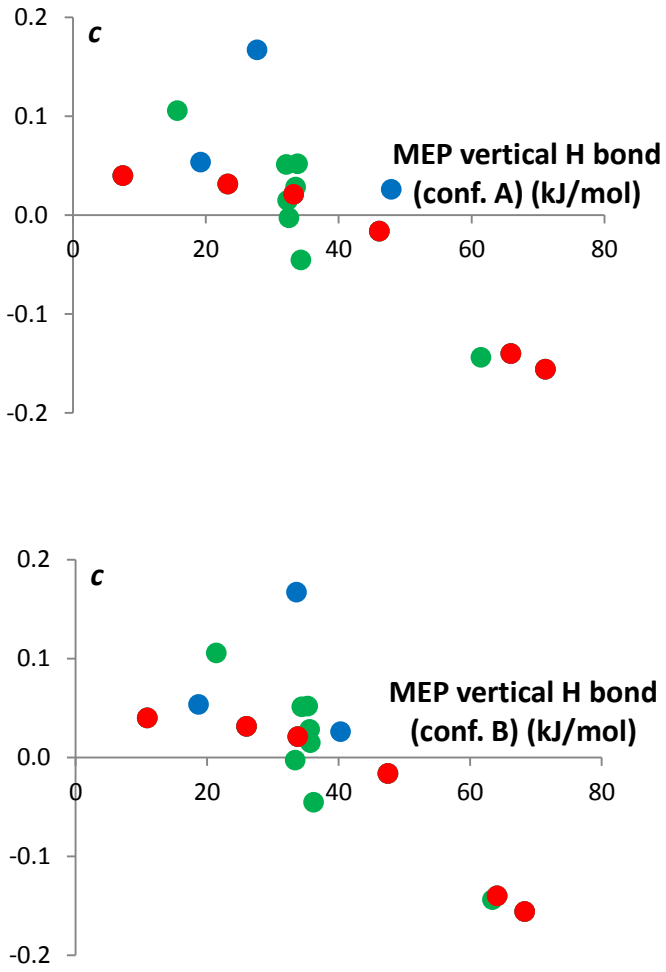

Figure 2.31. Graphs correlating the *c* coefficient with the MEPs at the *ortho* aromatic CH and at the formyl proton. The red points correspond to the *para*-series, the blue points to the *ortho*-series and the green points to the extended balances.

Overall, this electrostatic analysis indicates that the *b* and *c* coefficients cannot be wholly attributed to solvation of single hydrogen bond donor or acceptor sites. Nonetheless, the most polar sites are likely to have the most significant contributions to the *b* and *c* coefficients. This assertion is supported by the smaller magnitudes of the *c* coefficient compared to the *b* coefficient. Since the formyl oxygen is much more polar (–190 kJ mol^{-1} when X = *p*-NEt_2 and –144 kJ mol^{-1} when X = *p*-NO_2) than the edges of

the aromatic rings (X = +45 kJ mol^{-1} when X = *p*-NEt_2 and +113 kJ mol^{-1} when X = *p*-NO_2) it can be expected that there is a larger difference between the hydrogen-bond acceptor ability in conformer A vs. B compared to the changes in the hydrogen-bond donor ability.

2.14. The interplay of intramolecular and solvent effects: rationalising interesting observations

Closer examination of the folding free energies reveals some interesting trends in the conformational behaviour of the balances that might arise from the interplay of intramolecular and solvent effects. For example, balances bearing strongly electron-withdrawing substituents were seen to prefer conformer A in polar solvents, while conformer B was preferred in apolar solvents (Figure 2.32). Therefore, it is worth examining whether the proposed solvation model is able to rationalise these observations.

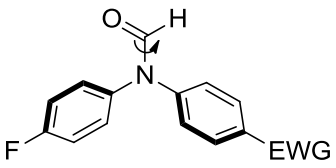

A major conformer in polar solvents

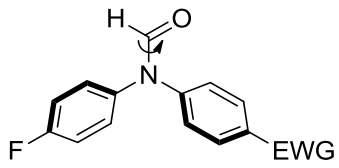

B major conformer in apolar solvents

Figure 2.32. A is the major conformer in polar solvents when the X-substituent is a strong EWG, but B dominates in apolar solvents.

The observation that the preferred conformer switches in a solvent-dependent manner while the X-substituent remains constant indicates that solvent effects in the most polar solvents must dominate over the intramolecular electrostatic effects. This raises the question of whether the derived *b* and *c* parameters are able to account for the effects of the solvent on these electron-poor balances, or whether some additional explanation is required.

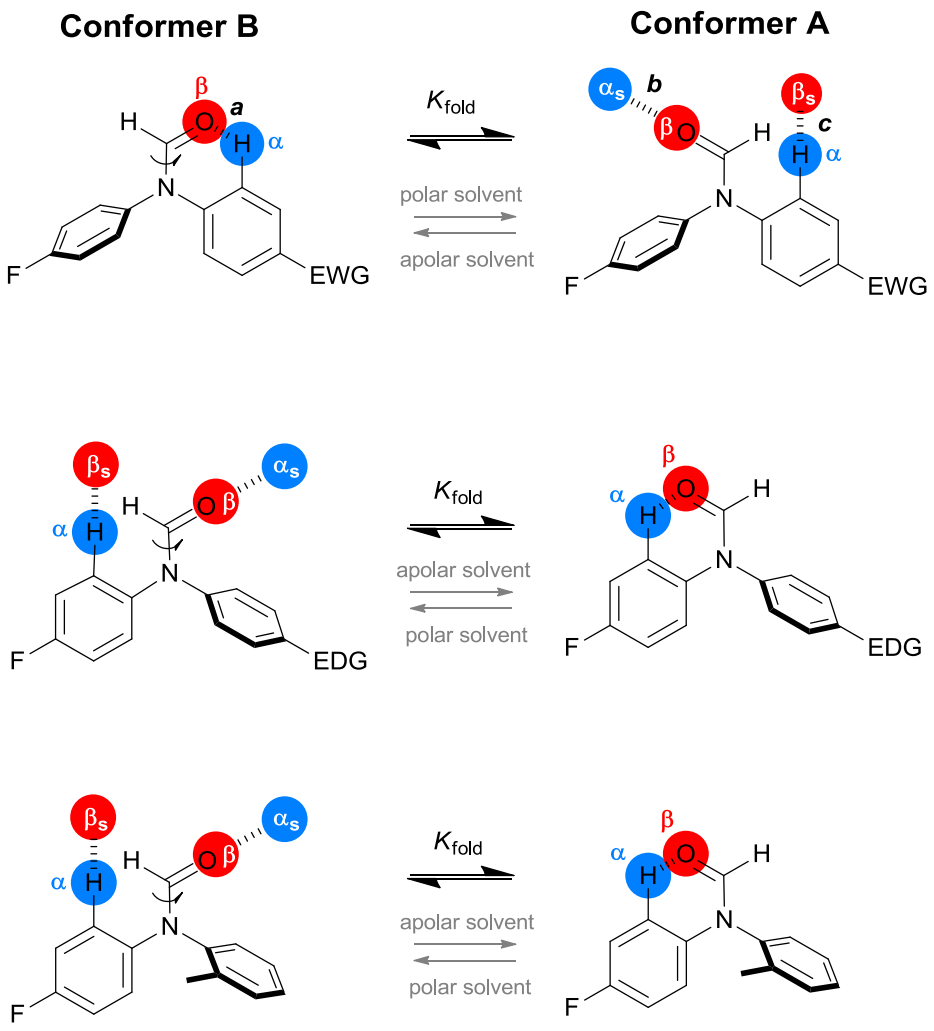

Figure 2.33. The major conformations and the favoured interactions in the presence of a polar or apolar solvent for EWG, EDG and *ortho*-substituted balances.

Taking the example of balance **11**, where X = *p*-NO_2, it can be seen that b = –0.50 and c = –0.16. In other words, increasing the hydrogen-bond donor or acceptor constant of the solvent contributes to driving the equilibrium towards conformer A (–ve ΔG). The model is most easily understood with the assistance of the schematic equilibria shown in Figure 2.33. Although the specific sites of solvation cannot be identified using MEP values (see graphs above), it is still possible to rationalise the conformational

equilibrium as being determined by the relative competition of the intramolecular interaction between the formyl oxygen and the aryl rings vs. solvation of these sites in the A and B conformers. According to this hypothesis, when a balance bearing a strong EWG is dissolved in an apolar solvent, then an internal hydrogen bond between the formyl group oxygen and the polar aromatic proton of the EWG-substituted ring dominates the position of the conformational equilibrium as indicated by the large positive *a* coefficient. In contrast, a solvent with a strong ability to accept hydrogen bonds such as DMSO will compete with the formyl oxygen in the binding of the polar aromatic protons, driving the equilibrium towards conformation A (Figure 2.33, top).

However when X is an EDG (Figure 2.33, centre) the favourable oxygen interaction with the edge of the slightly more polar fluorine-substituted ring (and repulsion from the electron-rich aromatic ring) is more important than the equivalent interaction with the X-substituted ring, and hence the *a* coefficient is negative. Under these circumstances a polar solvent competes with these intramolecular interactions and has the effect of driving the conformation towards the B conformer.

This interpretation involves consideration of the conformation of the aromatic rings as the substituents and solvents are varied. Unlike the C-N bond in the formyl group, the N-aryl bonds are rotating rapidly on the NMR timescale and are therefore not observed as discrete conformer signals in the NMR spectra. In the crystal structures of analogues of these compounds, aromatic rings bearing EWGs are more planar with the adjacent amide group, whilst rings bearing EDGs are twisted further from the plane of the amide (Figure 2.34). Similar effects can be expected in solution as shown in Figure 2.33 above, and balances bearing EDGs in apolar solvents are likely to prefer average conformations where the fluorine-substituted ring lies close to the plane of the formyl group. However, rings bearing a strong EWG X-substituent would favour a more planar conformation that allows conjugation between the EWG and the lone pair electrons of the formamide nitrogen, particularly in conformer B where an intramolecular interaction can take place between the formyl oxygen and the edge of the polar aromatic ring.

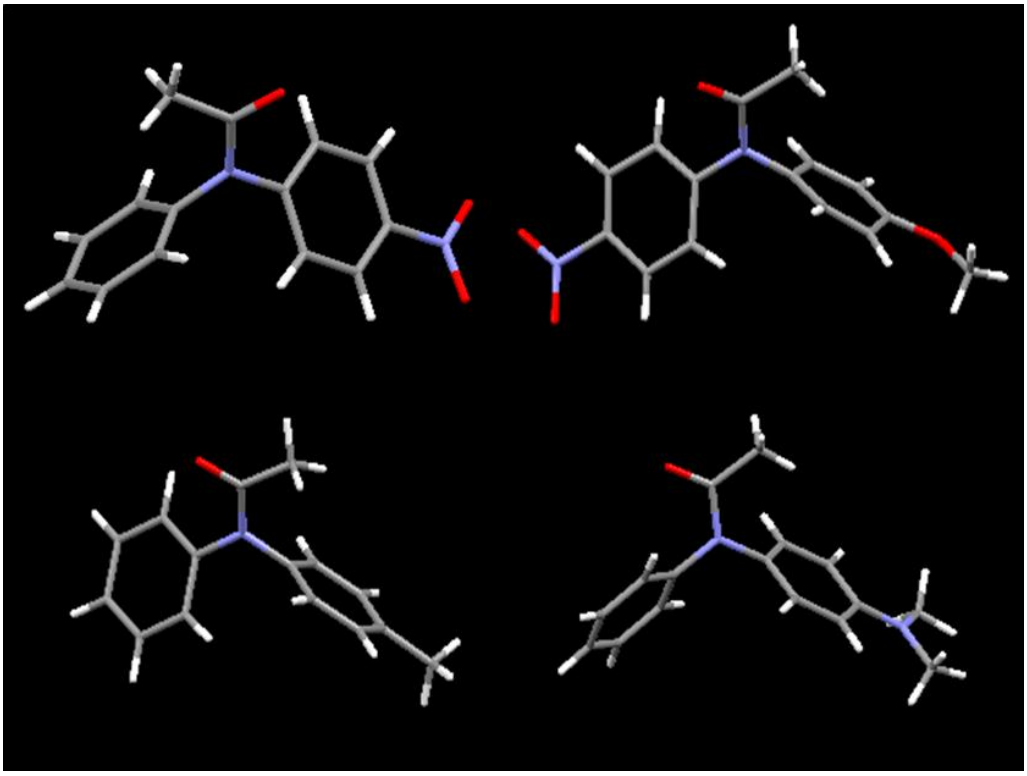

Figure 2.34. Crystal structures with EDG and EWG at the *para* positions of the aromatic rings from the CCDB (CCDB codes: LUVREZ, UHOPIQ, LUVRID, UHOPOW)

Other interesting effects can be seen in the *b* and *c* coefficients of the *ortho*-substituted balances, which are positive even when X = *ortho*-NO_2 (Table 2.8). This observation is striking since the balances substituted with *para*-EWGs have negative values for both *b* and *c* coefficients due to the solvation effects discussed above. Crystal structures and computational modelling show that *ortho*-substituents twist the substituted ring out of the plane of the formamide as shown at the bottom of Figure 2.33. This model explains the positive *b* and *c* coefficients. In conformer A, a weak internal H-bond can be formed with the edge of the fluorine-substituted ring in apolar solvents. However, in conformer B, the twist of the *ortho*-substituted ring makes this internal interaction impossible and the formyl oxygen and the edges of the ring will be more readily solvated. This results in larger positive *b* and *c* coefficients than seen in most of

the *para*-substituted balances since conformer B is always most readily solvated than conformer A due to the lack of a competitive aromatic edge-oxygen interaction.

Furthermore, some of the extended balances show some interesting results, which seemed unusual based on the expected through-bond electron-withdrawing or donating properties of the substituents on the third aromatic ring. These results fit within the model described above and reveal interesting electronic phenomena which are the focus of Chapter 3.

The analysis above shows that the solvation model employed can be used to isolate electrostatic effects on the position of conformational equilibria, and although specific solvation sites cannot always be determined, the dissected coefficients still facilitate physical interpretations that provide insights into the solvation of small molecules.

2.15. Conclusions

A new class of molecular torsion balances featuring a slowly rotating tertiary formyl amide was synthesised and fully characterised using NMR spectroscopy. The experimental folding free energy for each balance in a variety of solvents was determined using the equation $\Delta G = -RT\ln K_{fold}$, where K_{fold} was found from the integration of the peaks corresponding to the two conformers in the NMR spectra. Initial analyses revealed linear correlations between the folding free energies of the *para*-substituted balances and the Hammett constants of the substituents, which indicated that the trends in the conformational equilibrium are governed by intramolecular electrostatic effects, but the solvent has a large influence on the magnitude of these interactions.

It was possible to dissect the electrostatic interaction and the solvation effects on each balance by fitting the results to the equation $\Delta G_{calc} = a + b\alpha_s + c\beta_s$. The *a* coefficient correlated linearly with both calculated molecular electrostatic potentials and DFT/B3LYP/6-31G* folding energies, confirming the electrostatic origin of *a*. The *b* and *c* coefficients also correlated with calculated MEPs, but the lower quality correlations suggested that a dominant solvation point could not be unambiguously

identified. Nonetheless, the magnitude of the *b* and *c* coefficients provided mechanistic insights into the changes in the intramolecular interactions, conformational effects and competitive solvent interactions as the structures and properties of the balances were varied. Interpretation of the *a*, *b*, and *c* coefficients even allowed apparently anomalous behaviour of some balances to be fully accounted for within the same solvation model.

The approach provides a general method for dissecting electrostatic and solvent effects to reveal pseudo gas-phase behaviour from experimental data obtained in solution. Fundamental insights may be gained through this ability to deconvolute some of the major factors governing molecular behaviour in solution.

2.16. Acknowledgements

Catherine Adam performed the synthesis, characterisation and solvent studies for molecular torsion balances **7**, **10**, **11**, **14**, **15** and **17**.

2.17. References

1. Hughes, R. M.; Waters, M. L., *Curr. Opin. Struct. Biol.* **2006**, 16, 514-524.
2. Brandl, M.; Weiss, M. S.; Jabs, A.; Suhnel, J.; Hilgenfeld, R., *J. Mol. Biol.* **2001**, 307, 357-377.
3. Liu, H.; Gao, J.; Lynch, S. R.; Saito, Y. D.; Maynard, L.; Kool, E. T., *Science* **2003**, 302, 868-871.
4. Egli, M.; Tereshko, V.; Mushudov, G. N.; Sanishvili, R.; Liu, X.; Lewis, F. D., *J. Am. Chem. Soc.* **2003**, 125, 10842-10849.
5. Kryger, G.; Silman, I.; Sussman, J. L., *J Physiol. (Paris)* **1998**, 92, 191-4.
6. Finzel, B. C.; Baldwin, E. T.; Bryant, G. L., Jr.; Hess, G. F.; Wilks, J. W.; Trepod, C. M.; Mott, J. E.; Marshall, V. P.; Petzold, G. L.; Poorman, R. A.; O'Sullivan, T. J.; Schostarez, H. J.; Mitchell, M. A., *Protein Sci.* **1998**, 7, 2118-2126.
7. Jones, G. B., *Tetrahedron* **2001**, 57, 7999-8016.
8. Ruano, J. L. G.; Aleman, J.; Alonso, I.; Parra, A.; Marcos, V.; Aguirre, J., *Chem. Eur. J.* **2007**, 13, 6179-6195.
9. Meyer, E. A.; Castellano, R. K.; Diederich, F., *Angew. Chem. Int. Ed.* **2003**, 42, 1210-1250.
10. Wood, W. W.; Parker, F. R., *J. Chem. Phys.* **1957**, 27, 720-33.
11. Jones, J. R., *Proc. R. Soc. London, Ser. A* **1924**, 106, 441-62.
12. Jones, J. R., *Proc. R. Soc. London, Ser. A* **1924**, 106, 463-77.
13. Tomasi, J.; Mennucci, B.; Cammi, R., *Chem. Rev.* **2005**, 105, 2999-3093.

14. Cramer, C. J.; Truhlar, D. G., *Chem. Rev.* **1999**, 99, 2161-2200.
15. Tapia, O.; Goscinski, O., *Mol. Phys.* **1975**, 29, 1653-61.
16. Wong, M. W.; Frisch, M. J.; Wiberg, K. B., *J. Am. Chem. Soc.* **1991**, 113, 4776-82.
17. Zhou, R., *Proteins: Struct., Funct., Genet.* **2003**, 53, 148-161.
18. Zhang, L. Y.; Gallicchio, E.; Friesner, R. A.; Levy, R. M., *J. Comput. Chem.* **2001**, 22, 591-607.
19. Jover, J.; Bosque, R.; Sales, J., *QSAR and Comb. Sci.* **2008**, 27, 563-581.
20. http://www.sklogwiki.org/SklogWiki/index.php/Lennard-Jones_model, Lennard-Jones potential.
21. Rowley, L. A.; Nicholson, D.; Parsonage, N. G., *J. Comput. Phys.* **1975**, 17, 401-14.
22. Hunter, C. A., *Angew. Chem., Int. Ed.* **2004**, 43, 5310-5324.
23. Cook, J. L.; Hunter, C. A.; Low, C. M. R.; Perez-Velasco, A.; Vinter, J. G., *Angew. Chem., Int. Ed.* **2007**, 46, 3706-3709.
24. Cook, J. L.; Hunter, C. A.; Low, C. M. R.; Perez-Velasco, A.; Vinter, J. G., *Angew. Chem., Int. Ed.* **2008**, 47, 6275-6277.
25. Cabot, R.; Hunter, C. A., *Chem. Commun.* **2009**, 2005-2007.
26. Cockroft, S. L.; Hunter, C. A., *Chem. Commun.* **2006**, 3806-3808.
27. Cockroft, S. L.; Hunter, C. A., *Chem. Commun.* **2009**, 3961 - 3963.
28. Ōki, M., *Acc. Chem. Res.* **1990**, 23, 351-6.
29. Motherwell, W. B.; Moïse, J.; Aliev, A. E.; Nič, M.; Coles, S. J.; Horton, P. N.; Hursthouse, M. B.; Chessari, G.; Hunter, C. A.; Vinter, J. G., *Angew. Chem., Int. Ed.* **2007**, 46, 7823-7826.
30. Paliwal, S.; Geib, S.; Wilcox, C. S., *J. Am. Chem. Soc.* **1994**, 116, 4497-8.
31. Gardner, R. R.; Christianson, L. A.; Gellman, S. H., *J. Am. Chem. Soc.* **1997**, 119, 5041-5042.
32. Aliev, A. E.; Moïse, J.; Motherwell, W. B.; Nič, M.; Courtier-Murias, D.; Tocher, D. A., *Phys. Chem. Chem. Phys.* **2009**, 11, 97-100.
33. Hof, F.; Scofield, D. M.; Schweizer, W. B.; Diederich, F., *Angew. Chem. Int. Ed.* **2004**, 43, 5056-5059.
34. Fischer, F. R.; Schweizer, W. B.; Diederich, F., *Angew. Chem. Int. Ed.* **2007**, 46, 8270-8273.
35. Fischer, F. R.; Wood, P. A.; Allen, F. H.; Diederich, F., *Proc. Natl. Acad. Sci. U. S. A.* **2008**, 105, 17290-17294.
36. Carroll, W. R.; Pellechia, P.; Shimizu, K. D., *Org. Lett.* **2008**, 10, 3547-3550.
37. Zoltewicz, J. A.; Maier, N. M.; Fabian, W. M. F., *J. Org. Chem.* **1998**, 63, 4985-4990.
38. Yamasaki, R.; Tanatani, A.; Azumaya, I.; Saito, S.; Yamaguchi, K.; Kagechika, H., *Org. Lett.* **2003**, 5, 1265-1267.
39. Okamoto, I.; Yamasaki, R.; Sawamura, M.; Kato, T.; Nagayama, N.; Takeya, T.; Tamura, O.; Masu, H.; Azumaya, I.; Yamaguchi, K.; Kagechika, H.; Tanatani, A., *Org. Lett.* **2007**, 9, 5545-5547.
40. Klapars, A.; Huang, X.; Buchwald, S. L., *J. Am. Chem. Soc.* **2002**, 124, 7421-7428.
41. Phillips, D. P.; Zhu, X.-F.; Lau, T. L.; He, X.; Yang, K.; Liu, H., *Tetrahedron Lett.* **2009**, 50, 7293-7296.

42. Rahman, M.; Kundu, D.; Hajra, A.; Majee, A., *Tetrahedron Lett.* **2010**, 51, 2896-2899.
43. Lana, E. J. L.; Carazza, F.; Aparacida de Oliveira, R., *Helv. Chim. Acta* **2004**, 87, 1825-1831.
44. Maynard, G. D.; Ghosh, M.; Yuan, J.; Currie, K. S.; Mitchell, S.; Guo, Q.; Zhao, H. Preparation of 4,5-disubstituted-2-aryl pyrimidines as C5a receptor ligands. PCT Int. Appl. **2005**, US2005/015897, WO2005/110416 A2.
45. Paduraru, P. M.; Popoff, R. T. W.; Nair, R.; Gries, R.; Gries, G.; Plettner, E., *J. Comb. Chem.* **2008**, 10, 123-134.
46. Nishimura, N.; Yoza, K.; Kobayashi, K., *J. Am. Chem. Soc.* **2010**, 132, 777-790.
47. Tyagarajan, S.; Chakravarty, P. K.; Zhou, B.; Taylor, B.; Eid, R.; Fisher, M. H.; Parsons, W. H.; Wyvratt, M. J.; Lyons, K. A.; Klatt, T.; Li, X.; Kumar, S.; Williams, B.; Felix, J.; Priest, B. T.; Brochu, R. M.; Warren, V.; Smith, M.; Garcia, M.; Kaczorowski, G. J.; Martin, W. J.; Abbadie, C.; McGowan, E.; Jochnowitz, N.; Weber, A.; Duffy, J. L., *Bioorg. Med. Chem. Lett.* **2010**, 20, 7479-7482.
48. Tyagarajan, S.; Chakravarty, P. K.; Zhou, B.; Taylor, B.; Fisher, M. H.; Wyvratt, M. J.; Lyons, K.; Klatt, T.; Li, X.; Kumar, S.; Williams, B.; Felix, J.; Priest, B. T.; Brochu, R. M.; Warren, V.; Smith, M.; Garcia, M.; Kaczorowski, G. J.; Martin, W. J.; Abbadie, C.; McGowan, E.; Jochnowitz, N.; Parsons, W. H., *Bioorg. Med. Chem. Lett.* **2010**, 20, 5480-5483.
49. Ashton, P. R.; Harris, K. D. M.; Kariuki, B. M.; Philp, D.; Robinson, J. M. A.; Spencer, N., *J. Chem. Soc., Perkin Trans. 2* **2001**, 2166-2173.
50. Naumann, C.; Patrick, B. O.; Sherman, J. C., *Tetrahedron* **2002**, 58, 787-798.
51. Goldup, S. M.; Leigh, D. A.; Lusby, P. J.; McBurney, R. T.; Slawin, A. M. Z., *Angew. Chem., Int. Ed.* **2008**, 47, 3381-3384.
52. Gasparro, F. P.; Kolodny, N. H., *J. Chem. Educ.* **1977**, 54, 258-61.
53. Hammett, L. P., *J. Am. Chem. Soc.* **1937**, 59, 96-103.
54. Hansch, C.; Leo, A.; Taft, R. W., *Chem. Rev.* **1991**, 91, 165-95.
55. http://en.wikipedia.org/wiki/Solvent, Solvent (dielectric constant).
56. Reichardt, C., *Solvents and solvent effects in organic chemistry*. Third Edition ed.; Wiley-VCH: **2003**.
57. Smithrud, D. B.; Diederich, F., *J. Am. Chem. Soc.* **1990**, 112, 339-43.
58. Cabot, R.; Hunter, C. A.; Varley, L. M., *Org. Biomol. Chem.* **2010**, 8, 1455-1462.
59. Cabot, R.; Hunter, C. A., *Org. Biomol. Chem.* **2010**, 8, 1943-1950.
60. Abraham, M. H.; Platts, J. A., *J. Org. Chem.* **2001**, 66, 3484-3491.
61. Sahakitpichan, P.; Thasana, N.; Ruchirawat, S., *Synthesis* **2005**, 2934-2938.

Chapter 3

Experimental Measurement of Through-space Substituent Effects

Abstract

Non-covalent interactions are fundamental forces in many chemical and biological processes. The study of non-covalent interactions and molecular recognition phenomena is often challenging since numerous subtle effects may contribute to the overall observed behaviour. A number of computational approaches propose the existence of a direct through-space interaction of substituents with an aromatic system.[1,2] Such effects may be small, so their measurement might require a sensitive system. Here, a synthetic molecular torsion balance based on a slowly rotating tertiary amide, has been used to measure the electrostatic modulation of an aromatic ring via through-space substituent effects in a range of solvents. Through-space electronic communication was observed to occur between a phenyl ring and substituents placed *ortho* to each other on an aromatic ring. The effect was measured experimentally in addition to being predicted by density functional calculations. Methoxy groups positioned in this manner were seen to increase the electron density of the aromatic rings via a through-space effect. This through-space effect can be switched off by a conformational change induced by the placement of a bulky *tert*-butyl group adjacent to the methoxy group. Strikingly, nitro groups were seen to increase the electron density of the adjacent aromatic ring via through-space effects despite being strongly electron-withdrawing through bonds. The converse was also found to be true, since NH_2 and OH groups were seen to reduce electron density when the polar protons were positioned above an adjacent aromatic ring, despite the ability of these groups to donate electron density via resonance. To our knowledge this is the first

time that the through-space effects of substituents on the electrostatic potentials of aromatic rings have been unequivocally identified and measured.

3.1. Through-space substituent effects: background & theory

Most chemists are familiar with classic physical organic chemistry surrounding the effects of substituents on the interactions and reactivity of molecules. The electron-withdrawing and donating properties of substituents can be ranked and classified using σ_m and σ_p Hammett substituent constants[3-5] in aromatic systems and σ^* in aliphatic systems.[6-8] More detailed analyses further dissect these properties into R and F constants[9-11] which measure the through-bond resonance and field contributions to the electronic properties of substituents, respectively. Another popular way of viewing substituent effects is through the use of Molecular Electrostatic Potentials,[12,13] which have been used to study the inductive[14] and resonance effects of substituents.[15]

Conventionally it has been assumed that the majority of the electrostatic effects occur through bonds via resonance and inductive effects described above. However, theoreticians have recently proposed that the classic substituent effects on the electronic properties of aromatic rings can be adequately described only by considering through-space effects where strong resonant effects are not involved.[16]

In 2008 Wheeler and Houk performed computational studies on the effects of substituents in the model systems; $C_6H_6\cdots C_6H_5$-X, $C_6H_6\cdots$H-X, $C_6F_6\cdots C_6H_5$-X and $C_6F_6\cdots$H-X (Figure 3.1.i). By comparing face-to-face interactions in the benzene dimers with the corresponding benzene and H-X complexes, they concluded that there is a direct interaction between the substituent X and the unsubstituted aromatic ring.[2] Wheeler and Houk have suggested that the through-space effects of substituents are involved in stacking interactions[17], cation$\cdots\pi$ interactions[18] and anion$\cdots\pi$ interactions.[19]

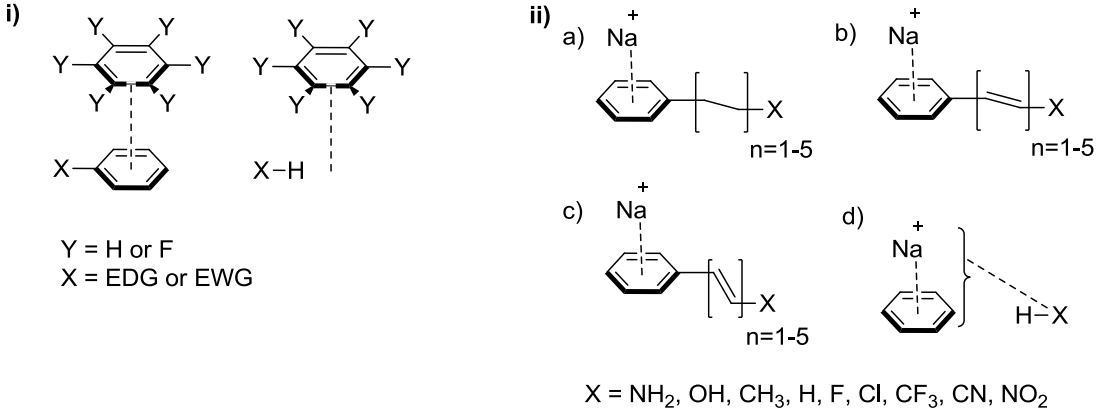

Figure 3.1. i) Model system used by Wheeler and Houk to study substituent effects in the benzene dimer[2], ii) Model system designed by Suresh to study substituent effects in the cation···π interaction[20].

In 2011 Suresh and co-workers performed a computational analysis of the cation···π interaction in the model systems shown in Figure 3.1.ii and were able to dissect the energetic contribution of resonance, inductive and through-space substituent effects.[20] The energy of system a) is due to inductive and through-space effects and of system b) is attributed to resonance, inductive and through-space substituent effects. In system c) the substituent is not in the same plane with the aromatic ring and thus there is no resonance effect, which can be calculated by subtracting the energy of b) and c). Finally the system d), where the substituent X is not connected to the ring, accounts for the through-space interaction. This analysis suggested that the energy of the cation···π interaction is mainly due to through-space effects for the electron-withdrawing substituents and due to resonance effects for the electron-donating groups.[20]

Through-space substituent effects were also studied by using Molecular Electrostatic Potentials.[1,21] Wheeler and Houk claimed that the changes in the MEP above a substituted arene is not always due to changes in the aryl π-system but mainly due to direct through-space interaction of the substituent.[1,16] Their research expanded from simple mono-substituted benzenes to complicated aromatic systems.[1] They compared the actual electrostatic potential surface of a substituted benzene (e.g.

$C_6H_5NO_2$) to the additive surface (e.g. C_6H_6 + HNO_2) and found that the actual and additive surfaces are quite similar, showing the existence of a through-space substituent effect.

Suresh and co-workers used the model system shown in Figure 3.2 to study the through-bond and through-space effects of substituents in alkyl, alkenyl and alkynyl systems, by the use of Molecular Electrostatic Potentials.[21] By comparing the minimum MEP on the aromatic ring of the systems shown in Figures 3.2a and 3.2b it was found that for the alkyl chain system there was a 79.6% contribution of the through-space effect and 20.4% through-bond effect. On the other hand the contribution of through-space effects in the substituted alkenyl and alkynyl systems shown in Figures 3.2c and 3.2e is only about 45%.[21]

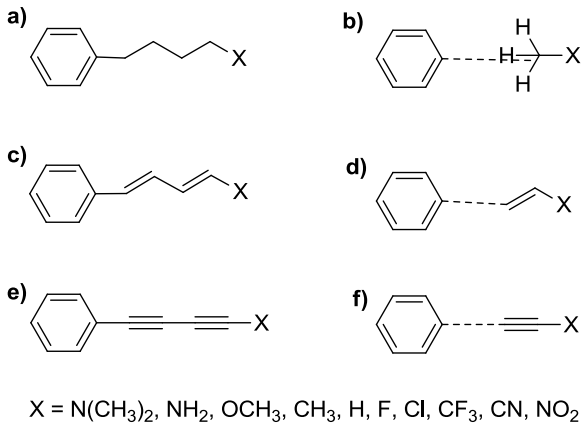

Figure 3.2. Model system designed by Suresh and co-workers to study the energetic contribution of through-bond and through-space substituent effects.[21]

It should be pointed out that the concept of through-space substituent effects is not new and has been identified in earlier studies of ionisation in carboxylic acids.[22-24] An interesting example of the through-space effect was presented in 1966 by calculating the ionisation constants of 2'-substituted biphenyl-4-carboxylic acids (Figure 3.3.).[22] As shown in Figure 3.3 the configuration of these acids resembles the di-*ortho*-substituted biphenyl torsion balances that we have studied and which are shown latter in this

chapter. The pK_a values of the 2'-substituted acids were compared to the pK_a values of the 4'-substituted carboxylic acids. All the substituents, except for the amino group, give weaker acids when they are at the 2' position compared to the 4' position. The authors claim that the observed effect is due to the fact that the steric bulkiness of the 2' substituent results in a displacement of the π-electrons of the adjacent aromatic ring towards the carboxylic acid, which weakens the acidity.[22]

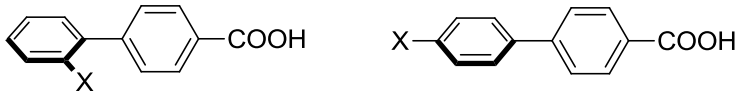

X = H, NO_2, NH_2, F, Cl, Br, I, Me, CN, Pr^i, MeO, Et, Ph

Figure 3.3. Model system studying the through-space effects of the *ortho* substituents to the adjacent ring.[22]

In cases of the *ortho*-effect[25-27] for the *ortho*-substituted benzoic acids a steric and a direct field effect between the two substituents was observed. However, to prove whether the theory surrounding such effects is correct and can be predicted computationally, a combined experimental and theoretical approach is required. Thus, the question is raised whether the proposed through-space effects can be identified and measured experimentally.

Here we use an experimental approach that provides a means of measuring electrostatic potentials which can then be compared with theoretical predictions. In this study we designed a simple molecular torsion balance which exists in two conformational states via slow rotation of a formyl group (Figure 3.4). This type of balances incorporates three aromatic rings to allow the investigation of the through-space effects of substituents placed *ortho* to the central ring (Figure 3.6). The through-space effects can be monitored experimentally, as the change in the electron density of the central ring affects the folding free energy of the formyl group. The energy

difference between the two conformers was correlated with the molecular electrostatic potentials at the central ring which were calculated computationally.

3.2. Introduction to the model system

The experimental part of this study employs a molecular torsion balance based on a tertiary amide with a slowly rotating formyl group (Figure 3.4). A series of balances with a range of X-substituents were synthesised and characterised as described in Chapter 2 (Sections 2.4 and 2.6), with the exception of compound **45**, which was synthesised as shown in Figure 3.5. Some of the balances bearing phenyl X-substituents might be expected to impart significant through-space effects on the electronic properties of the central aromatic ring (bottom of Figure 3.6). Meanwhile, the other balances (**6**, **7**, **3**, **5**, **10**, **11**), served as suitable references for identifying interesting electronic effects since the electron-withdrawing and donating properties of their simple substituents are well understood (top of Figure 3.6).

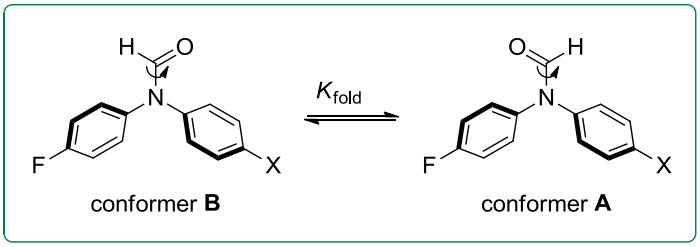

Figure 3.4. The equilibrium for the molecular torsion balance employed in this study.

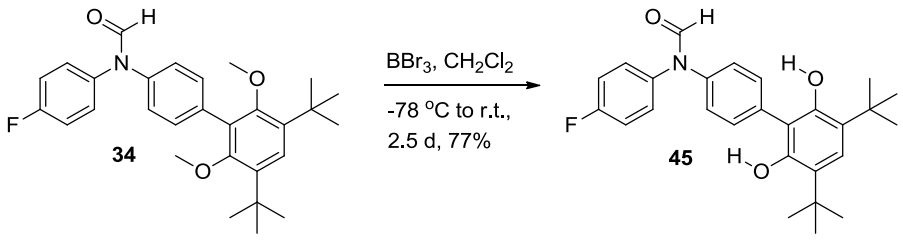

Figure 3.5. Synthesis of *N*-(3',5'-di-*tert*-butyl-2',6'-dihydroxy-[1,1'-biphenyl]-4-yl)-*N*-(4-fluorophenyl)-formamide (**45**).[28]

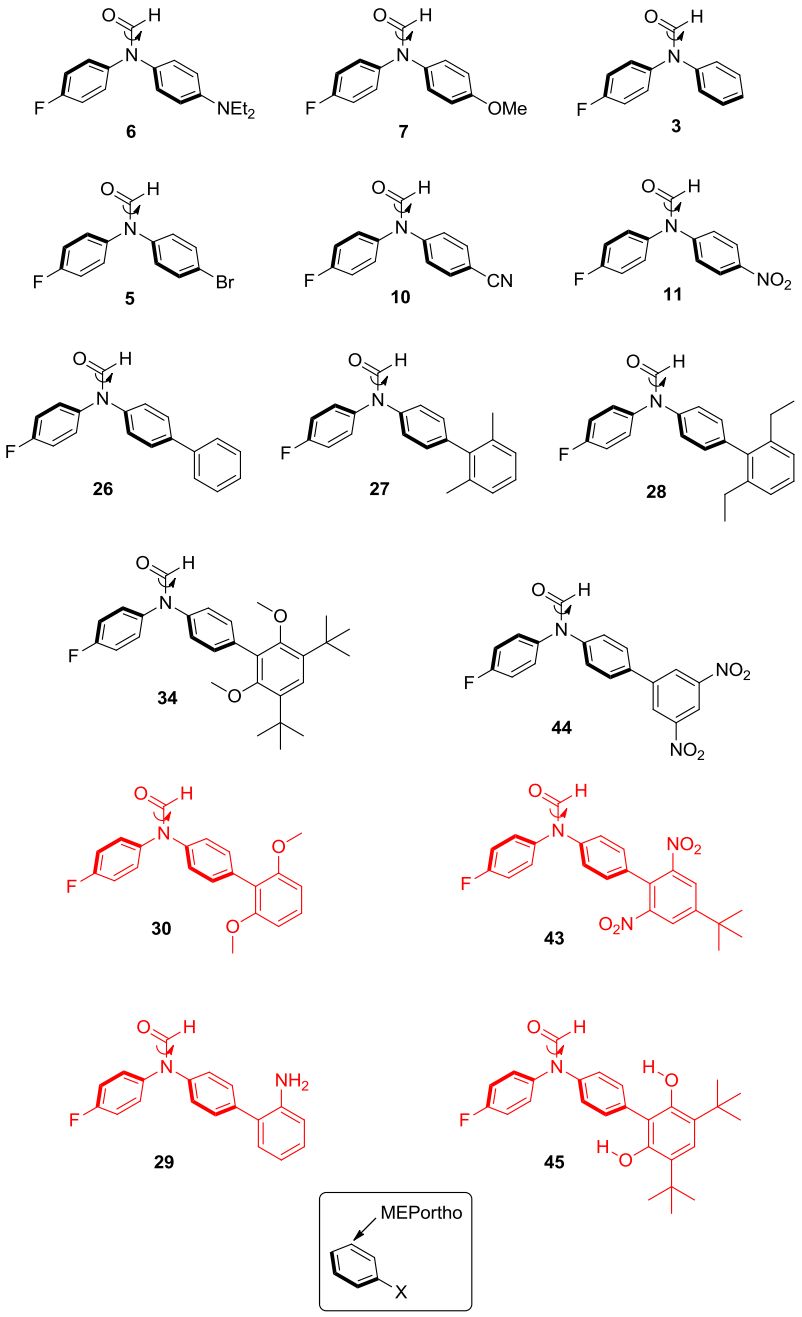

Figure 3.6. Molecular balances synthesised in this study and the position on the substituted ring or biphenyl where the MEP_{ortho} is taken. Pronounced through-space substituent effects were observed between methoxy, nitro, amino and hydroxyl substituents positioned over the faces of the aromatic rings in compounds **30, 43, 29** and **45** (shown in red), but not in the other compounds shown.

Each of these molecules exists in two conformations at room temperature, as was observed by distinct conformer signals in the NMR spectra. Since each of these balances contains an aromatic ring bearing a fluorine substituent, this allows ^{19}F-NMR spectra to be obtained in a variety of solvents. Integration of the ^{19}F-NMR peaks for each of the conformers was therefore used to obtain the folding equilibrium constant K_{fold}. Dominant conformers were assigned as detailed in Chapter 2 and in the experimental section of this thesis. Folding free energies were then calculated for each balance in each solvent using $\Delta G_{exp} = -RT \ln K_{fold}$ (Table 3.1).

3.3. Results and Discussion

Table 3.1 lists the experimental folding free energies ΔG_{exp} for all of the balances in each solvent investigated. These experimental data were correlated against the calculated molecular electrostatic potential of the X-substituted ring positioned *ortho* to the amide group (MEP_{ortho} as indicated in Figure 3.6). The molecular electrostatic potential at this *ortho* position was found to give better quality correlations with the experimental energies than the MEP taken *ipso* to the amide bond, or at the ring centre. Most of these correlations in different solvents gave R^2 values between 0.91 and 0.97 (Figure 3.7). The lower correlation coefficients in acetonitrile and DMSO can be attributed to the very small changes in the folding energies as the substituents were varied. Indeed, the change in the gradients of the graphs in Figure 3.7 clearly indicates that the intramolecular electrostatic effects that we seek to measure are diminished by the dominant solvent effects of the most polar solvents.

Overall, these graphs show that ΔG_{exp} becomes more negative (or less positive) when X is an electron-donating substituent. In other words, the equilibrium in Figure 3.4 moves towards the right when the electron density of the X-substituted aromatic ring increases. In contrast, the B conformer (in which the formyl oxygen is positioned above the X-substituted ring) is favoured when X is an electron-withdrawing substituent.

Table 3.1. Experimental folding free energies for each balance in every solvent examined, and the MEP at the *ortho* position, as indicated in Figure 3.6, for every balance. The indication n.s. refers to the cases where the balance was not soluble in the specific solvent.

X-substituent and compound number	MEP *ortho* (kJ/mol)	ΔG (kJ/mol) Chloroform	ΔG (kJ/mol) Acetone	ΔG (kJ/mol) Acetonitrile	ΔG (kJ/mol) Benzene	ΔG (kJ/mol) Ethyl acetate	ΔG (kJ/mol) Hexane	ΔG (kJ/mol) THF	ΔG (kJ/mol) DCM	ΔG (kJ/mol) Ethanol	ΔG (kJ/mol) Methanol	ΔG (kJ/mol) DMSO	ΔG *(kJ/mol)* Diethyl ether
H (3)	-70.6	-1.14	-0.85	-0.78	-0.68	-1.07	-1.14	-0.88	-0.81	-0.81	-0.81	-0.75	-1.11
Br (5)	-40.9	0.08	0.05	-0.15	0.08	0.18	0.37	0.23	0.08	-0.05	-0.08	-0.10	0.37
NEt_2 (6)	-96.5	-1.57	-1.53	-0.99	-1.39	-2.15	-2.75	-2.09	-1.11	-1.53	-1.07	-0.81	-2.40
OMe (7)	-76.8	-0.78	-0.71	-0.52	-0.75	-0.92	-1.48	-1.07	-0.58	-0.68	-0.52	-0.37	-1.27
CN (10)	-14.6	1.03	0.29	-0.15	0.78	0.65	n.s.	0.68	0.71	0.37	0.15	-0.55	1.27
NO_2 (11)	-7.5	1.39	0.46	0.02	1.07	0.96	n.s.	0.88	0.99	0.58	0.18	-0.37	1.98
Ph (26)	-66.1	-0.68	-0.58	-0.58	-0.46	-0.68	n.s.	-0.65	-0.58	-0.55	-0.62	-0.58	-0.65
PhdiMe (27)	-62.9	-0.99	-0.65	-0.55	-0.62	-0.65	n.s.	-0.85	-0.85	-0.62	-0.68	-0.65	-0.85
PhdiEt (28)	-61.6	-1.03	-0.62	-0.55	-0.58	-0.65	-0.92	-0.65	-0.96	-0.65	-0.75	-0.55	-0.78
PhdiOMe (30)	-97.9	-2.27	-1.11	-0.78	-1.82	-1.57	n.s.	-1.57	-1.14	-1.31	-1.14	-0.81	-2.09
PhdiOMetBu (34)	-60.5	-1.18	-0.71	-0.85	-0.32	-0.58	-0.85	-0.75	-1.07	n.s.	-0.71	-0.58	-0.49
Ph(o-diNO_2) (43)	-68.5	-0.96	-0.68	-0.32	-0.71	-0.55	n.s.	-0.75	-0.55	n.s.	-0.55	-0.75	-0.49
Ph(m-diNO_2) (44)	-15.3	0.62	-0.02	-0.21	1.48	0.35	n.s.	0.21	0.32	n.s.	0.05	-0.35	n.s.
$PhNH_2$ (29)	-55	-0.37	-0.62	-0.49	-0.13	-0.71	n.s.	-0.52	-0.49	-0.43	-0.49	-0.68	-0.55
PhdiOH*t*Bu (45)	-12.7	0.49	0.35	0.40	0.68	0.21	1.35	0.18	0.18	0.68	0.26	-1.22	0.23

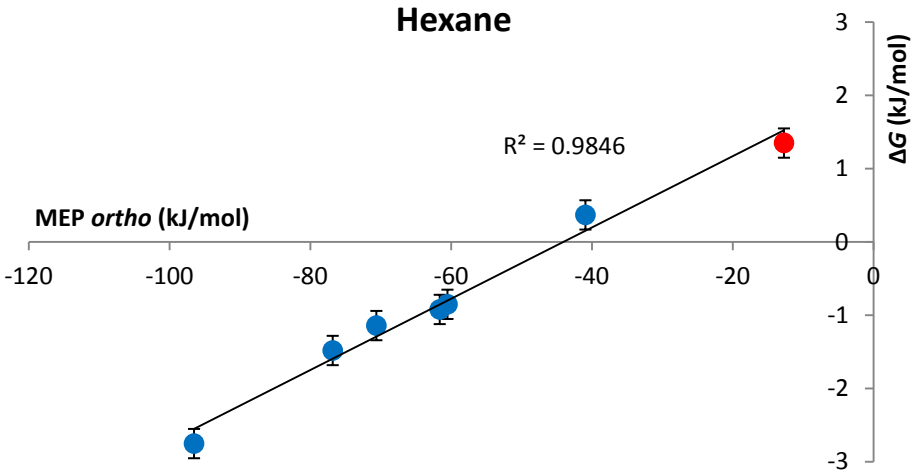
Hexane
R² = 0.9846
MEP *ortho* (kJ/mol)
ΔG (kJ/mol)
-120
-100
-80
-60
-40
-20
0
3
2
1
0
-1
-2
-3

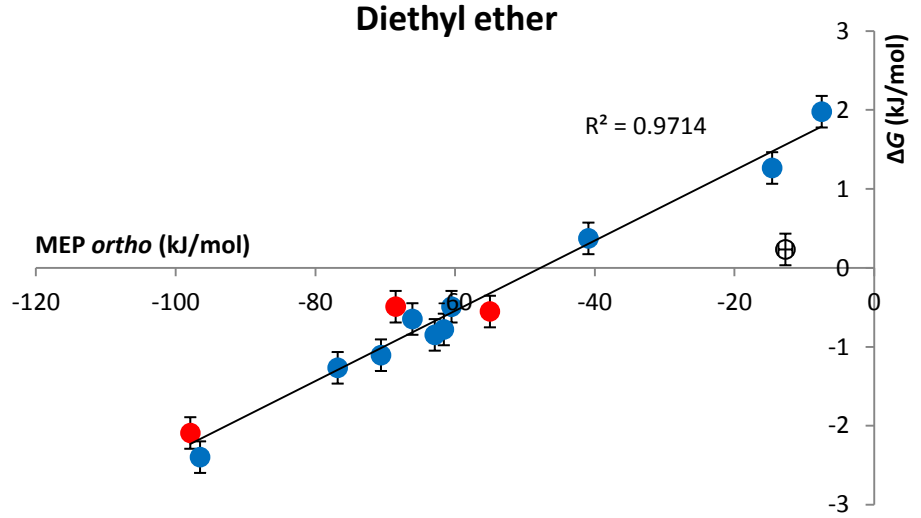
Diethyl ether
R² = 0.9714
MEP *ortho* (kJ/mol)
ΔG (kJ/mol)
-120
-100
-80
-60
-40
-20
0
3
2
1
0
-1
-2
-3

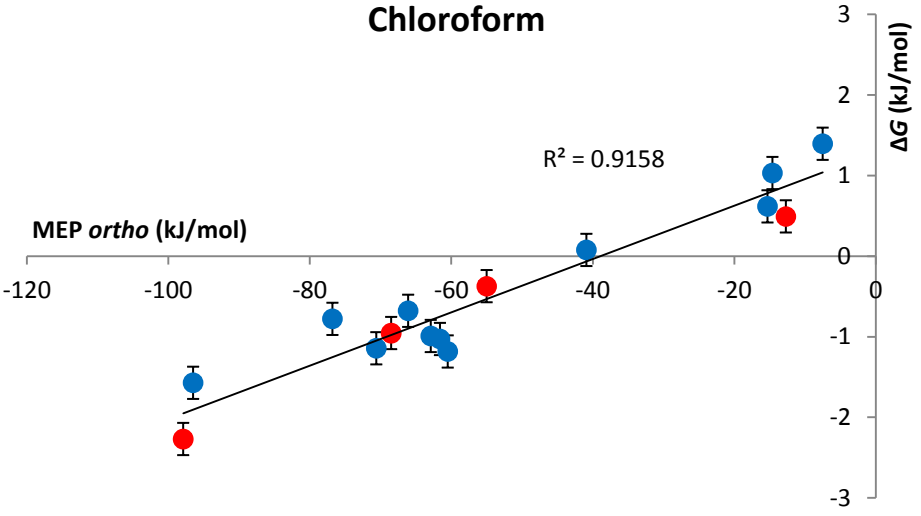
Chloroform
R² = 0.9158
MEP *ortho* (kJ/mol)
ΔG (kJ/mol)
-120
-100
-80
-60
-40
-20
0
3
2
1
0
-1
-2
-3

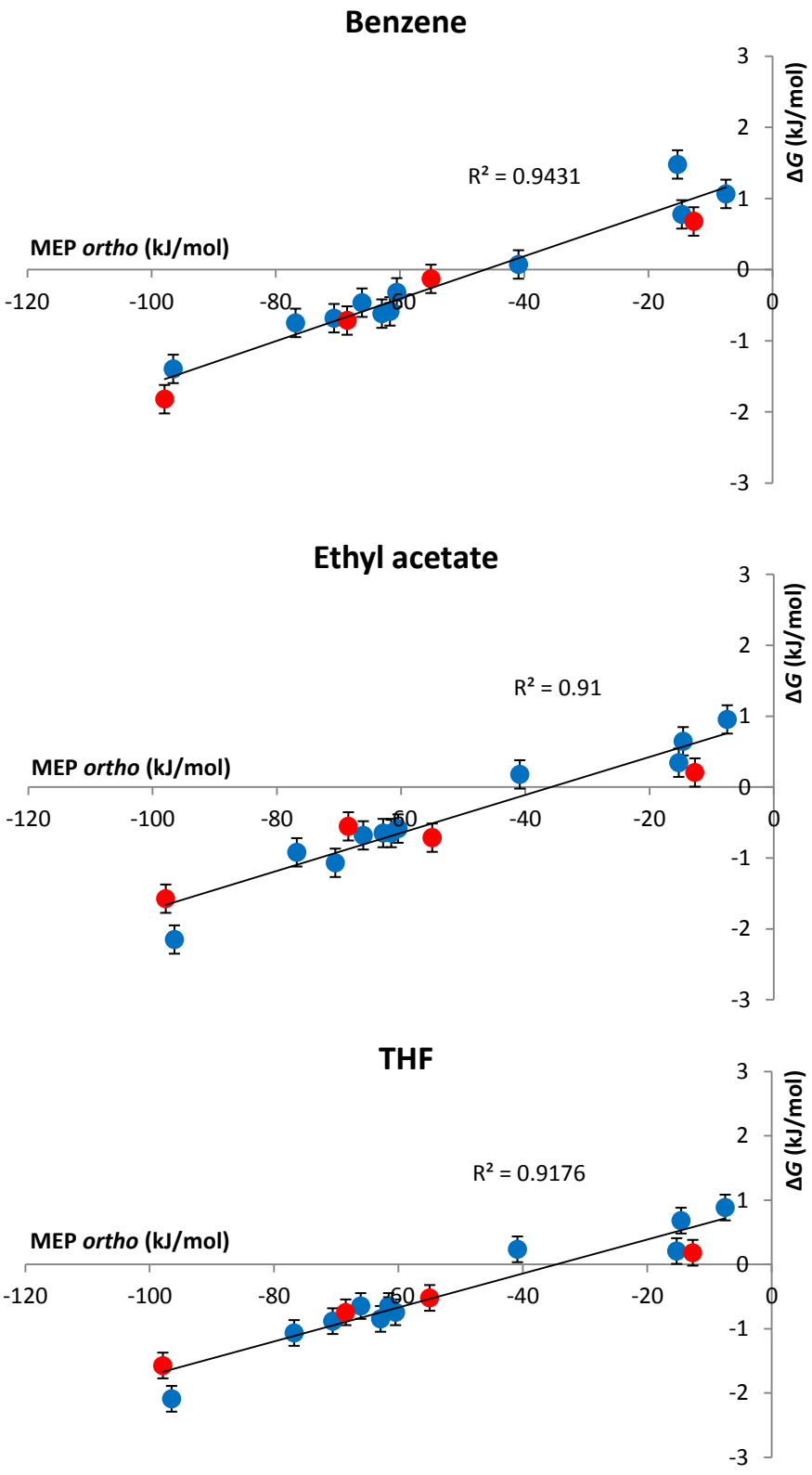
Benzene
R² = 0.9431
MEP ortho (kJ/mol)
ΔG (kJ/mol)
Ethyl acetate
R² = 0.91
MEP ortho (kJ/mol)
ΔG (kJ/mol)
THF
R² = 0.9176
MEP ortho (kJ/mol)
ΔG (kJ/mol)

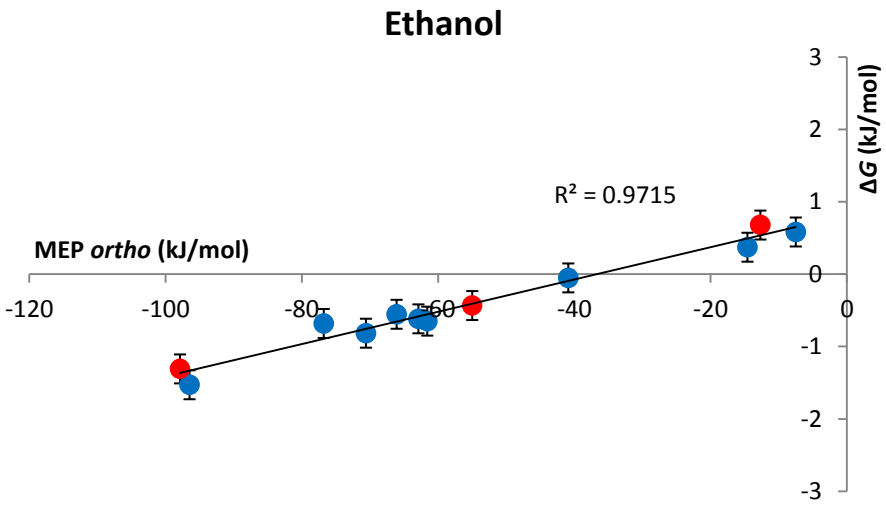
Ethanol
R² = 0.9715
MEP *ortho* (kJ/mol)
ΔG (kJ/mol)
-120
-100
-80
-60
-40
-20
0
3
2
1
0
-1
-2
-3

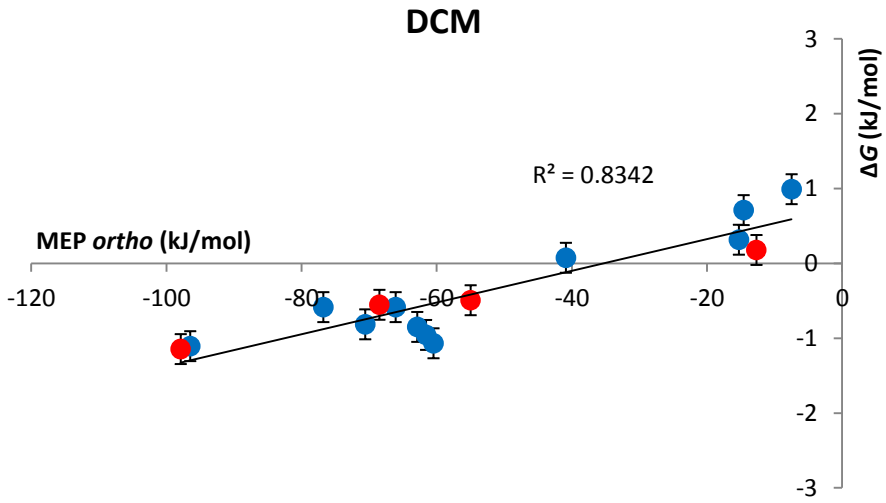
DCM
R² = 0.8342
MEP *ortho* (kJ/mol)
ΔG (kJ/mol)
-120
-100
-80
-60
-40
-20
0
3
2
1
0
-1
-2
-3

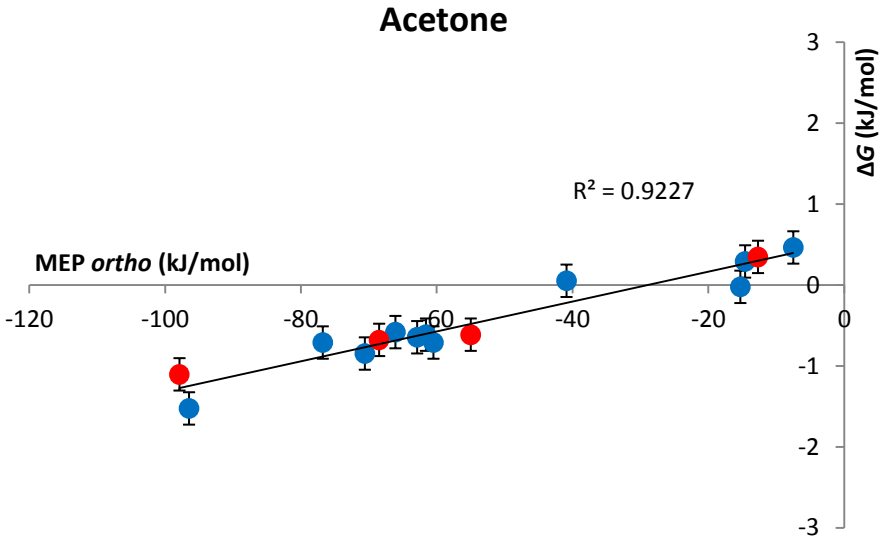
Acetone
R² = 0.9227
MEP *ortho* (kJ/mol)
ΔG (kJ/mol)
-120
-100
-80
-60
-40
-20
0
3
2
1
0
-1
-2
-3

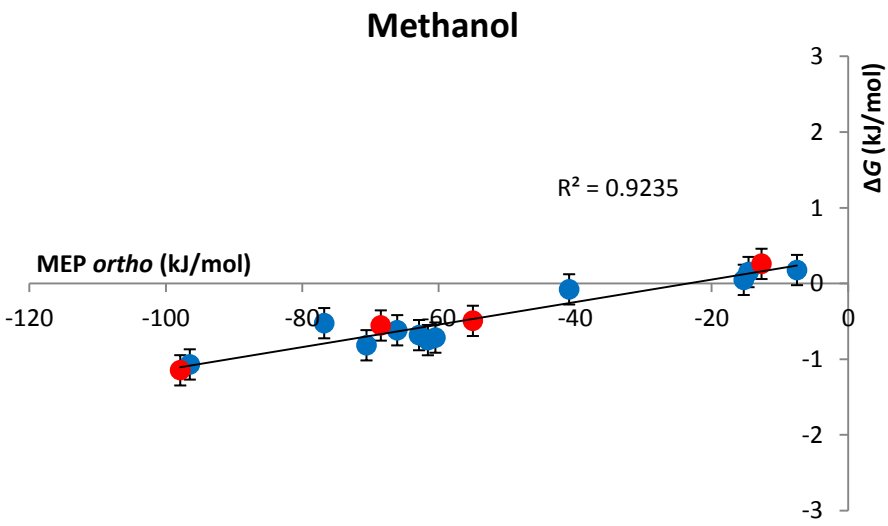
Methanol
R² = 0.9235
MEP ortho (kJ/mol)
ΔG (kJ/mol)
-120
-100
-80
-60
-40
-20
0
3
2
1
0
-1
-2
-3

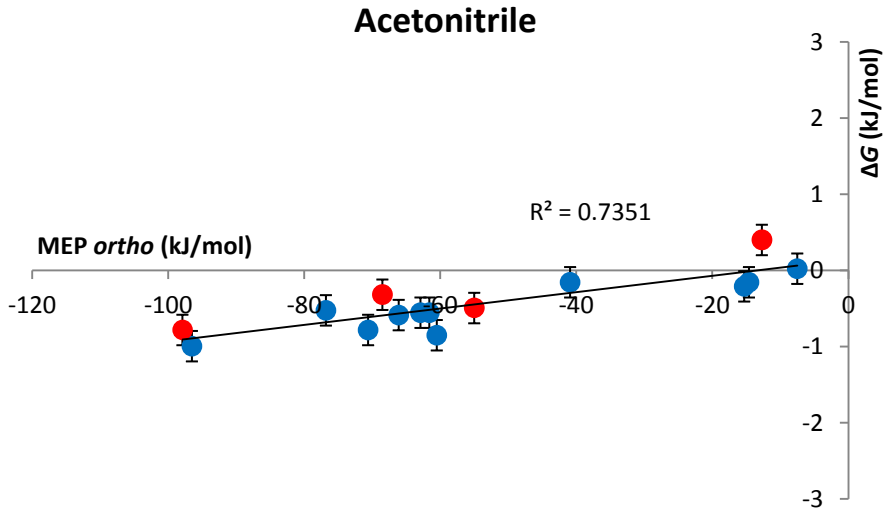
Acetonitrile
R² = 0.7351
MEP ortho (kJ/mol)
ΔG (kJ/mol)
-120
-100
-80
-60
-40
-20
0
3
2
1
0
-1
-2
-3

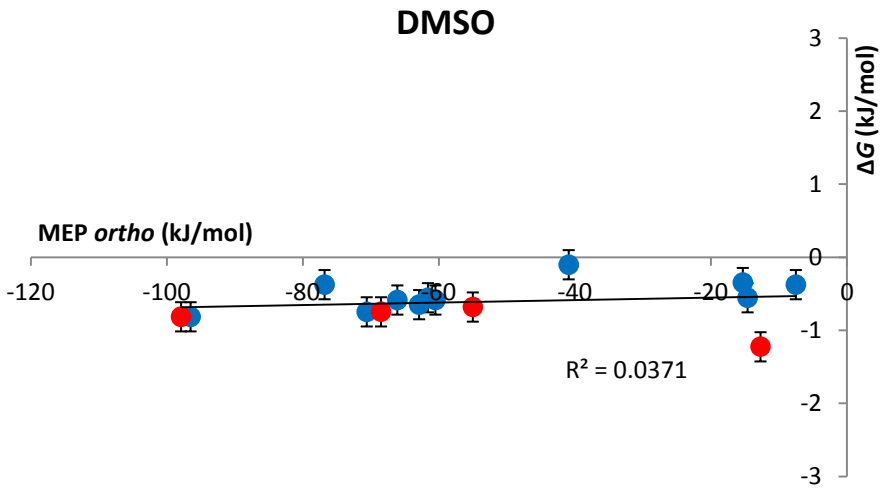
DMSO
R² = 0.0371
MEP ortho (kJ/mol)
ΔG (kJ/mol)
-120
-100
-80
-60
-40
-20
0
3
2
1
0
-1
-2
-3

Figure 3.7 (on the last four pages). Graphs correlating the molecular electrostatic potential at the *ortho* position with the experimental folding free energies for the balances in each solvent. The blue points on the graphs refer to the reference torsion balances used in this study and the red points refer to the PhdiOMe (**30**), Ph(*o*-diNO$_2$) (**43**), PhNH$_2$ (**29**) and PhdiOH*t*Bu (**45**) balances where through-space effects were observed. In the case of diethyl ether the PhdiOH*t*Bu (**45**) balance appeared to be a major outlier (hollow circle) and was excluded from the best fit line.

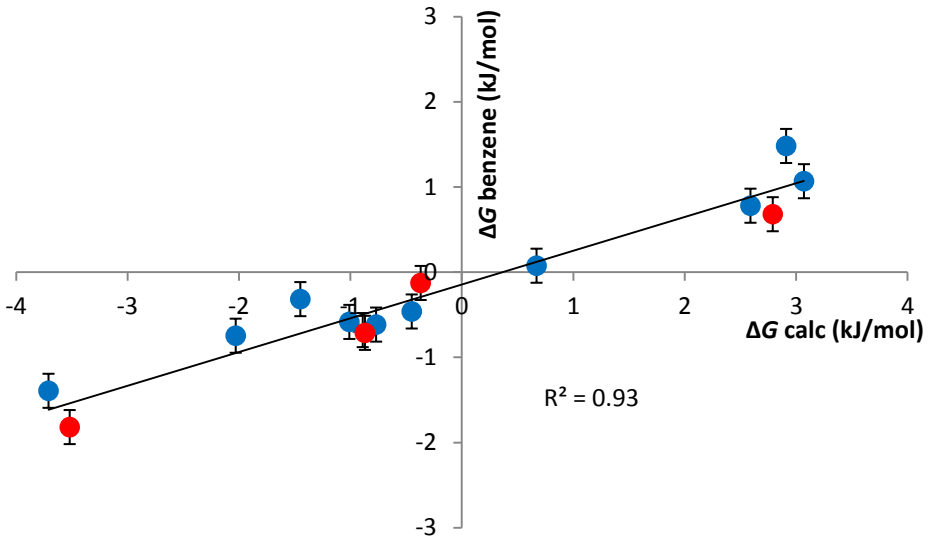

Figure 3.8. Graph correlating the calculated Δ*G* (found by subtracting the calculated energies of the two conformers of each balance minimised at B3LYP/6-31G* level in Spartan '08) with the experimental Δ*G* in benzene for all the balances. The blue points on the graphs refer to the reference torsion balances used in this study and the red points refer to the PhdiOMe (**30**), Ph(*o*-diNO$_2$) (**43**), PhNH$_2$ (**29**) and PhdiOH*t*Bu (**45**) balances where through-space effects were observed.

The two conformers of each balance were drawn in the program Spartan '08 and minimised at the B3LYP/6-31G* level. The difference of the calculated energies

between the two conformers was correlated with the experimental ΔG in benzene for all the balances, giving a linear correlation of $R^2 = 0.93$ (Figure 3.8). This graph shows that the through space effect can be predicted using usual B3LYP/6-31G* calculations, as the data for the PhdiOMe (**30**), Ph(*o*-diNO_2) (**43**), $PhNH_2$ (**29**) and PhdiOH*t*Bu (**45**) balances (red points) correlate well with the reference data.

It can be seen that all of the balances fit on these correlations, even those bearing phenyl groups as X substituents where through-space substituent effects might be observed. However, the quality of these correlations alone is not sufficient to prove that through-space effects are in operation, nor that these effects have been predicted computationally. Unambiguous identification of through-space electronic effects requires consideration of the structures and calculated properties of these compounds in comparison to their observed experimental behaviour.

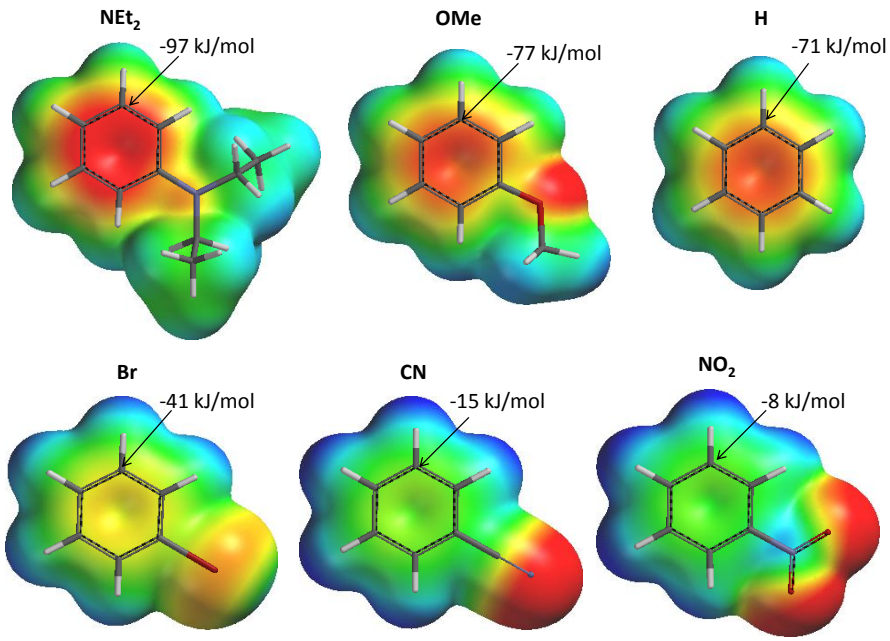

Figure 3.9. Density potential surfaces for the substituted benzene rings referring to the *para*-substituted reference balances and the MEP_{ortho} values taken at the *ortho*-position with reference to position of the formamide in the reference molecular balances. All structures and surfaces were minimised and calculated using B3LYP/6-31G* in Spartan '08.

Figure 3.9 shows the calculated MEPs of substituted aromatic rings bearing a range of electron withdrawing and donating substituents found in the simple reference balances (compounds **6**, **7**, **3**, **5**, **10**, **11**). The colours of the MEP surfaces are scaled from –100 kJ/mol to +100 kJ/mol (red to blue) throughout this chapter. This standardised scale assists the comparison of MEP surfaces between differently substituted molecules. It can be observed that electron-donating substituents such as NEt_2 increase the electron density of the faces of the aromatic rings, as indicated by the increased red colour relative to benzene. When a strong electron-withdrawing substituent is present (e.g. CN and NO_2), the green colouration of the aromatic ring indicates that the electrostatic potential is close to zero. Furthermore, protons on aromatic rings bearing electron-withdrawing groups have an increased positive potential relative to benzene as indicated by their dark blue colour. The potential surfaces in Figure 3.9 serve as a useful scale for analysing substituent effects and for the identification of possible through-space substituent effects as discussed below.

Through-space effects of nitro substituents

Figure 3.10 shows the calculated MEP surfaces for biphenyl moieties corresponding to those found in balances **27**, **43**, and **44**. It can be seen that the *ortho*-disubstituted biaryls are particularly sterically hindered; therefore it is worthwhile comparing these calculated structures with those found in the Cambridge Crystallographic Database (CCDB) before considering the calculated properties and experimental behaviour of the corresponding balances. Figure 3.11 shows structures found in the CCDB for the Ph – Ph(*o*-diNO_2) and Ph – Ph(*m*-diNO_2) moieties as seen in balances **43** and **44**. It can be seen that both the biaryl and nitro-aryl bond torsions found in the CCDB compare well with those in the calculated structures.

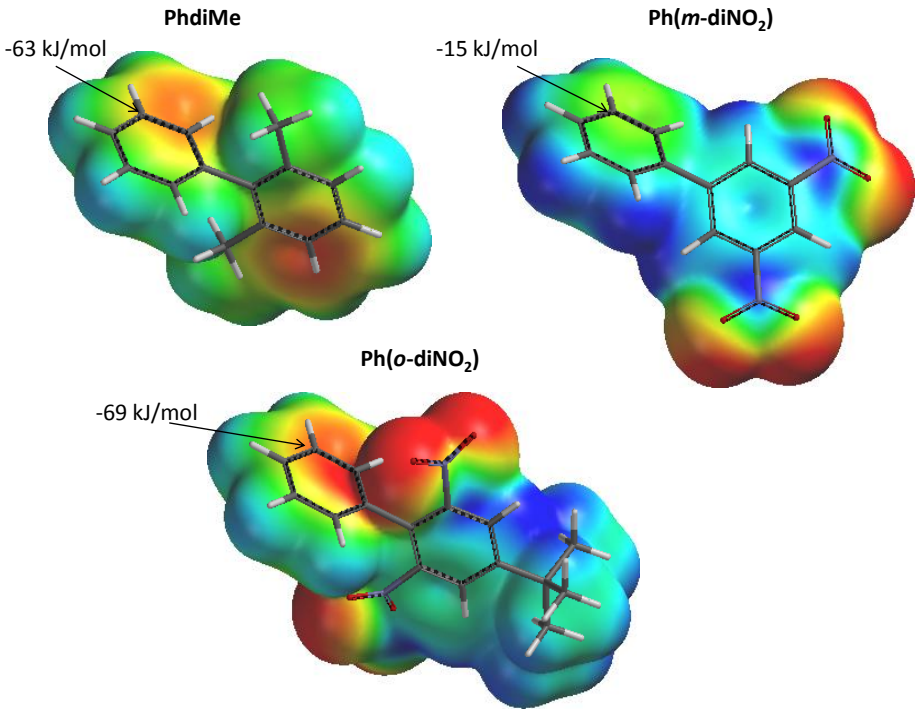

Figure 3.10. Density potential surfaces for nitro-substituted biphenyls and the MEP at the *ortho* positions.

The calculated MEPs of the Ph(*o*-diNO$_2$) and Ph(*m*-diNO$_2$) biphenyls suggest that a through-space substituent effect can take place when a nitro group is placed *ortho* to a phenyl group. The nitro groups in both of these examples have strong through-bond electron-withdrawing properties and remove similar amounts of electron density from the rings to which they are directly bonded (note the similar blue-green colour of the MEPs of the aromatic faces). However, there is a prominent difference between the MEPs on the face of the adjacent aromatic rings. Ph(*m*-diNO$_2$) has a MEP$_{ortho}$ of –15 kJ/mol, which is similar to that of the reference where X = CN (Figure 3.9). In contrast, Ph(*o*-diNO$_2$) is surprisingly electron-rich, with a MEP$_{ortho}$ of –69 kJ/mol, which is similar to that of benzene (Figure 3.9) or biphenyl (Figure 3.19).

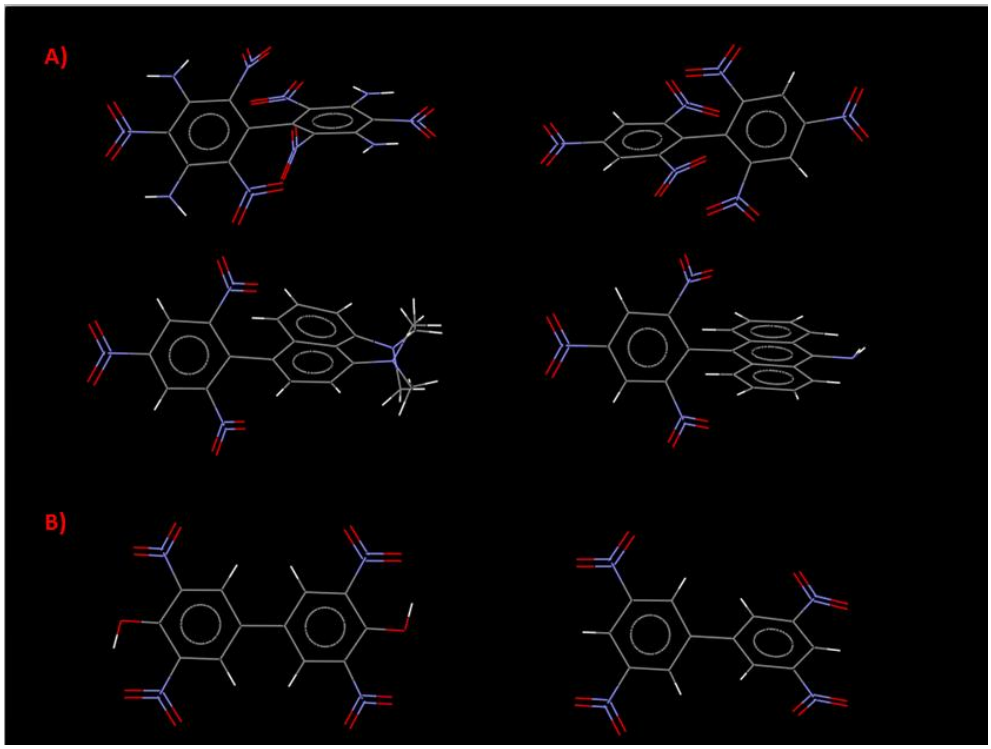

Figure 3.11. Crystal structures showing A) Ph – Ph(*o*-diNO$_2$) and B) Ph – Ph(*m*-diNO$_2$) biphenyl moieties from the CCDB (CCDB codes: A) FEKVOG, MOCJUK, NUPJIR, VINCIE, B) NIOBPH, VORLEU)

As expected based on the quality of the correlations in Figure 3.7, and in agreement with the theoretical MEP calculations it can be seen that the experimental folding free energies listed in Table 3.1 for balance **44**, (X = Ph(*m*-diNO$_2$), MEP$_{ortho}$ = –15 kJ/mol) are similar to those of reference balance **10** (X = CN, MEP$_{ortho}$ = –15 kJ/mol) in the range of solvents studied. Meanwhile, the experimental folding energies of balance **43** (X = Ph(*o*-diNO$_2$), MEP$_{ortho}$ = –69 kJ/mol) are most similar to those of reference balances **26** (X = Ph, MEP$_{ortho}$ = –66 kJ/mol) and **3** (X = H, MEP$_{ortho}$ = –71 kJ/mol).

NMR chemical shift data also provide useful experimental data on the electron-density.[29] As it can be observed from the chemical shifts of the aromatic protons of the

X-substituted ring, the more electron rich the ring, the lower the chemical shift (Table 3.2). This can be easily observed by comparing the chemical shifts in the reference NEt_2 (**6**) and NO_2 (**11**) balances, particularly for the protons *meta* to the amide that are closest to the substituent. In the NEt_2 (**6**), where the substituent is electron donating, the proton chemical shifts are lower compared to the NO_2 (**11**) balances, with the electron withdrawing nitro group (Table 3.2). The Ph(*o*-diNO_2) (**43**) and Ph(*m*-diNO_2) (**44**) balances have both two electron-withdrawing nitro groups, but the Ph(*o*-diNO_2) (**43**) balance appears to have lower chemical shifts for the aromatic protons of the central ring. This implies that the X-substituted ring of the Ph(*o*-diNO_2) (**43**) balance is more electron rich compared to the Ph(*m*-diNO_2) (**44**) balance, which can be attributed to the through-space electron-donation of the *ortho* nitro groups in balance **43**.

Table 3.2. Chemical shifts for all balances for the aromatic protons of the X-substituted ring (central ring) in $CDCl_3$. The positions *ortho* and *meta* refer to the positions relative to the amide group.

X-substituent	compound number	Chemical shifts (ppm) $CDCl_3$ of *ortho* proton		Chemical shifts (ppm) $CDCl_3$ of *meta* proton	
		conformer A	conformer B	conformer A	conformer B
H	**3**	7.16	7.29	7.42	7.40
Br	**5**	7.03	7.18	7.54	7.51
NEt_2	**6**	7.01	7.05	6.66	6.64
OMe	**7**	7.11	7.19	6.94	6.91
CN	**10**	7.20	7.44	7.68	7.63
NO_2	**11**	7.29	7.54	8.29	8.25
Ph	**26**	7.23	7.35	7.63	7.60
PhdiMe	**27**	7.21	7.36	7.21	7.10 - 7.19
PhdiEt	**28**	7.21	7.37	7.23	7.19
PhdiOMe	**30**	7.17	7.31	7.41	7.39
PhdiOMetBu	**34**	7.23	7.37	7.59	7.55
Ph(o-diNO_2)	**43**	7.18	7.40	7.30	7.25
Ph(m-diNO_2)	**44**	7.34	7.52	7.74	7.70
$PhNH_2$	**29**	7.25	7.37	7.52	7.50
PhdiOHtBu	**45**	7.37	7.54	7.51	7.48

Overall, these experiments and calculations combined show that nitro groups serve as through-space electron-donating groups when placed *ortho* to an aromatic ring. In the geometry examined here, the strong through-bond electron-withdrawing effects of the nitro substituents are approximately cancelled by an equally strong through-space donation of electron density from the electron-rich oxygen atoms.

Through-space effects of methoxy substituents

The central rings of balances **34** and **30** might be expected to have similar electron densities based on a consideration of the through-bond effects of the methoxy substituents. However, the electrostatic potential of the ring bonded to the PhdiOMe moiety contained within balance **30** has a MEP_{ortho} of –98 kJ/mol compared to only –61 kJ/mol in the PhdiOMetBu moiety from balance **34** (Figure 3.12). This increased electron density is shown by the intense red colour in Figure 3.12, which appears to arise via the through-space substituent effect of the methoxy oxygen atoms on the adjacent aromatic ring. Notably, the steric influence of the *tert*-butyl groups in PhdiOMetBu appears to switch off the through-space donation of electron density by the methoxy group.

The validity of these calculations is supported by the experimental results since the folding free energies of balance **30** (X = PhdiOMe, MEP_{ortho} = –98 kJ/mol) most closely resemble those of electron-rich control balance **6** (X = NEt_2, MEP_{ortho} = –97 kJ/mol) (Table 3.1). In contrast, the folding free energies of balance **34** (X = PhdiOMetBu, MEP_{ortho} = –61 kJ/mol) most closely resemble balances bearing electronically inert X-substituents such as **3** (X = H), **26** (X = Ph), **27** (X = PhdiMe), and **28** (X = PhdiEt), whose MEP_{ortho} values range from –62 to –71 kJ/mol. Further insight into the switching of through-space substituent effects can be obtained by examining the structures of compounds in the CCDB (Figure 3.13).

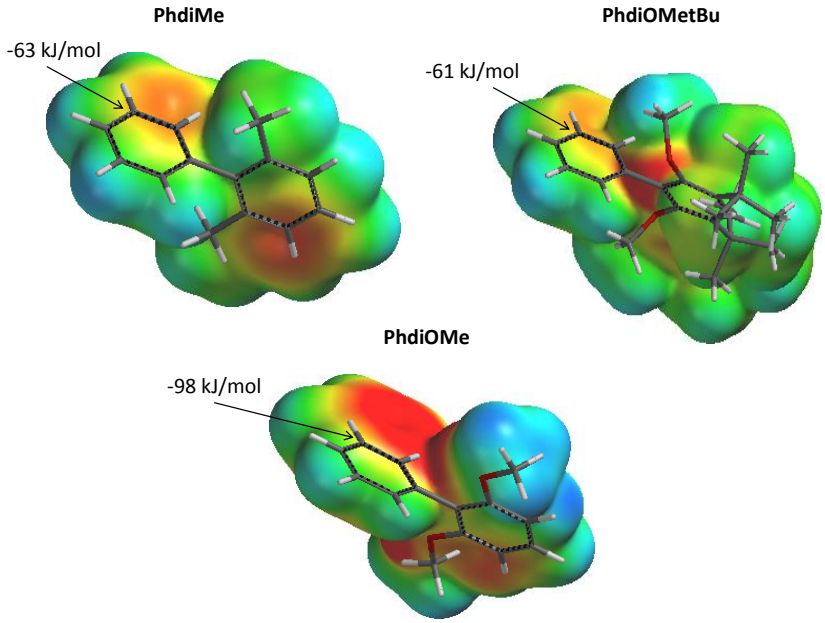

Figure 3.12. Density potential surfaces for methoxy-substituted biphenyls indicating the MEP at the *ortho* positions.

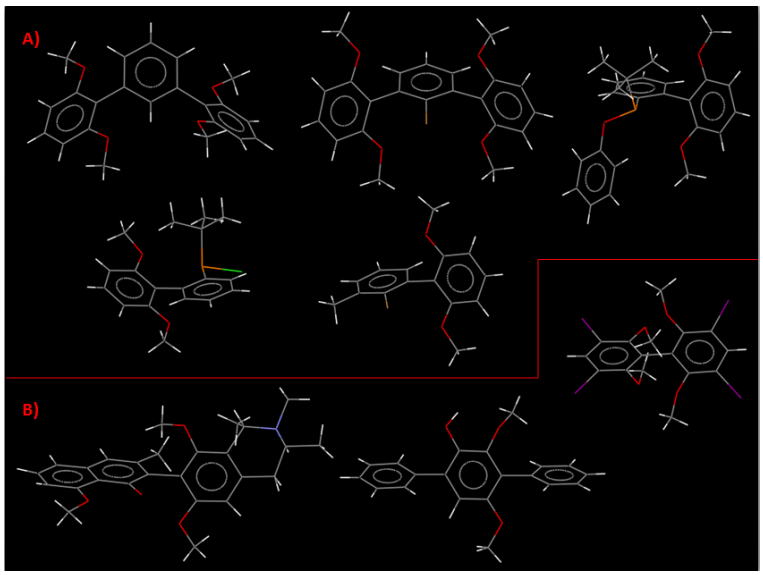

Figure 3.13. Crystal structures showing A) the Ph – PhdiOMe conformation and B) Ph – PhdiOMe when the methoxy groups are forced to adopt a certain arrangement due to the presence of bulky substituents. (CCDB codes: A) BESSEY, IRALAP, NILSOR, MABWUJ, IRALOD, B) DAXGAK, ETABUX, RALDOY)

Figure 3.13 shows the structures of Ph – PhdiOMe biaryl moieties found in the crystal database. The structures in Figure 3.13A contain methoxy groups flanked by a phenyl ring on one side. In these structures, the methoxy substituents are co-planar with the ring to which they are attached, with the methyl group pointing away from the *ortho*-phenyl group. Such a structure is also predicted in the calculations for the biaryl moiety of balance **30** (Figure 3.12). Figure 3.13B shows structures where a second bulky substituent is placed *ortho* to the methoxy group, which forces the methoxy groups to twist out of the plane of the aromatic ring as is the case in balance **34**.

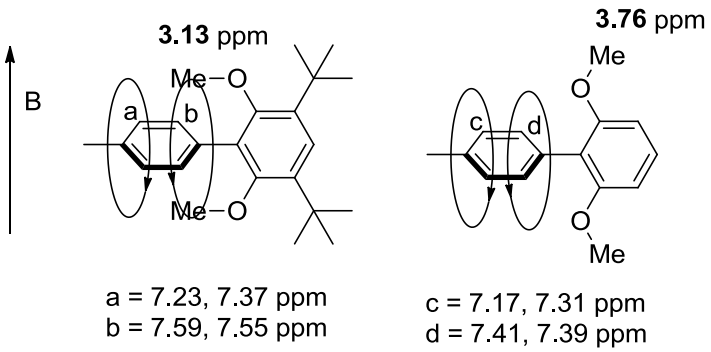

Figure 3.14. The resonances of the methoxy protons and aromatic protons of the central ring for the PhdiOMetBu (**34**) and PhdiOMe (**30**) balances. There are two chemical shifts for each aromatic proton of the central ring corresponding to the two conformers.

The proton NMR resonances also contain valuable information on the conformation of the methoxy groups in balances **30** and **34** which support the computational and solid-state structures discussed above. The chemical shift of the methoxy protons in the X = PhdiOMetBu balance **34** is 3.13 ppm, while in the X = PhdiOMe balance **30** this signal occurs at 3.76 ppm (Figure 3.14). This observation can be attributed to differences in conformation and the corresponding changes in the shielding effects of the neighbouring phenyl ring. In the case of the X = PhdiOMe balance **30**, the methoxy protons point away from the aromatic ring, and their chemical

shift is mostly affected by the externally applied magnetic field of the spectrometer, B. However, in the case of the PhdiOMetBu balance **34**, the methoxy groups are twisted towards the aromatic ring. As a result, the methoxy proton resonance is shifted upfield due to the induced magnetic field generated by the delocalised π electrons that opposes the externally applied field.[30]

These structural insights combined with the electrostatic potential calculations suggest that the introduction of *tert*-butyl groups adjacent to the methoxy groups twist the electron-rich lone-pairs of the oxygen atom away from the adjacent aromatic ring, which appears to switch off the through-space effect (PhdiOMetBu).

Additional experimental support for the through-space electronic effects occurring in the methoxy-substituted balances is provided by NMR data. The chemical shifts of the aromatic protons of the reference balances, as shown in Table 3.2, indicate that the more electron-rich an aromatic ring the lower the chemical shifts. The chemical shifts of the aromatic protons of the central ring for the balances **30** and **34** comply with this observation (balance **30** has lower chemical shifts compared to **34**), confirming that the central ring in balance **30** (X = PhdiOMe) is more electron rich than in balance **34** (Figure 3.12).

The calculations and experimental data confirm that methoxy groups serve as through-space electron-donors when placed *ortho* to an aromatic ring. It has also been shown that the electron-donating through-space effect of methoxy groups can be switched off via the introduction of bulky substituents which twist the oxygen-lone pairs away from the adjacent aromatic ring. These observations are most consistent with through-space electronic communication rather than through-bond electronic effects.

Through-space effects of amino substituents

Figure 3.15 shows the density potential surface of the amino-substituted biphenyl which corresponds to the $PhNH_2$ (**29**) balance. The MEP at the *ortho* position of the $PhNH_2$ biphenyl is –55 kJ/mol at the upper face of the surface, which is near in space to the amino group. Despite the fact that balance **29** is *mono*-substituted, the MEP*ortho* (–55 kJ/mol) at the position most affected by the through-space effect correlates nicely with

the experimental folding free energy of the balance **29** in a series of different solvents as shown in Figure 3.7.

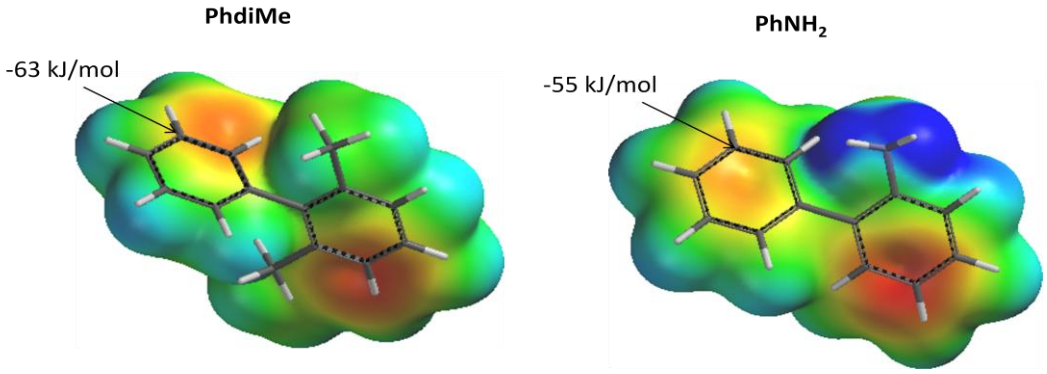

Figure 3.15. Density potential surface for the amino-substituted biphenyl indicating the MEP at the *ortho* positions.

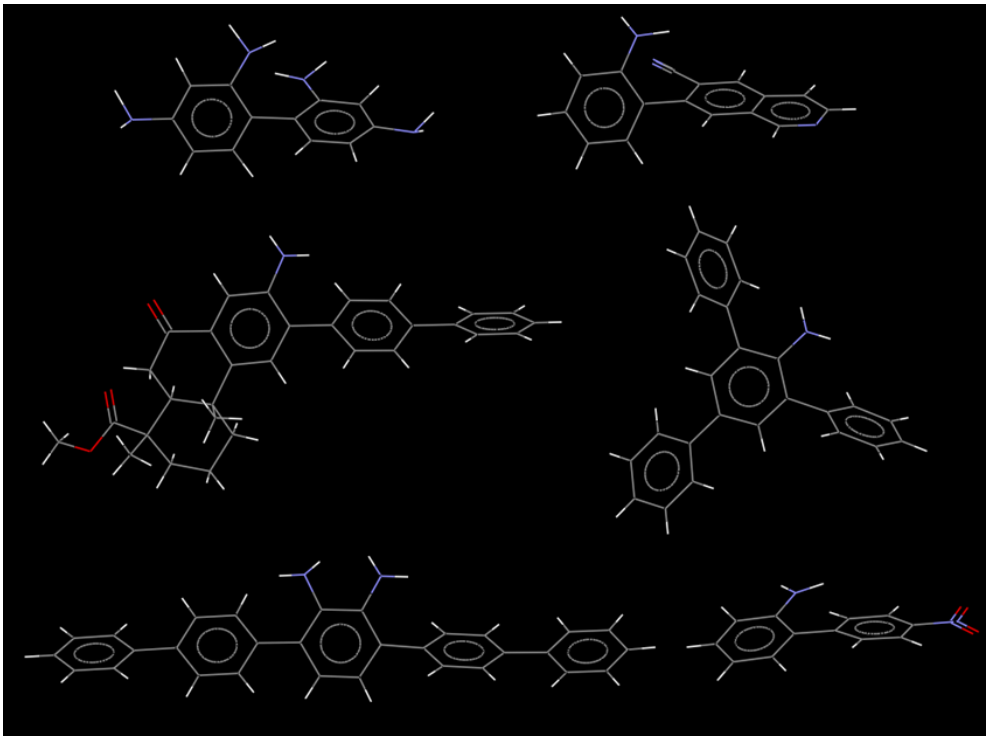

Figure 3.16. Crystal structures showing the Ph – $PhNH_2$ conformation. (CCDB codes: BUWCAX, CAPISQ, DIZLUU, YUPYUE, EFAHAV, DIWFEU)

The NH_2 group is electron donating via resonance, which is also apparent from the intense red colour of the aromatic ring with the *ortho* amino substituent in Figure 3.15. Interestingly, the MEP*ortho* of the $PhNH_2$ biphenyl (–55 kJ/mol) is less negative compared to the MEP*ortho* of the PhdiMe biphenyl (–63 kJ/mol). Thus, the calculations suggest that the amino protons reduce the electron density of the adjacent aromatic ring via through-space effects.

The relative conformation of the Ph – $PhNH_2$ biphenyls can also be shown in the crystal structures of Figure 3.16. As calculated in Spartan'08, the two rings are not coplanar and the amino protons are located above the second aromatic ring.

The chemical shifts of the aromatic protons in the X = $PhNH_2$ (**29**) balance listed in Table 3.2 are most similar to the X = CN control balance. Overall, the chemical shift data and the experimental folding free energies are consistent with the through-space electron-withdrawing effect of the NH_2 group when its polar protons are positioned above an aromatic ring.

Through-space effects of hydroxy substituents

Unfortunately the X = PhdiOHtBu compound **45** was found to be quite unstable and decomposed over a period of days. Nonetheless, it was still possible to obtain experimental folding free energies for balance **45** in a variety of solvents. As shown in Table 6.1 in the experimental chapter, the analysis of ^{19}F-NMR chemical shifts suggests that the preferred conformer of this balance may differ in acetone, ethyl acetate and DMSO relative to that observed in chloroform. However, due to the stability problems mentioned above, a full 2D NMR analysis was not performed in these solvents, and it was assumed that the balance **45**, (whose chemical shift data resembles the CN (**10**) and NO_2 (**11**) balances) only flipped conformers in DMSO (ΔG values found in Table 3.1). Although the free energies of balance **45** are likely to be less accurate than the other balances examined (due to the presence of small amounts of decomposition products in the NMR spectra), the data for the balance **45** correlated very well with calculated MEP values in all solvents with the exception of diethyl ether (Figure 3.7).

Figure 3.17 shows the density potential surface for the hydroxy-substituted biphenyl which corresponds to the PhdiOH*t*Bu (**45**) balance. The bulky *tert*-butyl groups force the hydroxyl groups to point over the adjacent aromatic ring, which dramatically decreases the MEP of the ring. This is obvious from the green colour at the ring centre and the intense blue colour of the aromatic protons. The MEP*ortho* of the PhdiOH*t*Bu biphenyl is –13 kJ/mol and it resembles the CN (**10**) balance (MEP*ortho* –15 kJ/mol).

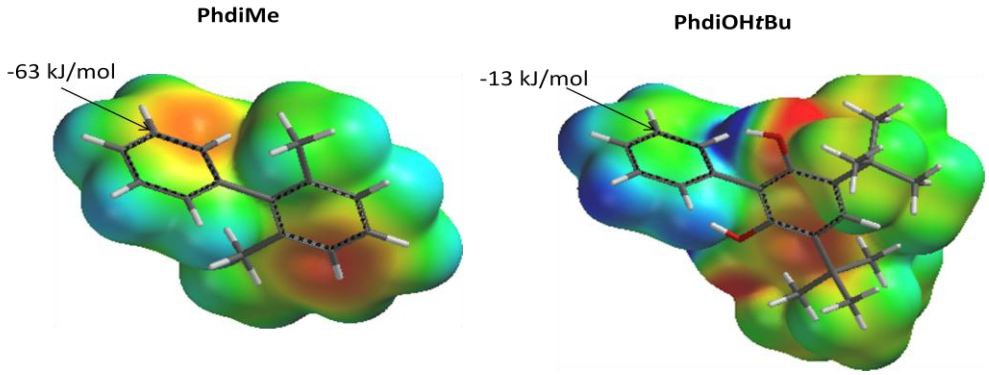

Figure 3.17. Density potential surface for the hydroxy-substituted biphenyl indicating the MEP at the *ortho* positions.

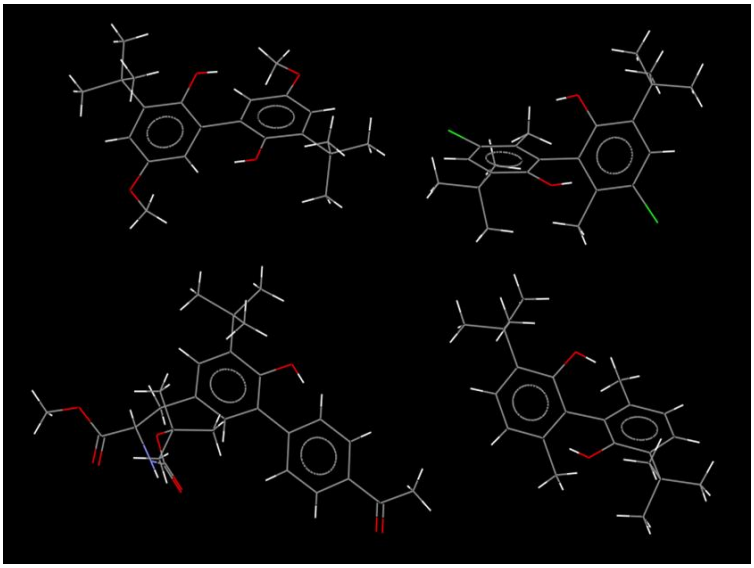

Figure 3.18. Crystal structures showing the Ph – PhOH*t*Bu conformation. (CCDB codes: FOVXOE, DUWHAF, GUGZIS, XILZEX)

The calculations indicate that the bulky *tert*-butyl groups force the hydroxyl protons to point over the adjacent aromatic ring, which is supported by the crystal structures shown in Figure 3.18. In addition, the OH protons of balance **45** appear at 4.63 and 4.68 ppm for conformers A and B respectively in $CDCl_3$, whereas the OH proton of phenol has a chemical shift of 5.35 ppm.[31] The OH protons in balance **45** are shielded by the induced field of the adjacent aromatic ring and therefore move upfield to a lower chemical shift.[30]

The NMR chemical shift data of the PhdiOH*t*Bu (**45**) balance in $CDCl_3$ listed in Table 3.2 also show that the aromatic protons of the central ring have chemical shifts most similar to the X = Br, CN, or NO_2 reference balances. Thus, it can be concluded from the NMR data and folding free energies that polar hydroxy protons positioned above an aromatic ring have the effect of reducing electron density via a through-space substituent effect.

Through-space effects of alkyl substituents

In Figure 3.19 it can be seen that electrostatic potentials of the biphenyls Ph, PhdiMe and PhdiEt are very similar and only slightly less negative than benzene (Figure 3.9). Accordingly, the folding free energies of balances **26**, **27** and **28** are very similar, supporting the results of the MEP calculations shown in Figure 3.19, and suggesting that electronic through-space effects are small in these cases (MEP_{ortho} –62 to –66 kJ/mol). Figure 3.20 shows structures from the CCDB showing the conformations of the Ph - Ph and Ph - PhdiMe biaryl systems found in balances **26** and **27**. Reassuringly, the crystal structures of the moieties closely resemble those in the calculated structures.

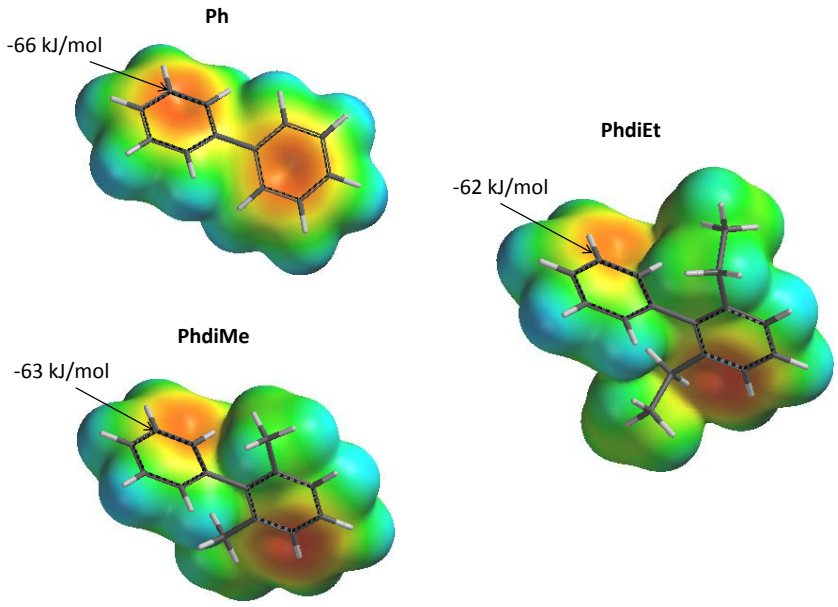

Figure 3.19. Density potential surfaces for alkyl-substituted biphenyls indicating the MEP at the *ortho* positions.

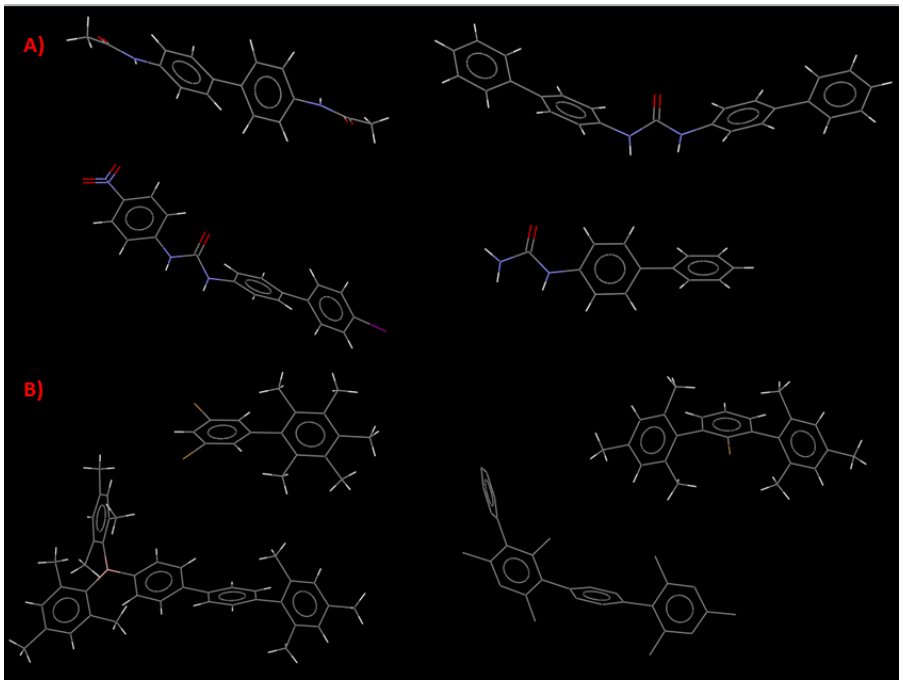

Figure 3.20. Crystal structures showing the relative angles of the A) Ph - Ph and B) Ph - PhdiMe systems found in balances **26** and **27**. (CCDB codes: A) ASIFIR, HAHCOJ, TIVQAR, QOGROT, B) VUYVUH, CORGUM, ASODUI, VINWEU)

3.4. Conclusions

Molecular Electrostatic Potential surface calculations predict through-space electronic communication to occur between aromatic rings and substituents placed in close proximity to each other. Calculations performed at the B3LYP/6-31G* level were shown to correctly predict the through-space electronic effects of substituents on experimental folding free energies in a series of molecular balances measured in a range of organic solvents.

The calculated and experimental observations could not be explained by classic through-bond substituent effects. For example, while nitro groups are strongly electron-withdrawing through bonds, nitro groups were shown to be strongly electron-donating through-space. Similarly, methoxy groups were found to be electron-donating through-space, but only when the oxygen lone-pairs point towards an aromatic ring. In this case, the through-space substituent effect could be switched off-entirely via a conformation change induced by a nearby *tert*-butyl group. The electron-density of aromatic rings was found to be reduced by nearby polar hydroxyl and amino protons, while alkyl groups placed in the same position did not have a significant electronic effect.

This combined experimental and theoretical study supports the hypothesis that the electron-density of an aromatic ring can be strongly perturbed by the through-space electronic effects of substituents. The unambiguous identification and experimental measurement of these effects has fundamental implications and could be harnessed in synthetic strategies[32,33], organo-catalysis[34] and supramolecular chemistry[35].

3.5. References

1. Wheeler, S. E.; Houk, K. N., *J. Chem. Theory Comput.* **2009**, 5, 2301-2312.
2. Wheeler, S. E.; Houk, K. N., *J. Am. Chem. Soc.* **2008**, 130, 10854-10855.
3. Hammett, L. P., *Chem. Rev.* **1935**, 17, 125-36.
4. Hammett, L. P., *J. Am. Chem. Soc.* **1937**, 59, 96-103.
5. Hansch, C.; Leo, A.; Taft, R. W., *Chem. Rev.* **1991**, 91, 165-95.
6. Taft, R. W., Jr., *J. Am. Chem. Soc.* **1952**, 74, 2729-32.
7. Taft, R. W., Jr., *J. Am. Chem. Soc.* **1952**, 74, 3120-8.

8. Taft, R. W., Jr., *J. Am. Chem. Soc.* **1953**, 75, 4231-8.
9. Swain, C. G.; Lupton, E. C., Jr., *J. Amer. Chem. Soc.* **1968**, 90, 4328-37.
10. Hansch, C.; Leo, A.; Unger, S. H.; Kim, K. H.; Nikaitani, D.; Lien, E. J., *J. Med. Chem.* **1973**, 16, 1207-16.
11. Swain, C. G.; Unger, S. H.; Rosenquist, N. R.; Swain, M. S., *J. Am. Chem. Soc.* **1983**, 105, 492-502.
12. Suresh, C. H.; Gadre, S. R., A Novel *J. Am. Chem. Soc.* **1998**, 120, 7049-7055.
13. Galabov, B.; Ilieva, S.; Schaefer, H. F., III, *J. Org. Chem.* **2006**, 71, 6382-6387.
14. Suresh, C. H.; Alexander, P.; Vijayalakshmi, K. P.; Sajith, P. K.; Gadre, S. R., *Phys. Chem. Chem. Phys.* **2008**, 10, 6492-6499.
15. Sayyed, F. B.; Suresh, C. H., *Tetrahedron Lett.* **2009**, 50, 7351-7354.
16. Wheeler, S. E., Understanding Substituent Effects in Noncovalent Interactions Involving Aromatic Rings. *Acc. Chem. Res.*, **2012** Ahead of Print.
17. Wheeler, S. E., *J. Am. Chem. Soc.* **2011**, 133, 10262-10274.
18. Wheeler, S. E.; Houk, K. N., *J. Am. Chem. Soc.* **2009**, 131, 3126-3127.
19. Wheeler, S. E.; Houk, K. N., *J. Phys. Chem. A* **2010**, 114, 8658-8664.
20. Sayyed, F. B.; Suresh, C. H., *J. Phys. Chem. A* **2011**, 115, 5660-5664.
21. Sayyed, F. B.; Suresh, C. H.; Gadre, S. R., *J. Phys. Chem. A* **2010**, 114, 12330-12333.
22. Byron, D. J.; Gray, G. W.; Wilson, R. C., *J. Chem. Soc. C* **1966**, 837-40.
23. Roberts, J. D.; Moreland, W. T., Jr., *J. Am. Chem. Soc.* **1953**, 75, 2167-73.
24. Bowden, K.; Grubbs, E. J., *Chem. Soc. Rev.* **1996**, 25, 171-177.
25. Hojo, M.; Utaka, M.; Yoshida, Z., Ortho effects. V. *Tetrahedron* **1971**, 27, 2713-23.
26. Hojo, M.; Utaka, M.; Yoshida, Z., Otho effects. VI. *Tetrahedron* **1971**, 27, 4031-8.
27. Komiyama, M., *Bull. Chem. Soc. Jpn.* **1988**, 61, 2079-82.
28. Chen, W.; Lin, Z.; Ning, M.; Yang, C.; Yan, X.; Xie, Y.; Shen, X.; Wang, M.-W., *Bioorg. Med. Chem.* **2007**, 15, 5828-5836.
29. Cativiela, C.; Garcia, J. I., *Can. J. Chem.* **1990**, 68, 1477-81.
30. http://en.wikipedia.org/wiki/Chemical_shift, chemical shifts.
31. http://riodb01.ibase.aist.go.jp/sdbs/, (National Institute of Advanced Industrial Science and Technology).
32. Clayden, J.; Vassiliou, N., *Org. Biomol. Chem.* **2006**, 4, 2667-2678.
33. Clayden, J., *Nat. Chem.* 3, **2011**, 842-843.
34. MacMillan, D. W. C., *Nature* **2008**, 455, 304-308.
35. Schneider, H. J., *Angew Chem Int Ed Engl* **2009**, 48, 3924-77.

Chapter 4

Solvent bridging interactions in molecular balances

Abstract

The role of water molecules in biological systems has been proven to be very important.[1-3] Interactions where water binds between a protein and a ligand may help to stabilise the complex (Figure 4.1).[4-6] The water molecules found within protein crystal structures can be classified in two groups: those that are conserved as bridging molecules in the interaction site and those which can be displaced by the ligand.[7,8] Water molecules that are strongly bound are often found in polar regions of a protein and form more hydrogen bonds than loosely bound water molecules found in mostly apolar environments.[7,8] Knowledge of the role of water molecules in a protein binding site is useful for the design of ligands with the essential structure to bind at an active site. Furthermore, bridging water molecules may be important in stabilising the structure of proteins.[9-11] It is very difficult to examine a specific bridging interaction in the structurally complicated dynamic systems found in biology where numerous factors contribute to the observed behaviour.

In this study we used small organic molecules to investigate the energetic contribution of solvent bridging interactions to the overall energy of the system. More specifically, we used synthetic molecular balances that exist as two conformers in equilibrium *via* the slow rotation of a bond.[12] The hydrophobic effect caused by D_2O for some molecular balances has been identified in the literature.[13-15]

Molecules which might form potential bridging interactions between functional groups in molecular balances were identified using computational modelling. Unfortunately the hydroxy-substituted balances had aggregation and stabilisation problems, though changes in folding energies were observed in other balances capable

of forming D_2O bridging interactions as the concentration of D_2O in a THF solution was changed. However, changes in the folding free energy were also observed in reference balances, suggesting that a general solvation effect was the cause of the effect rather than a specific bridging interaction.

Water bridging interactions in biological systems

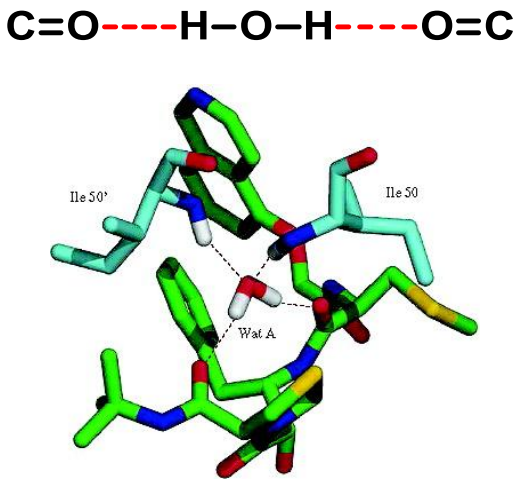

Figure 4.1. a) The bridging interaction of a water molecule between two carbonyls. b) Wat A acts as a bridge between HIV-1 protease and ligand KNI272. The water molecule forms four hydrogen bonds in total, two as a hydrogen bond donor to the ligand and two as a hydrogen bond acceptor to the protein.[7] (Reprinted with permission from: Barillari, C.; Taylor, J.; Viner, R.; Essex, J. W., *J. Am. Chem. Soc.* **2007**, 129, 2577-2587. Copyright 2007, American Chemical Society.)

4.1. Methodology for the investigation of bridging interactions

The design of the molecular torsion balances used for the investigation of bridging interactions is based on a tertiary formamide (Figure 4.2). These molecules exist as two conformers in equilibrium at room temperature due to the slow rotation of the formyl group arising from the double-bond character of the N-C bond. Signals corresponding to each conformer are therefore apparent in the NMR spectra and the ratio of these signals can provide the folding free energy of the balance.

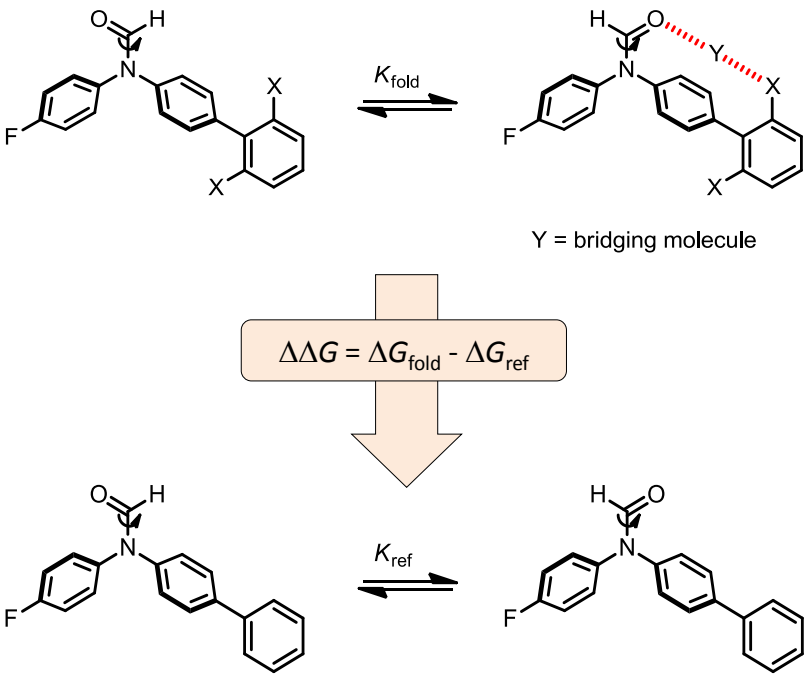

Figure 4.2. Schematic representation of the method followed for the determination of the energetic contribution of the bridging interaction.

The design of the molecular balance incorporates three aromatic rings, one is substituted with a fluorine atom, while the second aromatic ring is connected to a third ring *para* to the amide. The third aromatic ring in this design is di-*ortho*-substituted with methoxy, nitro or hydroxyl groups that could form a potential bridging interaction to the formyl group mediated by a solvent molecule (Figure 4.2, top right). These rings are *ortho*-disubstituted such that a bridging interaction may take place irrespective of the orientation of the third ring.

The distance between the formyl group and the other interacting substituent as shown in Figure 4.3 is more than 5 Å as found from the minimised structures of the balances calculated using DFT/B3LYP/6-31G* in Spartan '08. This distance is too large

for a direct hydrogen bond to take place, but large enough to accommodate a small-molecule bridging interaction.

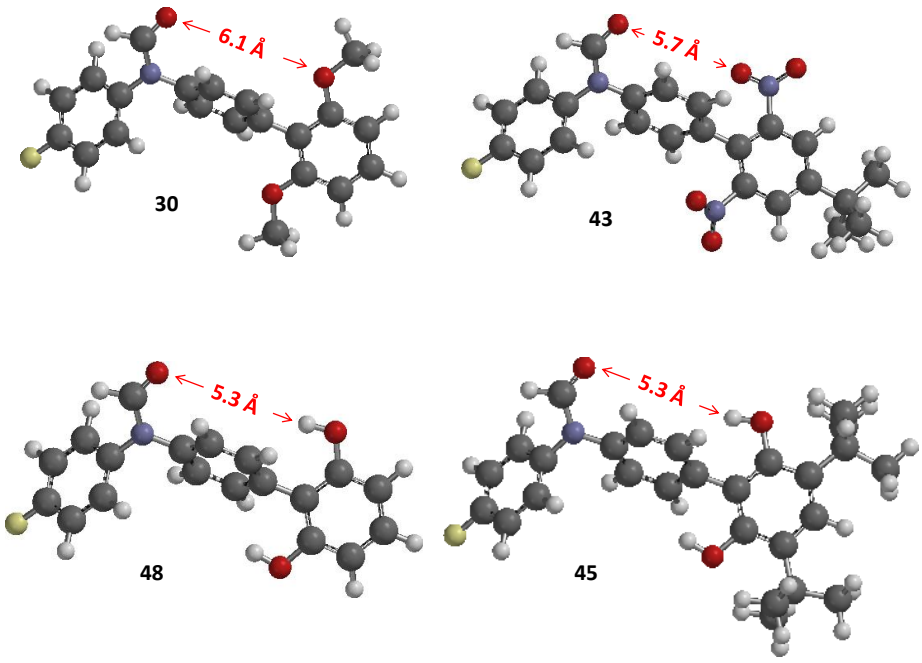

Figure 4.3. Computational structures of molecular torsion balances and the corresponding distances between the formyl and the other interacting group calculated in Spartan ’08 using B3LYP/6-31G*.

The two bridging partners shown in Figure 4.2 are the oxygen or proton of the formyl group and the X-substituents on the third aromatic ring. These partners can be hydrogen bond donors or acceptors depending on the donating or accepting ability of the bridging molecule Y. The X-substituents or the whole third ring could be removed in reference balances such that no bridging interaction can occur, while still taking into account the secondary electronic, steric and solvent effects on position of the conformation equilibrium. By measuring the folding energy of suitable reference compounds and subtracting it from the folding free energy of the torsion balance containing the bridging interaction, the actual energetic contribution of the interaction can be quantified (Figure 4.2).

The structures of all of the molecular balances discussed in this chapter are shown in Figure 4.4.

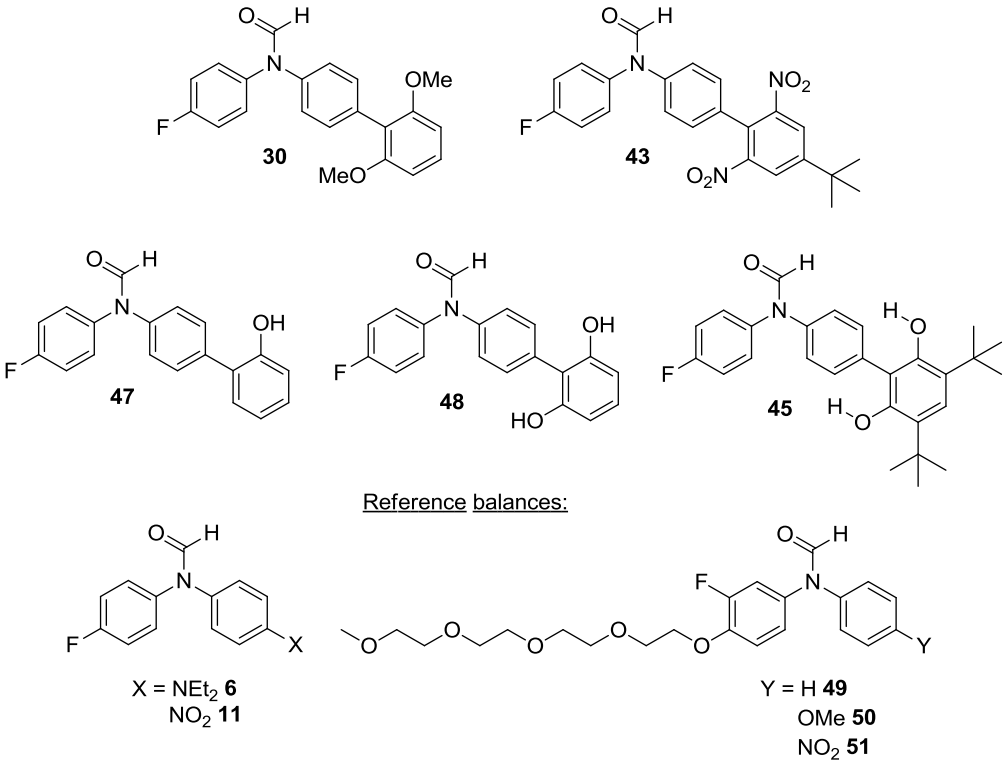

Figure 4.4. Molecular torsion balances that could show solvent bridging interactions and reference balances used in this study.

4.2. Modelling molecular balances with bridging molecules

The proposed molecular torsion balances were minimised at the DFT/B3LYP/6-31G* level in Spartan '08 to examine whether various bridging molecules could be accommodated between the formyl group and the substituent on the third aromatic ring of the balance.

Figure 4.5 shows space filling models of the PhdiOMe balance (**30**) with potential bridging molecules (H_2O, ethylene glycol, butylamine and aniline). A good fit between the formyl oxygen and the methoxy substituent is seen in all cases except for ethylene glycol. In the latter case, the binding cleft may be too small to accommodate both hydroxyl groups. Thus, ethylene glycol was rejected as a potential bridging candidate.

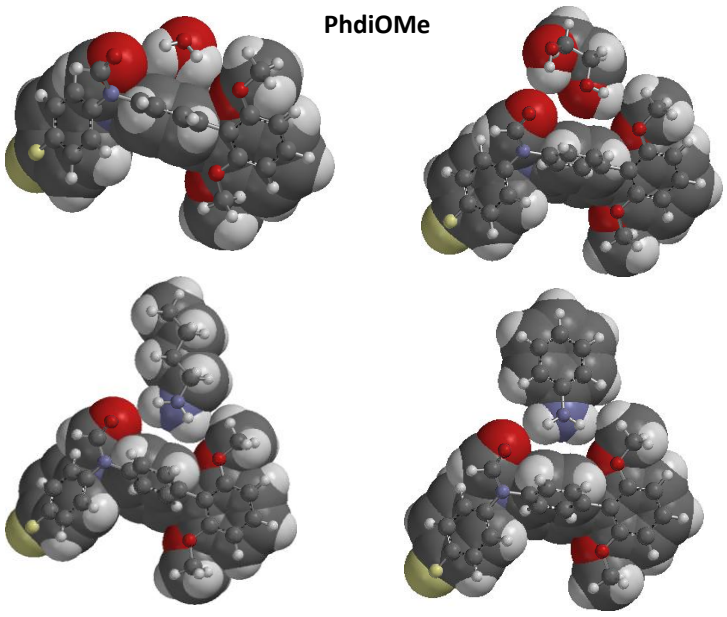

Figure 4.5. Space filling model of *N*-(2',6'-dimethoxy-[1,1'-biphenyl]-4-yl)-*N*-(4-fluorophenyl)formamide (**30**) with different bridging molecules.

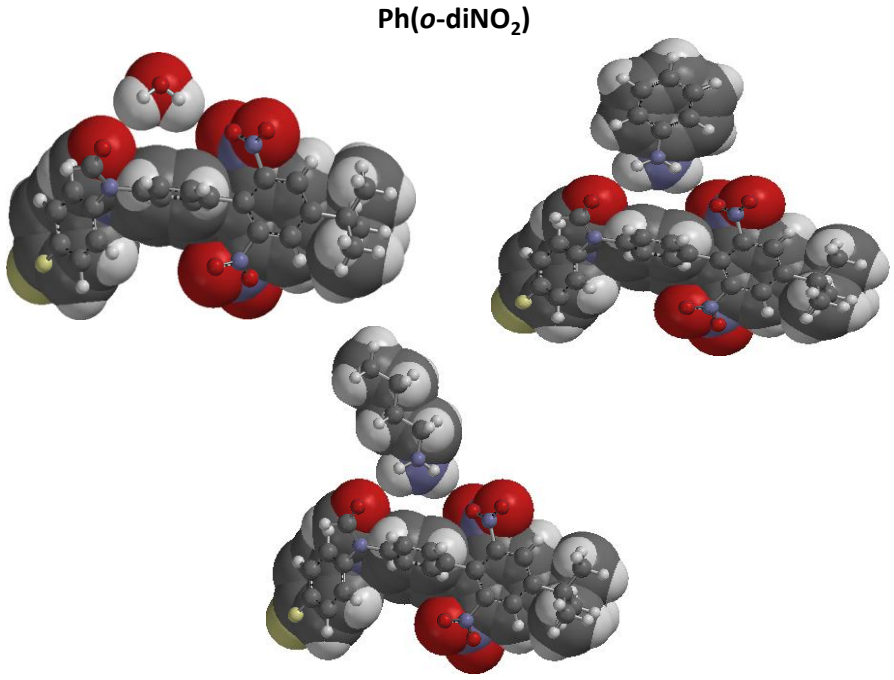

Figure 4.6. Space filling model of *N*-(4'-(*tert*-butyl)-2',6'-dinitro-[1,1'-biphenyl]-4-yl)-*N*-(4-fluorophenyl)formamide (**43**) with different bridging molecules.

Figure 4.6 shows the minimised structures of the Ph(*o*-diNO_2) balance (**43**) with bridging water, butylamine and aniline molecules. All three molecules appear able to form bridging hydrogen bonds and fit well within the cleft between the formyl and nitro groups.

In the case of the PhdiOH balance (**48**) it is difficult to predict whether the hydroxyl protons will point towards the adjacent formyl group or away from it. For example, a hydrogen bond could form between the proton of the hydroxyl substituent and the *n*-butanol oxygen atom and a second between the hydroxyl proton of *n*-butanol and the formyl oxygen. The PhdiOHtBu balance (**45**) was designed to overcome this conformational ambiguity since the two hydroxyl protons are forced to point towards the central aromatic ring due to the bulky *tert*-butyl groups. This design allows a molecule such as an alcohol to form a bridging interaction within the binding cleft (Figure 4.7).

PhdiOH &PhdiOHtBu

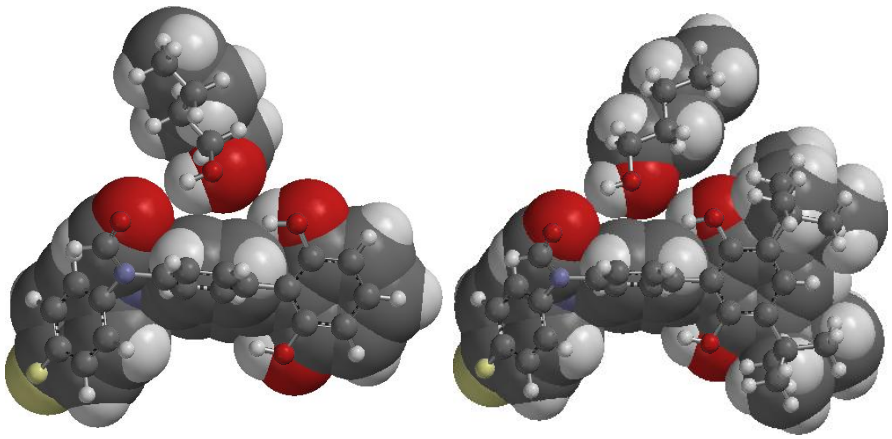

Figure 4.7. Space filling model of the *N*-(2',6'-dihydroxy-[1,1'-biphenyl]-4-yl)-*N*-(4-fluorophenyl)-formamide (**48**) and *N*-(3',5'-di-*tert*-butyl-2',6'-dihydroxy-[1,1'-biphenyl]-4-yl)-*N*-(4-fluorophenyl)-formamide (**45**) with *n*-butanol as a bridging molecule.

4.3. Synthesis of the molecular torsion balances

The syntheses of molecular balances referred to in this chapter are detailed in Chapters 2 and 3 except for compounds **47** and **48** as detailed below. The PEGylated balances described later were synthesised and characterised by Catherine Adam.

The *N*-(4-fluorophenyl)-*N*-(2'-hydroxy-[1,1'-biphenyl]-4-yl)formamide balance (**47**) was synthesised in an 84% yield via the Suzuki coupling reaction of *N*-(4-bromophenyl)-*N*-(4-fluorophenyl)formamide (**5**)[16] with (2-hydroxyphenyl)boronic acid (**46**). Tetrakis(triphenylphosphine)palladium(0) was used as a catalyst and sodium carbonate as a base (Figure 4.8).[17]

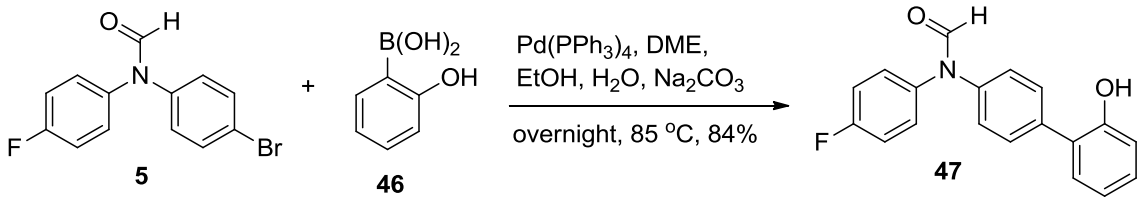

Figure 4.8. Synthesis of the *N*-(4-fluorophenyl)-*N*-(2'-hydroxy-[1,1'-biphenyl]-4-yl)formamide (**47**).

Following this successful reaction, the di-OH molecular torsion balance *N*-(2',6'-dihydroxy-[1,1'-biphenyl]-4-yl)-*N*-(4-fluorophenyl)-formamide (**48**) was synthesised in excellent yield (97%) after the deprotection of the methoxy groups of the *N*-(2',6'-dimethoxy-[1,1'-biphenyl]-4-yl)-*N*-(4-fluorophenyl)formamide (**30**)[16,17] with boron tribromide in dichloromethane (Figure 4.9).[18] Literature procedures used 4 eq of 1 M BBr_3 in CH_2Cl_2, but this was not sufficient for the synthesis of the di-OH-*t*-Bu balance (**45**).[18] However, 8 eq of BBr_3 was used successfully for the synthesis of torsion balances (**45**) and (**48**).

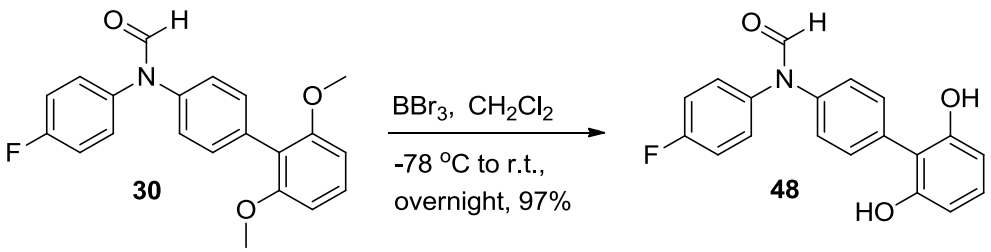

Figure 4.9. Synthesis of *N*-(2',6'-dihydroxy-[1,1'-biphenyl]-4-yl)-*N*-(4-fluorophenyl)-formamide (**48**).

4.4. Problems encountered with the hydroxy-substituted molecular torsion balances

Unfortunately, it was observed that the mono-OH (**47**) and di-OH (**48**) balances slowly crystallised in solvents such as $CDCl_3$, DCM, benzene and EtOAc during NMR experiments. No crystals were seen to form in more polar solvents such as acetone and acetonitrile. A concentration study was therefore performed in chloroform and methanol for the mono-OH (**47**) torsion balance to test for aggregation. In methanol the ratio of the two conformers was stable at all three concentrations examined (0.33 M, 0.1 M and 0.028 M), whereas the ratio changed in a concentration-dependant manner in chloroform (concentrations: 0.33 M, 0.1 M and 0.028 M), which was consistent with aggregation in apolar solvents (Figure 4.10). A likely explanation is that the hydroxyl groups of these balances are well solvated in polar solvents, but the hydroxyl groups are free to serve as aggregation points in more apolar solvents. Although the di-OH-*t*-Bu balance (**45**) is less likely to be affected by aggregation due to the bulky *tert*-butyl groups, it had limited stability and was found to decompose on the time-scale of a few days. This limited the accuracy of the NMR conformer integrals. Furthermore, silica also seemed to contribute to the decomposition of the molecule, rendering purification of the compound difficult.

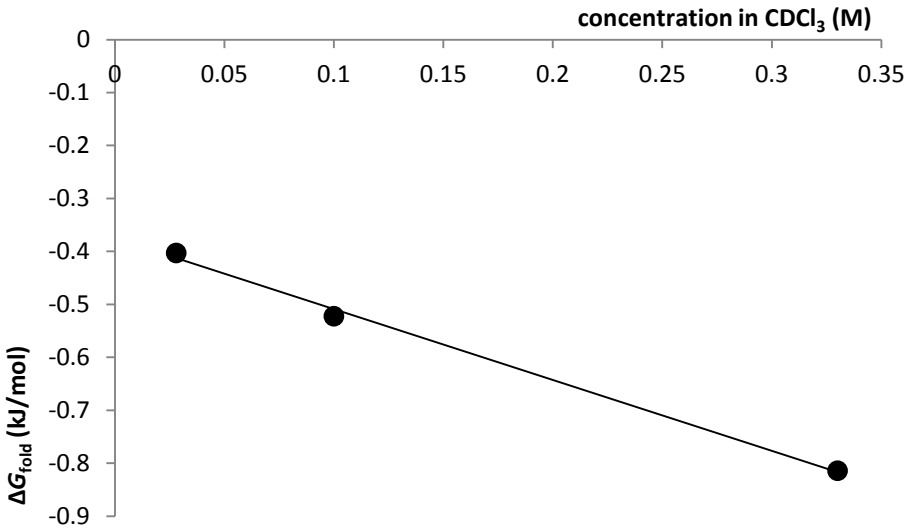

Figure 4.10. The folding free energy of the mono-OH (**47**) torsion balance is concentration-dependant in chloroform.

Nonetheless, it could still be determined that di-OH-*t*-Bu balance (**45**) preferred conformer B, while conformer A dominated for the mono-OH (**47**) and di-OH (**48**) balances. This observation is consistent with the through-space electronic substituent effects described in Chapter 3. A table containing approximate folding energies for the three hydroxy-substituted balances **47**, **48** and **45** in a range of organic solvents can be found in the experimental section (Chapter 6-Table 6.1). However, the limitations above meant that the hydroxy-substituted balances could not be used alongside the other molecular balances in the experimental investigations of solvent bridging interactions described below (Figure 4.4).

4.5. Investigation of potential deuterium oxide bridging interactions

N-(2',6'-dimethoxy-[1,1'-biphenyl]-4-yl)-*N*-(4-fluorophenyl)formamide (**30**) contains two methoxy substituents at the *ortho* positions of the third aromatic ring. As was shown

by molecular modelling (Figure 4.5), a water (or deuterium oxide) molecule could potentially bridge between the formyl and methoxy oxygen atoms (Figure 4.11).

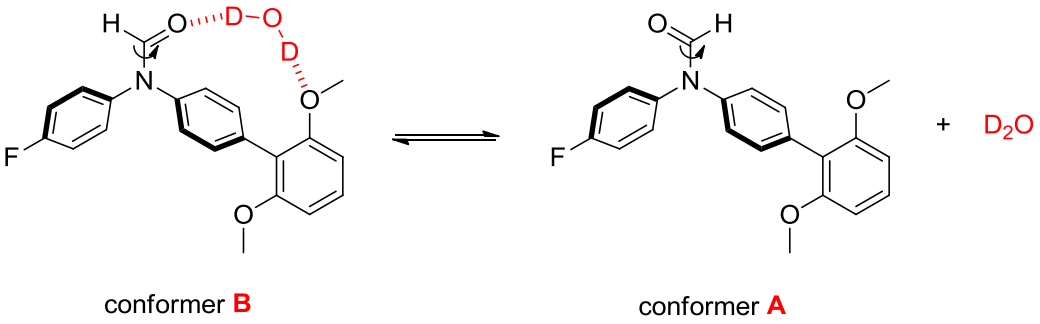

	Dry solvent		"Wet" solvent	
	A/B ratio	**Δ*G* (kJ/mol)**	**A/B ratio**	**Δ*G* (kJ/mol)**
$CDCl_3$	2.50	-2.27	2.44	-2.21
CH_3NO_2	1.37	-0.78	1.35	-0.75
CH_3CN	1.37	-0.78	1.39	-0.81

Figure 4.11. Equilibrium of the *N*-(2',6'-dimethoxy-[1,1'-biphenyl]-4-yl)-*N*-(4-fluorophenyl)formamide (**30**) with a D_2O bridging molecule. Table showing the A/B ratios and Δ*G* of the balance (**30**) in dry solvents and the same solvents after mixing with D_2O.

The table at the bottom of Figure 4.11 lists the conformer ratios for compound **30** measured in various solvents both with and without the addition of D_2O. In all cases, A is the major conformer. If the postulated bridging interaction is formed, it might be expected that the equilibrium should shift towards conformer B (Figure 4.11). Although chloroform is not miscible with water, small amounts of it can dissolve. However, "wetting" chloroform with D_2O resulted only in a minor change in the conformational ratio of compound **30**. This could indicate that either no bridging interaction is formed in the torsion balance, or that the binding constant of D_2O to the bridging site was too low to give a measurable effect at low concentrations of D_2O. Nitromethane is known to dissolve up to 10% water, but addition of 10% D_2O to nitromethane also gave a slight

change in the conformational ratio of balance **30**. Acetonitrile is fully miscible with water, but compound **30** proved to be quite insoluble in acetonitrile mixtures containing moderate amounts of D_2O. At the concentrations of D_2O in acetonitrile in which compound **30** was soluble, only a slight change in the conformational ratio was observed compared to dry acetonitrile (Figure 4.11). The conformational ratio difference in all three cases is within the limits of experimental error, and does not prove the existence of any significant bridging interaction.

Table 4.1. Conformational ratios and folding free energies of molecular balances in THF and D_2O solutions.

Balance	Solvent	A	B	ΔG_{fold}
PhdiOMe (30)	**THF**	1	0.54	-1.53
	10% D_2O	1	0.57	-1.39
	20% D_2O	1	0.6	-1.27
	30% D_2O	1	0.61	-1.22
***p*-NEt_2 (6)**	**THF**	1	0.43	-2.09
	15% D_2O	1	0.51	-1.67
	30% D_2O	1	0.53	-1.57
***p*-NO_2 (11)**	**THF**	0.7	1	0.88
	30% D_2O	0.91	1	0.23
	40% D_2O	0.93	1	0.18
PEG-H (49)	**THF**	1	0.8	-0.55
	D_2O	1	0.87	-0.35
PEG-OMe (50)	**THF**	1	0.71	-0.85
	D_2O	1	0.95	-0.13
PEG-NO_2 (51)	**THF**	0.59	1	1.31
	D_2O	1	0.64	-1.11

More promising results were obtained with THF, which is reasonably miscible with water (Table 4.1). In the case of balance **30**, the conformational ratio changed from A/B = 1/0.54 in dry THF to 1/0.61 in THF containing 30% (v/v) D_2O. Since the conformational ratio changed very little on going from 20% D_2O to 30% D_2O, NMR spectra were taken over a range of intervals spanning several minutes to several hours.

No change in the conformational ratio was observed, which proved that the conformational equilibrium occurred rapidly within the timescale of the experiments.

Before any evidence of a bridging interaction can be claimed, the aforementioned changes in the conformational ratio in the presence of deuterium oxide must be compared against the behaviour of reference balances under the same conditions (Table 4.1 and Figure 4.4).

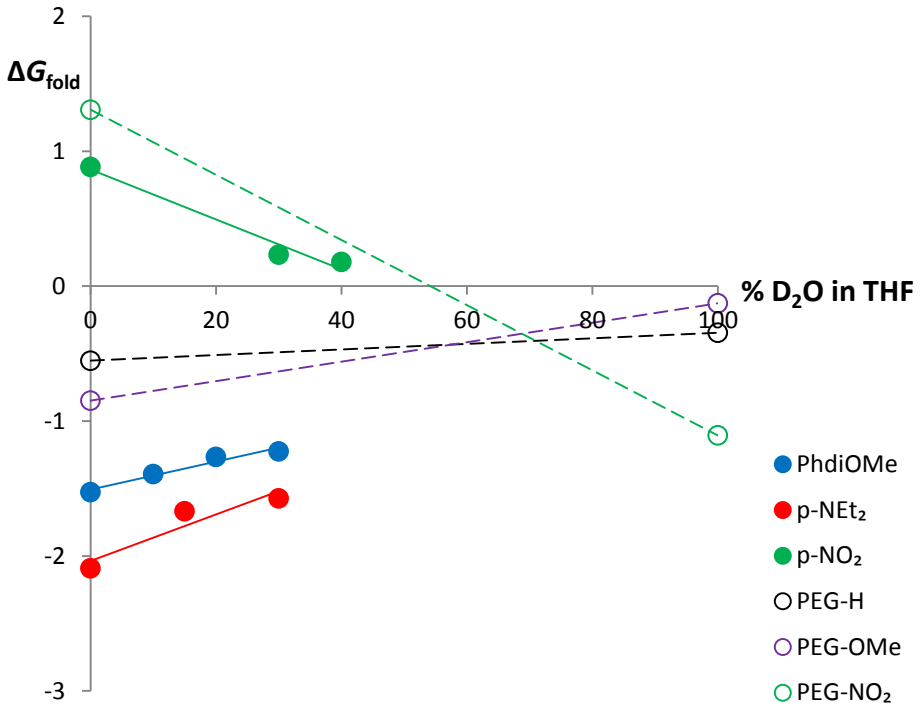

Figure 4.12. Folding free energies in various THF/D_2O mixtures for molecular torsion balances **30, 6, 11** (solid circles), and PEGylated balances **49, 50** and **51** (hollow circles).

Figure 4.12 shows the experimental folding free energy of various control balances as the percentage of deuterium oxide in THF is varied. Although the *p*-NEt_2 and *p*-NO_2 reference balances lack the substituents required to form bridging interactions, the conformational ratios of these compounds changed significantly as the proportion of D_2O dissolved in the THF was varied.

As was shown in Chapter 3, the *p*-NEt_2 balance (**6**) has similar electronic properties to the diOMe balance (**30**), therefore this balance serves as the most appropriate reference balance. It can be seen that the changes in the folding free energy of balance **30** as the concentration of D_2O is varied (blue line in Figure 4.12) are similar to those observed for the NEt_2 reference compound (red line in Figure 4.12). It can be therefore concluded that significant D_2O-mediated bridging interactions within the PhdiOMe balance (**30**) cannot be identified. One possible explanation is that the binding of water to this receptor is too weak to overcome the entropic penalty associated with complexation. The energy cost for bringing together two molecules in solution to form a bimolecular complex has been reported to be +6 kJ/mol.[19] Thus, a side experiment was performed in which a THF/30% D_2O solution saturated with ammonium carbonate was used to investigate whether the ammonium cation forms a bridging interaction in balance **30**. The ammonium cation might be expected to bind the bridging site more strongly than D_2O, but unfortunately, the addition of the salt caused both compound **30** to crash out of solution, and the phase separation of THF and D_2O.

Also notable was the change in the conformational ratio of the *p*-NO_2 balance (**11**) from A/B = 0.7/1 in THF to 0.93/1 in THF with 40% D_2O (Figure 4.12). This result mirrors the observation made in Chapter 2 that balances bearing strongly electron-withdrawing substituents were seen to prefer conformer A in polar solvents, while conformer B was preferred in apolar solvents (Table 2.1). To further examine this effect, another researcher in the group (Catherine Adam) performed a series of experiments on the *p*-NO_2 balance in mixtures of 20%, 40%, 60% and 80% of D_2O in acetone. With the addition of more D_2O, resonances in the ^{19}F-NMR corresponding to each conformer were seen to move closer together, before coalescing, and eventually crossing-over. The free folding energies were also seen to swap signs, which confirmed the gradual change in the preference for conformer A as more D_2O was added to the solution.

Since the simple reference balances are not soluble in D_2O, Catherine Adam also synthesised water-soluble PEGylated torsion balances as shown in Figure 4.13. Table 4.1 includes the folding free energies of these PEGylated balances in pure THF and pure

D_2O. As can be seen in the graph in Figure 4.12 the folding free energies of the PEG-H and PEG-OMe balances change slightly on moving from THF to D_2O, but those of the PEG-NO_2 balance change dramatically from a strong preference of conformer B in THF to a preference for conformer A in D_2O.

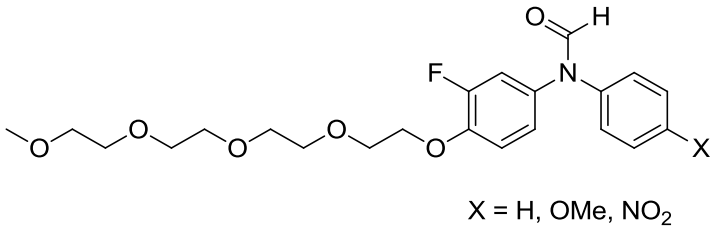

Figure 4.13. PEGylated molecular torsion balances.

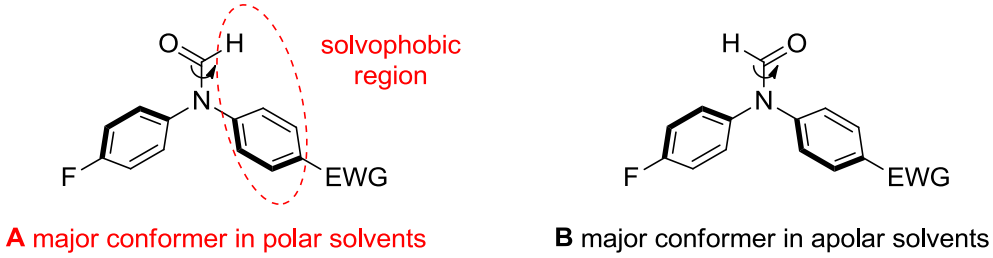

Figure 4.14. When the X-substituent is a strong EWG, conformer A is preferred in polar solvents, while conformer B is preferred in apolar solvents.

One possible hypothesis that competes with the solvation model presented in Chapter 2, is that the change in the preferred conformer as water is added is due to a solvophobic effect. Electrostatic calculations show that when the substituent is a strong EWG the face of the adjacent aromatic ring becomes very apolar with a partial charge close to zero. Thus, it could be reasoned that solvophobic polar solvents would drive the equilibrium towards conformer A, in which the apolar formyl group proton is positioned above the solvophobic region formed by the most apolar aromatic face (Figure 4.14).

Although, this solvophobic model seems feasible, the correlations of the dissected *a*, *b* and *c* coefficients with calculated electrostatic potentials and calculated folding energies presented in Chapter 2 strongly suggest that the solvophobic coefficient *d* is close to zero, indicating that solvophobic effects are not important in determining the position of the conformational equilibrium in this class of molecules. Since water is both a good hydrogen bond donor and a good hydrogen bond acceptor, the situation shown in Figure 4.15 applies, where both the formyl oxygen and the edge of the most polar aromatic ring are strongly solvated by water driving the equilibrium towards conformer A. This model provides a more general explanation for the observed conformational behaviour of the balances across the range of solvents examined.

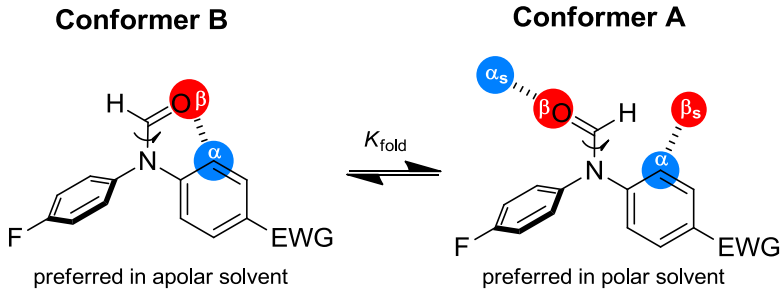

Figure 4.15. Solvation model for balances bearing electron-withdrawing groups (EWG).

4.6. Conclusions and future work

Computational modelling of molecular torsion balances containing potential bridging interactions was performed. The hydroxy-substituted balances were unsuitable for the investigation of bridging interactions due to aggregation and stability problems. The PhdiOMe torsion balance (**30**) was used for the study of D_2O bridging interactions in THF/D_2O mixtures. However control experiments performed with reference balances indicated that the observed changes in the conformational ratio as D_2O is added to THF arise from a general solvation effect rather than a specific bridging interaction. The result was consistent with the solvation model introduced in Chapter 2. Further

experimental support for this model was provided by data obtained for balances with electron-withdrawing substituents in THF/D_2O solvent mixtures.

Computational modelling also suggested that the PhdiNO_2 balance (**43**) might be a promising candidate for the examination of bridging interactions, however, there was insufficient time to obtain these data. Future work could expand the study to include analysis of this compound in D_2O/THF solvent mixtures.

One possible reason for the failure to identify bridging interactions in this system despite promising computational models is that the entropic penalty associated with binding the receptor site is too large to be overcome by the enthalpic stabilisation of forming the proposed bridging interactions. Further investigation into this hypothesis is required through combined experimental and theoretical studies. It is possible that the bridging interactions observed in protein crystal structures are stabilised by the protein cavity since they are protected from entropic "solvent buffeting".[20]

4.7. Acknowledgements

Catherine Adam performed studies on the *p*-NO_2 balance (**11**) in acetone/D_2O mixtures, in addition to synthesising and studying the PEGylated molecular torsion balances (**49**), (**50**) and (**51**).

4.8. References

1. Salonen, L. M.; Holland, M. C.; Kaib, P. S. J.; Haap, W.; Benz, J.; Mary, J.-L.; Kuster, O.; Schweizer, W. B.; Banner, D. W.; Diederich, F., *Chem. Eur. J.* **2012**, 18, 213-222.
2. Tarek, M.; Tobias, D. J., *Phys. Rev. Lett.* **2002**, 88, 138101/1-138101/4.
3. Otting, G.; Wuethrich, K., *J. Am. Chem. Soc.* **1989**, 111, 1871-5.
4. Meiering, E. M.; Wagner, G., *J. Mol. Biol.* **1995**, 247, 294-308.
5. McTigue, M. A.; Davies, J. F., II; Kaufman, B. T.; Kraut, J., *Biochemistry* **1992**, 31, 7264-73.
6. Filman, D. J.; Bolin, J. T.; Matthews, D. A.; Kraut, J., *J. Biol. Chem.* **1982**, 257, 13663-72.
7. Barillari, C.; Taylor, J.; Viner, R.; Essex, J. W., *J. Am. Chem. Soc.* **2007**, 129, 2577-2587.

8. Babor, M.; Sobolev, V.; Edelman, M., Complexes. *J. Mol. Biol.* **2002**, 323, 523-532.
9. Dougan, L.; Koti, A. S. R.; Genchev, G.; Lu, H.; Fernandez, J. M., *ChemPhysChem* **2008**, 9, 2836-2847.
10. Levy, Y.; Onuchic, J. N., *Annu. Rev. Biophys. Biomol. Struct.* **2006**, 35, 389-415.
11. Cheung, M. S.; Garcia, A. E.; Onuchic, J. N., *Proc. Natl. Acad. Sci. U. S. A.* **2002**, 99, 685-690.
12. Mati, I. K.; Cockroft, S. L., *Chem. Soc. Rev.* **2010**, 39, 4195-4205.
13. Gardner, R. R.; McKay, S. L.; Gellman, S. H., *Org. Lett.* **2000**, 2, 2335-2338.
14. Gardner, R. R.; Christianson, L. A.; Gellman, S. H., *J. Am. Chem. Soc.* **1997**, 119, 5041-5042.
15. Bhayana, B.; Wilcox, C. S., *Angew. Chem., Int. Ed.* **2007**, 46, 6833-6836.
16. Phillips, D. P.; Zhu, X.-F.; Lau, T. L.; He, X.; Yang, K.; Liu, H., *Tetrahedron Lett.* **2009**, 50, 7293-7296.
17. Lana, E. J. L.; Carazza, F.; Aparacida de Oliveira, R., *Helv. Chim. Acta* **2004**, 87, 1825-1831.
18. Chen, W.; Lin, Z.; Ning, M.; Yang, C.; Yan, X.; Xie, Y.; Shen, X.; Wang, M.-W., *Bioorg. Med. Chem.* **2007**, 15, 5828-5836.
19. Hunter, C. A., *Angew. Chem., Int. Ed.* **2004**, 43, 5310-5324.
20. Boes, F.; Pleiss, J., *Biophys. J.* **2009**, 97, 2550-2558.

Chapter 5

The interplay of steric and solvation effects on conformational equilibria

Abstract

Solvation phenomena affect most chemical and biological processes, and play an important role in determining the rate and outcome of chemical reactions.[1] Water molecules have been found to be important in the protein folding[2] and in the stabilisation of protein-ligand complexes.[3] Solvent effects can manifest themselves over long distances, as is observed in the long-range attraction between two hydrophobic surfaces in water.[4-7] The size and shape of the solvent molecule is also important in solvation processes, particularly in the presence of a sterically occluded solute such as that found in binding pockets or capsules.[8-10] The solvent can even control the self-assembly of capsules.[11] According to Rebek's 55% rule the binding of a guest molecule in the cavity of a receptor can occur when the ratio of the guest volume to the host volume is about 0.55.[12]

This short chapter outlines preliminary findings observed in molecular balances in $CDCl_3$ and CH_2Cl_2 solution, which suggest that the position of a conformational equilibrium might be affected either by the steric blocking of solvation sites or electrostatic changes induced by solvation. Although no clear conclusion can be made based on the existing data, the results warrant further investigation and new model systems are proposed to investigate the possible mechanisms by which these effects could occur.

5.1. Introduction to the model system

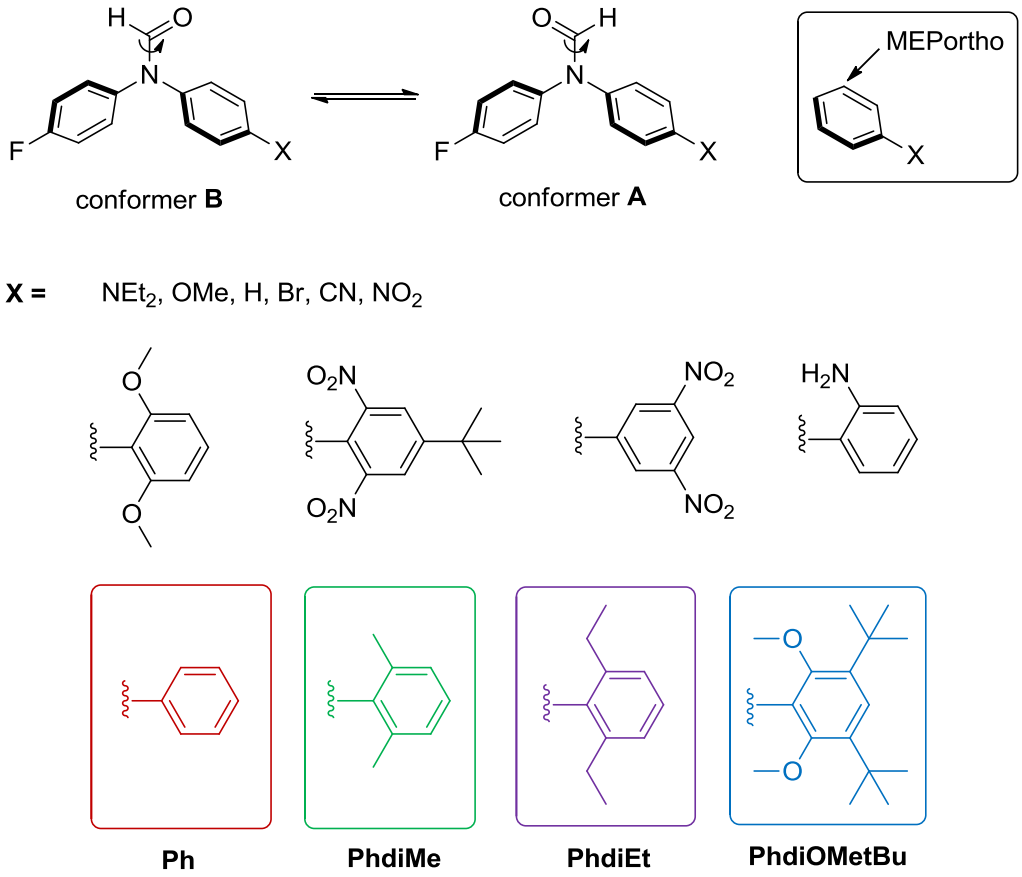

Figure 5.1. The molecular torsion balances used in this study. Control balances (black colour) and highlighted balances showing a possible steric effect (coloured).

The molecular torsion balances shown in Figure 5.1 are based on a slowly rotating tertiary amide and exist in equilibrium between two conformational states. All of them accommodate a *p*-fluoro-substituted aromatic ring and a second *p*-substituted ring with a variety of substituents. The torsion balances shown in black are the reference compounds and the coloured highlighted balances are the ones where the interplay of steric and solvation effects was observed (Figure 5.1).

As was described in Chapter 3, the folding free energies of this series of balances correlated very well with calculated electrostatic potential values (MEP_{ortho}) in most solvents. The formyl oxygen in the major conformer is usually located above the less electron-rich aromatic ring. However, some interesting results were observed for the correlations in dichloromethane and chloroform (Figure 5.2). The series of coloured compounds highlighted in Figure 5.1 are notable outliers (indicated by the coloured points in Figure 5.2), except for the Ph substituent (red), which fits on the best fit line. As we continue along the PhdiMe, PhdiEt and PhdiOMetBu series it can be seen that the data points become more distant from the best fit line. The table in Figure 5.3 shows that moving from the Ph to the PhdiOMetBu balance makes the folding free energy more negative, thus conformer A becomes more abundant.

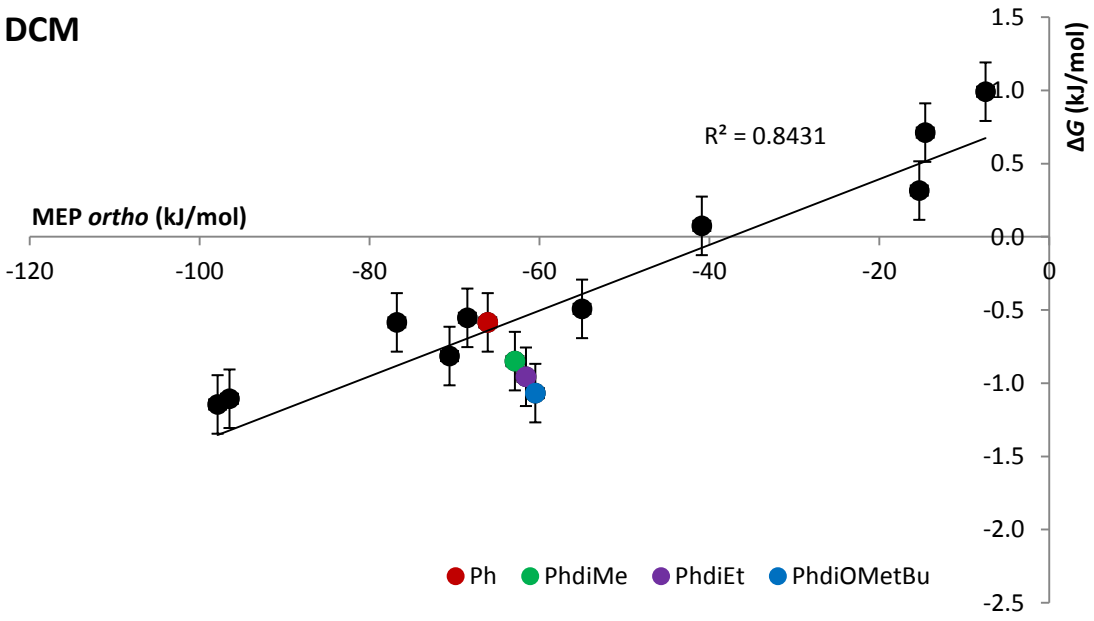

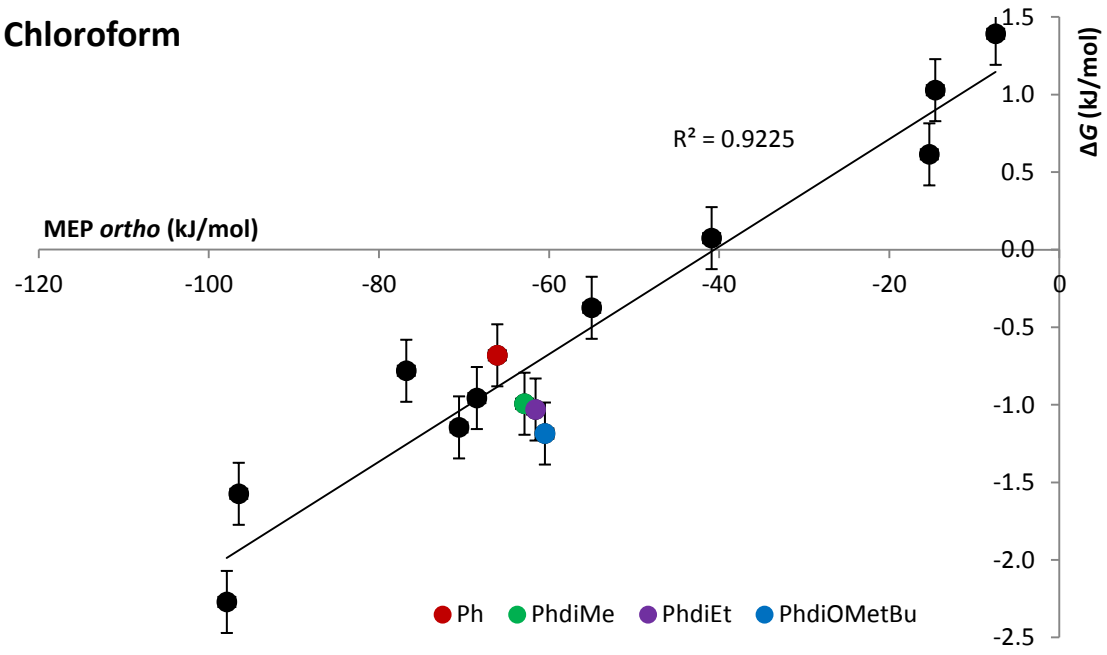

Figure 5.2. Graphs correlating the molecular electrostatic potential at the *ortho* position with the experimental folding free energies for the balances in chloroform and DCM. The compound series highlighted in Figure 5.1 are shown with coloured spots.

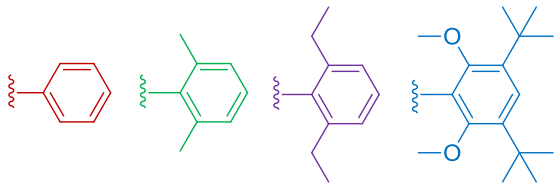

X-substituent	MEP_{ortho} (kJ/mol)	Δ*G* (kJ/mol) DCM	Δ*G* (kJ/mol) Chloroform
Ph	-66.1	-0.58	-0.68
PhdiMe	-62.9	-0.85	-0.99
PhdiEt	-61.6	-0.96	-1.03
PhdiOMetBu	-60.5	-1.07	-1.18

Figure 5.3. The MEP_{ortho} values and the experimental folding free energies for the Ph, PhdiMe, PhdiEt and PhdiOMetBu balances in DCM and chloroform.

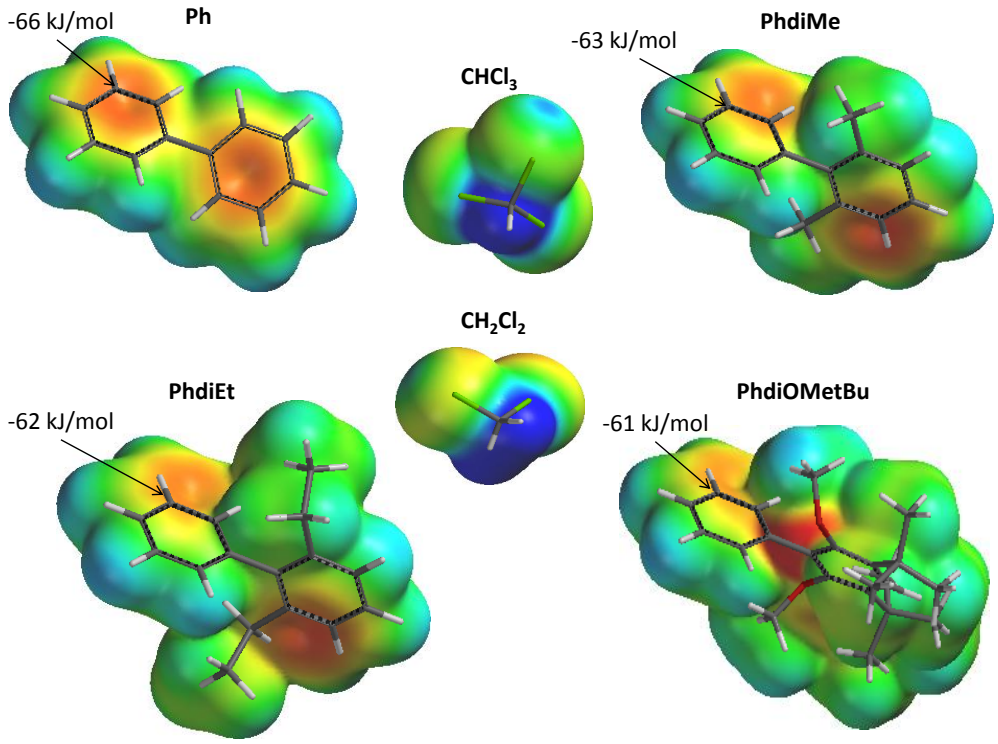

Figure 5.4. Density potential surfaces of the biphenyls with MEP_{ortho} values and solvent surfaces all in the same colour scale [–100 kJ/mol minimum potential (red colour) and +100 kJ/mol maximum potential (blue colour)].

The highlighted series of balances have similar electronic properties with MEP_{ortho} values ranging from –61 to –66 kJ/mol (Figure 5.4). However, these molecules have quite different sterics around the central ring. The size of the substituents on the third aromatic ring of the balance follow the sequence Ph < PhdiMe < PhdiEt < PhdiOMetBu, which suggests a possible steric effect. The PhdiOMetBu is the most sterically hindered of this series as the bulky *tert*-butyl groups force the methoxy groups to lie above the central ring of the system.

One possible explanation for this steric effect that also takes into account the solvation properties of chloroform and dichloromethane is presented in Figure 5.5. Chloroform and dichloromethane are expected to mostly solvate the system as hydrogen

bond donors since α_s = 2.2 and 1.9, β_s = 0.9 and 1.1 for chloroform and dichloromethane respectively.[13] A chloroform or DCM molecule can freely solvate the central aromatic ring of the balance in the absence of bulky substituents, as in the case of the Ph substituent. It could be hypothesised that solvation of the ring face by a hydrogen bond donor would decrease the electron density of this ring, shifting the equilibrium slightly towards conformer B (Figure 5.5 top). However, bulkier substituents would be expected to hinder solvation of the central ring making the ring more electron rich than it would be if it was solvated and shifting the equilibrium slightly towards conformer A (Figure 5.5 bottom)

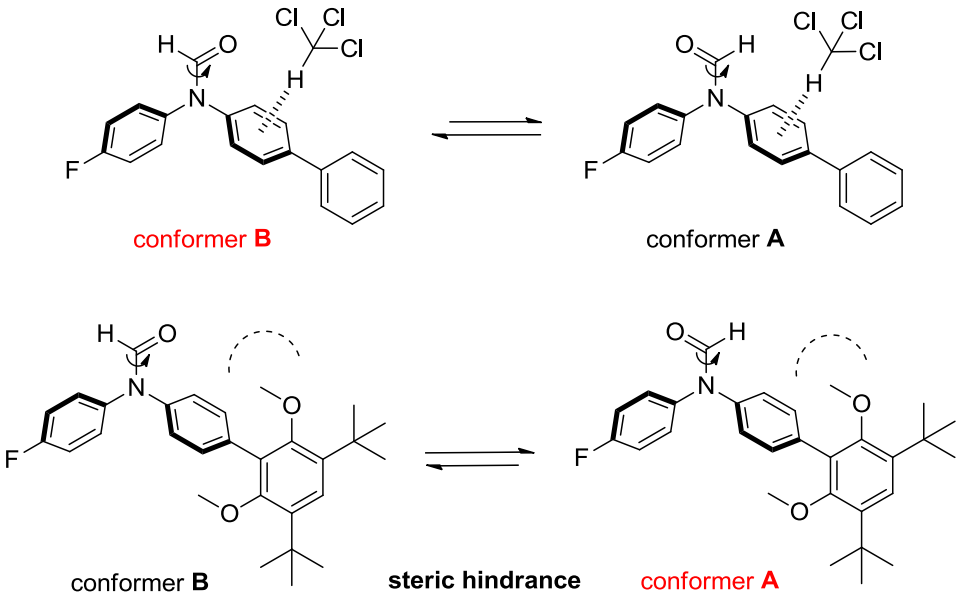

Figure 5.5. One possible explanation of the effects of steric hindrance on the position of the conformational equilibrium. There is only a subtle effect and the equilibrium is slightly shifted towards conformer A or B.

The fact that this steric effect is not apparent in the folding free energies measured in methanol and ethanol despite their high α_s values could be explained by the preference of these solvents to interact with themselves rather than the less polar aromatic ring, since alcohols also possess good hydrogen bond acceptors (β_s = 5.3),

whereas chloroform and DCM do not (β_s = 0.9 and 1.1).[13,14] This is consistent with the phenomenon of preferential solvation.[15-22]

A second possible explanation for the steric effect observed in this series of balances is shown in Figure 5.6. The formyl oxygen has a MEP of around –200 kJ/mol, which might suggest that it is the most likely moiety on the balance to be solvated by chloroform or dichloromethane. When there is no steric hindrance, for example in the balance with the Ph substituent, the formyl oxygen can be solvated easily in both conformations. However, when the substituent is the PhdiOMetBu the solvation of the formyl oxygen is more hindered in conformer B compared to conformer A. Thus, bulky substituents drive equilibrium slightly towards conformation A, and the folding free energies have more negative values.

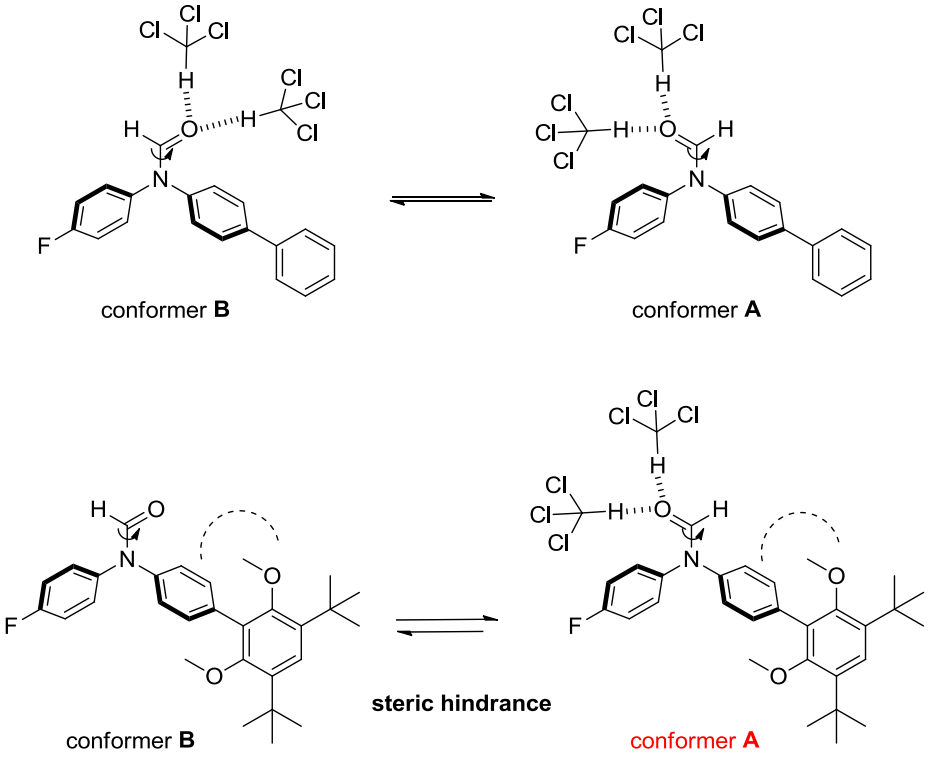

Figure 5.6. Second possible explanation of the steric effects observed in the system. The equilibrium is slightly shifted towards conformer A in balances with bulky substituents.

Neither of the models above can be confirmed with the experimental data obtained thus far; further work is required to examine these hypotheses as outlined below.

5.2. Future work: A pyridyl-balance for examining solvation-induced polarisation of aromatic rings

To test the hypothesis proposed in Figure 5.5 that solvation can modulate the electronic properties of an aromatic ring, a pyridine-based torsion balance was synthesised as shown below (Figure 5.8). Although no obvious solvation effects were observed in balances bearing hydrogen-bond acceptor groups such as CN, OMe, or NO_2 groups in solvents with the strongest hydrogen-bond donor constants (Chapter 2), this could be because any polarisation of the electrostatic potential of the ring resulting from substituent-solvent interactions was too weak to be observed, or that the hydrogen-bond acceptor groups were too weak. It was proposed that the pyridyl balance should overcome these limitations since the pyridine nitrogen is directly attached to the ring and is a very good hydrogen bond acceptor ($\beta = 7$), the acceptance of a hydrogen bond might be more likely to influence the position of the conformational equilibrium via polarisation of the electrostatic potential.[13]

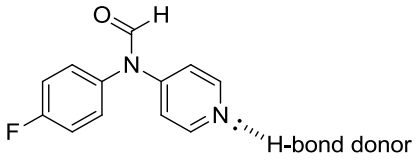

Figure 5.7. A pyridine-based torsion balance interacting with a hydrogen bond donor.

The *N*-(4-fluorophenyl)-*N*-(pyridin-4-yl)formamide (**53**) was synthesised from the *N*-(4-fluorophenyl)formamide (**9**) and the 4-iodopyridine (**52**) by using 50 mol% CuI as catalyst, 10 mol% *N*,*N*-dimethylethylenediamine as ligand and caesium fluoride as base, but in a very low yield (Figure 5.8).[23]

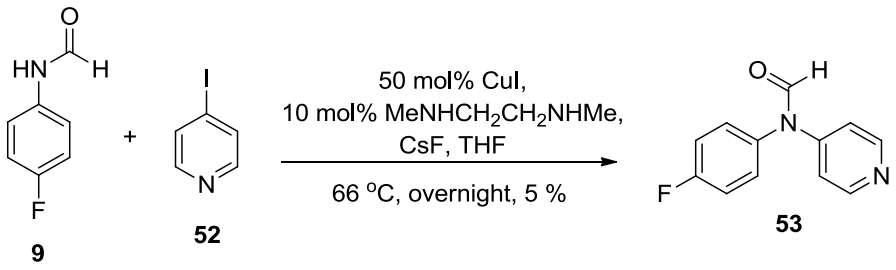

Figure 5.8. Synthesis of the *N*-(4-fluorophenyl)-*N*-(pyridin-4-yl)formamide (**53**).

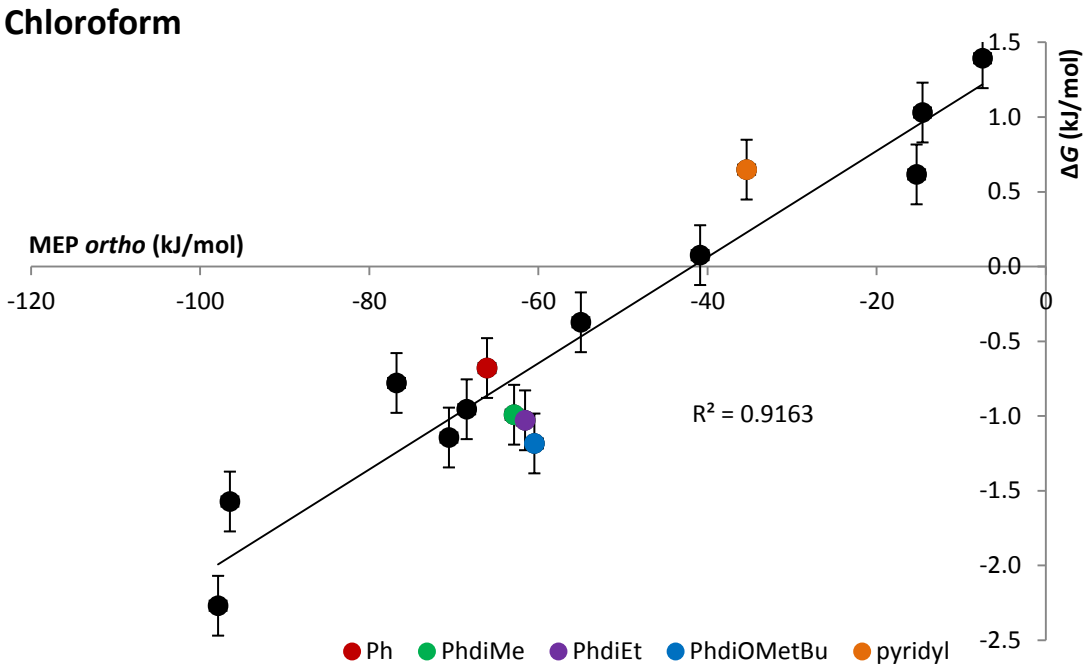

Figure 5.9. Graph correlating the molecular electrostatic potential at the *ortho* position with the experimental folding free energies for the balances in chloroform. The pyridyl-balance is shown in orange colour.

The ^{19}F-NMR showed two peaks corresponding to the two conformers in a ratio A/B = 0.77/1 in chloroform and the electron ionisation mass spectrum showed the correct mass. Unfortunately due to the very low yield, insufficient material was obtained

for a complete characterisation of the balance by ^{13}C-NMR and 2D NMR spectroscopies. Due to lack of time this balance was left to another group member to continue further investigations.

Nevertheless, knowing the conformational ratio in chloroform, a graph correlating the molecular electrostatic potential at the *ortho* position with the folding free energy, including the data for the pyridyl-balance, could be drawn (Figure 5.9). As it was expected, the pyridyl-balance in chloroform was an outlier, supporting the solvation-induced polarisation theory.

5.3. Future work: A molecular balance for examining steric effects on solvation

The second hypothesis that steric blocking of solvation of the formyl oxygen might account for the observation of patterns in the folding ratios of molecular balances in chloroform or dichloromethane (Figure 5.6) could be examined using molecular torsion balances bearing even bulkier *ortho* substituents (Figure 5.10).

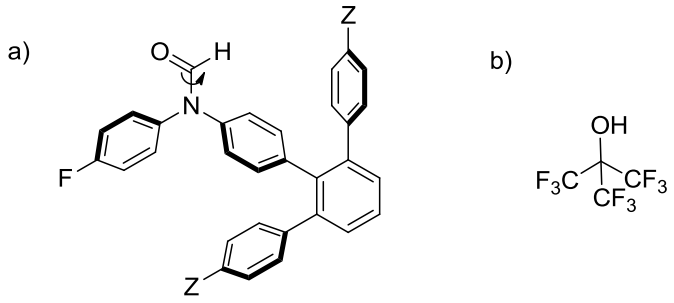

Figure 5.10. a) Molecular torsion balances with bulkier *ortho* substituents, b) Bulky solvent molecules with good hydrogen bond donor and poor hydrogen bond acceptor ability.

A solvation study of balances of the type proposed in Figure 5.10a could provide insight into the important solvation sites in these balances. Variation of the Z-

substituents would confirm whether solvation of the formyl group or the face of the aromatic ring was the key factor accounting for the outlying results in chloroform and dichloromethane. If folding energies were relatively independent of the steric bulk of Z, then solvation of the face of the central aromatic ring would be implicated as being important. In contrast, if folding free energies varied in accord with the steric bulk of the Z-substituent, then the importance of solvation of the formyl group would be confirmed.

Another possibility for further investigation could be the use of bulkier solvents featuring a good hydrogen bond donor but a poor hydrogen bond acceptor site. One example of such a solvent is the nonafluoro-*tert*-butyl alcohol (Figure 5.10b). Unfortunately, there was insufficient time to investigate either of these possibilities.

5.4. Conclusions

The correlation of the folding free energies of the molecular torsion balances with the molecular electrostatic potential at the *ortho* position revealed a series of outliers in dichloromethane and chloroform. It was observed that as phenyl substituents became larger in the Ph, PhdiMe, PhdiEt and PhdiOMetBu series, larger outliers were seen compared to the control balances. This steric hindrance effect was explained by two hypotheses and future work was proposed in order to test the assumptions.

5.5. References

1. Reichardt, C., *Org. Process Res. Dev.* **2007**, 11, 105-113.
2. Dougan, L.; Koti, A. S. R.; Genchev, G.; Lu, H.; Fernandez, J. M., *Chem. Phys. Chem* **2008**, 9, 2836-2847.
3. Barillari, C.; Taylor, J.; Viner, R.; Essex, J. W., *J. Am. Chem. Soc.* **2007**, 129, 2577-2587.
4. Christenson, H. K.; Yaminsky, V. V., *Colloids Surf., A* **1997**, 129 67-74.
5. Lin, Q.; Meyer, E. E.; Tadmor, M.; Israelachvili, J. N.; Kuhl, T. L., *Langmuir* **2005**, 21, 251-255.
6. Chandler, D., *Nature* **2005**, 437, 640-647.
7. Yaminsky, V.; Ohnishi, S., *Langmuir* **2003**, 19, 1970-1976.
8. Conn, M. M.; Rebek, J., Jr., *Chem. Rev.* **1997**, 97, 1647-1668.
9. Szabo, T.; Hilmersson, G.; Rebek, J., Jr., *J. Am. Chem. Soc.* **1998**, 120, 6193-6194.

10. Hamann, B. C.; Shimizu, K. D.; Rebek, J., Jr., *Angew. Chem., Int. Ed. Engl.* **1996**, 35, 1326-1329.
11. Tokunaga, Y.; Rudkevich, D. M.; Santamaria, J.; Hilmersson, G.; Rebek, J., Jr., *Chem. Eur. J.* **1998**, 4, 1449-1457.
12. Mecozzi, S.; Rebek, J., Jr., *Chem. Eur. J.* **1998**, 4, 1016-1022.
13. Hunter, C. A., *Angew. Chem., Int. Ed.* **2004**, 43, 5310-5324.
14. Abraham, M. H.; Platts, J. A., *J. Org. Chem.* **2001**, 66, 3484-3491.
15. Cabot, R.; Hunter, C. A., *Org. Biomol. Chem.* **2010**, 8, 1943-1950.
16. Cabot, R.; Hunter, C. A., *Chem. Soc. Rev.* **2012**, 41, 3485-3492.
17. Amenta, V.; Cook, J. L.; Hunter, C. A.; Low, C. M. R.; Vinter, J. G., *Org. Biomol. Chem.* **2011**, 9, 7571-7578.
18. Buurma, N. J.; Cook, J. L.; Hunter, C. A.; Low, C. M. R.; Vinter, J. G., *Chem. Sci.* **2010**, 1, 242-246.
19. Cook, J. L.; Hunter, C. A.; Low, C. M. R.; Perez-Velasco, A.; Vinter, J. G., *Angew. Chem., Int. Ed.* **2008**, 47, 6275-6277.
20. Marcus, Y., *J. Chem. Soc., Faraday Trans. 1* **1989**, 85, 381-8.
21. Rastrelli, F.; Saielli, G.; Bagno, A.; Wakisaka, A., *J. Phys. Chem. B* **2004**, 108, 3479-3487.
22. Sasirekha, V.; Vanelle, P.; Terme, T.; Meenakshi, C.; Umadevi, M.; Ramakrishnan, V., *J. Fluoresc.* **2007**, 17, 528-539.
23. Phillips, D. P.; Zhu, X.-F.; Lau, T. L.; He, X.; Yang, K.; Liu, H., *Tetrahedron Lett.* **2009**, 50, 7293-7296.

Chapter 6

Experimental section

6.1. Conformer assignment by NMR

All molecular torsion balances were fully characterised by NMR analysis in $CDCl_3$. The following figures present the NMR spectra (^{1}H, ^{13}C, HSQC, COSY, NOESY and HMBC) of the *N*-(4-fluorophenyl)-*N*-phenylformamide (**3**) and the full assignment of the two conformers. In this example proton resonances have been labelled numerically and carbon resonances alphabetically. Prime (') denotes the peaks corresponding to the minor conformer.

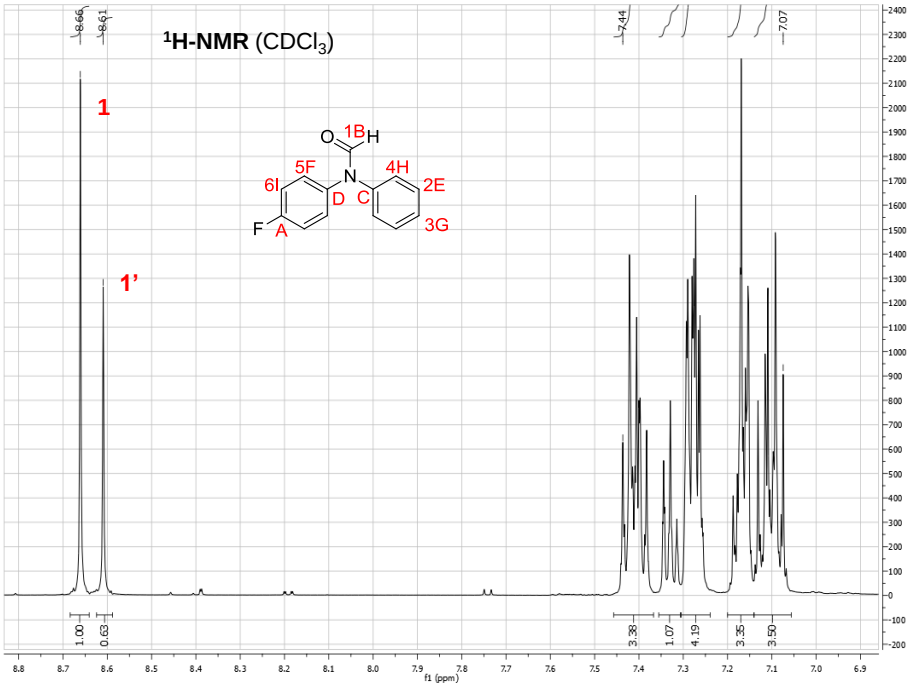

Figure 6.1. The ^{1}H-NMR spectrum of the *N*-(4-fluorophenyl)-*N*-phenylformamide (**3**) in $CDCl_3$ at r.t.

Two conformers (relative ratio of 1: 0.63) for each proton and carbon of the *N*-(4-fluorophenyl)-*N*-phenylformamide (**3**) exist in the ^{1}H and ^{13}C-NMR. The major and minor formyl protons (1 and 1') appear at 8.66 and 8.61 ppm respectively and the resonances of the aromatic protons appear in the region 7.07 – 7.44 ppm (Figure 6.1). Figure 6.2 shows the aromatic region of the ^{1}H-NMR of *N*-(4-fluorophenyl)-*N*-phenylformamide (**3**). From this it can be clearly recognised that the triplet at 7.33 ppm corresponds to the proton 3 of the major conformer. The integration of the peaks provide extra information about the number and type (major or minor) of resonances for each subsection of the complicated aromatic region, where most of the peaks overlap.

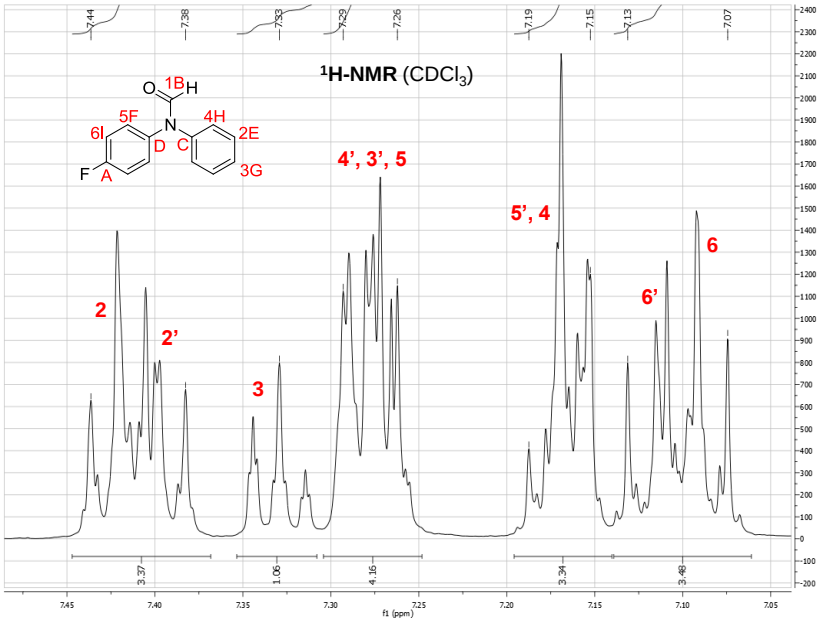

Figure 6.2. The aromatic region of ^{1}H-NMR spectrum of the *N*-(4-fluorophenyl)-*N*-phenylformamide (**3**).

The carbon peaks corresponding to the fluorine-substituted ring can be recognised in the ^{13}C-NMR spectra because they appear as doublets (Figure 6.3). The further away the carbon is from the fluorine, the smaller the *J* coupling appears (e.g. J_A = 246.9 Hz and J_D = 3.1 Hz). From the integration of the ^{13}C-NMR spectra, it was obvious that carbon G refers to one proton only, so it can be concluded that it is the carbon connected

to proton 3. From the HSQC spectrum the protons attached to each aromatic carbon can be assigned (Figure 6.4). In this way the resonances corresponding to the protons of the two conformers can be also assigned in the complicated aromatic region of the ^{1}H-NMR.

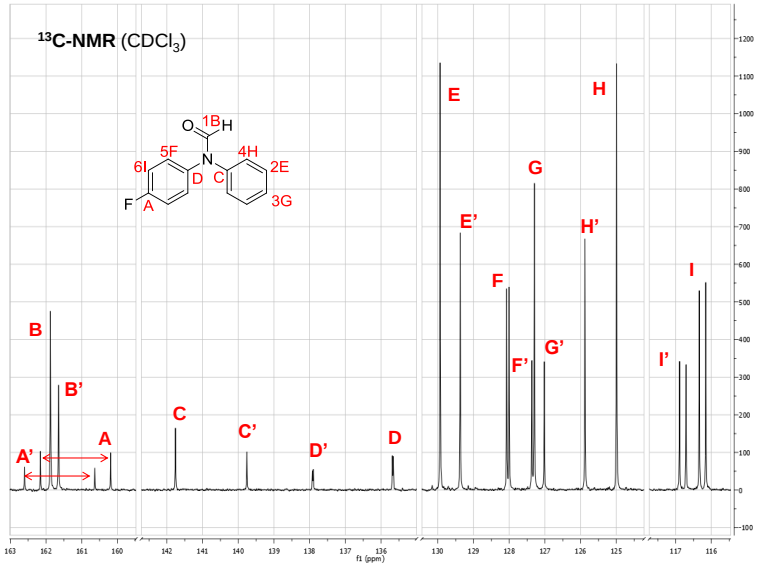

Figure 6.3. The ^{13}C-NMR spectrum of *N*-(4-fluorophenyl)-*N*-phenylformamide (**3**) in $CDCl_3$ at r.t.

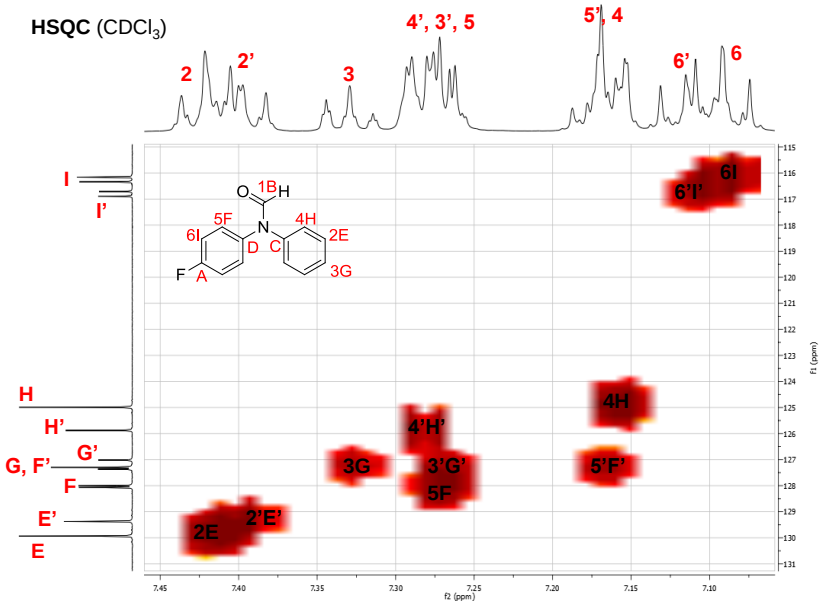

Figure 6.4. The HSQC spectrum of *N*-(4-fluorophenyl)-*N*-phenylformamide (**3**).

The proton – proton correlation experiment (COSY) shows the protons connected to each other by a single bond. From the interpretation of Figure 6.5 the relative positions of protons 2 and 4 on the ring can be identified.

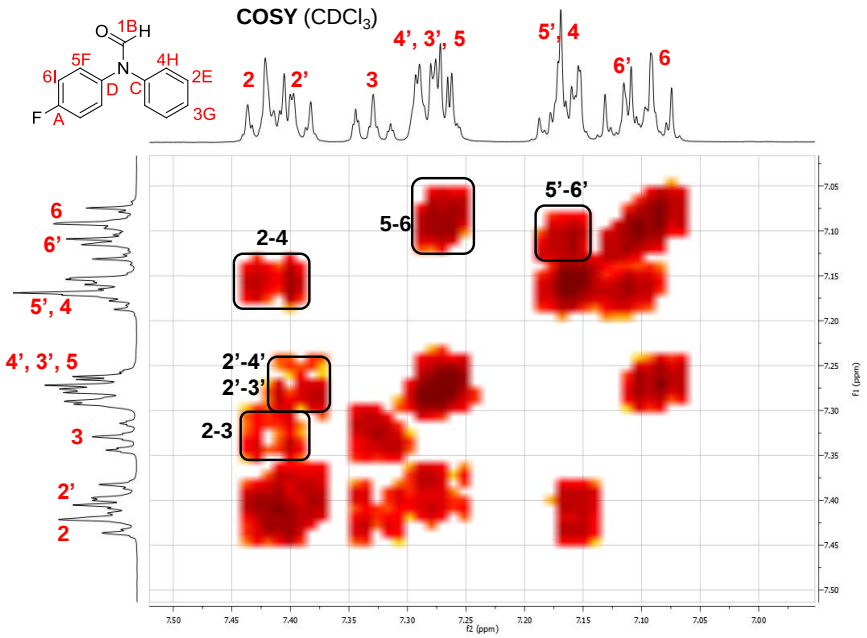

Figure 6.5. The COSY spectrum of *N*-(4-fluorophenyl)-*N*-phenylformamide (**3**).

All the synthesised balances, described in the previous chapters, exist as two conformers by slow rotation of the formyl group. The NOESY experiment shows the proton – proton correlation between protons that are close to each other in space. This experiment can be used to identify the major and the minor conformation for each torsion balance. The major formyl proton 1 correlates with proton 4 and the minor formyl proton 1' with proton 5' (Figure 6.6). Thus the major conformer is the one with the oxygen atom above the aromatic ring with the fluorine.

The NOESY experiment reveals both the major through-space NOE signals, which allow the assignment of the conformers in addition to minor NOE signals. These minor signals appear for two different reasons. Firstly, the distance between the formyl proton and the protons of the most distant ring is less than 5 Å, thus NOEs between these

protons can still appear. Secondly, there is exchange between the two conformers on the timescale of the NOESY experiment at room temperature.

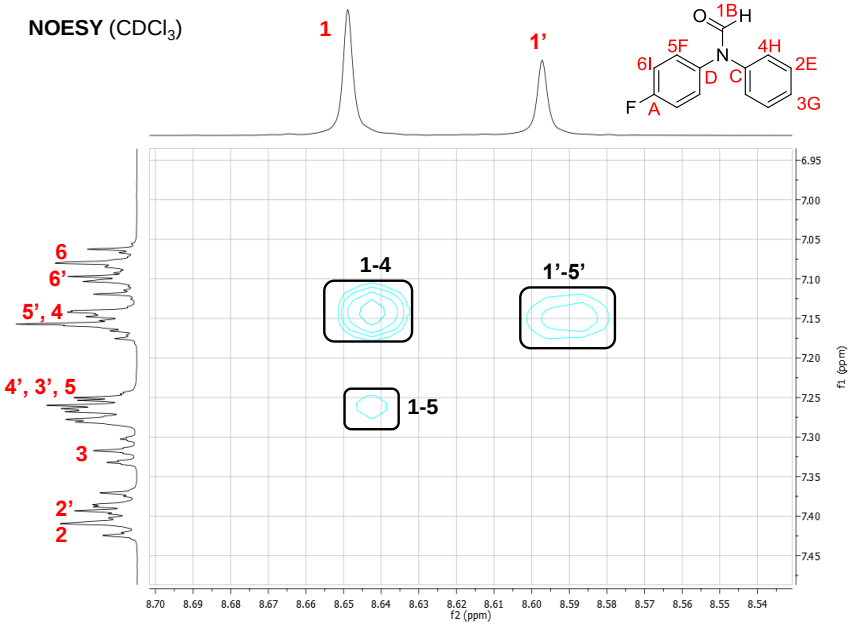

Figure 6.6. The NOESY spectrum of *N*-(4-fluorophenyl)-*N*-phenylformamide (**3**).

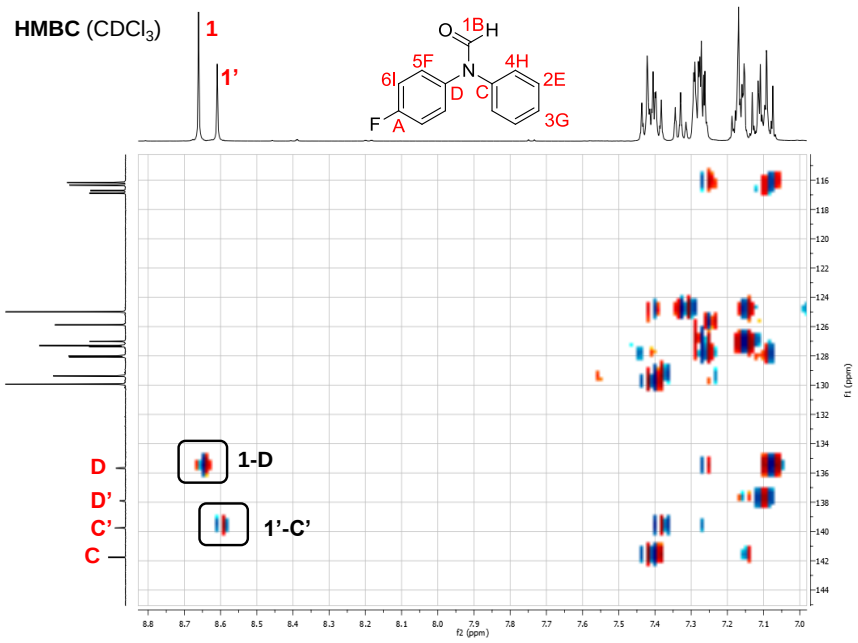

Figure 6.7. The HMBC spectrum of *N*-(4-fluorophenyl)-*N*-phenylformamide (**3**).

An interesting observation in the HMBC spectrum (proton – carbon correlation across multiple bonds) was that the formyl proton has a cross peak with the *trans* quaternary aromatic carbon. In the example depicted in Figure 6.7, the major formyl proton correlates with the D carbon and the minor with the C' carbon. This *trans* cross peak in the HMBC can be used as a means of rapidly assigning the major and minor conformer. In Figure 6.8 the result of the NMR assignment is shown.

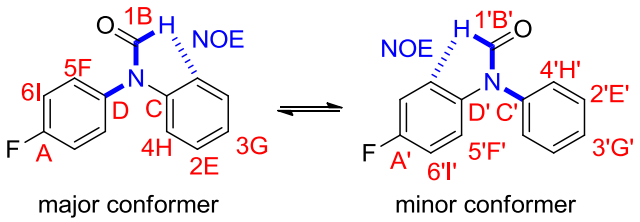

Figure 6.8. Full assignment of the two conformers of *N*-(4-fluorophenyl)-*N*-phenylformamide (**3**). The major NOE between the formyl proton and the aromatic proton, as well as the cross peaks 1-D and 1'-C' are shown in blue colour.

The solvation study of every molecular torsion balance was performed by using a series of deuterated and non-deuterated solvents. For all solvents except for $CDCl_3$, ^{19}F-NMR was the basic method used to find the ratio of the two conformers.

The fluorine chemical shift difference of the two conformers was plotted across the different solvents for all the balances. In this way any possible outliers (i.e. cases where the conformers have swapped in particular solvents) were identified. A full NMR analysis was done for the outliers, by using deuterated solvent, in order to check whether the major conformer is different to that assigned in $CDCl_3$ or not. For the few cases where a deuterated solvent was not available, it was assumed that the dominant conformer was the same as the assignment in $CDCl_3$ in the case of DCM outliers, and MeOH in the case of EtOH outliers. The majority of the balances did not appear to be outliers in the ^{19}F-ppm analysis and it was assumed that the conformational assignment in $CDCl_3$ was reserved for all the solvents.

A similar procedure to the one described above for the NMR assignment of *N*-(4-fluorophenyl)-*N*-phenylformamide (**3**), was used in all the molecular torsion balances synthesised. In the case of *N*-(4-fluorophenyl)-*N*-phenylformamide (**3**) some extra NMR analysis (shown below) was carried out, in order to ascertain the correct conformational assignment.

As was mentioned earlier, the rotation of the formyl group is rapid at room temperature and exchange between the two conformers is observed. For this reason the NMR tube was cooled down to –35 ^{o}C to slow down the exchange and avoid minor NOE signals. A 1-dimensional NOESY experiment, which was more easily interpreted and of higher resolution and sensitivity compared to the 2D NOESY experiment, was performed by irradiating the formyl proton of the major conformer and the signals of the response were observed (Figure 6.9). The major NOE appeared to occur with proton 4, which also appears as a doublet. This result further confirms the assignment described above.

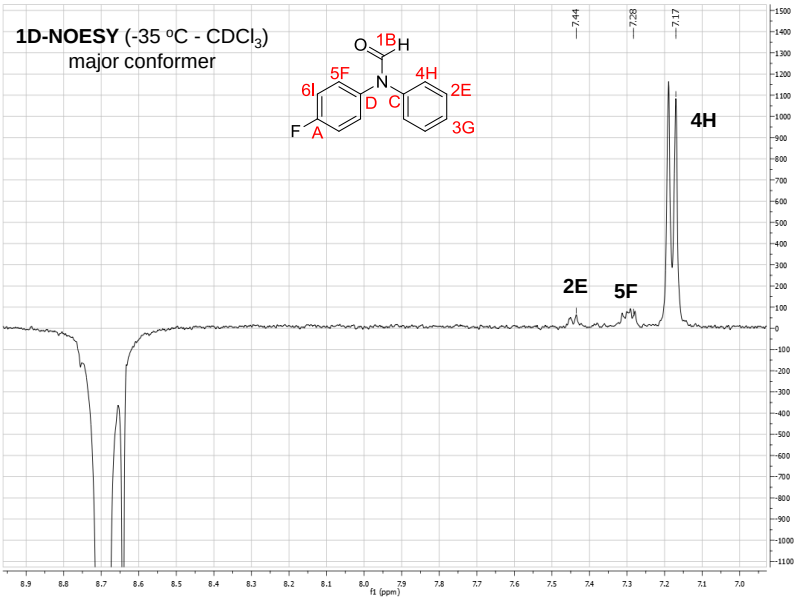

Figure 6.9. The 1D NOESY experiment on the major conformer of *N*-(4-fluorophenyl)-*N*-phenylformamide (**3**) at –35 ^{o}C in $CDCl_3$.

A second 1D NOESY experiment was carried out by irradiating the formyl proton of the minor conformer (Figure 6.10). The major NOE in this case appears with proton 5'. The peak corresponding to proton 5' is a multiplet, which is explained by the coupling of this proton with the fluorine atom attached to the same ring.

The final NMR experiment that was carried out was a combination of 1D NOESY and TOCSY experiments (Figure 6.11). First, a 1D NOESY spectrum was taken by irradiating the formyl proton of the major conformer at –35 ^{o}C. After that, a TOCSY was taken which shows how the magnetisation is initially transferred from proton 1 to proton 4 (NOESY experiment) and then from proton 4 to protons 2 and 3 across the aromatic ring (TOCSY experiment).

Based on this confirmation that the assignment of the balance using the classic ^{1}H, ^{13}C, HSQC, COSY, NOESY and HMBC experiments was correct, the characterisation of the other compounds was based only on these simple experiments.

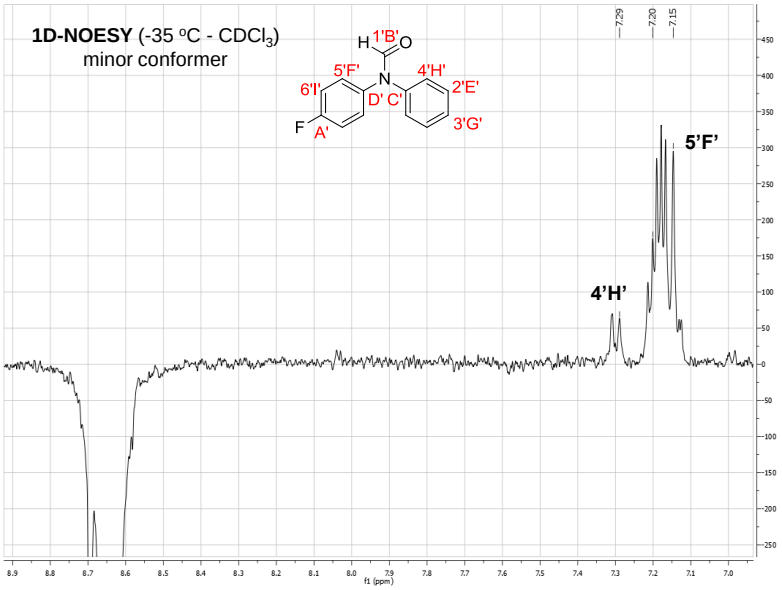

Figure 6.10. The 1D NOESY experiment on the minor conformer of *N*-(4-fluorophenyl)-*N*-phenylformamide (**3**) at –35 ^{o}C in $CDCl_3$.

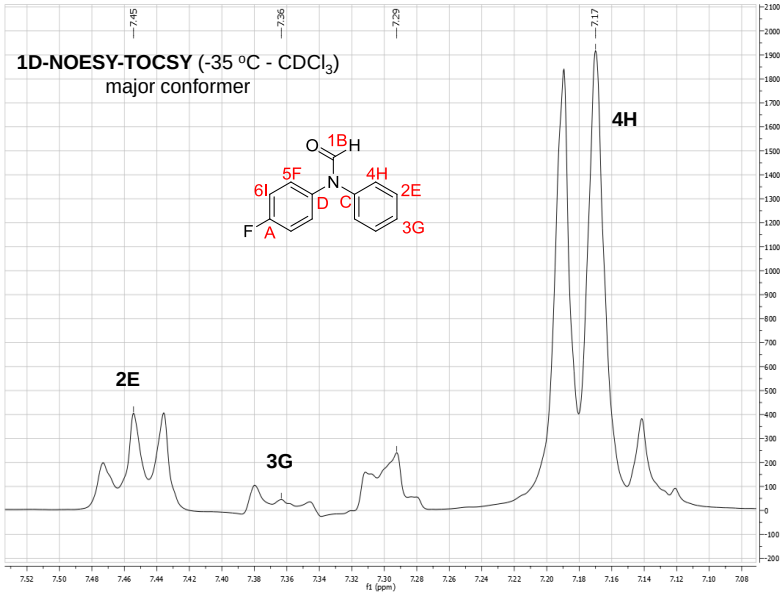

Figure 6.11. The 1D NOESY - TOCSY experiment on the major conformer of *N*-(4-fluorophenyl)-*N*-phenylformamide (**3**) at –35 ^{o}C in $CDCl_3$.

6.2. Variable temperature NMR

To prove that these molecular balances exist as two conformers and that the second set of peaks in the spectrum does not correspond to an impurity, a variable temperature NMR experiment can be used. At low temperatures the exchange of the conformers is slow, but as the sample is heated the exchange is faster, thus resulting in a single signal.

The Figures 6.12 – 6.14 show the VT NMR experiments for three of the balances in DMSO-d_6. In Figure 6.12 the two formyl protons corresponding to the two conformers coalesce at 70 ^{o}C, giving a single peak. By cooling the sample down, the two formyl peaks reappear. Figures 6.13 and 6.14 show two more complicated compounds (three-ring system) and the coalescence temperatures are found to be 79 ^{o}C and 75 ^{o}C respectively. In Figure 6.14 a complication in the interpretation of the VT NMR is added by the presence of the OH signal close to the formyl signals as the OH chemical shift changes on increasing the temperature.

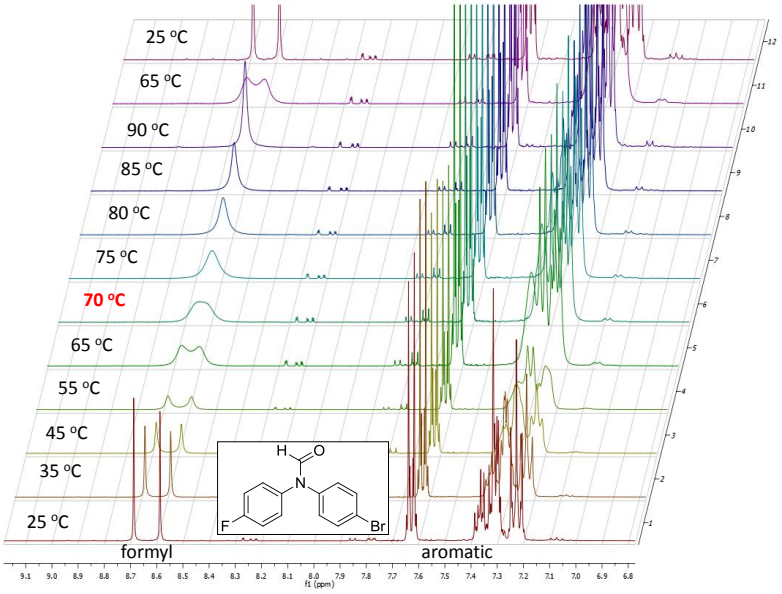

Figure 6.12. VT NMR experiment for *N*-(4-bromophenyl)-*N*-(4-fluorophenyl)formamide (**5**) in DMSO-d_6.

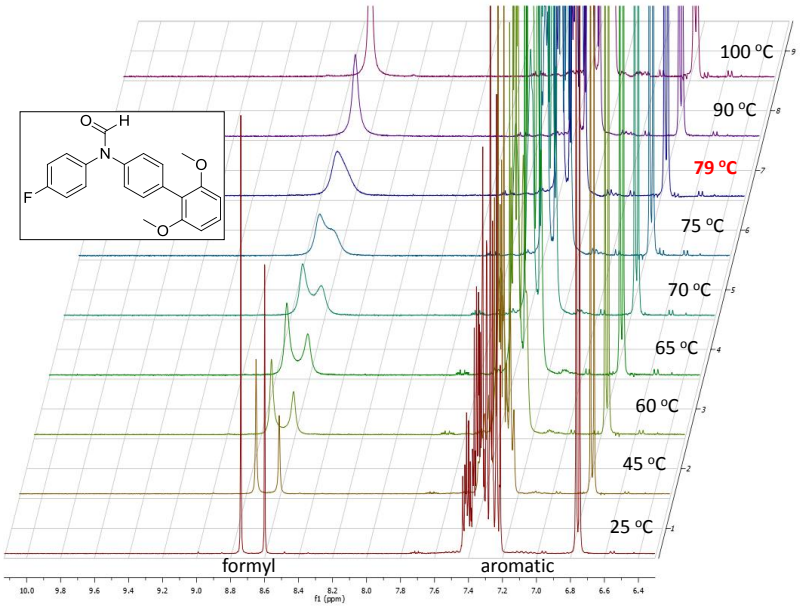

Figure 6.13. VT NMR experiment for *N*-(2',6'-dimethoxy-[1,1'-biphenyl]-4-yl)-*N*-(4-fluorophenyl)formamide (**30**) in DMSO-d_6.

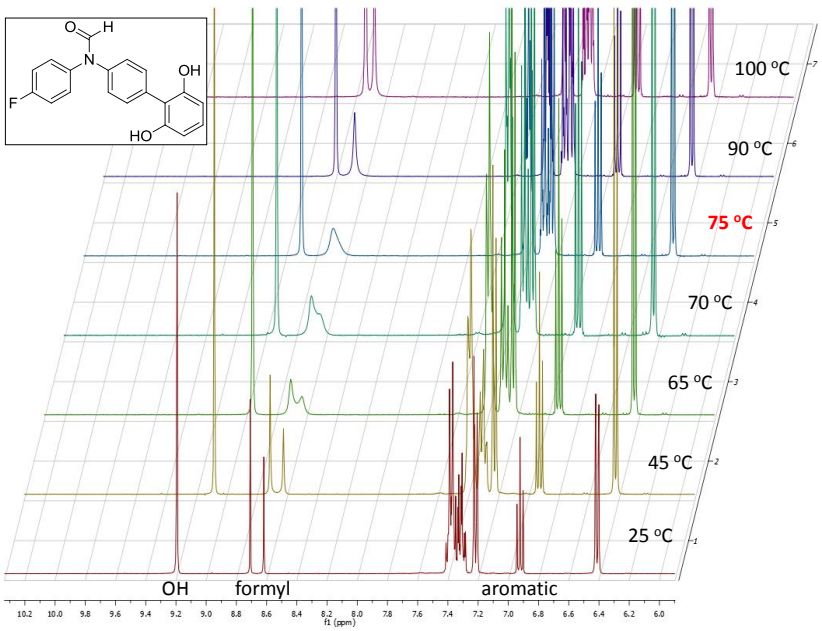

Figure 6.14. VT NMR experiment for *N*-(2',6'-dihydroxy-[1,1'-biphenyl]-4-yl)-*N*-(4-fluorophenyl)-formamide (**48**) in DMSO-d_6.

6.3. EXSY NMR experiment

A molecular torsion balance exists in two conformational states by slow rotation of a particular bond. The two conformers are in equilibrium and exchange with each another. EXSY experiments provide a simple method of determining the barrier to rotation, which basically consists of a series of 1D NOESY experiments where the mixing time is varied.[1]

This method was used to calculate the activation energy barrier for the rotation of the formyl group in *N*-(4-fluorophenyl)-*N*-phenylformamide (**3**), which serves as a typical example of the molecular balances studied in this thesis. 1D NOESY NMRs were taken of this compound in $CDCl_3$ with mixing times ranging from 0.01 s to 0.7 s. The formyl proton of the major conformer was specifically irradiated and the exchange of the formyl proton with the minor conformer was measured at each mixing time. The

integral ratio for the response signal compared to the irradiated peak was plotted against the mixing times for each experiment to give the linear correlation as shown in Figure 6.15.[1] When the mixing time is zero there is obviously no exchange peak, thus the straight line in the graph should pass through the origin of the graph (0,0). The slope of the line corresponds to the rate constant of conformational exchange, k (s^{-1}).

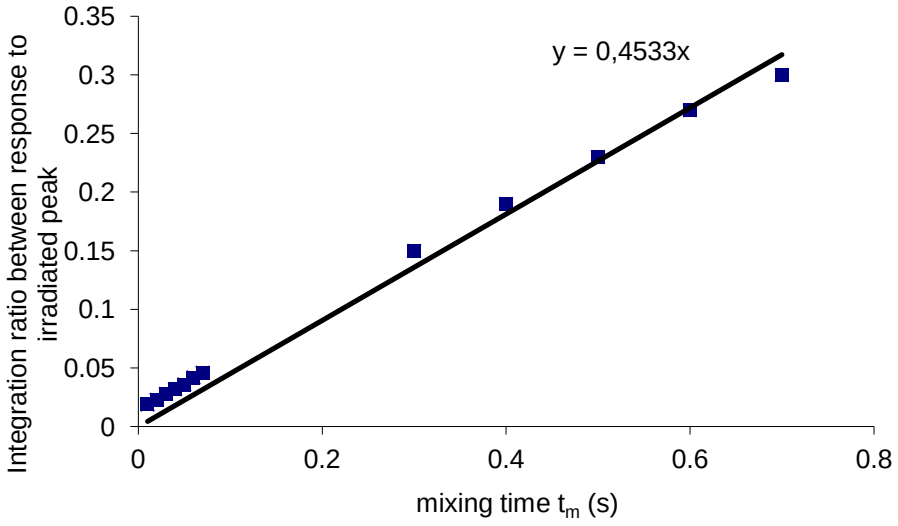

Figure 6.15. Graph of the integral ratio between the response signal compared to the irradiated peak versus mixing time for *N*-(4-fluorophenyl)-*N*-phenylformamide (**3**) at 25 ^{o}C.

The rate constant in this experiment was found to be $\boldsymbol{k = 0.4533\ s^{-1}}$.

$$k = \frac{k_B T}{h} e^{-\frac{\Delta G^{\neq}}{RT}} \rightarrow \Delta G^{\neq} = -RT ln \frac{kh}{k_B T} = 74.9 \frac{kJ}{mol}$$

where R = 8.314 J·K^{-1}·mol^{-1}, k_B = 1.38 x 10^{-23} J·K^{-1} and h = 6.63 x 10^{-34} J·s

The barrier to rotation for the formyl group was determined to be **74.9 kJ/mol**, which is similar to that of the acetyl group in *N*,*N*-dimethylacetamide (~71.1 kJ/mol).[2]

6.4. Error analysis for ΔG_{fold} determination

The free energy difference between the two conformations of a torsion balance is derived from the folding equilibrium constant. This was calculated by integrating the peaks corresponding to the same nuclei in the two conformations either in the ^{1}H or ^{19}F NMR. The errors involved in the integration of the signals were calculated by taking ^{1}H and ^{19}F NMRs of 10 mixtures of 2-fluoro-4-methoxyphenol and 1-fluoro-4-methoxybenzene, in 5/95, 15/85, 25/75, till 95/5 concentration ratios, which were then integrated by four different people. For every sample, the standard deviation of the integrals reported by each of the four researchers was determined to give an average standard deviation of the integral ratios. The reported error is twice the standard deviation, corresponding to the 95% confidence interval. This was found to be 0.13 kJ / mol for ^{19}F NMR and 0.11 kJ / mol for ^{1}H NMR integrations. Thus, an error bar of ± 0.2 kJ / mol should adequately account for experimental errors involved in the determination of folding free energies.

6.5. Experimental procedures

Materials and instruments

All chemicals were obtained from commercial sources and used without further purification. Purification of reaction products was carried out using column chromatography with silica gel (40 - 63 μm), or preparatory-TLC using Analtech Uniplate silica gel thin layer chromatography plates (20 x 20 cm). Solvent ratios are reported in parentheses next to the purification method used in each case. Reactions were monitored by TLC on Merck aluminium sheets coated with silica gel 60F, with further detection by UV light (254 nm). All reactions were performed in the dark, under a N_2 atmosphere using dry solvents unless otherwise stated.

Routine NMR analysis of synthetic products was performed on a Bruker 400 MHz or 500 MHz spectrometer. ^{19}F and variable temperature NMR experiments were performed on a Bruker 400 MHz spectrometer. EXSY experiment was performed on a

Bruker 600 MHz spectrometer. Chemical shifts are reported in parts per million (δ) relative to tetramethylsilane and all coupling constants (*J*) are given in Hertz (Hz). Signal splitting patterns in ^{1}H NMR spectra could not be determined in cases where conformer signals resulted in overlapping peaks. The chemical shifts of aromatic protons were often identified using HSQC spectra and the signals were recorded as multiplets (m). ^{1}H and ^{13}C NMR spectra were referenced by using the known chemical shift of the deuterated solvent.[15] In the ^{19}F spectra when a non-deuterated solvent was used, TFA in D_2O was used as an internal reference. ^{13}C and some ^{19}F spectra have been ^{1}H decoupled.

Mass spectrometry was performed by the University of Edinburgh technician-supported mass spectrometry service, using a Thermo MAT 900 XP spectrometer for electron ionisation or a Finnigan MAT LCQ for electrospray ionisation.

The IR spectra were taken on neat samples using a Shimadzu IRAffinity-1 machine. Absorptions are reported in cm^{-1} and the absorptions in the fingerprint region are not reported. Melting points were measured in a Gallenkamp melting point apparatus and are uncorrected.

Ab initio calculations were performed using Spartan '08 V 1.2.0. The calculations were run using a DFT/B3LYP/6-31G* basis set to obtain the equilibrium geometries of model compounds that were used for the determination of electrostatic surface potentials and HOMOs.

Preparation of *N*-(4-fluorophenyl)-*N*-phenylformamide (3)[3]

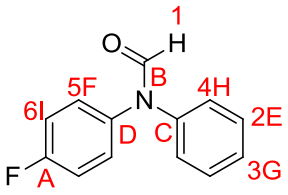

First attempt: The procedure described below was first attempted with 5 mol % CuI and 10 mol % ethylenediamine and the product was synthesised in 14% yield.

Second attempt: A dry flask was charged with CuI (17.1 mg, 20 mol %) and K_3PO_4 (191 mg, 0.9 mmol), evacuated, and backfilled with nitrogen. Ethylenediamine (12 µl, 40 mol %), 1-fluoro-4-iodobenzene (0.05 ml, 0.45 mmol), formanilide (65 mg, 0.54 mmol) and toluene (1 ml) were added under nitrogen. The reaction mixture was stirred overnight at 80 °C. The resulting suspension was allowed to reach room temperature and filtered through a pad of silica gel. The filtrate was concentrated under *vacuo* and the residue was purified with prep-TLC (DCM) to afford the product as a brown solid (52 mg, yield 54%)

m.p. = 69 – 71 °C; ESI-HRMS: obtained *m/z* 216.081301 $(M + H)^+$ (composition: $C_{13}H_{11}O_1N_1F_1$); IR (neat) / cm^{-1} 2924.09, 2852.72, 1676.14 (amide), 1591.27, 1504.48, 1492.9, 1462.04; ^1H NMR ($CDCl_3$) δ 8.66 (1, s, 1H), 8.61 (1', s, 1H), 7.42 (2, m, 2H), 7.4 (2', m, 2H), 7.33 (3, t, *J* = 7.4 Hz, 1H), 7.29 (4', m, 2H), 7.26 – 7.28 (5 and 3', m, 3H), 7.18 (5', m, 2H), 7.16 (4, m, 2H), 7.12 (6', m, 2H), 7.09 (6, m, 2H); ^{13}C NMR ($CDCl_3$) δ 161.62 (A', d, *J* = 247.7 Hz), 161.17 (A, d, *J* = 246.9 Hz), 161.88 (B), 161.65 (B'), 141.76 (C), 139.76 (C'), 137.91 (D', d, *J* = 3.1 Hz), 135.67 (D, d, *J* = 3.1 Hz), 129.94 (E), 129.37 (E'), 128.04 (F, d, *J* = 8.4 Hz), 127.33 (F', d, *J* = 8.8 Hz), 127.3 (G), 127.02 (G'), 125.88 (H'), 124.99 (H), 116.80 (I', d, *J* = 22.9 Hz), 116.25 (I, d, *J* = 22.7 Hz); ^{19}F NMR ($CDCl_3$) δ -114.27 (minor, tt, *J* = 8.0, 4.8 Hz), -114.61 (major, tt, *J* = 8.2, 4.9 Hz).

Preparation of *N*-(4-bromophenyl)-*N*-(4-fluorophenyl)formamide (5)[3,4]

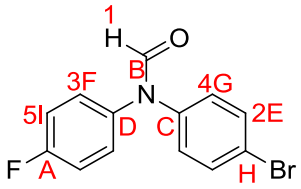

Initial attempts: a) The general procedure described for the preparation of the *N*-(4-fluorophenyl)-*N*-phenylformamide was followed by using *N*-(4-bromophenyl)formamide instead of formanilide this time, in order to synthesise the *N*-

(4-bromophenyl)-*N*-(4-fluorophenyl)formamide. The use of 5 mol % CuI and 10 mol % ethylenediamine gave the desired product in 6% yield. Increasing the amount of catalyst did not improve the yield.[3]

b) Into a flask were placed caesium fluoride (171 mg, 1.13 mmol), copper(I) iodide (4.3 mg, 5 mol %), 1-fluoro-4-iodobenzene (0.05 ml, 0.45 mmol), *N*-(4-bromophenyl)formamide (108 mg, 0.54 mmol) and *N*,*N*-dimethylethylenediamine (4.8 µl, 10 mol %). The flask was sealed, evacuated, and backfilled with nitrogen 2–3 times, then it was charged with THF (1 ml), evacuated and backfilled with nitrogen twice more and was allowed to stir at room temperature overnight. The yield of this reaction was very poor (4%). The same reaction was attempted under the following conditions: i) r.t for 3 days gave 7% yield, ii) 66 °C for 2 days gave 9% yield, iii) with increase of the catalysts (20 mol % CuI and 40 % mol *N*,*N*-dimethylethylenediamine) at 66 °C overnight gave 12% yield.[4]

Final attempt: Into a flask were placed caesium fluoride (171 mg, 1.13 mmol), copper(I) iodide (43 mg, 50 mol %), 1-fluoro-4-iodobenzene (0.05 ml, 0.45 mmol), *N*-(4-bromophenyl)formamide (108 mg, 0.54 mmol) and *N*,*N*-dimethylethylenediamine (4.8 µl, 10 mol %). The flask was sealed, evacuated, and backfilled with nitrogen 2–3 times, then it was charged with THF (2 ml), evacuated and backfilled with nitrogen twice more and was allowed to stir at 66 °C overnight. The reaction mixture was diluted with EtOAc and quenched with saturated ammonium chloride. The aqueous layer was extracted with EtOAc and the combined organics were washed with brine, dried over magnesium sulfate, filtered, and concentrated under *vacuo*. The crude product was purified with flash chromatography (from 1:1 hexane:DCM to pure DCM) to give the *N*-(4-bromophenyl)-*N*-(4-fluorophenyl)formamide as a white solid in 85% yield (113 mg).[4]

m.p. = 84 – 87 °C; EI-HRMS: obtained *m/z* 292.984671 M^+ (composition: $C_{13}H_9O_1N_1Br_1F_1$, expected *m/z* 292.98515); IR (neat) / cm^{-1} 1668.43 (amide), 1639.49, 1602.85, 1583.56, 1504.48, 1485.19; ^{1}H NMR ($CDCl_3$) δ 8.63 (1', s, 1H), 8.57 (1, s, 1H), 7.54 (2', m, 2H), 7.51 (2, m, 2H), 7.25 (3', m, 2H), 7.18 (4, m, 2H), 7.16 (3, m, 2H), 7.12 (5, m, 2H), 7.10 (5', m, 2H), 7.03 (4', m, 2H); ^{13}C NMR ($CDCl_3$) δ 161.82 (A, d, *J* = 248.4 Hz), 161.34 (A', d, *J* = 247.7 Hz), 161.52 (B'), 161.40 (B), 140.85 (C'),

138.86 (C), 137.33 (D, d, J = 3.1 Hz), 135.20 (D', d, J = 3.2 Hz), 133.10 (E'), 132.44 (E), 128.11 (F', d, J = 8.5 Hz), 127.62 (F, d, J = 8.6 Hz), 127.14 (G), 126.30 (G'), 120.86 (H'), 120.27 (H), 117.03 (I, d, J = 22.9 Hz), 116.44 (I', d, J = 22.8 Hz); ^{19}F NMR ($CDCl_3$) δ -113.50 (major, tt, J = 7.7, 4.9 Hz), -113.99 (minor, tt, J = 8.2, 4.8 Hz).

Preparation of *N*-(4-(diethylamino)phenyl)-*N*-(4-fluorophenyl)formamide (6)[4]

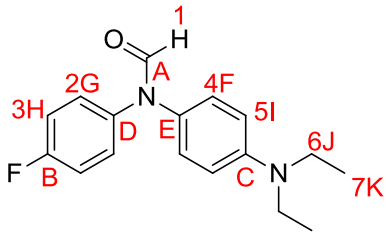

Into a flask were placed caesium fluoride (171 mg, 1.13 mmol), copper(I) iodide (43 mg, 50 mol %), 1-fluoro-4-iodobenzene (0.05 ml, 0.45 mmol), *N*-(4-(diethylamino)phenyl)formamide (104 mg, 0.54 mmol) and *N*,*N*-dimethylethylenediamine (4.8 µl, 10 mol %). The flask was sealed, evacuated, and backfilled with nitrogen 2–3 times, then it was charged with THF (1 ml), evacuated and backfilled with nitrogen twice more and was allowed to stir at 66 °C overnight. The reaction mixture was diluted with EtOAc and quenched with saturated ammonium chloride. The aqueous layer was extracted with EtOAc and the combined organics were washed with brine, dried over magnesium sulfate, filtered, and concentrated under *vacuo*. The crude product was purified with prep-TLC (DCM) to give 82 mg of product as a yellow oil (64%).

EI-HRMS: obtained *m/z* 286.147467 M^+ (composition: $C_{17}H_{19}O_1N_2F_1$, expected *m/z* 286.14814); IR (neat) / cm^{-1} 2966.52, 2926.01, 2893.22, 2870.08, 1681.93 (amide), 1610.56, 1516.05, 1504.48; ^{1}H NMR ($CDCl_3$) δ 8.6 (1', s, 1H), 8.52 (1, s, 1H), 7.31 (2, dd, J = 9.0, 4.9 Hz, 2H), 7.14 (2', dd, J = 8.9, 4.7 Hz, 2H), 7.07 (3', m, 2H), 7.05 (4', m, 2H), 7.03 (3, m, 2H), 7.01 (4, m, 2H), 6.66 (5, m, 2H), 6.64 (5', m, 2H), 3.37 (6, m, 2H), 3.35 (6', m, 2H), 1.18 (7, m, 3H), 1.16 (7', m, 3H); ^{13}C NMR ($CDCl_3$) δ 162.24 (A),

161.87 (A'), 161.16 (B', d, J = 246.8 Hz), 160.56 (B, d, J = 245.5 Hz), 147.29 (C), 146.94 (C'), 138.74 (D'), 136.70 (D), 129.19 (E), 127.60 (F), 127.46 (F'), 127.24 (E'), 126.82 (G, d, J = 8.1 Hz), 126.12 (G', d, J = 8.4 Hz), 116.44 (H', d, J = 22.9 Hz), 115.79 (H, d, J = 22.6 Hz), 112.08 (I), 111.91 (I'), 44.59 (J), 44.55 (J'), 12.66 (K'), 12.60 (K); ^{19}F NMR ($CDCl_3$) δ -115.66 (minor, tt, J = 7.8, 4.8 Hz), -116.05 (major, tt, J = 8.3, 4.9 Hz).

Attempted synthesis of *N*-(2-cyanophenyl)-*N*-(4-fluorophenyl)formamide (19)[4]

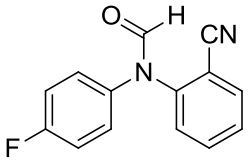

Into a flask were placed caesium fluoride (167 mg, 1.1 mmol), copper(I) iodide (42 mg, 50 mol %), 2-iodobenzonitrile (100 mg, 0.44 mmol), *N*-(4-fluorophenyl)formamide (74 mg, 0.53 mmol) and *N*,*N*-dimethylethylenediamine (4.7 μl, 10 mol %). The flask was sealed, evacuated, and backfilled with nitrogen 2–3 times, then it was charged with THF (2 ml), evacuated and backfilled with nitrogen twice more and it was allowed to stir at 66 °C overnight. The reaction mixture was diluted with EtOAc and quenched with saturated ammonium chloride. The aqueous layer was extracted with EtOAc and the combined organics were washed with brine, dried over magnesium sulfate, filtered, and concentrated under *vacuo*. No reaction was observed and after one night only the starting materials remained.

Attempted synthesis of *N*-(2-(dimethylamino)phenyl)-*N*-(4-fluorophenyl)formamide (21)[4]

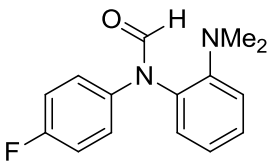

Into a flask were placed caesium fluoride (190 mg, 1.25 mmol), copper(I) iodide (48 mg, 50 mol %), 2-bromo-*N*,*N*-dimethylaniline (0.07 ml, 0.5 mmol), *N*-(4-fluorophenyl)formamide (83 mg, 0.6 mmol), and *N*,*N*-dimethylethylenediamine (5.4 µl, 10 mol %). The flask was sealed, evacuated, and backfilled with nitrogen 2–3 times, then it was charged with THF (2.5 ml), evacuated and backfilled with nitrogen twice more and it was allowed to stir at 66 °C overnight. The reaction mixture was diluted with EtOAc and quenched with saturated ammonium chloride. The aqueous layer was extracted with EtOAc and the combined organics were washed with brine, dried over magnesium sulfate, filtered, and concentrated under *vacuo*. No reaction was observed and after one night only the starting materials remained.

Preparation of *N*-(2-bromophenyl)-*N*-(4-fluorophenyl)formamide (23)[4]

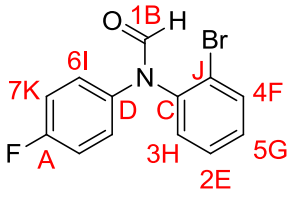

Into a flask were placed caesium fluoride (342 mg, 2.26 mmol), copper(I) iodide (86 mg, 50 mol %), 1-fluoro-4-iodobenzene (0.1 ml, 200 mg), *N*-(2-bromophenyl)formamide (216 mg, 1.08 mmol), and *N*,*N*-dimethylethylenediamine (9.6 µl, 10 mol %). The flask was sealed, evacuated, and backfilled with nitrogen 2–3 times, then it was charged with THF (4 ml), evacuated and backfilled with nitrogen twice more and it was allowed to stir at 66 °C overnight. The reaction mixture was diluted with EtOAc and quenched with saturated ammonium chloride. The aqueous layer was extracted with EtOAc and the combined organics were washed with brine, dried over magnesium sulfate, filtered, and concentrated under *vacuo*. The crude product was purified with prep-TLC (DCM) and was obtained in 29% yield (76 mg). The compound seems to exist in 4 conformational states which are apparent in the NMR. A full characterisation was not performed as this

compound was not included in our studies, due to the presence of 4 conformers. The different conformers are not denoted with prime (').

EI-LRMS: obtained *m/z* 294 (composition: $C_{13}H_9BrFNO$, expected MW 294.11906); ^{1}H NMR ($CDCl_3$) δ 8.74 (1, s, 1H), 8.69 (1, s, 1H), 8.41 (1, s, 1H), 8.4 (1, s, 1H), 7.99 (2, dd, *J* = 8, 1.4 Hz, 1H), 7.97 (2, dd, *J* = 8, 1.4 Hz, 1H), 7.74 (2, dd, *J* = 8.1, 1.4 Hz, 1H), 7.71 (2, dd, *J* = 8.1, 1.4 Hz, 1H), 7.41 – 7.5 (3, m, 1H), 7.34 – 7.37 (4, m, 1H), 7.26 – 7.32 (5, 6, m, 3H), 7.13 – 7.16 (6, m, 2H), 7.03 – 7.1 (7, m, 2H); ^{13}C NMR ($CDCl_3$) δ 162.06 (B), 162.03 (B), 161.43 (B), 161.33 (B), 161.2 (A, d, *J* = 247 Hz), 160.63 (A, d, *J* = 246.4 Hz), 142.99 (C), 141.91 (C), 140.98 (E), 140.74 (E), 139.8 (C), 138.36 (C), 136.95 (D, d, *J* = 3.0 Hz), 136.82 (D, d, *J* = 2.9 Hz), 135.35 (D, d, *J* = 3.0 Hz), 135.29 (D, d, *J* = 3.0 Hz), 134.52 (E), 134.28 (E), 131.06 (F), 130.70 (F), 130.56, 130.40 (G), 130.25, 130.21, 130.16 (G), 130.00 (H), 129.81 (H), 129.08 (H), 128.89 (H), 126.30 (I, d, *J* = 8.3 Hz), 126.10 (I, d, *J* = 8.2 Hz), 125.05 (I, d, *J* = 8.4 Hz), 124.88 (I, d, *J* = 8.4 Hz), 123.67 (J), 123.02 (J), 116.63 (K, d, *J* = 22.9 Hz), 116.62 (K, d, *J* = 22.9 Hz), 115.89 (K, d, *J* = 22.8 Hz), 115.83 (K, d, *J* = 22.7 Hz); ^{19}F NMR ($CDCl_3$) δ -115.12, -115.31, -115.34, -115.52.

Preparation of *N*-([1,1'-biphenyl]-4-yl)-*N*-(4-fluorophenyl)formamide (26)[5]

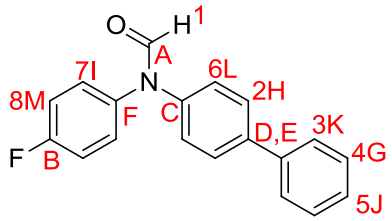

A two-neck flask, equipped with a reflux condenser, septum, and stirring bar, was filled with *N*-(4-bromophenyl)-*N*-(4-fluorophenyl)formamide (200 mg, 0.68 mmol) and $Pd(Ph_3P)_4$ (24 mg, 0.02 mmol) in DME (8 ml) under a N_2 atmosphere. The mixture was stirred for 10 min at 50 ^{o}C. To this solution was added the phenylboronic acid (115 mg, 0.95 mmol), dissolved in a minimum amount of EtOH:DME 1:2, followed by aq.

Na_2CO_3 (2 M, 9.26 mmol). This mixture was refluxed (85 ^oC) under stirring. After overnight stirring, the flask was cooled to r.t., and the mixture was treated with saturated aq. NH_4Cl solution and extracted with $CHCl_3$. The organic layer was washed with brine, dried, filtered, and concentrated in *vacuo*. The product (yellow solid) was purified first with column chromatography (DCM) and then with prep-TLC (DCM) and the yield of the reaction was 78% (155 mg).

m.p. = 111 – 114 °C; EI-HRMS: obtained *m/z* 291.105367 M^+ (composition: $C_{19}H_{14}O_1N_1F_1$, expected *m/z* 291.10594); IR (neat) / cm^{-1} 2920.23, 1685.79 (amide), 1606.7, 1504.48, 1485.19; ^1H NMR ($CDCl_3$) δ 8.72 (1, s, 1H), 8.63 (1', s, 1H), 7.63 (2, m, 2H), 7.60 (2', m, 2H), 7.59 (3', m, 2H), 7.57 (3, m, 2H), 7.46 (4, m, 2H), 7.44 (4', m, 2H), 7.40 (5', m, 1H), 7.37 (5, m, 1H), 7.35 (6', m, 2H), 7.32 (7, m, 2H), 7.23 (6, m, 2H), 7.21 (7', m, 2H), 7.14 (8', m, 2H), 7.11 (8, m, 2H); ^{13}C NMR ($CDCl_3$) δ 161.78 (A), 161.72 (A'), 161.70 (B', d, *J* = 247.8 Hz), 161.24 (B, d, *J* = 247.1 Hz), 140.88 (C), 140.34 - 140.31 (D, E'), 139.92 - 139.89 (D', E), 138.93 (C'), 137.79 (F'), 135.59 (F), 129.09 (G), 128.98 (G'), 128.56 (H), 128.12 (I, d, *J* = 8.6 Hz), 128.04 (H'), 127.90 (J), 127.66 (J'), 127.47 (I', d, *J* = 8.5 Hz), 127.21 (K'), 127.15 (K), 126.01 (L'), 125.15 (L), 116.88 (M', d, *J* = 22.9 Hz), 116.32 (M, d, *J* = 22.8 Hz); ^{19}F NMR ($CDCl_3$) δ -114.03 (minor, tt, *J* = 8.0, 4.8 Hz), -114.42 (major, tt, *J* = 8.2, 4.8 Hz).

Preparation of *N*-(2',6'-dimethyl-[1,1'-biphenyl]-4-yl)-*N*-(4-fluorophenyl) formamide (27)[5]

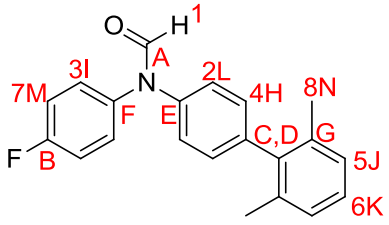

A two-neck flask, equipped with a reflux condenser, septum, and stirring bar, was filled with *N*-(4-bromophenyl)-*N*-(4-fluorophenyl)formamide (200 mg, 0.68 mmol) and

$Pd(Ph_3P)_4$ (24 mg, 0.02 mmol) in DME (8 ml) under a N_2 atmosphere. The mixture was stirred for 10 min at 50 ^oC. To this solution was added the (2,6-dimethylphenyl)boronic acid (142 mg, 0.95 mmol), dissolved in a minimum amount of EtOH:DME 1:2, followed by aq. Na_2CO_3 (2 M, 9.26 mmol). This mixture was refluxed (85 ^oC) under stirring. After overnight stirring, the flask was cooled to r.t., and the mixture was treated with saturated aq. NH_4Cl solution and extracted with $CHCl_3$. The organic layer was washed with brine, dried, filtered, and concentrated in *vacuo*. The product (white solid) was purified with prep-TLC (1:1 hexane:DCM and then DCM) and the yield of the reaction was 59% (129 mg).

m.p. = 150 – 153 °C; EI-HRMS: obtained *m/z* 319.136311 M^+ (composition: $C_{21}H_{18}O_1N_1F_1$, expected *m/z* 319.13724); IR (neat) / cm^{-1} 2924.09, 1681.93 (amide), 1504.48, 1465.9; ^1H NMR ($CDCl_3$) δ 8.76 (1, s, 1H), 8.63 (1', s, 1H), 7.36 (2', m, 2H), 7.33 (3, m, 2H), 7.25 (3', m, 2H), 7.21 (2 and 4, m, 4H), 7.10 - 7.19 (4', 5, 5', 6, 6', 7' and 7, m, 12H), 2.06 (8 and 8', s, 12H); ^{13}C NMR ($CDCl_3$) δ 161.93 (A), 161.74 (B', d, *J* = 247.9 Hz), 161.71 (A'), 161.28 (B, d, *J* = 247.1 Hz), 140.98 (C'), [140.56, 140.28, 140.23 (C, D, E)], 139.64 (D'), 138.40 (E'), 137.89 (F', d, *J* = 3.1 Hz), 136.24 (G'), 136.09 (G), 135.63 (F, d, *J* = 3.1 Hz), 130.67 (H), 129.99 (H'), 128.24 (I, d, *J* = 8.5 Hz), 127.76 (I', d, *J* = 8.5 Hz), 127.58 (J), 127.48 (J'), 127.40 (K and K'), 125.42 (L'), 124.70 (L), 116.90 (M', d, *J* = 22.9 Hz), 116.36 (M, d, *J* = 22.8 Hz), 21.04 (N'), 21.01 (N); ^{19}F NMR ($CDCl_3$) δ -113.98 (minor, tt, *J* = 8.0, 4.8 Hz), -114.44 (major, tt, *J* = 8.2, 4.9 Hz).

Preparation of (2,6-diethylphenyl)boronic acid (25)[6]

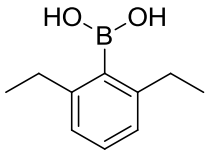

2,6-diethyl bromobenzene (0.24 ml, 1.41 mmol) was added dropwise, to a stirred solution of *n*-BuLi (0.62 ml, 1.55 mmol) in THF (3 ml) at –78 ^oC under nitrogen. After

stirring at –78 °C for 30 min, $B(OMe)_3$ (0.24 ml, 2.12 mmol) was added slowly, and the mixture was warmed to r.t. and stirred overnight. 2 N HCl (2 ml) was added and the mixture was stirred for 1 h. The organic layer was separated and the aqueous layer was extracted with ether (x2). The combined organic layers were dried over $MgSO_4$ and the solvents were removed in *vacuo*. A quick column (DCM to DCM:5% MeOH) to remove the remaining starting material was performed and then the crude product (207 mg, ≈ 82% yield) was used in the next step.

Preparation of *N*-(2',6'-diethyl-[1,1'-biphenyl]-4-yl)-*N*-(4-fluorophenyl)formamide (28)[5]

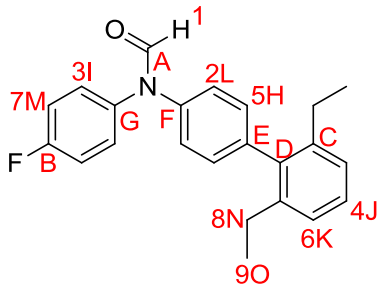

A two-neck flask, equipped with a reflux condenser, septum, and stirring bar, was filled with *N*-(4-bromophenyl)-*N*-(4-fluorophenyl)formamide (245 mg, 0.83 mmol) and $Pd(Ph_3P)_4$ (29 mg, 0.025 mmol) in DME (10 ml) under a N_2 atmosphere. The mixture was stirred for 10 min at 50 °C. To this solution was added the (2,6-diethylphenyl)boronic acid (207 mg, 1.16 mmol), dissolved in a minimum amount of EtOH:DME 1:2 (2.5 ml), followed by aq. Na_2CO_3 (2 M, 11.3 mmol). This mixture was refluxed (85 °C) under stirring. After overnight stirring, the flask was cooled to r.t., and the mixture was treated with saturated aq. NH_4Cl solution and extracted with $CHCl_3$. The organic layer was washed with brine, dried, filtered, and concentrated in *vacuo*. The product was obtained as a yellow solid in 42% yield (121 mg) after purification with prep-TLC (2:1 hexane:DCM and then only DCM) and a second prep-TLC (DCM).

m.p. = 93 – 97 °C; EI-HRMS: obtained *m/z* 347.167834 M^+ (composition: $C_{23}H_{22}O_1N_1F_1$, expected *m/z* 347.16854); IR (neat) / cm^{-1} 2960.73, 2926.01, 2870.08,

1681.93 (amide), 1604.77, 1506.41, 1454.33; ^{1}H NMR ($CDCl_3$) δ 8.77 (1, s, 1H), 8.63 (1', s, 1H), 7.37 (2', m, 2H), 7.24 - 7.35 (3, 3', 4 and 4', m, 6H), 7.23 (5, m, 2H), 7.21 (2, m, 2H), 7.19 (5', m, 2H), 7.13 - 7.18 (7', 6, 6' and 7, m, 8H), 2.35 (8', m, 4H), 2.34 (8, m, 4H), 1.05 (9, m, 6H), 1.04 (9', m, 6H); ^{13}C NMR ($CDCl_3$) δ 161.96 (A), 161.77 (B', d, J = 247.9 Hz), 161.71 (A'), 161.31 (B, d, J = 247.1 Hz), 142.41 (C'), 142.28 (C), 140.31 (D), 139.88 (D'), 139.57 (E), 139.44 (F), 138.96 (E'), 138.45 (F'), 137.87 (G', d, J = 3.1 Hz), 135.60 (G, d, J = 3.2 Hz), 131.08 (H), 130.38 (H'), 128.30 (I, d, J = 8.5 Hz), 128.08 (J), 127.88 (J'), 127.87 (I', d, J = 8.5 Hz), 125.83 (K), 125.71 (K'), 124.92 (L'), 124.20 (L), 116.92 (M', d, J = 22.9 Hz), 116.38 (M, d, J = 22.7 Hz), 26.95 (N), 26.92 (N'), 15.66 (O and O'); ^{19}F NMR ($CDCl_3$) δ -113.90 (minor, tt, J = 8.1, 4.8 Hz), -114.38 (major, tt, J = 8.2, 4.9 Hz).

Preparation of *N*-(2'-amino-[1,1'-biphenyl]-4-yl)-*N*-(4-fluorophenyl)formamide (29)[5]

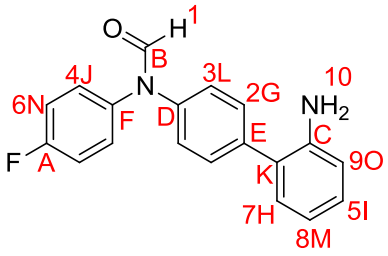

A two-neck flask, equipped with a reflux condenser, septum, and stirring bar, was filled with *N*-(4-bromophenyl)-*N*-(4-fluorophenyl)formamide (465 mg, 1.58 mmol) and $Pd(Ph_3P)_4$ (55 mg, 0.047 mmol) in DME (20 ml) under a N_2 atmosphere. The mixture was stirred for 10 min at 50 ^{o}C. To this solution was added the 2-aminobenzeneboronic acid (300 mg, 2.19 mmol), dissolved in a minimum amount of EtOH:DME 1:2, followed by aq. Na_2CO_3 (2 M, 21.51 mmol). This mixture was refluxed (85 ^{o}C) under stirring. After overnight stirring, the flask was cooled to r.t., and the mixture was treated with saturated aq. NH_4Cl solution and extracted with $CHCl_3$. The organic layer was washed with brine, dried, filtered, and concentrated in *vacuo*. The product was obtained as a

brown solid in 67% yield (326 mg) after purification with column chromatography (DCM).

m.p. = 116 – 118 °C; EI-HRMS: obtained *m/z* 306.117193 M^+ (composition: $C_{19}H_{15}O_1N_2F_1$, expected *m/z* 306.11684); IR (neat) / cm^{-1} 3480 (NH_2), 3390 (NH_2), 1672.28 (amide), 1614.42, 1504.48, 1489.05; ^{1}H NMR ($CDCl_3$) δ 8.72 (1, s, 1H), 8.63 (1', s, 1H), 7.52 (2, m, 2H), 7.50 (2', m, 2H), 7.37 (3', d, *J* = 8.5 Hz, 2H), 7.32 (4, m, 2H), 7.25 (3, m, 2H), 7.22 (4', m, 2H), 7.11 - 7.19 (5, 5', 6', 6, 7 and 7', m, 8H), 6.85 (8, m, 1H), 6.83 (8', m, 1H), 6.76 - 6.79 (9 and 9', m, 2H), 3.77 (10, s, 2H); ^{13}C NMR ($CDCl_3$) δ 161.79 (B), 161.75 (B'), 161.73 (A', d, *J* = 248.0 Hz), 161.29 (A, d, *J* = 247.3 Hz), 143.68 (C'), 143.58 (C), 140.66 (D), 138.68 (D'), 138.65 (E), 138.24 (E'), 137.72 (F', d, *J* = 3.3 Hz), 135.50 (F, d, *J* = 3.3 Hz), 130.59 (G), 130.53 (H'), 130.48 (H), 130.03 (G'), 129.08 (I), 128.89 (I'), 128.24 (J, d, *J* = 8.7 Hz), 127.59 (J', d, *J* = 8.7 Hz), 126.60 (K'), 126.23 (K), 126.04 (L'), 125.06 (L), 118.97 (M), 118.82 (M'), 116.89 (N', d, *J* = 23.1 Hz), 116.35 (N, d, *J* = 23.0 Hz), 115.96 (O), 115.82 (O'); ^{19}F NMR ($CDCl_3$) δ -113.91 (minor, tt, *J* = 8.0, 4.8 Hz), -114.31 (major, tt, *J* = 8.2, 4.9 Hz).

Preparation of *N*-(2',6'-dimethoxy-[1,1'-biphenyl]-4-yl)-*N*-(4-fluorophenyl) formamide (30)[5]

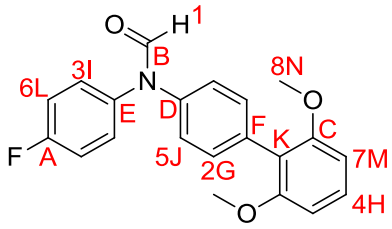

A two-neck flask, equipped with a reflux condenser, septum, and stirring bar, was filled with *N*-(4-bromophenyl)-*N*-(4-fluorophenyl)formamide (500 mg, 1.7 mmol) and $Pd(Ph_3P)_4$ (59 mg, 0.05 mmol) in DME (22 ml) under a N_2 atmosphere. The mixture was stirred for 10 min at 50 ^oC. To this solution was added the (2,6-dimethoxyphenyl)boronic acid (431 mg, 2.37 mmol), dissolved in a minimum amount of

EtOH:DME 1:2, followed by aq. Na_2CO_3 (2 M, 23.15 mmol). This mixture was refluxed (85 ^oC) under stirring. After overnight stirring, the flask was cooled to r.t., and the mixture was treated with saturated aq. NH_4Cl solution and extracted with $CHCl_3$. The organic layer was washed with brine, dried, filtered, and concentrated in *vacuo*. The product (white solid) was purified with column chromatography (DCM) in 91% yield (545 mg).

m.p. = 146 – 148 °C; EI-HRMS: obtained *m/z* 351.126276 M^+ (composition: $C_{21}H_{18}O_3N_1F_1$, expected *m/z* 351.12707); IR (neat) / cm^{-1} 1681.93 (amide), 1587.42, 1504.48, 1469.76; ^1H NMR ($CDCl_3$) δ 8.75 (1, s, 1H), 8.61 (1', s, 1H), 7.41 (2, m, 2H), 7.39 (2', m, 2H), 7.36 (3, m, 2H), 7.29 - 7.34 (4, 5' and 4', m, 4H), 7.26 (3', m, 2H), 7.17 (5, m, 2H), 7.15 (6', m, 2H), 7.12 (6, m, 2H), 6.68 (7, d, *J* = 8.4 Hz, 2H), 6.66 (7', d, *J* = 8.4 Hz, 2H), 3.77 (8, s, 6H), 3.74 (8', s, 6H); ^{13}C NMR ($CDCl_3$) δ 162.14 (B), 161.71 (A', d, *J* = 247.6 Hz), 161.70 (B'), 161.26 (A, d, *J* = 246.8 Hz), 157.78 (C'), 157.64 (C), 139.98 (D), 138.12 (D'), 137.91 (E', d, *J* = 3.0 Hz), 135.62 (E, d, *J* = 3.1 Hz), 133.17 (F), 132.66 (F'), 132.52 (G), 131.90 (G'), 129.27 (H), 128.99 (H'), 128.41 (I, d, *J* = 8.5 Hz), 127.98 (I', d, *J* = 8.6 Hz), 124.43 (J'), 123.77 (J), 118.62 (K'), 118.04 (K), 116.73 (L', d, *J* = 22.8 Hz), 116.22 (L, d, *J* = 22.7 Hz), 104.30 (M and M'), 56.01 (N), 55.95 (N'); ^{19}F NMR ($CDCl_3$) δ -114.20 (minor, tt, *J* = 8.1, 4.8 Hz), -114.64 (major, tt, *J* = 8.2, 4.9 Hz).

Preparation of 1,5-di-*tert*-butyl-2,4-dimethoxybenzene (32)[7]

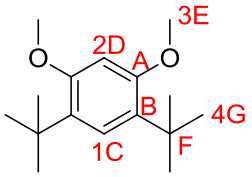

The 4,6-di-tert-butylresorcinol (10 g, 0.045 mol) was added to a suspension of NaH (60% dispersion in mineral oil, 5.4 g, 0.225 mol) in DMF (200 ml). The iodomethane (14 ml, 0.225 mol) was then added and the reaction mixture was stirred at room

temperature overnight. When reaction was complete, a solution of saturated NH_4Cl was slowly added and the aqueous phase was extracted with $CHCl_3$ (x2). The combined organic layers were washed with water (x10), dried, filtered and concentrated under reduced pressure. The product (white solid) was obtained with flash chromatography (3:1 hexane:DCM) in 68% yield (7.65 g).

m.p. = 66 – 71 °C; EI-HRMS: obtained *m/z* 250.19279 M^+ (composition: $C_{16}H_{26}O_2$, expected *m/z* 250.19328); IR (neat) / cm^{-1} 2953.02, 2854.65, 1610.56, 1570.06, 1504.48, 1462.04; ^1H NMR ($CDCl_3$) δ 7.19 (1, s, 1H), 6.48 (2, s, 1H), 3.85 (3, s, 6H), 1.36 (4, s, 18H); ^{13}C NMR ($CDCl_3$) δ 157.22 (A), 129.12 (B), 124.98 (C), 97.48 (D), 55.32 (E), 34.59 (F), 30.18 (G).

Preparation of (3,5-di-*tert*-butyl-2,6-dimethoxyphenyl)boronic acid (33)[8,9]

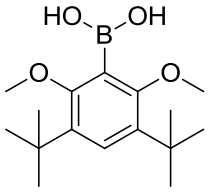

Initial attempts: a) To a stirred solution of 1,5-di-*tert*-butyl-2,4-dimethoxybenzene in THF at –78 °C under nitrogen was added *n*-BuLi followed immediately by $B(OMe)_3$. After stirring at –78 °C for 30 min, the mixture was warmed to r.t. and stirred overnight. The resulting mixture was quenched with 2 N HCl and extracted with DCM (x2). The combined extracts were washed with water and brine, dried and concentrated. This reaction did not work.[8]

b) The above reaction was repeated but the addition of the reagents was performed at 0 °C and also after adding the *n*-BuLi the reaction was stirred at 0 °C for 1 hour before adding the $B(OMe)_3$. Again the reaction was unsuccessful.

Final attempt: To a solution of 1,5-di-*tert*-butyl-2,4-dimethoxybenzene (1 g, 4 mmol) in dry THF (10 ml) at 0 °C under nitrogen was added dropwise a solution of *n*-BuLi (1.7 ml, 4.3 mmol) over 5 min. The reaction mixture was stirred at 0 °C for 30 min and then

at r.t. for 3.5 hours. The mixture was cooled to –78 ^{o}C and $B(OMe)_3$ (0.9 ml, 7.8 mmol) was added. The resulting mixture was allowed to warm to r.t. and stirred overnight. The reaction mixture was quenched with 2 N HCl at 0 ^{o}C and stirred for 30 min at r.t. The product was extracted with EtOAc, washed with water and brine, dried and concentrated. A quick column (from DCM to DCM:10% MeOH) was performed to remove some of the impurities and then the crude boronic acid (323 mg, ≈ 27% yield) was used directly in the next step without further purification.[9]

Preparation of *N*-(3',5'-di-*tert*-butyl-2',6'-dimethoxy-[1,1'-biphenyl]-4-yl)-*N*-(4-fluorophenyl)formamide (34)[5]

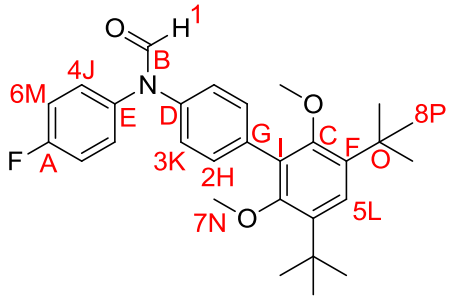

A two-neck flask, equipped with a reflux condenser, septum, and stirring bar, was filled with *N*-(4-bromophenyl)-*N*-(4-fluorophenyl)formamide (485 mg, 1.65 mmol) and $Pd(Ph_3P)_4$ (57 mg, 0.05 mmol) in DME (25 ml) under a N_2 atmosphere. The mixture was stirred for 10 min at 50 ^{o}C. To this solution was added the (3,5-di-*tert*-butyl-2,6-dimethoxyphenyl)boronic acid (671 mg, 2.28 mmol), dissolved in a minimum amount of EtOH:DME 1:2, followed by aq. Na_2CO_3 (2 M, 22.47 mmol). This mixture was refluxed (85 ^{o}C) under stirring. After overnight stirring, the flask was cooled to r.t., and the mixture was treated with saturated aq. NH_4Cl solution and extracted with $CHCl_3$. The organic layer was washed with brine, dried, filtered, and concentrated in *vacuo*. The product (white solid) was purified with column chromatography (DCM) in 33% yield (254 mg).

m.p. = 154 – 157 °C; EI-HRMS: obtained *m/z* 463.250806 M^+ (composition: $C_{29}H_{34}O_3N_1F_1$, expected *m/z* 463.25227); IR (neat) / cm^{-1} 2954.95, 1687.71 (amide), 1506.41, 1469.76; ^1H NMR ($CDCl_3$) δ 8.77 (1, s, 1H), 8.63 (1', s, 1H), 7.59 (2, d, *J* = 8.5 Hz, 2H), 7.55 (2', d, *J* = 8.6 Hz, 2H), 7.37 (3', d, *J* = 8.5 Hz, 2H), 7.32 (4, m, 2H), 7.29 (5, m, 1H), 7.27 (5', m, 1H), 7.23 (3, m, 2H), 7.21 (4', m, 2H), 7.15 (6', m, 2H), 7.12 (6, m, 2H), 3.13 (7 and 7', s, 12H), 1.40 (8, s, 18H), 1.39 (8', s, 18H); ^{13}C NMR ($CDCl_3$) δ 161.90 (B), 161.71 (A', d, *J* = 247.9 Hz), 161.67 (B'), 161.26 (A, d, *J* = 247.1 Hz), 156.17 (C'), 156.03 (C), 140.42 (D), 138.57 (D'), 137.95 (E', d, *J* = 3.1 Hz), 137.29 (F), 137.09 (F'), 135.64 (E, d, *J* = 3.2 Hz), 135.32 (G), 134.74 (G'), 132.64 (H), 131.92 (H'), 128.64 (I'), 128.35 (I), 128.13 (J, d, *J* = 8.5 Hz), 127.61 (J', d, *J* = 8.5 Hz), 125.35 (K'), 125.00 (L), 124.72 (L'), 124.49 (K), 116.92 (M', d, *J* = 22.9 Hz), 116.38 (M, d, *J* = 22.8 Hz), 60.50 (N'), 60.47 (N), 35.23 (O), 35.21 (O'), 31.15 (P and P'); ^{19}F NMR ($CDCl_3$) δ -114.01 (minor, tt, *J* = 8.0, 4.8 Hz), -114.41 (major, tt, *J* = 8.2, 4.9 Hz).

Attempted synthesis of *N*-(2',6'-bis(trifluoromethyl)-[1,1'-biphenyl]-4-yl)-*N*-(4-fluorophenyl)formamide (36)[5,10,11]

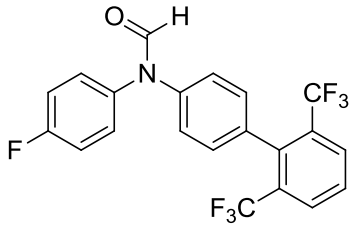

First attempt: A two-neck flask, equipped with a reflux condenser, septum, and stirring bar, was filled with *N*-(4-bromophenyl)-*N*-(4-fluorophenyl)formamide (82 mg, 0.28 mmol) and $Pd(PPh_3)_4$ (10 mg, 0.008 mmol) in DME (4 ml) under a N_2 atmosphere. The mixture was stirred for 10 min at 50 ^oC. To this solution was added the 2,6-bis(trifluoromethyl)benzeneboronic acid (100 mg, 0.39 mmol), dissolved in a minimum amount of EtOH:DME 1:2, followed by aq. Na_2CO_3 (2 M, 3.8 mmol). This mixture was refluxed (85 ^oC) under stirring. After overnight stirring, the flask was cooled to r.t., and

the mixture was treated with saturated aq. NH_4Cl solution and extracted with $CHCl_3$. The organic layer was washed with brine, dried, filtered, and concentrated in *vacuo*.[5]

Second attempt: A two-neck flask, equipped with a reflux condenser, septum, and stirring bar, was filled with the *N*-(4-bromophenyl)-*N*-(4-fluorophenyl)formamide (82 mg, 0.28 mmol) and $Pd(dppf)Cl_2$ (6 mg, 3 mol%) in ethanol (3.5 ml) under a N_2 atmosphere. To this solution was added the 2,6-bis(trifluoromethyl)benzeneboronic acid (100 mg, 0.39 mmol) followed by Et_3N (0.16 ml, 1.12 mmol). This mixture was refluxed at 78^{o}C under stirring. After overnight stirring, the flask was cooled to r.t., and the mixture was treated with saturated aq. NH_4Cl solution and extracted with $CHCl_3$. The organic layer was washed with brine, dried, filtered, and concentrated in *vacuo*.[10]

Third attempt: A two-neck flask, equipped with a reflux condenser, septum, and stirring bar, was filled with the *N*-(4-bromophenyl)-*N*-(4-fluorophenyl)formamide (82 mg, 0.28 mmol), palladium(II) acetate (5.8 mg, 0.026 mmol) and triphenylphosphine (14 mg, 0.054 mmol) in *n*-propanol (4 ml) under a N_2 atmosphere. To this solution was added the 2,6-bis(trifluoromethyl)benzeneboronic acid (100 mg, 0.39 mmol) followed by aq. Na_2CO_3 (2 M, 3.8 mmol). This mixture was refluxed at 97 ^{o}C under stirring. After overnight stirring, the flask was cooled to r.t., and the mixture was treated with saturated aq. NH_4Cl solution and extracted with $CHCl_3$. The organic layer was washed with brine, dried, filtered, and concentrated in *vacuo*.[11] None of the three attempts worked and the *N*-(2',6'-bis(trifluoromethyl)-[1,1'-biphenyl]-4-yl)-*N*-(4-fluorophenyl)formamide could not be synthesised.

Preparation of 2-bromo-5-(*tert*-butyl)-1,3-dinitrobenzene (38)[12]

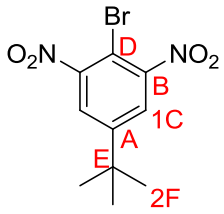

4-*tert*-butylbromobenzene (1.6 ml, 9.38 mmol) was added dropwise to vigorously stirred fuming nitric acid (5 ml) at 0 ^{o}C during 30 minutes. The mixture was stirred at 25 ^{o}C for 1 hour and then at 50 ^{o}C for 20 minutes after which time the mixture was poured on to vigorously stirring ice–water (20 mL). The precipitate was collected by filtration and washed with water (2 × 5 mL) and saturated aqueous $NaHCO_3$ solution (3 × 5 mL). The solid was dissolved in a mixture of EtOH (20 mL) and acetone (2 mL), with the resulting concentration of the solution under reduced pressure affording the product as yellow coloured needles (99.8% yield, 2.838 g).

m.p. = 115 – 119 °C; EI-HRMS: obtained *m/z* 301.990079 M^+ (composition: $C_{10}H_{11}O_4N_2Br_1$, expected *m/z* 301.99022); IR (neat) / cm^{-1} 1598.99, 1537.27 (NO_2), 1479.4, 1463.97, 1348.24 (NO_2); ^{1}H NMR ($CDCl_3$) δ 7.88 (1, s, 2H), 1.38 (2, s, 9H); ^{13}C NMR ($CDCl_3$) δ 154.56 (A), 151.83 (B), 124.91 (C), 104.11 (D), 35.76 (E), 30.81 (F).

Preparation of (4-((4-fluorophenyl)amino)phenyl)boronic acid (39)[8]

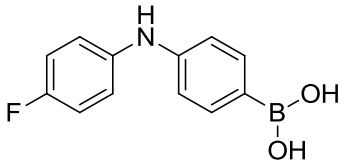

To a stirred solution of *N*-(4-bromophenyl)-*N*-(4-fluorophenyl)formamide (200 mg, 0.68 mmol) in THF (5 ml) at –78 ^{o}C under nitrogen was added *n*-BuLi (0.54 ml, 1.36 mmol) followed immediately by $B(OMe)_3$ (0.15 ml, 1.33 mmol). After stirring at –78 ^{o}C for 30 min, the mixture was warmed to r.t. and stirred overnight. The resulting mixture was quenched with 2 N HCl and extracted with DCM (x2). The combined extracts were washed with water and brine, dried and concentrated. A quick column (DCM to DCM:2% MeOH) was performed to remove major impurities and then the crude boronic acid (64 mg, ≈ 41% yield) was used without further purification in the next step.

Preparation of 4'-(*tert*-butyl)-*N*-(4-fluorophenyl)-2',6'-dinitro-[1,1'-biphenyl]-4-amine (41)[5]

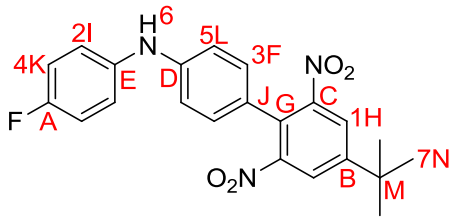

A two-neck flask, equipped with a reflux condenser, septum, and stirring bar, was filled with the 2-bromo-5-(*tert*-butyl)-1,3-dinitrobenzene (95 mg, 0.31 mmol) and $Pd(Ph_3P)_4$ (11 mg, 0.009 mmol) in DME (4 ml) under a N_2 atmosphere. The mixture was stirred for 10 min at 50 ^oC. To this solution was added the (4-((4-fluorophenyl)amino)phenyl)boronic acid (100 mg, 0.43 mmol), dissolved in a minimum amount of EtOH:DME 1:2, followed by aq. Na_2CO_3 (2 M, 4.22 mmol). This mixture was refluxed (85 ^oC) under stirring. After overnight stirring, the flask was cooled to r.t., and the mixture was treated with saturated aq. NH_4Cl solution and extracted with $CHCl_3$. The organic layer was washed with brine, dried, filtered, and concentrated in *vacuo*. The product was obtained after a prep-TLC (1:1 hexane:DCM) as an orange oil in 61% yield (78 mg).

ESI-HRMS: obtained *m/z* 408.13541 $(M - H)^+$ (calculated *m/z* 408.13672); IR (neat) / cm^{-1} 3410 (amine), 2968.45, 2929,87, 1608.63, 1523.76 (NO_2), 1352.1 (NO_2); ^1H NMR ($CDCl_3$) δ 7.91 (1, s, 2H), 7.12 (2, m, 2H), 7.08 (3, m, 2H), 7.01 (4, m, 2H), 6.93 (5, m, 2H), 5.73 (6, s, 1H), 1.42 (7, s, 9H); ^{13}C NMR ($CDCl_3$) δ 158.86 (A, d, *J* = 241.6 Hz), 153.69 (B), 151.17 (C), 145.50 (D), 137.64 (E, d, *J* = 2.8 Hz), 129.43 (F), 127.03 (G), 123.61 (H), 122.48 (I, d, *J* = 7.9 Hz), 121.44 (J), 116.23 (K, d, *J* = 22.5 Hz), 115.70 (L), 35.65 (M), 30.96 (N); ^{19}F NMR ($CDCl_3$) δ -120.23 (tt, *J* = 8.1, 4.7 Hz).

Preparation of *N*-(4'-(*tert*-butyl)-2',6'-dinitro-[1,1'-biphenyl]-4-yl)-*N*-(4-fluorophenyl)formamide (43)[13]

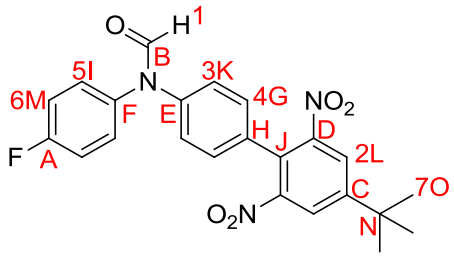

A mixture of 4'-(*tert*-butyl)-*N*-(4-fluorophenyl)-2',6'-dinitro-[1,1'-biphenyl]-4-amine (51 mg, 0.12 mmol) and formic acid (1 ml) was heated at 80 ^{o}C for 6 h. The mixture was cooled to room temperature and diluted with ethyl acetate. The resulting solution was washed with sodium bicarbonate (x2), followed by brine, dried over magnesium sulfate, filtered, and concentrated. The crude product was purified with prep-TLC (DCM) and obtained as yellow crystals in 59% yield (31 mg).

m.p. = 166 – 170 °C; EI-HRMS: obtained *m/z* 437.137891 M^+ (composition: $C_{23}H_{20}O_5N_3F_1$, expected *m/z* 437.1387); IR (neat) / cm^{-1} 2960, 2880, 1687.71 (amide), 1606.7, 1531.48 (NO_2), 1502.55, 1355.96 (NO_2); ^{1}H NMR ($CDCl_3$) δ 8.76 (1, s, 1H), 8.58 (1', s, 1H), 8.03 (2, s, 2H), 7.99 (2', s, 2H), 7.40 (3', d, *J* = 8.5 Hz, 2H), 7.30 (4, m, 2H), 7.28 (5, m, 2H), 7.25 (4', m, 2H), 7.23 (5', m, 2H), 7.18 (3, m, 2H), 7.16 (6', m, 2H), 7.13 (6, m, 2H), 1.45 (7, s, 9H), 1.44(7', s, 9H); ^{13}C NMR ($CDCl_3$) δ 162.01 (A', d, *J* = 248.5 Hz), 161.67 (B), 161.60 (B'), 161.51 (A, d, *J* = 247.7 Hz), 154.94 (C), 154.58 (C'), 150.85 (D'), 150.72 (D), 142.57 (E), 140.89 (E'), 137.18 (F', d, *J* = 2.9 Hz), 135.01 (F, d, *J* = 3.4 Hz), 129.91 (G), 129.52 (H), 129.14 (G'), 128.61 (I, d, *J* = 8.6 Hz), 128.51 (I', d, *J* = 8.6 Hz), 126.43 (J'), 126.14 (J), 124.70 (K'), 124.21 (K or L), 124.09 (K or L), 124.01 (L'), 117.11 (M', d, *J* = 22.9 Hz), 116.57 (M, d, *J* = 22.9 Hz), 35.80 (N), 35.74 (N'), 30.92 (O and O'); ^{19}F NMR ($CDCl_3$) δ -113.19 (minor, tt, *J* = 8.0, 4.8 Hz), -113.85 (major, tt, *J* = 8.2, 4.8 Hz).

Preparation of *N*-(4-fluorophenyl)-3',5'-dinitro-[1,1'-biphenyl]-4-amine (42)[5]

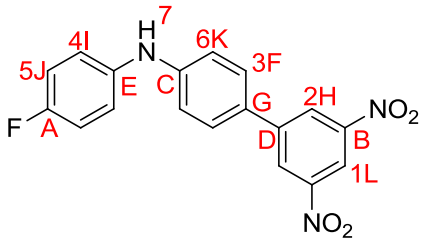

A two-neck flask, equipped with a reflux condenser, septum, and stirring bar, was filled with the 1-iodo-3,5-dinitrobenzene (129 mg, 0.44 mmol) and $Pd(Ph_3P)_4$ (15 mg, 0.013 mmol) in DME (5.6 ml) under a N_2 atmosphere. The mixture was stirred for 10 min at 50 ^oC. To this solution was added the (4-((4-fluorophenyl)amino)phenyl)boronic acid (140 mg, 0.61 mmol), dissolved in a minimum amount of EtOH:DME 1:2, followed by aq. Na_2CO_3 (2 M, 6 mmol). This mixture was refluxed (85 ^oC) under stirring. After overnight stirring, the flask was cooled to r.t., and the mixture was treated with saturated aq. NH_4Cl solution and extracted with $CHCl_3$. The organic layer was washed with brine, dried, filtered, and concentrated in *vacuo*. The product was obtained after a column chromatography (1:1 hexane:DCM) as a red solid in 98% yield (152 mg).

m.p. = 205 – 207 °C; ESI-HRMS: obtained *m/z* 352.0732 $(M - H)^+$ (calculated *m/z* 352.0728); IR (neat) / cm^{-1} 3380 (amine), 3090, 2910, 1597.06, 1506.41 (NO_2), 1346.31 (NO_2); ^1H NMR ($CDCl_3$) δ 8.91 (1, t, *J* = 1.9 Hz, 1H), 8.71 (2, d, *J* = 2.0 Hz, 2H), 7.58 (3, d, *J* = 8.6 Hz, 2H), 7.16 (4, dd, *J* = 8.8, 4.7 Hz, 2H), 7.05 – 7.08 (5 and 6, m, 4H), 5.84 (7, s, 1H); ^{13}C NMR ($CDCl_3$) δ 159.17 (A, d, *J* = 242.6 Hz), 149.16 (B), 146.34 (C), 144.57 (D), 137.29 (E, d, *J* = 2.8 Hz), 128.48 (F), 127.45 (G), 125.87 (H), 122.83 (I, d, *J* = 8.0 Hz), 116.46 (J, d, *J* = 22.6 Hz), 116.16 (K), 116.05 (L); ^{19}F NMR ($CDCl_3$) δ -119.34 (tt, *J* = 8.2, 4.7 Hz).

Preparation of *N*-(3',5'-dinitro-[1,1'-biphenyl]-4-yl)-*N*-(4-fluorophenyl)formamide (44)[13]

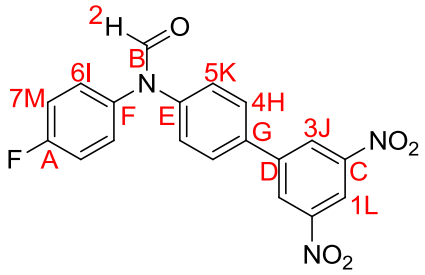

A mixture of *N*-(4-fluorophenyl)-3',5'-dinitro-[1,1'-biphenyl]-4-amine (152 mg, 0.43 mmol) and formic acid (3.5 ml) was heated at 80 ^{o}C for 6 h. The mixture was cooled to room temperature and diluted with ethyl acetate. The resulting solution was washed with sodium bicarbonate (x2), followed by brine, dried over magnesium sulfate, filtered, and concentrated. The crude product was purified with prep-TLC (DCM) and obtained as yellow crystals in 78% yield (128 mg).

m.p. = 184 – 186 °C; EI-HRMS: obtained *m/z* 381.075365 M^{+} (composition: $C_{19}H_{12}O_5N_3F_1$, expected *m/z* 381.0761); IR (neat) / cm^{-1} 1678.07 (amide), 1598.99, 1539.2 (NO_2), 1506.41, 1344.38 (NO_2); ^{1}H NMR ($CDCl_3$) δ 9.03 (1', t, *J* = 1.9 Hz, 1H), 9.01 (1, t, *J* = 1.9 Hz, 1H), 8.79 (2', s, 1H), 8.76 (3', d, *J* = 1.9 Hz, 2H), 8.75 (3, d, *J* = 2.0 Hz, 2H), 8.63 (2, s, 1H), 7.74 (4', d, *J* = 8.4 Hz, 2H), 7.70 (4, d, *J* = 8.5 Hz, 2H), 7.52 (5, d, *J* = 8.6 Hz, 2H), 7.34 (5', d, *J* = 8.6 Hz, 2H), 7.3 (6', m, 2H), 7.24 (6, m, 2H), 7.19 (7, m, 2H), 7.15 (7', m, 2H); ^{13}C NMR ($CDCl_3$) δ 162.03 (A, d, *J* = 248.9 Hz), 161.72 (B), 161.58 (A', d, *J* = 248.0 Hz), 161.40 (B'), 149.21 (C'), 149.16 (C), 143.91 (D), 143.51 (D' or E'), 143.36 (D' or E'), 141.48 (E), 137.10 (F, d, *J* = 3.3 Hz), 134.99 (G'), 134.95 (F', d, *J* = 3.1 Hz), 134.50 (G), 128.86 (H'), 128.55 (I', d, *J* = 8.7 Hz), 128.15 (H), 128.08 (I, d, *J* = 8.9 Hz), 126.91 (J and J'), 126.22 (K), 125.09 (K'), 117.61 (L'), 117.41 (L), 117.21 (M, d, *J* = 22.9 Hz), 116.65 (M', d, *J* = 22.8 Hz); ^{19}F NMR ($CDCl_3$) δ -112.94 (major), -113.44 (minor).

Preparation of *N*-(3',5'-di-*tert*-butyl-2',6'-dihydroxy-[1,1'-biphenyl]-4-yl)-*N*-(4-fluorophenyl)-formamide (45)[14]

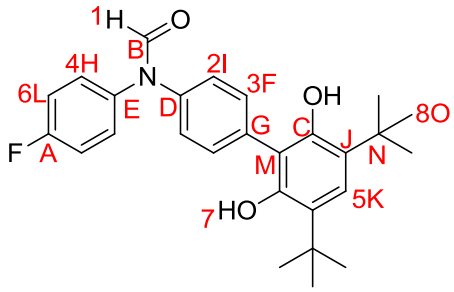

First attempt: The procedure described below was first attempted with 4 equivalents of 1 M solution of BBr_3 in CH_2Cl_2 and stirred overnight but it seemed that only one methoxy group was deprotected.

Second attempt: To a solution of *N*-(3',5'-di-*tert*-butyl-2',6'-dimethoxy-[1,1'-biphenyl]-4-yl)-*N*-(4-fluorophenyl)formamide (100 mg, 0.22 mmol) in CH_2Cl_2 (5 ml) was added dropwise 1 M solution of BBr_3 in CH_2Cl_2 (1.73 ml, 1.73 mmol) at –78 ^{o}C. The reaction mixture was stirred for 2.5 days at r.t. under nitrogen. The reaction mixture was then hydrolysed by careful shaking with water, thus precipitating a solid which was dissolved by the addition of 1 M sodium hydroxide, then neutralised with 1 M hydrochloric acid, extracted with ethyl acetate (x3), and the organic layer was dried over anhydrous magnesium sulphate and the ethyl acetate was removed under reduced pressure. The product (yellow solid) was obtained after purification with prep-TLC (2:1 hexane:EtOAc) in 77% yield (74 mg), but it was proved to be unstable.

m.p. = 70 – 73 °C (it decomposed at this temperature); EI-HRMS: obtained *m/z* 435.220595 M^+ (composition: $C_{27}H_{30}O_3N_1F_1$, expected *m/z* 435.22097); IR (neat) / cm^{-1} 3560 (OH), 2960.73, 1681.93 (amide), 1600.92, 1506.41; ^{1}H NMR ($CDCl_3$) δ 8.77 (1', s, 1H), 8.62 (1, s, 1H), 7.54 (2, m, 2H), 7.51 (3', m, 2H), 7.48 (3, m, 2H), 7.37 (2', m, 2H), 7.31 (4', m, 2H), 7.24 - 7.27 (4, 5 and 5', m, 4H), 7.2 (6, m, 2H), 7.17 (6', m, 2H), 4.68 (7, s, 2H), 4.63 (7', s, 2H), 1.41 (8', s, 18H), 1.40 (8, s, 18H); ^{13}C NMR ($CDCl_3$) δ 162.06 (A, d, J = 248.9 Hz), 161.88 (B), 161.64 (B'), 161.64 (A', d, J = 248.1 Hz),

149.48 (C), 149.41 (C'), 142.75 (D'), 140.85 (D), 137.11 (E, d, J = 3.2 Hz), 134.96 (E', d, J = 3.0 Hz), 133.59 (F'), 132.95 (F), 130.35 (G'), 129.78 (G), 128.70 (H', d, J = 8.8 Hz), 128.15 (H, d, J = 8.9 Hz), 127.29 (I), 127.02 (J'), 126.85 (J), 125.92 (I'), 125.04 (K and K'), 117.19 (L, d, J = 23.2 Hz), 116.67 (L', d, J = 23.0 Hz), 115.82 (M), 115.63 (M'), 34.75 (N), 34.74 (N'), 30.08 (O'), 30.05 (O); ^{19}F NMR ($CDCl_3$) δ -112.96 (major, tt, J = 8.0, 4.8 Hz), -113.46 (minor, tt, J = 8.2, 4.8 Hz).

Preparation of *N*-(4-fluorophenyl)-*N*-(2'-hydroxy-[1,1'-biphenyl]-4-yl)formamide (47)[5]

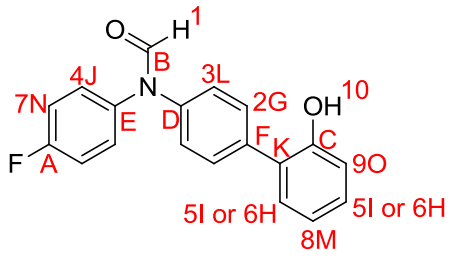

A two-neck flask, equipped with a reflux condenser, septum, and stirring bar, was filled with *N*-(4-bromophenyl)-*N*-(4-fluorophenyl)formamide (305 mg, 1.04 mmol) and $Pd(Ph_3P)_4$ (36 mg, 0.031 mmol) in DME (12 ml) under a N_2 atmosphere. The mixture was stirred for 10 min at 50 ^{o}C. To this solution was added the 2-hydroxybenzeneboronic acid (200 mg, 1.45 mmol), dissolved in a minimum amount of EtOH:DME 1:2, followed by aq. Na_2CO_3 (2 M, 14.16 mmol). This mixture was refluxed (85 ^{o}C) under stirring. After overnight stirring, the flask was cooled to r.t., and the mixture was treated with saturated aq. NH_4Cl solution and extracted with $CHCl_3$. The organic layer was washed with brine, dried, filtered, and concentrated in *vacuo*. The product was obtained as a white solid in 84% yield (269 mg) after purification with column chromatography (DCM to DCM:10% MeOH) and a second column (3:1 hexane:EtOAc).

m.p. = 123 – 126 °C; EI-HRMS: obtained *m/z* 307.100123 M^+ (composition: $C_{19}H_{14}O_2N_1F_1$, expected *m/z* 307.10086); IR (neat) / cm^{-1} 3138.18 (OH), 1658.78 (amide), 1600.92, 1504.48, 1450.47; ^{1}H NMR ($CDCl_3$) δ 8.70 (1, s, 1H), 8.62 (1', s,

1H), 7.57 (2, d, *J* = 8.6 Hz, 2H), 7.53 (2', d, *J* = 8.6 Hz, 2H), 7.39 (3', d, *J* = 8.5 Hz, 2H), 7.31 (4, m, 2H), 7.22 - 7.27 (5, 5', 6, 6', 4' and 3, m, 8H), 7.15 (7', m, 2H), 7.12 (7, m, 2H), 6.98 - 7.03 (8 and 8', m, 2H), 6.94 - 6.97 (9 and 9', m, 2H), 5.65 (10, s, 1H), 5.49 (10', s, 1H); ^{13}C NMR ($CDCl_3$) δ 161.96 (B), 161.91 (B'), 161.81 (A', d, *J* = 248.2 Hz), 161.36 (A, d, *J* = 247.4 Hz), 152.74 (C and C'), 140.86 (D), 139.08 (D'), 137.54 (E', d, *J* = 3.1 Hz), 136.77 (F), 136.11 (F'), 135.37 (E, d, *J* = 3.2 Hz), 130.73 (G), 130.52 (H), 130.45 (H'), 130.14 (G'), 129.52 (I), 129.43 (I'), 128.31 (J, d, *J* = 8.5 Hz), 127.67 (J', d, *J* = 8.6 Hz), 127.33 (K'), 127.05 (K), 126.18 (L'), 124.95 (L), 121.16 (M), 121.05 (M'), 116.95 (N', d, *J* = 22.9 Hz), 116.39 (N, d, *J* = 22.4 Hz), 116.30 (O), 116.23 (O'); ^{19}F NMR ($CDCl_3$) δ -113.65 (minor, tt, *J* = 8.0, 4.8 Hz), -114.12 (major, tt, *J* = 8.2, 4.9 Hz).

Preparation of *N*-(2',6'-dihydroxy-[1,1'-biphenyl]-4-yl)-*N*-(4-fluorophenyl)-formamide (48)[14]

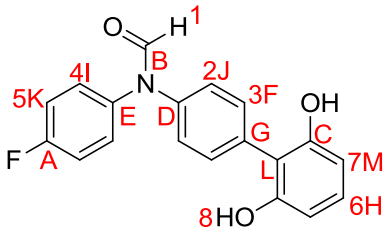

To a solution of *N*-(2',6'-dimethoxy-[1,1'-biphenyl]-4-yl)-*N*-(4-fluorophenyl)formamide (200 mg, 0.56 mmol) in CH_2Cl_2 (12 ml) was added dropwise 1 M solution of BBr_3 in CH_2Cl_2 (4.48 ml, 4.48 mmol) at –78 ^{o}C. The reaction mixture was stirred overnight at r.t. under nitrogen. The reaction mixture was then hydrolysed by careful shaking with water, thus precipitating a solid which was dissolved by the addition of 1 M sodium hydroxide, then neutralised with 1 M hydrochloric acid, extracted with ethyl acetate (x3), and the organic layer was dried over anhydrous magnesium sulphate and the ethyl acetate was removed under reduced pressure. The product (white solid) was obtained after purification with column chromatography (1:1 hexane:EtOAc) in 97% yield (175 mg).

m.p. = 176 – 180 °C; EI-HRMS: obtained *m/z* 323.094912 M^+ (composition: $C_{19}H_{14}O_3N_1F_1$, expected *m/z* 323.09577); IR (neat) / cm^{-1} 3300 (OH), 1672.28 (amide), 1600.92, 1581.63, 1506.41, 1490.97, 1460.11; ^1H NMR ($CDCl_3$) δ 8.68 (1, s, 1H), 8.58 (1', s, 1H), 7.41 - 7.46 (2', 3 and 3', m, 6H), 7.28 (4, m, 2H), 7.25 (2, m, 2H), 7.23 (4', m, 2H), 7.15 (5', m, 2H), 7.09 - 7.12 (5, 6 and 6', m, 4H), 6.55 (7, d, *J* = 1.8 Hz, 2H), 6.53 (7', d, *J* = 1.8 Hz, 2H), 5.29 (8, s, 2H), 5.16 (8', s, 2H); ^{13}C NMR ($CDCl_3$) δ 162.01 (B and B'), 161.99 (A', d, *J* = 248.7 Hz), 161.54 (A, d, *J* = 247.8 Hz), 153.82 (C), 153.78 (C'), 141.67 (D), 140.01 (D'), 137.16 (E', d, *J* = 3.1 Hz), 135.02 (E, d, *J* = 3.1 Hz), 132.49 (F), 131.91 (F'), 130.82 (G'), 129.93 (G), 129.76 (H and H'), 128.62 (I, d, *J* = 8.5 Hz), 128.06 (I', d, *J* = 8.6 Hz), 126.64 (J'), 125.14 (J), 117.08 (K', d, *J* = 22.9 Hz), 116.53 (K, d, *J* = 22.9 Hz), 114.79 (L'), 114.62 (L), 108.09 (M), 107.99 (M'); ^{19}F NMR ($CDCl_3$) δ -113.10 (major, tt, *J* = 8.0, 4.7 Hz), -113.70 (minor, tt, *J* = 8.2, 4.8 Hz).

Preparation of *N*-(4-fluorophenyl)-*N*-(pyridin-4-yl)formamide (53)[4]

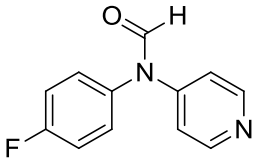

Into a flask were placed caesium fluoride (554 mg, 3.65 mmol), copper(I) iodide (139 mg, 50 mol %), 4-iodopyridine (300 mg, 1.46 mmol), *N*-(4-fluorophenyl)formamide (244 mg, 1.76 mmol) and *N*,*N*-dimethylethylenediamine (16 μl, 10 mol %). The flask was sealed, evacuated, and backfilled with nitrogen 2–3 times, then it was charged with THF (7 ml), evacuated and backfilled with nitrogen twice more and was allowed to stir at 66 °C overnight. The reaction mixture was diluted with EtOAc and quenched with saturated ammonium chloride. The aqueous layer was extracted with EtOAc and the combined organics were washed with brine, dried over magnesium sulfate, filtered, and concentrated under *vacuo*. The crude product was purified with prep-TLC (1:1 hexane:EtOAc) and the *N*-(4-fluorophenyl)-*N*-(pyridin-4-yl)formamide was obtained in 5% yield (16 mg). Not enough product was obtained to allow a full

characterisation and it was left to another group member to resynthesise and characterise this compound.

EI-LRMS: obtained *m/z* 216.1 M^+ (composition: $C_{12}H_9FN_2O$, expected *m/z* 216.06989); ^{1}H NMR ($CDCl_3$) δ 8.96, 8.62, 8.57, 7.35, 7.1 - 7.27, 7.01, ^{19}F NMR ($CDCl_3$) δ -111.45 (major), -112.24 (minor).

6.6. Tables with data

Table 6.1. The conformer ratios and the experimental folding free energies for the OH-substituted molecular torsion balances in each solvent examined. Grey entries indicate the cases where conformational assignment may be ambiguous (as identified based on ^{19}F-NMR chemical shift analysis as detailed in Chapter 2).

conformer preference possibly reversed relative to $CDCl_3$

overlapping peaks

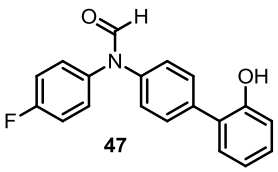

47

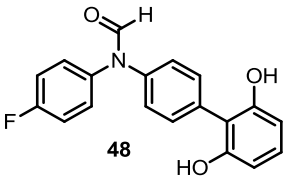

48

Solvent	ratio A/B	Δ*G* exp (kJ/mol)	ratio A/B	Δ*G* exp (kJ/mol)
Chloroform	1.20	-0.46	1.04	-0.10
Acetone	1.43	-0.88	1.61	-1.18
Acetonitrile	1.37	-0.78	1.45	-0.92
Benzene	1.20	-0.46	1.16	-0.37
Ethyl acetate	1.61	-1.18	1.85	-1.53
Hexane	n.s.	n.s.	n.s.	n.s.
THF	1.47	-0.96	1.92	-1.62
DCM	1.19	-0.43	1.03	-0.08
Ethanol	1.56	-1.11	n.s.	n.s.
Methanol	1.49	-0.99	1.67	-1.27
DMSO	1.33	-0.71	1.41	-0.85
Diethyl ether	1.67	-1.27	1.92	-1.62

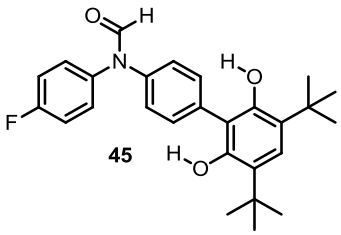

45

Solvent	ratio A/B	Δ*G* exp (kJ/mol)
Chloroform	0.82	0.49
Acetone	0.87 or 1.15	± 0.35
Acetonitrile	0.85	0.40
Benzene	0.76	0.68
Ethyl acetate	0.92 or 1.09	± 0.21
Hexane	0.58	1.35
THF	0.93	0.18
DCM	0.93	0.18
Ethanol	0.76	0.68
Methanol	0.90	0.26
DMSO	0.61 or 1.64	± 1.22
Diethyl ether	0.91	0.23

Table 6.2. Tables presenting the chemical shifts (ppm) of the conformers A and B (following the same conformational assignment as in $CDCl_3$) for every balance in each solvent observed in the ^{19}F-NMR spectra, and the difference between these chemical shifts. Coloured boxes indicate where detailed NMR analyses were performed to confirm the conformer assignments. Red boxes indicate where the dominant conformer was found to be different to that observed in $CDCl_3$. Green boxes indicate that the dominant conformer was the same as that observed in $CDCl_3$. Grey boxes indicate outliers in DCM and EtOH, which were assumed to have the same conformational preference as seen in $CDCl_3$ and MeOH respectively. Cases that were not soluble in a particular solvent are mentioned as "n.s." = not soluble, and data not obtained as "n.d." = not determined.

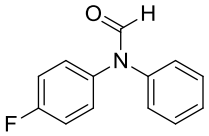

3

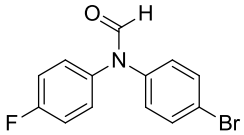

5

	A (ppm)	B (ppm)	B-A (ppm)	A (ppm)	B (ppm)	B-A (ppm)
Chloroform	-114.61	-114.27	0.34	-113.99	-113.5	0.49
Acetone	60.45	60.55	0.1	60.94	61.16	0.22
Acetonitrile	-116.65	-117.05	-0.4	-116.48	-116.22	0.26
Benzene	-115.46	-115.21	0.25	-114.9	-114.56	0.34
Ethyl acetate	-116.64	-116.23	0.41	-116.3	-115.75	0.55
Hexane	-115.86	-114.62	1.24	-115.15	-113.82	1.33
THF	-117.17	-116.63	0.54	-116.41	-115.78	0.63
DCM	-115.77	-115.67	0.1	-115.39	-115.13	0.26
Ethanol	-115.56	-115.52	0.04	-115.13	-114.98	0.15
Methanol	-116.59	-116.82	-0.23	-116.34	-116.21	0.13
DMSO	-115.07	-115.62	-0.55	-115.12	-114.69	0.43
Diethyl ether	-116.71	-115.7	1.01	-115.99	-114.87	1.12

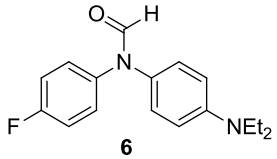

6

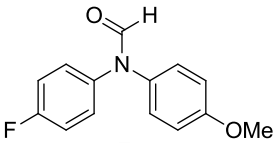

7

	A (ppm)	B (ppm)	B-A (ppm)	A (ppm)	B (ppm)	B-A (ppm)
Chloroform	-116.06	-115.67	0.39	-115.25	-114.83	0.42
Acetone	59.06	59.26	0.2	-116.78	-116.63	0.15
Acetonitrile	-117.82	-118.12	-0.3	-117.13	-117.46	-0.33
Benzene	-116.93	-116.64	0.29	-113.83	-113.55	0.28
Ethyl acetate	-118.14	-117.62	0.52	-117.4	-116.94	0.46
Hexane	-117.94	-116.57	1.37	-116.77	-115.4	1.37
THF	-118.56	-117.96	0.6	-117.74	-117.18	0.56
DCM	-117.3	-117.14	0.16	-116.36	-116.19	0.17
Ethanol	-116.81	-116.64	0.17	-120.76	-120.66	0.1
Methanol	-117.72	-117.82	-0.1	-116.35	-116.54	-0.19
DMSO	-116.32	-116.76	-0.44	-115.68	-116.18	-0.5
Diethyl ether	-118.61	-117.49	1.12	-117.53	-116.51	1.02

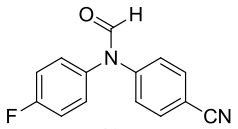

10

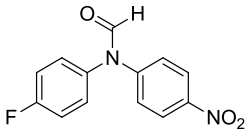

11

	A (ppm)	B (ppm)	B-A (ppm)	A (ppm)	B (ppm)	B-A (ppm)
Chloroform	-112.65	-112.03	0.62	-112.35	-111.67	0.68
Acetone	-117.23	-116.9	0.33	-114.36	-113.98	0.38
Acetonitrile	-115.36	-115.25	0.11	-114.28	-114.25	0.03
Benzene	-111.3	-110.91	0.39	-113.31	-112.91	0.4
Ethyl acetate	-114.95	-114.38	0.57	-114.69	-114.09	0.6
Hexane	n.s.	n.s.	n.s.	n.s.	n.s.	n.s.
THF	-115.21	-114.54	0.67	-114.99	-114.28	0.71
DCM	-113.92	-113.54	0.38	-113.67	-113.21	0.46
Ethanol	-118.63	-118.37	0.26	-118.65	-118.31	0.34
Methanol	-114.62	-114.67	-0.05	-114.48	-114.39	0.09
DMSO	-114.01	-113.77	0.24	-113.77	-113.59	0.18
Diethyl ether	-114.53	-113.58	0.95	-114.38	-113.22	1.16

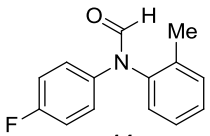

14

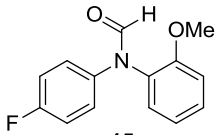

15

	A (ppm)	B (ppm)	B-A (ppm)	A (ppm)	B (ppm)	B-A (ppm)
Chloroform	-116.25	-115.97	0.28	-116.05	-115.86	0.19
Acetone	-117.61	-117.52	0.09	-117.46	-117.57	-0.11
Acetonitrile	-117.66	-117.32	0.34	-117.11	-117.48	-0.37
Benzene	-119.35	-119.51	-0.16	-119.37	-119.58	-0.21
Ethyl acetate	-118.04	-118	0.04	-118.13	-118.09	0.04
Hexane	-117.31	-116.79	0.52	-117.65	-116.96	0.69
THF	-118.3	-118.22	0.08	-118.52	-118.42	0.1
DCM	-117.14	-117.28	-0.14	-117.12	-117.08	0.04
Ethanol	-116.94	-116.91	0.03	-116.79	-116.81	-0.02
Methanol	-117.42	-117.27	0.15	-117.06	-117.24	-0.18
DMSO	-116.56	-116.01	0.55	-116.57	-115.95	0.62
Diethyl ether	-118.14	-117.73	0.41	-118.39	-117.94	0.45

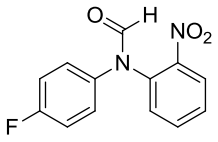

17

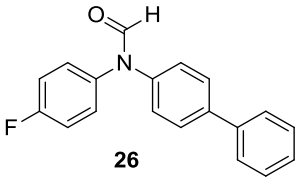

26

	A (ppm)	B (ppm)	B-A (ppm)	A (ppm)	B (ppm)	B-A (ppm)
Chloroform	-114.01	-113.48	0.53	-114.42	-114.04	0.38
Acetone	-116.01	-115.7	0.31	60.62	60.79	0.17
Acetonitrile	-115.72	-115.66	0.06	-116.43	-116.76	-0.33
Benzene	n.d.	n.d.	n.d.	-115.28	-114.99	0.29
Ethyl acetate	-116.27	-115.9	0.37	-116.48	-116	0.48
Hexane	n.s.	n.s.	n.s.	n.s.	n.s.	n.s.
THF	-116.58	-116.14	0.44	-116.83	-116.23	0.6
DCM	-115.24	-114.78	0.46	-115.46	-115.31	0.15
Ethanol	-115.36	-115.09	0.27	-115.69	-115.59	0.1
Methanol	-115.78	-115.66	0.12	-116.52	-116.7	-0.18
DMSO	-115.1	-115.28	-0.18	-114.89	-115.36	-0.47
Diethyl ether	-116.12	-115.37	0.75	-116.59	-115.48	1.11

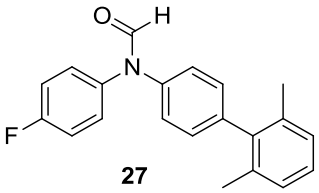

27

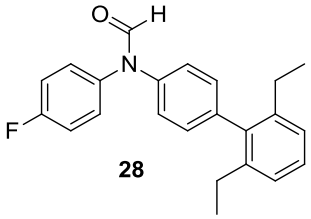

28

	A (ppm)	B (ppm)	B-A (ppm)	A (ppm)	B (ppm)	B-A (ppm)
Chloroform	-114.44	-113.98	0.46	-114.39	-113.91	0.48
Acetone	60.59	60.82	0.23	60.65	60.92	0.27
Acetonitrile	-116.54	-116.84	-0.3	-116.49	-116.77	-0.28
Benzene	-115.27	-114.89	0.38	-115.2	-114.75	0.45
Ethyl acetate	-116.45	-115.93	0.52	-116.38	-115.84	0.54
Hexane	n.s.	n.s.	n.s.	-115.92	-114.44	1.48
THF	-116.81	-116.1	0.71	-116.76	-115.97	0.79
DCM	-115.89	-115.66	0.23	-115.54	-115.27	0.27
Ethanol	-115.43	-115.3	0.13	-115.3	-115.14	0.16
Methanol	-116.49	-116.66	-0.17	-116.4	-116.55	-0.15
DMSO	-114.89	-115.28	-0.39	-114.81	-115.17	-0.36
Diethyl ether	-116.79	-115.58	1.21	-116.48	-115.23	1.25

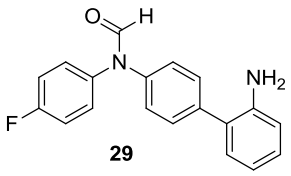

29

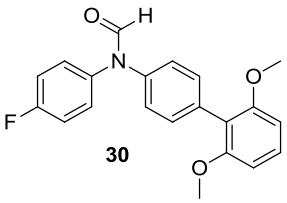

30

	A (ppm)	B (ppm)	B-A (ppm)	A (ppm)	B (ppm)	B-A (ppm)
Chloroform	-114.31	-113.91	0.4	-114.64	-114.2	0.44
Acetone	60.56	60.73	0.17	60.52	60.73	0.21
Acetonitrile	-115.95	-116.29	-0.34	-116.41	-116.77	-0.36
Benzene	-115.15	-114.99	0.16	n.d.	n.d.	n.d.
Ethyl acetate	-116.47	-116	0.47	-116.93	-116.41	0.52
Hexane	n.s.	n.s.	n.s.	n.s.	n.s.	n.s.
THF	-116.8	-116.26	0.54	-117.31	-116.58	0.73
DCM	-115.42	-115.25	0.17	-115.61	-115.51	0.1
Ethanol	-115.46	-115.41	0.05	-115.88	-115.73	0.15
Methanol	-116.53	-116.76	-0.23	-116.71	-116.87	-0.16
DMSO	-114.98	-115.45	-0.47	-114.89	-115.31	-0.42
Diethyl ether	-116.55	-115.53	1.02	-117.08	-115.89	1.19

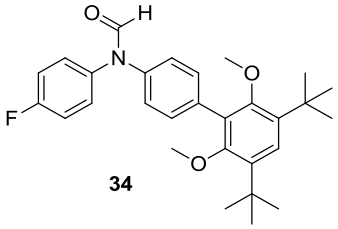

34

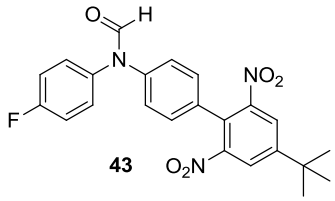

43

	A (ppm)	B (ppm)	B-A (ppm)	A (ppm)	B (ppm)	B-A (ppm)
Chloroform	-114.41	-114.01	0.4	-113.86	-113.19	0.67
Acetone	60.53	60.72	0.19	-115.33	-114.96	0.37
Acetonitrile	-116.62	-116.89	-0.27	-115.14	-115.34	-0.2
Benzene	-115.15	-114.83	0.32	-114.75	-114.03	0.72
Ethyl acetate	-116.62	-116.2	0.42	-115.92	-115.23	0.69
Hexane	-115.76	-114.44	1.32	n.s.	n.s.	n.s.
THF	-116.77	-116.14	0.63	-116.28	-115.29	0.99
DCM	-115.9	-115.69	0.21	-115.17	-114.8	0.37
Ethanol	-115.39	-115.33	0.06	-115.01	-114.69	0.32
Methanol	-116.44	-116.64	-0.2	-115.36	-115.39	-0.03
DMSO	-114.95	-115.41	-0.46	-114.41	-114.72	-0.31
Diethyl ether	-116.44	-115.4	1.04	-115.99	-114.48	1.51

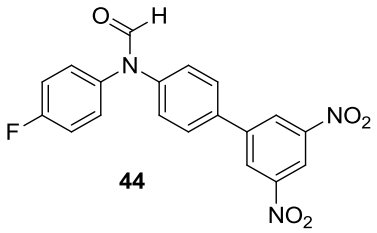

44

	A (ppm)	B (ppm)	B-A (ppm)
Chloroform	-113.44	-112.94	0.5
Acetone	-115.1	-115.31	-0.21
Acetonitrile	-115.39	-115.12	0.27
Benzene	-114.02	-113.7	0.32
Ethyl acetate	-115.73	-115.22	0.51
Hexane	n.s.	n.s.	n.s.
THF	-116.1	-115.51	0.59
DCM	-114.77	-114.51	0.26
Ethanol	n.s.	n.s.	n.s.
Methanol	-115.3	-115.42	-0.12
DMSO	-114.92	-114.48	0.44
Diethyl ether	n.s.	n.s.	n.s.

Table 6.3. Calculation of ΔG_{exp} and ΔG_{calc} for the *para*-substituted balances when the solvophobic term d≠0. The boxes highlighted in orange are the cases where the peaks of the two conformers in the NMR spectra were overlapping. In these cases the two peaks were separated by using the GSD function in MestReNova and then they were integrated.

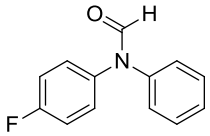

3

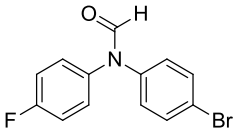

5

Solvent	A/B	ΔG exp	ΔG calc	A/B	ΔG exp	ΔG calc
Chloroform	1.59	-1.14	-1.00	0.97	0.08	0.05
Acetone	1.41	-0.85	-0.90	0.98	0.05	0.10
Acetonitrile	1.37	-0.78	-0.89	1.06	-0.15	0.07

Benzene	1.32	-0.68	-0.95	0.97	0.08	0.23
Ethyl acetate	1.54	-1.07	-0.91	0.93	0.18	0.11
Hexane	1.59	-1.14	-0.95	0.86	0.37	0.27
THF	1.43	-0.88	-0.96	0.91	0.23	0.22
DCM	1.39	-0.81	-0.98	0.97	0.08	0.10
Ethanol	1.39	-0.81	-0.81	1.02	-0.05	-0.12
Methanol	1.39	-0.81	-0.81	1.03	-0.08	-0.12
DMSO	1.35	-0.75	-0.73	1.04	-0.10	-0.09
Diethyl ether	1.56	-1.11	-0.96	0.86	0.37	0.23

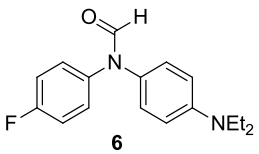

6

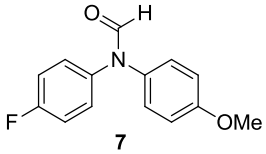

7

Solvent	A/B	Δ*G* exp	Δ*G* calc	A/B	Δ*G* exp	Δ*G* calc
Chloroform	1.89	-1.57	-1.43	1.37	-0.78	-0.70
Acetone	1.85	-1.53	-1.66	1.33	-0.71	-0.81
Acetonitrile	1.49	-0.99	-1.57	1.23	-0.52	-0.77
Benzene	1.75	-1.39	-2.06	1.35	-0.75	-1.10
Ethyl acetate	2.38	-2.15	-1.68	1.45	-0.92	-0.83
Hexane	3.03	-2.75	-2.20	1.82	-1.48	-1.20
THF	2.33	-2.09	-2.00	1.54	-1.07	-0.99
DCM	1.56	-1.11	-1.61	1.27	-0.58	-0.82
Ethanol	1.85	-1.53	-0.99	1.32	-0.68	-0.44
Methanol	1.54	-1.07	-0.99	1.23	-0.52	-0.44
DMSO	1.39	-0.81	-1.16	1.16	-0.37	-0.52
Diethyl ether	2.63	-2.40	-2.03	1.67	-1.27	-1.02

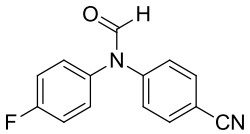

10

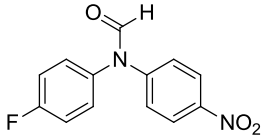

11

Solvent	A/B	Δ*G* exp	Δ*G* calc	A/B	Δ*G* exp	Δ*G* calc
Chloroform	0.66	1.03	1.01	0.57	1.39	1.31
Acetone	0.89	0.29	0.47	0.83	0.46	0.76
Acetonitrile	1.06	-0.15	0.45	0.99	0.02	0.72
Benzene	0.73	0.78	0.73	0.65	1.07	1.06
Ethyl acetate	0.77	0.65	0.51	0.68	0.96	0.80

Hexane	n.s.	n.s.	n.s.	n.s.	n.s.	n.s.
THF	0.76	0.68	0.76	0.7	0.88	1.15
DCM	0.75	0.71	0.91	0.67	0.99	1.21
Ethanol	0.86	0.37	0.02	0.79	0.58	0.14
Methanol	0.94	0.15	0.02	0.93	0.18	0.14
DMSO	1.25	-0.55	-0.39	1.16	-0.37	-0.27
Diethyl ether	0.6	1.27	0.75	0.45	1.98	1.14

6.7. References

1. Naumann, C.; Patrick, B. O.; Sherman, J. C., *Tetrahedron* **2002**, 58, 787-798.
2. Gasparro, F. P.; Kolodny, N. H., *J. Chem. Educ.* **1977**, 54, 258-61.
3. Klapars, A.; Huang, X.; Buchwald, S. L., *J. Am. Chem. Soc.* **2002**, 124, 7421-7428.
4. Phillips, D. P.; Zhu, X.-F.; Lau, T. L.; He, X.; Yang, K.; Liu, H., *Tetrahedron Lett.* **2009**, 50, 7293-7296.
5. Lana, E. J. L.; Carazza, F.; Aparacida de Oliveira, R., *Helv. Chim. Acta* **2004**, 87, 1825-1831.
6. Maynard, G. D.; Ghosh, M.; Yuan, J.; Currie, K. S.; Mitchell, S.; Guo, Q.; Zhao, H. Preparation of 4,5-disubstituted-2-aryl pyrimidines as C5a receptor ligands. PCT Int. Appl. **2005**, US2005/015897, WO2005/110416 A2.
7. Paduraru, P. M.; Popoff, R. T. W.; Nair, R.; Gries, R.; Gries, G.; Plettner, E., *J. Comb. Chem.* **2008**, 10, 123-134.
8. Sahakitpichan, P.; Thasana, N.; Ruchirawat, S., *Synthesis* **2005**, 2934-2938.
9. Nishimura, N.; Yoza, K.; Kobayashi, K., *J. Am. Chem. Soc.* **2010**, 132, 777-790.
10. Tyagarajan, S.; Chakravarty, P. K.; Zhou, B.; Taylor, B.; Eid, R.; Fisher, M. H.; Parsons, W. H.; Wyvratt, M. J.; Lyons, K. A.; Klatt, T.; Li, X.; Kumar, S.; Williams, B.; Felix, J.; Priest, B. T.; Brochu, R. M.; Warren, V.; Smith, M.; Garcia, M.; Kaczorowski, G. J.; Martin, W. J.; Abbadie, C.; McGowan, E.; Jochnowitz, N.; Weber, A.; Duffy, J. L., *Bioorg. Med. Chem. Lett.* **2010**, 20, 7479-7482.
11. Tyagarajan, S.; Chakravarty, P. K.; Zhou, B.; Taylor, B.; Fisher, M. H.; Wyvratt, M. J.; Lyons, K.; Klatt, T.; Li, X.; Kumar, S.; Williams, B.; Felix, J.; Priest, B. T.; Brochu, R. M.; Warren, V.; Smith, M.; Garcia, M.; Kaczorowski, G. J.; Martin, W. J.; Abbadie, C.; McGowan, E.; Jochnowitz, N.; Parsons, W. H., *Bioorg. Med. Chem. Lett.* **2010**, 20, 5480-5483.
12. Ashton, P. R.; Harris, K. D. M.; Kariuki, B. M.; Philp, D.; Robinson, J. M. A.; Spencer, N., *J. Chem. Soc., Perkin Trans. 2* **2001**, 2166-2173.
13. Rahman, M.; Kundu, D.; Hajra, A.; Majee, A., *Tetrahedron Lett.* **2010**, 51, 2896-2899.
14. Chen, W.; Lin, Z.; Ning, M.; Yang, C.; Yan, X.; Xie, Y.; Shen, X.; Wang, M.-W., *Bioorg. Med. Chem.* **2007**, 15, 5828-5836
15. Gottlieb, H. E.; Kotlyar, V.; Nudelman, A., *J. Org. Chem.* **1997,** 62, 7512-7515.